Burst Pressure of Pipeline with Longitudinal Crack in Dent Defects Using Extended Finite Element Method

by

Allan Ray Okodi

A thesis submitted in partial fulfillment of the requirements for the degree of

Doctor of Philosophy

in

Structural Engineering

Department of Civil and Environmental Engineering
University of Alberta

ABSTRACT

Pipelines are exposed to mechanical damage due to external interference while in service. The damages can be in form of dents, wrinkles, gouges, or cracks. In some instances, two or more of the damages may occur at the same location on the pipe and act as one defect. One of the combined defects in pipeline comprises of a crack inside a dent, commonly referred to as dent-crack defect. Field observations show pipeline with dent-crack defects fail by leakage or rupture at low pressure, requiring pipelines to be shutdown, which is a highly consequential choice in pipeline operations. Very little is known about how the constituting dents and cracks interact as they degrade integrity of the pipeline, partly because few researches have been conducted on the effect of dent-cracks in pipeline. Currently there are no predictive analytical models accepted in the pipeline industry to assess integrity of pipelines with dent-crack defects. The assessments could be done experimentally and by using traditional finite element method, which are both very expensive and time consuming methods. The traditional finite element method works well for problems in a continuum, but are not suited for modelling discontinuities like cracks, especially where the discontinuity is not static, like a propagating crack. The extended finite element method (XFEM) is specifically designed for modelling crack propagation. It is less tedious to use than the traditional finite element method because it does not require re-meshing the body each time the crack propagates. However, its effectiveness for assessment of crack propagation in pipelines has not been widely investigated. This thesis presents the results, discussion, conclusions and recommendations of a numerical evaluation of the effect of dent-crack defects on integrity of pipeline, conducted using the extended finite elements method implemented in the finite element analysis software, Abaqus. The first part of the evaluation focused on establishing the effectiveness of the XFEM methodology implemented in Abaqus for analysis of crack propagation and

prediction of burst pressure of pipeline with plain longitudinal cracks. Models of specimens of longitudinally cracked API X60 pipeline with known experimentally determined burst pressure were developed in Abaqus, allowing for XFEM crack propagation, and used to predict burst pressure of the pipeline. In addition, the burst pressures were predicted using the modified NG-18 equation, CorLAS and Failure Assessment Diagrams (FAD), which are industry accepted analytical methods for assessment of burst pressure. The predictions of different methods were compared with burst test results to assess effectiveness of the XFEM models. The comparisons showed that well calibrated XFEM models can accurately predict burst pressure of cracked pipeline. In the second part of the study, models of specimens of API X70 grade of pipeline having longitudinal cracks inside rectangular dents were calibrated and validated using burst test data obtained in literature and used in a parametric analysis of pipeline with various sizes of dent-crack defects. The effect of varying crack length, crack depth, dent depth, denting pressure, location of cracks inside dents and dent restraint condition, on burst pressure of pipeline with dent-crack defects were evaluated in order to establish the relative impact of the various parameters on integrity of the pipeline. The results showed that crack depth and location of crack inside the dent are the most severe parameters for pipeline integrity. Affected pipeline could have significant remaining burst strength depending on the sizes of the defects and the pipe could be retained in service upon an engineering assessment.

PREFACE

The work presented in this thesis was conducted as part of a research collaboration between the pipeline research team at the University of Alberta, led by Prof. Samer Adeeb and the team at Enbridge pipeline Inc., led by Dr. Nader Yoosef-Ghodsi. The author was responsible for developing the key concepts, data acquisition, numerical modelling, interpretation of results and reporting of findings of the research. The lead collaborators were primarily responsible for acquisition of funding, providing general direction of the study and necessary technical support to ensure quality of the work and proper interpretation of results.

The thesis is set up in seven chapters and all materials obtained from published or unpublished sources and used in the thesis have been appropriately acknowledge by way of references. In addition, all copyrighted materials have been used with permission of the copyright owners, in form of licenses.

The introduction presented in Chapter 1 and the literature review in Chapter 2 are the author's original work and where appropriate, references for citations have been provided within the text. Chapters three to six are derived from papers that have either already been published in journals and conference proceedings or submitted by the author for publication.

Chapter 3 is derived from a research article published in the International Journal of Pressure Vessels and Piping, Elsevier Science Direct: Okodi, A., Lin, M., Yoosef-Ghodsi, N., Kainat, M., Hassanien ,S., Adeeb, S., Crack Propagation and Burst Pressure of Longitudinally Cracked Pipeline Using Extended Finite Element Method, International Journal of Pressure Vessels and Piping (2020), 10.1016/j.ijpvp.2020.104115.

Chapter 4 is derived from a published conference proceeding: Okodi, A., Cheng, J.J.R., Li, Y., Kainat, M., Adeeb, S., Yoosef-Ghodsi, N., Extended Finite Element Investigation of Burst Pressure of Pipeline with Combined Dent and Crack Defects, Proceedings of the ASME 2020 Pressure Vessels & Piping Conference, July 19 - 24, 2020, Minneapolis, Minnesota, USA, PVP2020-21318.

Chapter 5 is derived from a research article published in the MDPI Journal of Applied Sciences, Special issue on Advanced Numerical Approaches for Crack Growth Simulation: Okodi, A., Li, Y., Cheng, J.J.R., Kainat, M.,Yoosef-Ghodsi, N., Adeeb, S., Crack Propagation and Burst Pressure of Pipeline with Restrained and Unrestrained Concentric Dent-Crack Defects Using Extended Finite Element Method, Journal of Pressure Sciences (2020), 10.3390/app10217554.

Chapter 6 is derived from a research article submitted for publication in the Journal of Pipeline Sciences and Engineering: Okodi, A., Li, Y., Cheng, J.J.R., Kainat, M.,Yoosef-Ghodsi, N., Adeeb, S., Effect of location of crack in dent on burst pressure of pipeline with combined dent and crack defects.

A.R. Okodi

Dedicated to my Loving family

and

Dear parents.

ACKNOWLEDGEMENTS

First, I would like to give sincere thanks to the Almighty God, for it is not by my strength or power alone, but by His grace and Will that I was able to walk this journey. Glory be to Him.

In equal measure, I would like to express my deepest and heart felt gratitude to my Supervisor, Dr. Samer Adeeb, for affording me the opportunity to be a part of your research team and providing me the resources and an excellent environment to thrive. Your unrelenting guidance were energizing and made seemingly steep milestones surmountable.

I would also like to thank the rest of my doctoral committee members: Dr. Roger J.J. Cheng, Dr. Yong Li, Dr. Robert Driver, Dr. Douglas Tomlinson, Dr. Carlos Cruz Noguez, and Dr. Lijun Deng for their guidance and encouragement. Sincere thanks also go to Dr. Frank Cheng at the University of Calgary for accepting the arduous yet, crucial responsibility of the external examiner of this dissertation.

In a special way, I would like to thank all my professors at the University of Alberta: Prof. Robert Driver, Prof. Ben Jar, Prof. Samer Adeeb, Dr. Carlos Cruz Noguez, Dr. Yong Li, Dr. Douglas Tomlinson, Dr. Mustafa Gul, Dr. Ali Imanpour, from whom I learnt a lot. Your excellent tutorship and unquestionable commitment to students laid a firm foundation for me to succeed in this program and I will always remember you.

I would also like to thank the management of NSERC and Enbridge Pipelines Inc. This work would not have been possible without your financial support and commitment to promoting research.

Many thanks go to my friends Ronald Ekylimpa, Sylvester Agbo, Meng Lin, Odin Guzman Sanchez, Lomude Mori, Xinfang Zhang, Jesus Salazar, Chike Okoloekwe, Nguyen Lisa Duong, Kairs Wong, Yueying Li, Remi Avione, Mhedard Palizi, Saher Salama Attia, Leichuan Tan, Azam Abdollahi, Xiaoben Liu, Janine Woo, Ahmed Abdelmoety, Jonelle Baptiste, Onyekachi Ndubuaku, Nahid Elyasi, Owusu Prempeh, Susana Somuah Mensah, Qian Zhang, Diana Abdulhameed, Parmod Dev, Bisi Adewale, Peter Uchechukwu Umezurike, Bernado Garcia,

Shaghayegh Abtahi, and Razak Oduro, for your invaluable social support and academic collaborations.

My sincere appreciation goes to the Management and staff of Makerere University, my alma mater. Special mention goes to Dr. Yasin Naku Ziraba and Dr. Robinah Kulabako for your encouragement and support.

I would also like to say many thanks to my parents and siblings for their enduring love and prayers. Special thanks go to my dear father, The Hon. Justice Ruby Aweri Opio, JSC. Your dedicated support and encouragement of education opened the first doors to this journey.

Finally, I owe a debt of gratitude to my lovely wife, Rebecca Aryemo and my children, for her loving support and understanding, without which I would not have been able to stay focused on this dissertation.

TABLE OF CONTENTS

LIST OF TABLES

LIST OF FIGURES

LIST OF SYMBOLS AND ABBREVIATIONS

a	Crack depth
2c	Crack length
D, OD, D_e	External diameter of a pipe
R	External radius of a pipe
t	Wall thickness
L	Length of pipe specimen
d	Depth of plain dent
d_p	Depth of plain dent measured before the pipe is pressurized
d_d^p	Depth of dent measured after the pipe is pressurized
r_{dc}	Radius of curvature of dent in circumferential orientation
r_{dl}	Radius of curvature of dent in longitudinal orientation
P	Internal pressure
σ_u	Ultimate stress
ε_0	True critical strain of material from tests
ε_f	Strain limit for ductile fracture
ε_{eq}	Equivalent strain
ε_e	Elastic strain
ε_p	Plastic strain
σ_m	Hydrostatic stress
σ_{eq}	von Mises Stress
$\sigma_1, \sigma_2, \sigma_3$	Principal stresses
σ_{fs}	Failure stress
$\overline{\sigma}$	Flow stress
M_T	Folias' factor
CVN	Charpy V-notch Impact Energy
σ_{ys}	Yield stress
E	Youngs modulus
E'	E, under plane stress condition
P_f	Failure pressure

A	Area of a crack
A_0	Reference area of a cracked region of the body
J	J-Integral
J_{1c}	J-Fracture toughness
K_r	Fracture ratio
L_r	Load ratio
K	Elastic stress intensity factor
K_I	Mode I stress intensity factor
K_{II}	Mode II stress intensity factor
K_{III}	Mode III Stress intensity factor
K_{Ic}	Critical stress intensity factor
K_{mat}	Measured fracture toughness of material
G	Energy release rate
G_c	Critical energy release rate (Fracture energy)
Maxpe	Maximum principal strain
Maxps	Maximum principal stress
γ_s	Surface energy
γ_P	Plastic dissipation of energy
w_f	Work of fracture
U	Strain energy
ν	Poisson's ratio
P_{dent}	Pressure inside pipe during denting of pipe
T_0	Maximum traction
δ_0	Maximum separation
Γ_0	Energy absorbed by cohesive elements during fracture
η	Stress triaxiality
P_y	Yield pressure
PEEQ	Equivalent plastic strain
EPRG	European Pipeline Research Group
ASME	American Society Mechanical Engineers
CSA	Canadian Standards Association

SMYS	Specified Minimum Yield Strength
FAD	Failure Assessment Diagram
API	American Petroleum Institute
SCC	Stress Corrosion Crack
XFEM	Extended Finite Element Method
FEM	Finite Element Methods
FEA	Finite Element Analysis
SENT	Single Edge Notch Tension test
DFDI	Ductile Failure Damage Indicator
SLD	Strain Limit Damage
LEFM	Linear Elastic Fracture Mechanics
EPFM	Elastic-Plastic Fracture Mechanics
CMOD	Crack Mouth Opening Displacement
CTOD	Crack Tip Opening Displacement
CZM	Cohesive Zone Modeling
TSL	Traction Separation Law
BPR	Burst Pressure Ratio
BSI	British Standards Institution
EDM	Electro-Discharging Machine
LVDT	Linear Variable Differential Transducers
MAOP	Maximum Allowable Operating Pressure (80% yield pressure)
AER	Alberta Energy Regulator
CEPA	Canadian Energy Pipeline Association
NEB	National Energy Board

1. INTRODUCTION

Nearly 60% of annual Canadian energy production comprises of oil and natural gas [1] sourced from remote locations and delivered through an extensive network of approximately 800,000 kilometers pipelines. Pipelines are widely regarded as safe and cost effective for bulk transportation of energy products and a lot of resources are invested to prevent failure and maintain them in service. The pipeline industry in North America has a very good safety record for transportation of oil and gas products [2,3] due to strict local and national regulatory frameworks that ensure energy companies follow good design, operation and maintenance practices and promote use of improved materials and methods in pipeline construction. For example, the Alberta Energy Regulator (AER) in Canada requires energy companies to report all safety incidents in pipelines even where the incidents do not result in any form of failure of pipelines and no products are spilled in the environment. Incidents are viewed as opportunity to better understand what causes them so that the industry can work toward preventing them and improving pipeline performance. Figure 1.1 shows the distribution of primary energy sources produced in Canada in 2017.

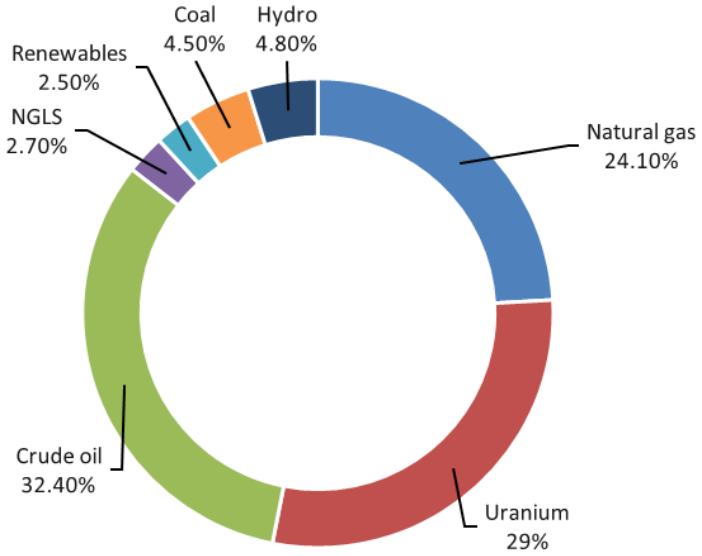

Figure 1.1 Canadian primary energy production-2017 [1]

1.1 Causes of pipeline safety incidents

Despite strict regulation and good safety practices, research shows safety incidents are common in both onshore and offshore pipelines in North America [4]. Most of the incidents are attributed to external interference and corrosion or metal loss. External interference, also known as mechanical

damage, refers to a collection of defects that occur when pipelines are hit by foreign objects during third party activities, which is pipeline industry expression for activities other than normal pipeline operation and maintenance. In onshore pipelines, third party damages (fig. 1.2a) are mainly due to excavations for developments such as roads, railways and building projects, while in offshore pipelines, the damages are due to impact of ship anchors or other foreign under water objects (Fig. 1.2b). Damages can also occur during construction of pipelines due to improper handling while lifting, stacking, transporting, and laying pipes. A common cause of damage during construction is where pipelines are laid on hard rocks that can pierce the bottom or where boulders used in backfilling the pipeline impact and damage the top surface, creating dents and wrinkles in the pipe wall. The damage may be accompanied with local metal loss in forms of scratch, or gouge in pipe wall resulting in combined scratch in dent, or gouge in dent defects. A scratch is a defect characterized by loss of coating and minimal loss of metal, while a gouge occurs with significant loss of metal from the pipe surface. Similarly, dents might be arbitrarily formed near welds (Fig1.2c), which can cause the welds to crack, resulting in cracks inside dents [5].

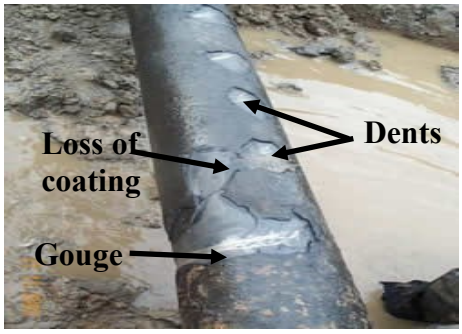

(a) Excavator impact (onshore pipeline)

(b) Dent and rupture (offshore pipeline)

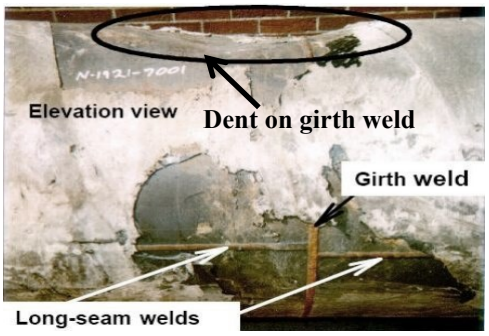

(c) Dents and loss of coating (onshore pipeline)

Figure 1.2 Defects due to third party impact on pipeline (Leis and Francini 1999)

Excessive mechanical damage can cause sudden failure in pipeline, characterized by loss of content due to leaks and ruptures. In many cases however, less severe damages like shallow dents, shallow gouges, and scratches, which do not cause loss of pipeline contents are created and are of little consequence to pipeline operations as affected pipelines continue to sustain high operating pressures in the short term, without failure [1,4,6]. In the long term however, any damage can compromise the structural integrity of the pipeline. High stresses and strains within the damaged region of the pipe could affect fatigue strength and cause failure at low pressure [5,7]. In addition, the regions where the inconsequential defects are located often act as sites where other more perilous defects like cracks and corrosions initiate in pipelines [7]. Studies show that reductions in fatigue life due to occurrence of mechanical damages in pipelines increase with depths of the mechanical damage [8] and with increasing D/t ratio of pipe outside diameter (D) to wall thickness(t) [9]. This is particularly important because currently, the trend in the pipeline industry is biased towards stronger grades of pipes that can allow use of very thin walled, and large diameter pipes to transport ever increasing volumes of pressurized products at lower cost.

Defects due to external interference were responsible for 8% of safety incidents reported in Alberta in 2017 (Fig 1.3a) [2]. 36% of the incidents (Fig 1.3b) resulted in failure and shut down of pipelines due to leaks and ruptures, while 64% were of low consequences and classified as “hits”, because they did not cause loss of contents but as mentioned above, could eventually progress to cause failure in the long term. Onshore pipelines are usually buried in the ground and defects may occur in the pipes and remain undetected for a long time, allowing them to grow and attract other opportunistic defects like cracks and corrosion, further deteriorating the pipe’s integrity. Defects due to external interference can therefore be very consequential for pipelines and require immediate attention when detected. The pipelines must be regularly inspected and where the defects are detected, an engineering assessment of fitness for service is conducted and appropriate actions taken to repair the defect or replace affected pipe.

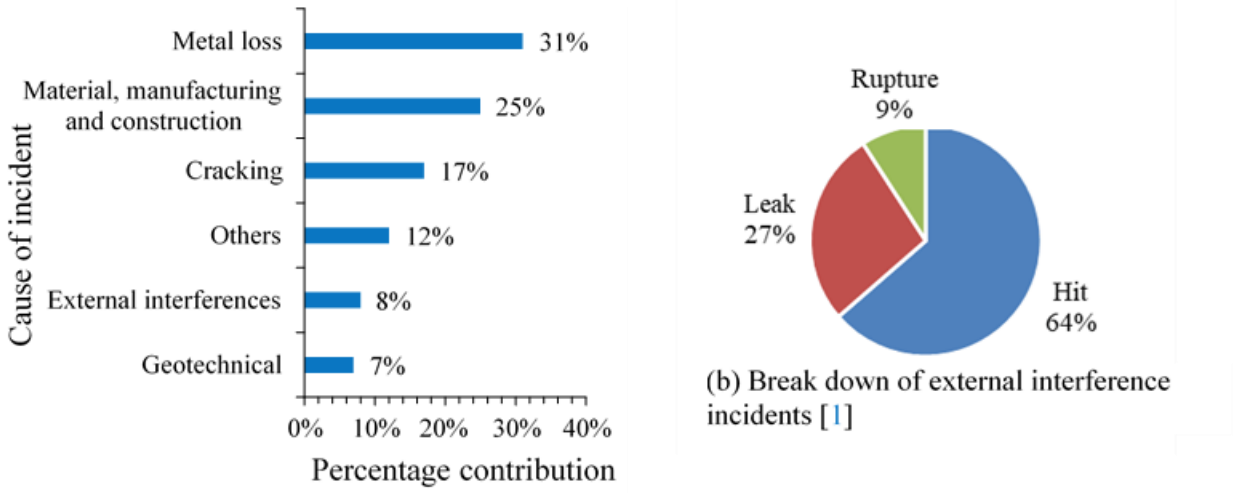

(a)Distribution of causes of pipeline incidents [2]

(b) Break down of external interference incidents [1]

Figure 1.3 Causes of pipeline safety incidents in Alberta -2017

1.1.1 Dents in pipeline

A dent is one of the most common form of mechanical damage in pipeline. The most important parameters that determine the effect of dents on integrity of pipelines are dent depth, d_d^p and radii of curvature r_{dc} and r_{dl} in circumferential and longitudinal orientations respectively (Fig1.4) [10]. Shallow, unconstrained plain dents with smooth curvature spring back elastically and rebound under internal pressure to regain the original pipe geometry. They are not considered to be severe defects because the damaged pipes can sustain pressure levels equivalent to yield strength of pipe material. This happens because in absence of stress risers like cracks, yielding within the dents occur over a large area and there is enough ductility to yield and accommodate large plastic flow without failure. Some dented pipes have been observed to fail at locations far away from the dent [11]. Dents cause local strain and stress concentrations which weaken in-service performance and reduce fatigue lives of the pipes [7,11]. Lancaster and Palmer (1996) [11] showed that strains in pressurized pipes with circular dents are highest in the axial extremities of the dents with the highest strains being between 10 to 28 times the strains in the undeformed region of the pipe. For a pipe having a dent combined with a gouge, Lancaster and Palmer (1996) [11]showed that cracking may begin within the gouge at the region of highest strain concentration factor. Rinehart and Keating (2007) [12] showed that stress concentration factors in two dimensional shallow, long dents in cylinders are always greater than 2 and can rise to between 10 and 20 in deep dents.

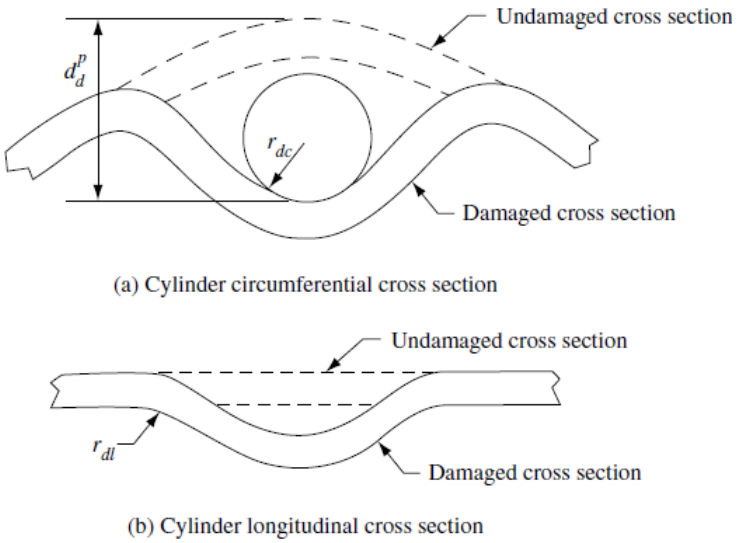

Figure 1.4 Plain dent parameters - EPRG method [10]

In addition, Rinehart and Keating showed that stress concentration in dents increase with ratios of dent depth to pipe thickness and dent depth to pipe diameter, reinforcing the conclusion that deep dents are more problematic for thin walled pipes with large diameters [9]. The deep dents are also undesirable because they impede flow of contents and movement of in line inspection equipment. Dents of any profile occurring in proximity of welds are undesirable as they may cause cracks in the weld zones.

There are many codes [13-18] that can be used to assess the effect of plain dents on integrity of pipeline. But since plain dents do not affect burst capability of pipelines, the objective of the assessment procedures is to rank the dents in the order of severity and prioritize them for detailed engineering analysis, dig out and repair of affected pipes. Except for ASME B31.8 [18], all other codes assess dent severity based upon depth. The ASME B31.8 uses a strain-based procedure in which the combined membrane and bending strains in dents are calculated and compared with a prescribed allowable total strain threshold to determine whether the dent is critical. According to the code guideline, plain dents are considered acceptable if the strains associated with the dents do not exceed 6% strain. The likelihood of puncture in dents and cracking in buckles increases when material strain exceeds 12% [5]. Therefore, the 6% strain is a suitable threshold for screening localized rock-induced deformations for incipient damage. The Canadian standards code CSA Z662-07[15] requires that dents of depth ≥6% of the pipe's outside diameter (D) should be repaired regardless of location on the pipe. Although tests show that pipes with deeper plain dents can

sustain pressure equivalent to yield strength of the material without failure, the 6%D upper limit on dent depth is necessary for free movement of in line inspection equipment and free flow of contents. The CSA Z662-07[15] also requires dents of any depth located near welds to be repaired unless determined through an engineering assessment that they will not crack the welds.

Research by European Pipeline Research Group (EPRG) [19] shows pipelines with plain dents of depth less than 10% of pipe outside diameter or stress levels less than 72% of the specified yield strength (SMYS) of the material will not fail under internal pressure, hence the EPRG capped the maximum allowable depth of plain dents in unpressurised pipes at 10%D (equation 1-1).

$$\frac{d_p}{D} \leq 10\% \qquad (1-1)$$

Where d_p is the depth of the plain dent measure before the pipe is pressurized and D is as defined before. The allowable maximum dent depth in pressurized pipes drops to 7% to account to the rebound of dents under internal pressure.

$$\frac{d_d^p}{D} \leq 7\% \qquad (1-2)$$

Where d_d^p is the depth of the plain dent measured after the rebound of the dent has occurred.

1.1.2 Crack and crack-like defects in pipeline

Cracks are planar discontinuities caused by linear rapture of the material, predominantly characterized by length, depth, and a sharp root/tip radius. The main cause of cracks in pipeline is mechanical damage, but they may also be caused by environmental action on a stressed pipe. Environmental cracking is due to interaction between susceptible pipe metal and aggressive electrolytes in the environment. It is more common in piping systems in petrochemical plants than transportation pipelines [13]. The corrosive electrolytes embrittle the otherwise ductile metal causing brittle fracture under internal pressure. An example of environmental cracking is the stress corrosion cracking. A major difference between mechanically induced cracks and environmental cracks is that mechanical cracks are usually planar (single) cracks, while the latter appear in multiples, often as branches of a major crack. In addition, crack-like defects that are not caused by linear rapture of the pipe material may also be found in the pipeline. Such defects have the same characteristics as cracks and can be conservatively assessed as cracks. Examples of crack-like

defects include lack of fusion and lack of penetration in welds, deep undercuts and root under cuts of welds, sharp localized corrosion, aligned porosity, and aligned inclusions within the sheet metal. The crack-like defects are classified as through-wall, surface, embedded, edge or corner flaws [10] as shown in figure 1.5.

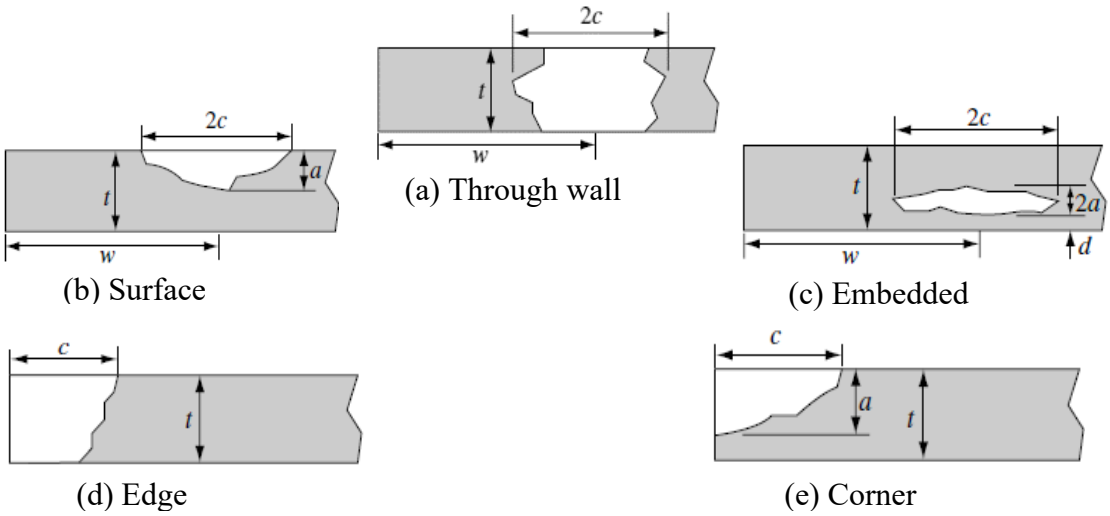

Figure 1.5 Crack-like defects-American Petroleum Institute classification [10,13]

The effect of cracks in pipeline is two-fold. From a fracture mechanics and materials perspective, cracks are stress risers or stress intensifiers in the material at the crack tip [20], while from a structural and geometric perspective, the cracks reduce the thickness of pipe wall available to transfer applied loads into the pipe supports or ground. The pipes are therefore structurally weaker at locations of crack. Cracks in pipelines can occur in either longitudinal or circumferential orientations on the pipe. Longitudinal cracks in pressurized pipelines are particularly dangerous because they occur in a plane normal to the maximum principal stress (hoop stress) and are therefore more likely to propagate at low internal pressure than circumferential cracks.

Assessment of burst pressure the pipe starts with determination of the size of crack, with crack length and depth being the main parameters of interest [21-24] The API 579 code [13] allows the assessment procedure for mechanical cracks to be applied to environmental cracks provided a dominant crack whose behavior largely controls the structural response of the pipe can be identified from the multiple environmental cracks using the flaw characterization techniques in

the code. The code further recommends damage mechanics for assessment of environmental cracks where a dominant branch cannot be defined.

Once the cracks are sized, the assessment of burst pressure follows fracture mechanics principles. Linear elastic fracture mechanics is employed to analyze fracture of brittle materials. Elastic-plastic fracture mechanics is used to analyze fracture of nonlinear elastic materials by extending the linear elastic mechanics theory to elastic-plastic materials. The radius of crack tip is infinitesimally small, therefore in theory, loading the crack tip causes infinite amount of stress, which explains why cracks are viewed as stress risers or intensifiers. The high stress intensity causes yielding and plastic deformation of the material at the crack tip and eventually causes crack growth if the loading is sustained. The size of the region at the crack tip that undergoes plastic deformation depends on the mechanical properties of the material. More plastic deformation occurs in elastic-plastic materials than in linear elastic materials. Therefore, linear elastic materials usually fail by brittle fracture while fracture of elastic plastic materials are ductile and present with significant plasticization of the ligament ahead of the crack tip.

There are many analytical models available to the pipeline industry for assessing the effect of cracks on integrity of pipelines and determining burst pressure [25-28], some of which have been developed into codes. These models include the Battelle NG-18 equation, CorLAS, and Failure Assessment Diagrams (FAD) in BS7910 and API 579 codes. The performance of these models has been compared by several researchers [27-29] with the conclusion that they vary in levels of accuracy of prediction, but the assessments are reliable.

1.1.3 Combined defects

Mechanical damage may cause multiple defects like dents, scratches, gouges and cracks simultaneously within the same region of the pipe. Dents formed near brittle welds may cause the welds to crack during denting, elastic spring back or re-rounding of the dent. Cracks could also initiate at the root of the dents because of the reduced fatigue life of the material within the dent. When in close proximity of each other, the multiple defects have been found to have a combined effect on the integrity of pipelines [10]. Dents and cracks in proximity of each other similarly act as one defect [21-24] and the combined defect, commonly referred to as dent-crack is regarded in pipeline industry as one of the most injurious mechanical defects [15-16].

1.2 Problem statement

Pipelines with dent-crack defects have been found to fail at low pressure even where the crack was negligible in size when the defects were first identified [30]. For example, dent-crack defects were responsible for the failure of Enbridge pipeline Inc.'s Line 2 near Odessa, Saskatchewan in September 2009 and Trans-Northern Pipelines Inc.'s Ottawa Lateral line near Farran's point, Ontario in October 2009 [31]. In both cases a longitudinal crack developed within shallow dents (0.51%D and 2.7% D respectively) at the bottom of the pipe, causing leakage at the 6 O'clock position at what was reported as normal operating pressure. Metallurgical investigations revealed that the cracks propagated by fatigue, demonstrating the dangers of dent-crack defects on integrity of pipelines. The dents reduced the fatigue life of the pipe and fatigue cracks developed due to fluctuations of internal pressure during different phases of pipeline operations.

Due to its severity on pipeline integrity, industry codes [15-18] recommend that pipeline with dent-crack defects with dent depths of more 4% of the outside diameter of the pipe be cut and replaced as pipe rings without fitness for service assessment, while those with dent depths less than 4%D can be repaired by grinding up to a depth less than 10% of pipe wall thickness. The ASME B31.4 code [15] does not formally permit pipeline with dent crack defects to be kept in service.

There are currently no analytical models accepted by the pipeline industry for assessing integrity of pipelines with dent-crack defects[10]. Assessments could be done experimentally and numerically, which are both expensive methods that do not give results fast enough for quick integrity decision making. A few attempts have been made to propose predictive models for pipeline with dent-crack defects. Oryniak et.al (2007) [32] proposed a theoretical solution based on estimates of stress distribution in a dent having an axial crack starting from the deepest point of a dent. The effect of dent is accounted for by allowing for geometric nonlinearity in the model. Bending stresses through the crack caused by the geometric nonlinearity are added to the stresses caused by the internal pressure and the sum of stresses is used to calculate the stress intensity factor and determine the pressure required to propagate a crack in dent. The formula is conservative as it does not capture re-rounding of the dent and has not been validated experimentally.

Bai and Song (1997) [33] calculate burst strength of pipes with dent-crack defects by considering a notch inside an infinitely long dent. A factor of safety is applied to the predictions to account for

the difference in stress environment in a notch from the environment at the tip of cracks. the models make predictions based on plastic collapse stress concept and not fracture and is non-conservative for specimens that fail by fracture.

The pipeline defect assessment manual [4,6,34] recommends use of dent-gouge fracture models for assessing a dent combined with any other defect but its effectiveness for dent-crack defect assessment is questionable because of the variation in stress environment at the tip of cracks from the environment at the base of gouges.

Very little research has been done on dent-crack defects in pipelines, partly due to the practical difficulty of creating artificial cracks for experiments. Usually the cracks are created as notches and gouges with a small fatigue crack at the tip. Researchers at the University of Windsor, Canada completed four full scale burst tests and parametric finite element analysis of specimens of API X70 grade of pipeline with longitudinal cracks inside rectangular dents [21-24]. Their work is one of the first published full scale burst tests of line pipe with dent-crack defects. The cracks were cut as fine notches in the pipe using electro discharge machine (EDM) prior to denting the pipe. Fatigue load was applied to induce a small real crack at the tip of the notch. The parametric finite element analysis was conducted by varying crack depth, crack length, dent depth and denting pressure. The results show the pipes had significant residual burst strengths, which varied with the size of defect parameters and suggests that the recommendations in the codes [15-18], to cut and replace pipe rings with dent-crack defects might be too conservative and wasteful. But it is important to note that very few specimens were tested in the study, thus more data is required a firm conclusion on the effect of dent-cracks on burst pressure of pipelines. A single test was conducted using API X55 and another using API X70 to assess the influence of pipeline grade and location of crack within the dent on burst pressure. The results showed that the location of a crack inside the dent does not change burst pressure if the crack is inside the dent. The API X55 pipe had lower burst strength than the API X70 pipe, which is understandable but, it was more likely to sustain pressure equivalent to 80 percent of its specified minimum yield strength (SMYS) before failure than the API X70 grade. The results strongly suggest pipelines with dent-cracks can be kept in service with fitness for service assessment although, the conclusions are based on few experiments.

There is need for more studies involving a wider range of combinations of defect parameters to generate more data on the effect of dent-crack defects on integrity of pipelines and facilitate a broader understanding of the interaction between various dent-crack defect parameters as they degrade pipeline integrity. The current study makes use of the extended finite element (XFEM) procedure in Abaqus [35] to numerically analyze the effect of dent-crack effects on burst pressure of pipelines. The XFEM procedure is more suited for analysis of crack propagation and prediction of burst pressure than the traditional finite element method but its application in pipeline has not yet been widely investigated. Different parameters of dent-crack defects, including dent depth, denting pressure, dent constraint condition, crack location in dent and crack geometry were considered in this study. The study was completed through finite element modelling of full-scale burst tests of four specimens of API X70 grade of pipeline with various sizes of dent-crack defects formed at different denting pressures and for different dent restraint conditions.

1.3 Significance of the study

Dents and cracks are common defects in pipelines. They are often found in close proximity of each other on the pipe and act as one defect. The combined defect is commonly referred to as dent-crack defect and is known to be very severe on pipeline integrity that the ASME B31.4 code [15] does not formally allow affected pipes to remain in service. However, a recent study [21-24] have shown that pipes could have significant remaining burst strength and could be kept in service with engineering assessment. But the study involved tests of a few specimens, thus more research is needed to verify its findings. The extended finite element method used in this research is considered more suitable for analysis of crack propagation than the traditional finite element method as it does not require the body to be re-meshed each time the crack grows. Hence it is less tedious to use, which enables more analysis to be completed in reasonable time and allows many possible defect scenarios to be analyzed than would be probable with the traditional finite element methods. It is anticipated that the extensive data generated in this study will facilitate a broader understanding of the interaction between the constituting dents and cracks in a dent-crack defect. The results will be useful in integrity assessment and maintenance of existing pipeline with dent-crack defects as a guide to operators on safe pressures at which pipelines with different sizes of dents and cracks can be operated without the risk of propagating the crack or bursting the pipe. The results will be shared with the pipeline industry through publications in conference

proceedings and peer reviewed journals to be considered a source of information that can be used to improve the existing code recommendations on treatment of dent-crack defects in pipelines. It is expected that a lot of pipes that are currently being replaced because of dent-crack defects will be repaired and kept in service and that there will be significant savings in the cost of pipeline operation and maintenance.

1.4 Objectives of the study

The aim of this research project is to provide a guide for engineering assessment of pipeline having longitudinal crack inside rectangular dent, based on an extensive data on burst pressure of the pipeline generated using XFEM.

1.4.1 Specific objectives

i. To evaluate the potential of XFEM criterion implemented in Abaqus software for predicting burst pressure of pipeline.
ii. To evaluate the effect of crack geometry on burst pressure of pipeline with dent-crack defects.
iii. To evaluate the effect of dent depth and operating pressure during dent formation on burst pressure of pipeline with dent-crack defects.
iv. To determine the effect of location of crack inside dent on burst pressure of pipeline with dent-crack defects.

1.5 Methodology

This work was accomplished in four steps using the analytical methods and numerical simulations as described below:

i. Results of 3 full-scale burst tests of specimens of API X60 pipe having mechanically formed longitudinal cracks of sizes 60mm×3mm, 140mm×7mm and 200mm×10mm were sourced from literature [29]. The crack growth resistance curves of the pipe material based on results of single edge notch tension test (SENT) was also obtained from literature. The experimental results were used to calibrate and validate an XFEM model of the pipe using the general-purpose finite element analysis (FEA) software package (Abaqus) [35].

ii. The XFEM model was used to predict burst pressures of the 3 pipe specimens. In addition, the burst pressure of the specimens was predicted using analytical methods available in the pipeline industry [25-29]. The predicted burst pressures were compared with test results to evaluate the performance of XFEM as a method for analyzing crack propagation and predicting burst pressure of cracked pipelines.

iii. Results of 4 full-scale burst tests of specimens of API X70 pipe having mechanically formed dent-crack defects with sizes of sizes 20mm×4.3mm, 60mm×4.3mm, 100mm×4.3mm and 200mm×4.3mm were obtained from literature [21] and used to calibrate and validate XFEM model to simulate burst tests of the pipe specimens.

iv. The validated XFEM model was used in parametric numerical analysis to investigate the influence of various dent-crack defect parameters on burst pressure of pipelines with dent-crack defects subjected to internal pressure. The parameters evaluated were crack length, crack depth and dent depth. Other parameters analyzed were internal pressure during dent formation, dent restraint condition i.e. unrestrained and restrained dents, and location of crack within the dent, namely: cracks at the center of dents and cracks in flanks of dents.

Burst pressure of the pipe is the pressure required to propagate a surface crack into a through wall crack. The proposed test matrix included two variations of the crack depth, four variations of crack length, four variations of the denting pressure, three variations of dent depths, two variations of dent restraints, and two variations of crack location within the dent. The parametric analyses were conducted such that all possible combinations of crack geometry, dent depth, dent restraint, crack location and denting pressure were considered in the investigation, resulting in a total of 384 finite element analysis runs performed in this study.

1.6 Organization of the thesis

The present thesis has seven chapters. The first of which is the introduction, followed by literature review in chapter 2, which gives a detailed background on current methods of assessment of dents and cracks in pipeline. Chapter 3 presents an assessment conducted in this study to determine suitability of XFEM procedure implemented in Abaqus software for analysis of crack propagation and prediction of burst pressure of pipeline. Burst pressures of cracked pipeline is predicted numerically and by using analytical methods available in pipeline industry and results discussed

in the chapter. Chapter 4 presents a calibration of numerical models with XFEM to predict burst pressure of pipeline having longitudinal cracks inside rectangular dents. The effect of defect parameters such as crack length, crack depth, dent depth and denting pressure on burst pressure is assessed. In chapter 5, the effect of varying the loading sequence on the burst pressure of pipeline with dent-crack defects is discussed. The dents are assessed under restrained (constrained) and unrestrained (unconstrained) conditions to determine the effect of varying dent restraint condition on burst pressure. In addition, the effect of releasing the indenter from the surface of a pipe with a restrained dent when the pipeline is operating at its maximum allowable pressure on crack propagation and burst pressure of the pipeline is discussed in this chapter. Chapter 6 presents an assessment of the effect of varying crack location on burst strength and discusses the influence of various parameters of dent-crack defects on burst strength. The last chapter presents a summary of the work done in this research, scientific contributions, conclusion drawn on the assessment of burst pressure and recommendations for future work.

1.7 References

[1].Natural Resources Canada (NRCan) Energy fact book 2019-2020

[2].National Energy Board, Canada, annual report to parliament, 2017-18, https://www.neb-one.gc.ca/, Accessed April 2019

[3].Canadian Energy Pipeline Association, Transmission Pipeline Industry Performance Report, 2018 snapshot, https://pr18.cepa.com/, Accessed April 2018

[4].Cosham, A., and Hopkins, P., 2004, "The effect of dents in pipelines-guidance in the pipeline defect assessment manual," International Journal of Pressure Vessels and Piping, 81(2), pp. 127-139.

[5].Rosenfeld, M. 2001. "Proposed New Guidelines for ASME B31.8 on Assessment of Dents and Mechanical Damage". Topical Report GRI-01/0084. Des Plaines, IL: GRI.

[6].Cosham, A., and Hopkins, P. 2001. "A New Industry Document Detailing Best Practices in Pipeline Defect Assessment." In Fifth International Onshore Pipeline Conference, Amsterdam, The Netherlands. http://www.penspenintegrity.com/downloads/virtual-library/industry-bestpractice.pdf.

[7].Baker, M. 2004a. "Dent Study". Delivery Order DTRS56-02-D-70036. Integrity Management Program. Office of Pipeline Safety.

[8].Alexander, C, and Kiefner, J. 1997. Final Report on Effects of Smooth and Rock Dents on Liquid Petroleum Pipelines: To the American Petroleum Institute, October 10, 1997. American Petroleum Institute.

[9].Fowler, J. 1993. "Criteria for Dent Acceptability in Offshore Pipeline." In the Offshore Technology Conference, Houston, Texas, May 1993. doi:10.4043/7311-MS. http://www.onepetro.org/mslib/servlet/onepetropreview?id=OTC-7311-MS.

[10].Keith A, Escoe B. Piping and pipelines assessment guide. British library cataloguing-in publication data, vol. I. Elsevier; 2006.

[11].Lancaster, E., and Palmer, S. 1996. "Strain Concentrations in Pressurized Dented Pipes." Proceedings of the Institution of Mechanical Engineers, Part E: Journal of Process Mechanical Engineering 210 (1) (February 1): 29–38. doi:10.1243/PIME_PROC_1996_210_290_02.

[12].Rinehart, A., and Keating, B. 2007. "Stress Concentration Solution for a 2D Dent in an Internally Pressurized Cylinder." Journal of Engineering Mechanics 133 (7) (July): 792–800. doi:10.1061/(ASCE)0733-9399(2007)133:7(792).

[13].ASME. “Fitness-for-service, API Recommended Practice 579-1/ASME FFS-1 2007, Second Edition”, The American Society of Mechanical Engineers, New York, USA, June 2007.

[14].BSI. BS7910: 2005, “Guide to methods for assessing the acceptability of flaws in metallic structure”, London, UK, British standards institution, July 2005.

[15].ASME. (2012). “Pipeline transportation systems for liquids and slurries.” ASME B31.4. New York.

[16].CSA Z662-2007, Oil and gas Pipeline Systems Ontario, Canada, 2007

[17].API 1160-2001, Managing System Integrity for Hazardous Liquid, Washington DC, USA 2001

[18].ASME B31.8-2010, Gas Transmission Distribution Piping System, New York, USA 2010

[19].WRC Bulletin 465, “Technologies for the Evaluation of Non-Crack-Like Flaws in Pressurized Components,” September 2001, Welding Research Council

[20].Anderson T.L, “Fracture mechanics fundamentals and applications”, Taylor and Francis, 2005.

[21].Ghaednia, H., “Burst strength of NPS30 Steel pipes with dent-crack defect’(2015). Electronic theses and dissertation 5713. https://scholar.uwindsor.ca/etd/5713

[22].Ghaednia, H.,Silva, J., Kenno S., Das S., Wang, R, Kania, R “Pressure test of 30in diameter X65 grade pipes with dent-crack defect’(2015), https://www.researchgate.net/publication/272741123

[23].Ghaednia, H., Das, S., Wang, R., and Kania, R. (2015b). “Safe burst strength of pipeline with dent-crack defect: Effect of crack depth and operating pressure.” Eng. Fail. Anal.,55,288-299.

[24].Ghaednia, H., Das, S., Wang, R., and Kania, R. (2017). “Dependence of burst strength on crack length of a pipe with dent-crack defects”. Pipeline systems and Eng. Practice, 2017,8(2):04016019.

[25].Jaske, C.E, “CorLAS User manual”, Version 2.25, 2010.

[26].Rothwell, A. B. Coote, R I “A critical review of the assessment methods for axial planar surface flaws in pipe”, Paper#21009, 52, Pipeline Technology conference, Oostende, Belgium, 2009

[27].Samarth, T., Ming G., Ravi K., Shahani K., Kania R., “Evaluation of existing fracture mechanics models for burst pressure predictions, theoretical and experimental aspects”,

IPC2014-33563 proceedings of the 10th international pipeline conference, Calgary Canada 2014

[28].Zijian, Y., Zhang S, Zhou W., "Model error assessment of burst capacity models for energy pipelines containing surface cracks", International Journal of Pressure Vessels and Piping, 2014

[29].Cravero, S. and Ruggeri, C., "Structural Integrity Analysis of Axially Cracked Pipelines Using Conventional and Constraint-Modified Failure Assessment Diagrams", International Journal of Pressure Vessels and Piping, 2006.

[30].Lancaster E.R., Palmer S.C.," Burst pressure of pipes containing dents and gouges", IMechE 1996, Proceedings of the Institution of Mechanical Engineers, UK, Vol 210

[31].National Energy board, Safety advisory NEB SA 2010-01, 18th June 2010; http://www.neb-one.gc.ca, Accessed 11 July 2019

[32].Orynyak, I., Yakovleva, E., & Rozgonyuk, V. (2007). Application of the cheng-finnie method to the calculation of stress intensity factors in thin-walled pipes with long axial cracks with allowance for geometric nonlinearity. *Strength of Materials, 39*(5), 455-465.

[33].Bai, Y., & Song, R. (1997). Fracture assessment of dented pipes with cracks and reliability-based calibration of safety factor. *International Journal of Pressure Vessels and Piping, 74*(3), 221-229.

[34].Macdonald, K. A., & Cosham, A. (2005). Best practice for the assessment of defects in pipelines – gouges and dents. Engineering Failure Analysis

[35].Abaqus 6.14, Documentation,2014. Dassault Systèmes

2. LITERATURE REVIEW

2.1 Defects in pipeline

Pipeline can develop any of the following defects while in service: *Corrosions* due to chemical or electrochemical action on pipe wall; *Gouges*, which are surface metal losses due to a foreign object's impact on the pipe wall [1]; *Wrinkles* are local deformations usually characterized by ridges and troughs on pipe wall and are visible manifestations of local buckling[2,3]; *Cracks* are material discontinuities in which two planar surfaces very close to each other converge in a sharp tip [4]; *Dents* are local depressions in pipe wall due to impact by a foreign body, which produce gross disturbance in curvature [5]; and *Combined defects* which comprise of two or more of the above defects occurring within the same region of a pipeline wall. Examples of combined defects include *cracks in dents*, *gouges in dents*, *crack in corrosion*, and *corroded dents* [6].

2.2 Dents

2.2.1 Classification of dents

Francini and Yoosef-Ghodsi (2008) [7] summarized definitions of different categories of dents thus: a *smooth dent* causes a gradual change in curvature of the pipe while a *plain dent* is a smooth dent without any other defect. A *kinked* or *creased* dent is a dent that causes an abrupt change in curvature of the pipe wall and has a radius of the curvature less than 5 times the thickness of pipe wall. *Unconstrained* and *constrained* dents refer to the freedom of the dent to spring back elastically and re-round under internal pressure for the pipe to regain its circular geometry. The freedom is restricted in *constrained* dents because the indenter, such as a rock remains in place to prevent elastic rebound and re-rounding under internal pressure. Constrained dents are also referred to as *rock dents*. In this study the effect of smooth dent with cracks on burst pressure of pipeline was analyzed considering both constrained and unconstrained states of the dent. Figure 2.1 show the profile of a typical smooth dent: w is the width of dent, and d the dent depth.

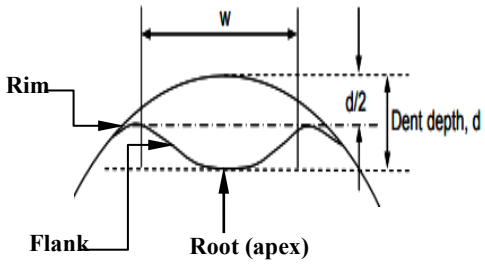

Figure 2.1 Dent nomenclature

2.2.2 Effect of dents on pipeline integrity

More than 80% of excavated pipelines present with some form of dent [8]. As a result, considerable effort has been spent in the past to study the effect of dents on integrity of pipelines, notably by Belanos and Ryan (1958)[9], Wang, K.C. et.al (1982) [10], Hopkins et.al (1983) [11], and Bjørnøy et.al (2000) [12]. Full scale tests show that plain dents do not affect burst pressure of pipelines as they attempt to move outwards under internal pressure, allowing the pipe to reign its original circular shape. However, they cause stress and strain concentrations within the affected region of the pipe [13-16], which are accommodated by ductility of the pipe material. The location of peak strain and magnitude of peak stress vary with shape of dent. In short localized dents, the peak strain occurs in the flank (Figure 2.1) of dent, while in long dents, the peak stress and strains occur at the root and the peak stress in short dents are lower than in long dents [16].

2.2.3 Assessment of dents

2.2.3.1 Stress-based assessment

In stress-based assessment of the effect of dents on burst pressure of pipeline, the dents are considered to fail by plastic collapse when the flow/collapse stress of the material is exceeded [17]. Orynyak et al. [18] proposed a model for estimating the burst pressure of a dented pipe by assuming that the dent region fails by plastic hinge mechanism when a critical stress develops in the pipe wall under internal pressure. The burst stress is obtained by reducing the ultimate plastic bending moment by a factor that depends on dent geometry. The model is developed for pipes with longitudinally infinite indentations only.

For a dent of width 2c and depth H, failure is by plastic collapse as plastic hinges develop at A, B, and C (Figure 2.2) resulting into a mechanism.

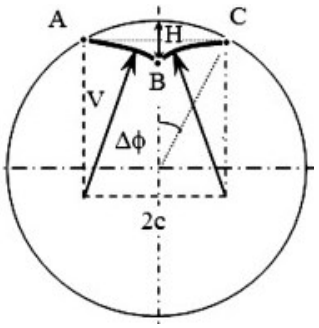

Figure 2.2 Orynyak's representation of the geometry of a typical dent [18]

Points A and B are located on an arc of a circle of radius of curvature, V. The dent depth H is connected to V by equation 2-1.

$$H = 2V\left(1 - \cos {}^{c}/_{V}\right) \qquad (2-1)$$

Where $\Delta\emptyset = {}^{c}/_{V}$ is the angle of the pipe surface tangent at A.

Orynyak's pipe strength reduction factor α due to dent geometry is given by the formula,

$$\alpha = \frac{PR}{\sigma_u t} = \sqrt{\frac{V^2}{t^2}\left(\frac{c}{V}\right)^4 + 1} - \frac{V}{t}\left(\frac{c}{V}\right)^2 \qquad (2-2)$$

Where P is the applied internal pressure, R the external radius of the pipe, t is wall thickness of the pipe and c is half width of the dent. And α can also be expressed as a function of a dimensionless length of the dent γ as below.

$$\alpha = \sqrt{\gamma^4 + 1} - \gamma^2 \qquad (2-3)$$

Where $\gamma = \frac{c}{\sqrt{Rt}}$

The burst pressure denoted, $P_{L,O} = \frac{\alpha\sigma_u t}{R}$ $\qquad (2-4)$

Where σ_u is the ultimate strength of the material determined from simple tensile test.

Allouti et.al [19] compared burst pressure of pipes having various dent geometries obtained from experiments to those predicted using the Oryniak model. Their results show that the model is too conservative and can underestimate the burst pressure of dented pipes by a factor of 8. The experimental results also showed that the burst strength was not affected by dent geometry. In fact, failure by tearing occurred in other places other than the dent location. This is attributed to the difference in Vickers's microhardness at the root of the dent and away from the dent. There was 30% difference in the hardness between the root and away from the dent. This microhardness is converted into ultimate strength and increases the limit pressure P_L of the root of the dent therefore the pipe cannot burst at the root of the dent, rather the bursting occurs away from the dent where the ultimate strength is not improved by strain hardening due to Vickers micro hardening. Allouti et.al [19] opine that a strain-based approach would be more suitable for assessing dents.

2.2.3.2 Strain-based assessment

Strain based criteria is mainly used to assess dent severity and prioritize digs for further investigations. A limit value of strain is used as the critical strain beyond which cracks may develop inside dents and the pipe fails. The ASME B31.8-2004 established an allowable strain in plain dents to be 6% [20] based on the allowable strain limit in the field bend and, the likelihood of crack initiation in the material exceeding 12% strain [15]. The 6% strain limit has effectively helped pipeline operators to manage integrity threats from plain dents but is considered as a fitness-for-purpose limit of plain dents and can be very conservative for failure assessment and may result in unnecessary excavations and repairs. Therefore, alternative criteria based on plastic strain limit damage have been proposed in literature to improve the strain limits used for assessment of plain dents. They include the Material elongation-based criterion [7], the Strain Limit Damage criterion [21] and Ductile Failure Damage Indicator (DFDI) criterion [22].

Material elongation-based criterion uses the material elongation obtained from tensile test divided by a factor of safety of 2 as the strain limit for plain dents. The limit assumes that the fracture strain of a material is approximately equal to the elongation. However, the true fracture strain is significantly higher than the material's elongation by a factor of approximately 2.5. therefore, the criterion is also conservative. For example, with a gauge length of 50mm, the minimum elongation of a typical pipeline steel ranges from 18% to 24% [21] and the maximum allowable equivalent strain in a dent according to the model would range from 9% to 12%, demonstrating that the model is very conservative and should only be used for a fitness for purpose assessment but not for predicting conditions for cracking in dents.

The Strain Limit Damage (SLD) uses a combined stress triaxiality got from elastic-plastic finite element analysis and specified minimum material properties to estimate the accumulated strain damage due to plain dents in pipeline. Accumulated strain damage greater than or equal to 1 shows the material has reached its strain damage limit and cannot sustain additional loading. The SLD criterion is conservative in nature because it uses a specified minimum allowable reduction in cross sectional area and elongation to failure. Therefore, it is best used for fitness for purpose assessment of dent severity but cannot predict condition for crack initiation in dents.

The DFDI criterion uses both the stress triaxiality obtained from finite element analysis and the material's true critical strain (ε_0), obtained from tests to determine the limit strain of the dents. The criterion is based on the concept that ductile fracture process follows void initiation, growth and coalescence on a micro scale and resulting in formation of cracks during large-scale plastic deformation. The generalized strain limit for ductile fracture (ε_f), is expressed in terms of the stress triaxiality $\left(\frac{\sigma_m}{\sigma_{eq}}\right)$ and the critical strain of the material (ε_0)[23,24].

$$\varepsilon_f = 1.65\varepsilon_0 e^{\left(-\frac{3\sigma_m}{2\sigma_{eq}}\right)} \qquad (2-5)$$

Where $\sigma_m = \frac{1}{3}(\sigma_1 + \sigma_2 + \sigma_3)$ is the hydrostatic stress,

$\sigma_{eq} = \frac{1}{\sqrt{2}}\sqrt{(\sigma_1 - \sigma_2)^2 + (\sigma_2 - \sigma_3)^2 + (\sigma_3 - \sigma_1)^2}$ is the von Mises stress, and $\sigma_1, \sigma_2, \sigma_3$ are the principal stresses in the respective directions. ε_0 is the critical strain of the material for incipient cracking and is usually in the range of 0.3 to 0.6 for typical pipeline steel [21]. The ductile strain limit in uni-axial tensile condition is equal to the critical strain of the material i.e. $\varepsilon_f = \varepsilon_0$.

The extent of plastic damage in the body is shown by the equivalent strain (ε_{eq}). The degree of plastic damage (dD) caused by small increments in the equivalent strain $(d\varepsilon_{eq})$is defined by the expression:

$$dD = \frac{d\varepsilon_{eq}}{\varepsilon_f} \qquad (2-6)$$

The integral of the degree of plastic damage in the domain of the equivalent strain gives the total ductile damage in the body and is the ductile failure damage indictor. its value ranges from 0 to 1. A value of 1 or higher signifies failure of the plain dent under the prevailing loading condition

$$DFDI = \int_0^{\varepsilon_{eq}} \frac{d\varepsilon_{eq}}{1.65\varepsilon_0 e^{\left(-\frac{3\sigma_m}{2\sigma_{eq}}\right)}} \qquad (2-7)$$

The maximum equivalent strain is determined from the dent profile data following curvature strain-based methods. The materials critical strain is determined from tensile test conducted using specialized equipment. Use of the actual material critical strain in the DFDI method makes it

capable of predicting crack initiation in plain dents. Therefore, the method can be used for failure assessment of dents in pipeline. The maximum principal stresses used in the analysis is usually determined by finite element analysis. But it is not practical to conduct FEM analysis for all dents in pipelines since they are usually very many. For a thin walled pipe subjected to internal pressure, Arumugam et.al [21] proposed the following expressions for determining the DFDI of plain dents under biaxial and uniaxial stress conditions. For biaxial stress ($\sigma_1 \neq 0, \sigma_1 = \sigma_2, \text{and } \sigma_3 = 0$

$$\text{DFDI}_{\text{upperbound}} = \frac{1.65\varepsilon_{\text{eq}}}{\varepsilon_0} \qquad (2-8)$$

For uniaxial stress condition, $\sigma_1 \neq 0, \sigma_2 = \sigma_3 = 0$

$$\text{DFDI}_{\text{lowerbound}} = \frac{\varepsilon_{\text{eq}}}{\varepsilon_0} \qquad (2-9)$$

2.2.4 Current code provisions on dents

The pipeline industry has several codes for assessing effects of plain dents on the integrity of pipelines. The provisions in three of them [20,25,26] considered representative of the whole are reviewed here. All, except ASME B31.8 [20] assess severity dents based on depth and none of them evaluate the burst pressure of dented pipes.

The Canadian Standards CAN/CSA-Z662-15[25] does not consider a plain dent as injurious unless its depth exceeds 6% of the pipe's outside diameter (D) or if it is 2%D deep and is located near a weld or in a corroded region of the pipe. Dents near cracks and with maximum strain ≥4% are considered injurious. All dents containing gouges, scratches, or cracks are regarded as defects that must be subjected to engineering assessments to determine their effects on integrity.

The provisions in ASME B31.4-2012 [26] are like CAN/CSA-Z662-15. The ASME B31.4 further requires that dents containing metal loss resulting from corrosion or due to grinding where less than 87.5% of the nominal wall thickness remains should be considered as defects and subjected to engineering assessment for integrity. The ASME B31.8 code [20] uses a strain-based procedure in which the combined membrane and bending strains are compared with a prescribed allowable total strain. Like the CSA-Z662-15 code, the ASME B31.8 also considers 6%D dent depth as injurious but may allow larger depths if maximum strains in the dents are less than 6% and

movement of inspection equipment is not impeded. Dents are not allowed near brittle welds but considered acceptable near ductile welds if the depths are less than 2%D and maximum strains due to the dents are less than 4% strain.

The code gives a non-mandatory procedure to estimate strains inside dents using dimensions of the dent and pipe (Figure 2.3). R_0 is the undeformed radius of the pipe, R_1 and R_2 are radii of curvature of the dent in circumferential and longitudinal directions respectively. R_1 is negative for re-entrant dents and positive otherwise while R_2 is generally always negative. Other dimensions are pipe thickness t, dent depth d and dent length L. The strains are given by equations (2-10).

Bending strains in the circumferential direction:

$$\varepsilon_1 = \frac{t}{2}\left(\frac{1}{R_0} - \frac{1}{R_1}\right) \qquad (2-10a)$$

Bending strains in the longitudinal direction:

$$\varepsilon_1 = -\frac{t}{2}\frac{1}{R_2} \qquad (2-10b)$$

Extensional strains in the longitudinal direction:

$$\varepsilon_1 = \frac{1}{2}\left(\frac{d}{L}\right)^2 \qquad (2-10c)$$

Strain on internal surface of pipe:

$$\varepsilon_i = [\,\varepsilon_1{}^2 - \varepsilon_1(\varepsilon_2 + \varepsilon_3) + (\varepsilon_2 + \varepsilon_3)^2]^{1/2} \qquad (2-10d)$$

Strain on outside surface of pipe:

$$\varepsilon_o = [\,\varepsilon_1{}^2 + \varepsilon_1(-\varepsilon_2 + \varepsilon_3) + (-\varepsilon_2 + \varepsilon_3)^2]^{1/2} \qquad (2-10e)$$

The overall strain $\varepsilon_{max} = \mathrm{Max}[\,\varepsilon_i, \varepsilon_o]$

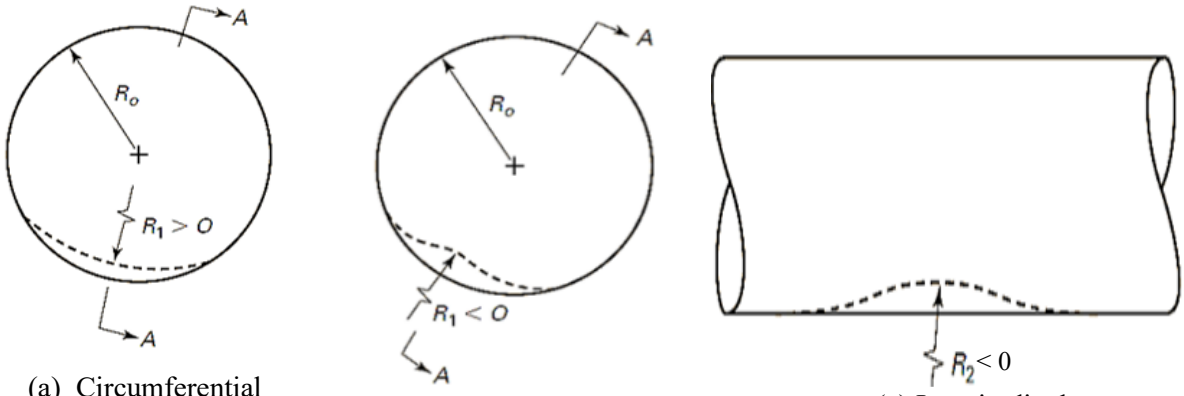

(a) Circumferential (Non re-entrant dent)

(b) Circumferential (Re-entrant dent)

(c) Longitudinal (Re-entrant dent)

Figure 2.3 Surface curvatures and sign conventions for calculation of strains in dents [20]

2.3 Cracks in pipeline

The development of cracks in pipeline depends on prevailing service condition. Pipes serving under corrosive conditions, external interference, and high stresses are likely to develop cracks [27]. The cracks may initiate on the external surface and grow in both thickness and longitudinal or circumferential directions of the pipe. For pressurized pipes, the maximum principle stress acts perpendicular to the longitudinal axis of the pipe. Therefore, cracks in the longitudinal plane propagate before those in the circumferential plane of the pipe. The cracks affect the strength of the pipes by reducing wall thickness and by acting as stress risers in the material at crack tip.

2.3.1 Assessment of cracks

2.3.1.1 Analytical methods

There are several methods available to the pipeline industry for assessing integrity of cracked pipelines. Common methods include the NG-18 equation [28,29], CorLAS methodology [30] and the failure assessment diagrams [31,32].

The Battelle NG-18 equation

The NG-18 equation (also called the Ln-secant equation) is a semi-empirical fracture mechanics-based analytical model for prediction of ductile failure stress levels in flawed pipes with through-wall and surface cracks. The original equation developed by Kiefner et.al [28] in 1973 has since

been found too conservative for long, shallow surface cracks, and poor for pipes with sub-optimal toughness. Kiefner [29] in 2008 addressed this weakness through a modified version shown in equation (2-15) below.

$$\sigma_{fs} = \frac{\left(\frac{\overline{\sigma}}{M_T}\right)\cos^{-1}(e^{-x})}{\cos^{-1}(e^{-y})} \qquad (2-15)$$

Where $x = \left(\frac{12\frac{CVN}{A_0}E\pi}{8c\overline{\sigma}^2}\right)$ and $y = x\left(1-\left(\frac{d}{t}\right)^{0.8}\right)^{-1}$

$\sigma_{fs}, \overline{\sigma}, M_T, CVN, A_0, E, a, t, 2c$ are failure stress, flow stress, Young's modulus, Folia's factor [33], upper shelf impact energy, reference area, wall thickness, crack depth, and crack length respectively. The flow stress is determined from yield stress using the formula $\overline{\sigma} = \sigma_{ys} + 68.95MPa$. The predicted failure/burst pressure of the assessed pipe is the pressure corresponding to the lowest possible failure stress. Failure stress of the component is calculated using equation (2-15) and the results used in equation (2-16) below to predicted failure pressure P_f.

$$P_f = \{\sigma_{fs}\}\frac{2t}{D}\left(\frac{1-\frac{A}{A_0}}{1-\frac{A}{A_0 M_T}}\right) \qquad (2-16)$$

The CorLAS method

CorLAS [30] is a software that uses inelastic fracture mechanics principles to account for stress corrosion cracks (SCC) crack growth in pipelines. For a surface crack defect, the software employs equation (2-17), by Shih et.al [34] for burst pressure predictions based on fracture toughness.

$$J = Q_f F_{sf}\left[\frac{\sigma^2\pi a}{E} + f_3(n)a\varepsilon_p\sigma\right] \qquad (2-17)$$

Where J, Q_f, F_{sf}, σ, a, E, $f_3(n)$, n, ε_p are respectively the applied J-integral, elliptical shape factor, free surface factor, applied stress, crack depth, Young's modulus, strain-hardening factor, strain hardening exponent, and plastic strain. J-integral values are computed iteratively and compared with the fracture toughness J_{1c} of the material and failure is predicted when $J = J_{1c}$. Figure 2.4 illustrates the relationship between applied J-integral and resistance (R) of a material to crack

growth. The rising slope of the R-curve indicate stable crack growth. Instability (crack growth) occurs when the applied J-integral is tangential to the R-curve.

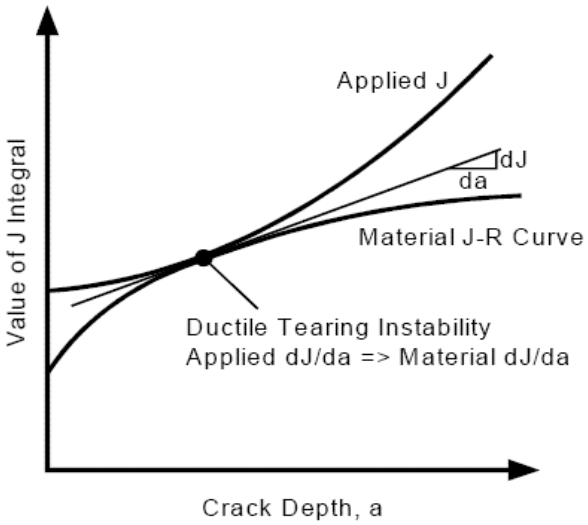

Figure 2.4 Illustration of ductile tearing instability

CorLAS allows two correlations of fracture toughness with Charpy impact energy.

Option 1: J_{1c} (in-lb/in^2) =10 CVN (ft-lb), which gives the lower estimate of fracture toughness, and Option 2: J_{1c} (in-lb/in^2) =$12\frac{CVN}{A_c}(\text{ft}-\text{lb})$, adopted from Ln-Sec model [28,29] gives the higher value of fracture toughness. Consequently, CorLAS has three fracture toughness options referred to as CorLAS options 1, 2 and 3 corresponding to measured fracture toughness and correlation options 1 and 2 respectively. CorLAS also predicts failure stress based on flow stress, where instead of using fracture toughness, flow stress defined by $\overline{\sigma} = \sigma_{ys} + 68.95\text{MPa}$ or $\overline{\sigma} = \frac{\sigma_{ys}+\sigma_u}{2}$ (MPa) is used, where $\overline{\sigma}, \sigma_{ys}, \sigma_u$ are the flow stress, yield and ultimate tensile strengths respectively. It should be noted that flow stress option 1 is also used in the Modified Ln-sec equation while option 2 is typically used in the analysis of plastic collapse of engineering materials and is adopted in this study because of the ductile nature of thin walled pipelines. Failure stress is evaluated using both fracture toughness and flow stress criteria and the lower value is used in equation (2-16) above to predict failure pressure.

Failure assessment diagram (FAD)

FAD is a graphical procedure used to assess the integrity of flawed components [31,32]. FAD comprises of a failure line that relates fracture toughness and strength properties of the component. The abscissa shows progression towards plastic collapse represented by the Load ratio L_r associated with the primary stress in the pipe. The ordinate shows progression towards failure by fracture represented by the fracture ratio K_r. The failure line is defined by the expression $K_r = f(L_r)$. It shows the acceptable and unacceptable limits for combinations of K_r and L_r of the material being assessed. Where $K_r = \frac{K_I}{K_{mat}}$, $L_r = \frac{\sigma_{ref}}{\sigma_{ys}}$, σ_{ref} is the reference stress due to applied load, σ_{ys} the yield strength of the material, K_I is the elastic stress intensity factor, K_{mat} is the material fracture toughness. Integrity assessment is based on determining the location of the assessment point (K_r, L_r) with respect to the failure line. A flawed component is considered safe if the assessment point falls below the failure line whereas it is unsafe if the assessment point is above the failure line. Increasing the load and or size of defects shifts the assessment point towards the failure line. A schematic representation of the FAD methodology is illustrated in figure 2.5.

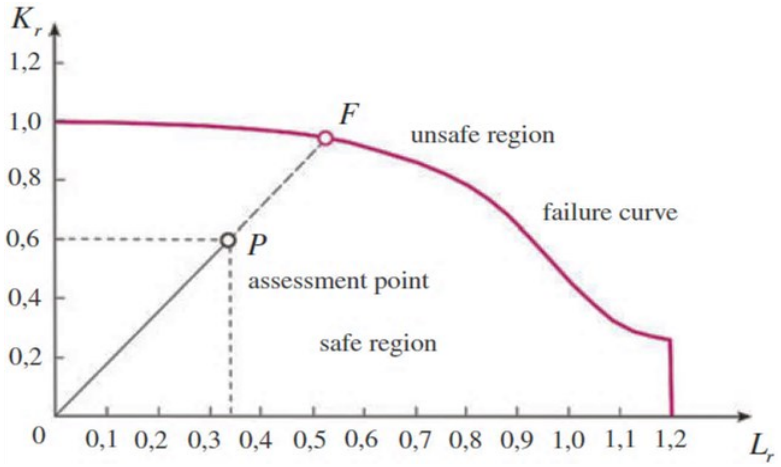

Figure 2.5 Failure assessment diagram-American Petroleum Institute [6]

FAD methodology allows three levels of assessment in order of increasing accuracy. Level 1 is the simplest form of FAD assessment, used when there is limited information on material properties or loading conditions. The material is assumed to have an elastic-perfectly plastic behavior. The crack is acceptable if $K_r \leq 0.707$ and $L_r \leq 0.8$. $L_r = \frac{\sigma_{ref}}{\sigma_{flow}}$, where $\sigma_{flow} = \frac{\sigma_y + \sigma_u}{2} \leq 1.2\sigma_y$. K_r is as defined before. Levels 2 and 3 use the actual properties of the pipe material and

are more accurate than level1. A flaw is acceptable if the assessed point lies within the region bounded by the FAD assessment line. Otherwise it is unacceptable.

The assessment line for FAD Level 2 is given by equation (2-18).

$$K_r = (1 - 0.14(L_r)^2)(0.3 + 0.7\exp[-0.65(L_r)^6]) \qquad (2-18)$$

The limiting value for L_r is given by:

$$L_{rmax} = \frac{\sigma_y + \sigma_u}{2\sigma_{ys}} \qquad (2-19)$$

Level 3 gives the best estimate for the strength of the cracked component. The assessment line is given by:

$$K_r(L_r) = \left(\frac{E\varepsilon_{ref}}{L_r\sigma_{ys}} + \frac{(L_r)^3\sigma_{ys}}{2E\varepsilon_{ref}}\right)^{-0.5} \text{ for } 0.0 < L_r \leq L_{rmax} \qquad (2-20)$$

$$K_r(L_r) = 1.0 \quad \text{for } L_r = 0.0.$$

WhereK_r, and L_r, are as before defined, E is Youngs modulus, ε_{ref} is the load ratio obtained from true stress-strain curve at a true stress equal to $L_r\sigma_{ys}$, L_{rmax}=1.25 for carbon steels.

2.4 Dents combined with cracks

Dents formed near brittle welds may cause the welds to crack during dent formation or during re-rounding under internal pressure, causing combined dent and crack defects in the pipeline [20,25,26]. In addition, stress and strain concentration in dents reduce fatigue life of the pipe, making it susceptible to stress corrosion cracking (SCC) under pressure cycles in normal operations [13-16]. Dents in pressurized pipes are especially dangerous if they occur on longitudinal weld seams. Cracks developed along the longitudinal weld seams may propagate at low pressure because the maximum hoop stress acts perpendicular to the longitudinal plane of the pipe [35]. Field observations show pipes with dented seam welds have very low burst pressures [6] when they crack, proving the two defects combine to act as one defect. The combined defect, commonly known as dent-crack defect [36-38] is widely regarded in pipeline industry as one of the most injurious defects.

2.4.1 Burst pressure of pipeline with combined dent and crack defects

Research on effect of dents combined with cracks on burst pressure of pipelines are very few [36-38]. Most of the research has focused on dents combined with gouges [39,40]. The stress environment at the tip of cracks are more severe than the environment at the base of gouges. Therefore, the results of studies of dents combined with gouges may not accurately explain the effect of dents combined with cracks on burst strength of pipeline. Other studies [10,19,21] have focused on determining the limiting strain at which cracks could initiate at the root of dents in pressurized pipeline. This is a serviceability condition and does not address the burst capacity of the pipeline, which is an ultimate failure limit state.

To the author's knowledge, there has been no research that extensively discusses the effect of dents combined with cracks on burst pressure of pipeline prior to the commencement of this study. In particular, the use of extended finite element methods for predicting burst pressure of pipeline having dents combined with cracks has not yet been explored. For this reason, a review of some research conducted on burst pressure of pipeline with dents combined with cracks is presented below. The author noticed that all reviewed research did not substantively address the effect of location of cracks inside dents on burst pressure and neglected the effect of dent restraint.

Research by Orynyak et.al (2007) [41]

Orynyak et.al [41] developed an analytical model (equation 2-21) for determining the stress intensity factor at the tip of a crack that initiates at the deepest point of a dent. The model treats dents as sources of geometric nonlinearity in the pipe. Bending stress is estimated, by treating the dent profile as the deflected shape of an elastic beam, with the maximum dent depth (d) substituting for maximum deflection(w). Based on fracture mechanics principles, the amplitude of the plasticity (K_I) at crack tip is proportional to the product of the combined stresses and the square root of crack length [43]. The combined stresses are due to bending (dent) and tension (pressure).

$$K_I = \left(\left(\frac{PR_0}{t}\right) Y_0 + (\sigma_{MD} - \sigma_M) Y_M\right)\sqrt{\pi a} \qquad (2-21)$$

Where σ_{MD} is the maximum bending stress generated by the distortion of the un-cracked pipe surface by the dent while σ_M is the associated bending stress through the crack. Y_0 and Y_M are the

dimensionless stress intensity factors for the case of bending and tensile stresses acting at infinite distance away from the crack and R_0 is the external radius of the pipe.

The stress intensity factor equations are developed within the framework of elastic formulation and does not account for the material behavior or re-rounding of dents under internal pressure, which would undoubtedly reduce the bending stresses in the pipe. Therefore, the formulation is conservative and may only be used for fitness for service but not for failure assessment model.

Research by Bai Y. and Song R. (1997) [42]

Bai and Song [42] proposed an analytical model (equation 2-23) for assessing fracture of a notch inside a dent and provided factors of safety for reliability. The equation for the dent combined with a notch is a modification of their expression for notch failure stress (equation 2-22) to account for the effect of dent on the notch.

$$\sigma_{notch} = \frac{2\sigma_p}{\pi}\cos^{-1}\left(\exp\left(-\frac{\pi K_{mat}^2}{8a\sigma_p^2}\right)\right) \qquad (2-22)$$

Where σ_{notch} denotes the notch stress at failure, σ_p is the collapse stress of the pipe, and a is the notch depth. K_{mat} is the material fracture toughness obtained by theoretical correlation with pipe toughness expressed in terms of the Charpy V-Notch energy (CVN). It is however important to note that Samarth et.al [44] have shown that using theoretical correlation relationships to determine K_{mat} from CVN can overestimate the material toughness. This is particularly important because the burst estimate is based on notch which is less injurious than a crack.

Bai and Song [42] modified the fracture toughness, compliance geometry, and flow stress equations of the notch and got the following expression for fracture of the notch inside the dent.

$$\sigma_{dent+notch} = \frac{2\sigma_p}{\pi}\cos^{-1}\left(\exp\left(-\frac{\pi K_{mat}^2}{Y^2 8a\sigma_p^2}\right)\right) \qquad (2-23)$$

Y, being a geometry function that varies with the crack aspect ratio $\left(\frac{a}{c}\right)$ [45], c being half of the length of the crack. Pressure at which the notch inside the dent fractures is designated the failure pressure (P) and is given by equation (2-24).

$$P = 2\sigma_{dent+notch} \times \frac{t}{D} \qquad (2-24)$$

Allowing for a factor of safety γ, the estimated safe operation pressure is given by equation 2-25.

$$P_L = \frac{1}{\gamma} \times 2\frac{t}{D}\frac{2\sigma_p}{\pi}\cos^{-1}\left(\exp\left(-\frac{\pi K_{mat}^2}{Y^2 8a\sigma_p^2}\right)\right) \qquad (2-25)$$

The values of factor of safety γ, are: 1.617 for target reliability index of 3.09, 1.89 for a target index of 3.71 and 2 for a target reliability index of 3.926. $\gamma = 2$ is recommended where no calibration of the model parameters is done. The model has been found to be too conservative when used to predict burst pressure of pipes with dent-crack defects.

Research by Ghaednia et.al (2015,2017) [36-38]

Ghaednia et.al [36-38] completed four full-scale burst tests and parametric finite element analysis of specimens of API X70 grade of pipeline with longitudinal cracks inside rectangular dents. The cracks were cut as fine notches in the pipe using electro-discharge machine (EDM) prior to denting the pipe. Fatigue load was used to create a 0.3mm real crack at the tip of the notch. Traditional finite element method software Abaqus, was used to conduct parametric analysis of the effect of crack depth, crack length, dent depth and denting pressure on burst pressure. The J-integral concept was used to determine failure pressure and the pipe was deemed to fail when the J-integral value at any integration point around the crack tip exceeded the critical value for the material by 15%.

A burst test of a specimen of API X55 was conducted for comparison with API X70 behavior to assess the influence of pipeline grade on burst pressure. Another test was conducted with the dent orientation on the pipeline skewed to vary the location of crack within the dent in order to assess the effect of location of the crack on burst pressure. The results showed that location of crack inside dent has no effect on burst pressure if the crack is inside the dent. The API X55 pipe had lower burst strength than the API X70 pipe, which is understandable, however, the API X55 grade was more likely to sustain pressure equivalent to 80 percent of its specified minimum yield strength before failure than the API X70 grade.

Although the number of tests conducted were few, the results strongly suggest pipelines with dent-cracks have significant residual strength and can be kept in service with fitness for service assessment.

2.5 Fracture of engineering materials

The deformation of a material depends on its mechanical properties, represented by the stress strain curve (Figure 2.6). The material is initially elastic and obeys Hooke's law until its yield strength σ_y, at B. The slope of line AB is the Young's modulus E of the material. Beyond B the material is inelastic, and its response is nonlinear (BCE) but may be approximated as linear in practical applications. Rise in stresses along BCE is due to plastic deformation and strain hardening. Point D is the location of zero stress. When the deformed specimen is hypothetically relieved of all stresses along line CD, elastic strain ε_e is released but plastic strains ε_p remains. Maximum stress occurs at point E, which represents the tensile strength of the material. Necking of the material begins at E and progresses up to F where fracture occurs.

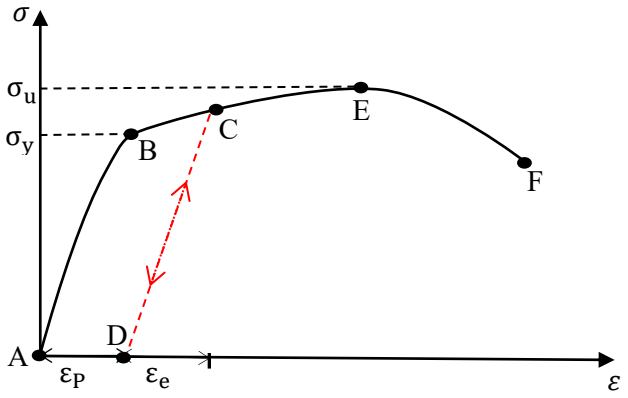

Figure 2.6 Typical stress-strain curve for elastic-plastic material

2.5.1 Ductile versus brittle fracture

Engineering materials fail by ductile or brittle fracture depending on their fracture toughness. Materials of low toughness fail by brittle fracture while tough materials fail by ductile fracture. Fracture toughness is a material property which describes its ability to resist crack growth. Its value depends on many factors including: composition and microstructure of the material, loading rate, geometric effects of crack tip, and temperature of the material. Steel for example is a very tough and ductile material at high temperature but becomes brittle at low temperature. Brittle fracture is characterized by rapid crack propagation with no apparent plastic deformation. The crack continues to propagate in the material if loading is sustained. Ductile fracture follows extensive plastic deformation (necking) of the material. The crack propagates gradually and typically stops unless the loading is increased. Figure 2.7 shows stress-strain curves and fracture surfaces of brittle

and ductile fracture. Extensive plastic deformation that occurs in ductile fracture can be seen in these figures. Observations of fractured surfaces show ductile fracture surfaces have longer necking regions and rougher appearances than brittle fracture surfaces. Brittle fracture surfaces are typically smooth and shiny.

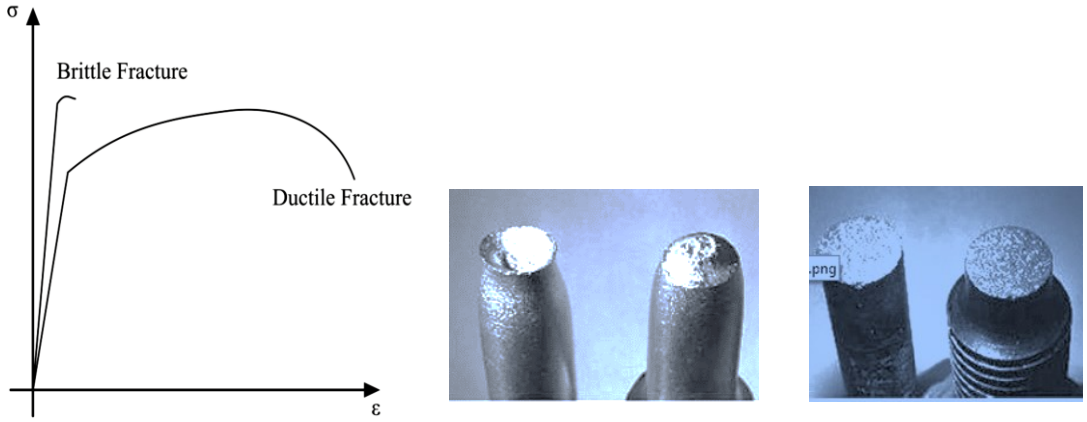

(a) Stress-strain curve (b) Ductile fracture surface (c) Brittle fracture surface

Figure 2.7 Illustration of ductile and brittle fracture [46]

2.6 Fracture mechanics

Fracture mechanics theory seeks to explain fracture of materials and predict failure of cracked bodies using three main concepts, namely: Linear Elastic fracture mechanics (LEFM); Elastic-Plastic Fracture Mechanics (EPFM); and local approach, like Cohesive Zone Modelling (CZM). An overview of each of the concepts presented in subsequent sections.

2.6.1 Linear elastic fracture mechanics

Linear elastic fracture mechanics (LEFM) provides a framework for analyzing fracture of elastic materials. It is a useful tool for solving fracture problems in structures with pre-existing cracks. LEFM uses stress intensity and energy criteria to quantify resistance to crack growth.

2.6.1.1 Crack opening modes

There are three types of loading that a cracked body can experience, as Figure 2.8 illustrates. Mode I loading, where the principal load is applied normal to the crack plane and it tends to open the crack. Mode II corresponds to in-plane shear loading and tends to slide one crack face with respect to the other. Mode III refers to out-of-plane shear. A cracked body can be loaded in any

one of these modes, or a combination of two or three modes. In general, Mode I loading is the most common in pipeline industry and engineering design.

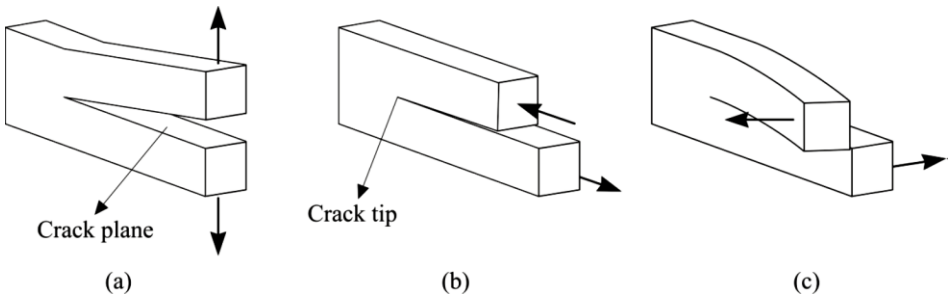

Figure 2.8 Crack opening modes: (a) Mode I (b) Mode II (c) Mode III [43]

2.6.1.2 Stress intensity factor

The local stress-strain field at crack-tip in an infinitely large body subjected to uniform stress at locations remote from the crack can be described using a single parameter called the stress intensity factor, denoted K. The stress intensity factor is the amplitude of the crack-tip stress singularity. Stresses near the crack tip increase in proportion to the stress intensity factor. If K is known, it is possible to solve for all components of stress, strain, and displacement near the crack tip as a function of r and θ (figure 2.9).The stress intensity factor is also a measure of the amount of energy available for fracture around a crack front in a linear elastic material. When it becomes critical, the crack grows, and the material fails. This critical value denoted K_c is the fracture toughness of the material.

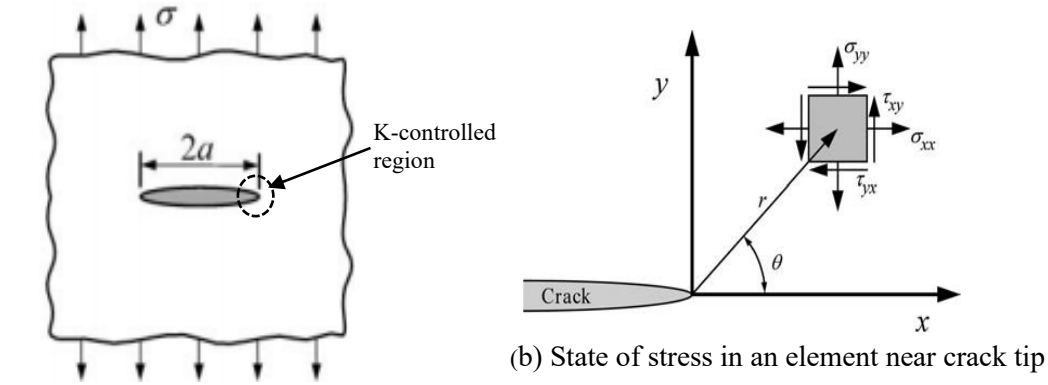

(a) Cracked body under remote stress

(b) State of stress in an element near crack tip

Figure 2.9 Crack in an infinitely large body subjected to uniform stress [43]

The elastic stress field ahead of crack tip in linear elastic body subjected to mode I loading is defined in terms of the Mode I stress intensity factor K_I as follows:

$$\sigma_x = \frac{K_I}{\sqrt{2\pi r}}\cos\left(\frac{\theta}{2}\right)\left[1 - \sin\left(\frac{\theta}{2}\right)\left(\frac{3\theta}{2}\right)\right]$$

$$\sigma_y = \frac{K_I}{\sqrt{2\pi r}}\cos\left(\frac{\theta}{2}\right)\left[1 + \sin\left(\frac{\theta}{2}\right)\left(\frac{3\theta}{2}\right)\right] \qquad (2-26)$$

$$\tau_{xy} = \frac{K_I}{\sqrt{2\pi r}}\sin\left(\frac{\theta}{2}\right)\cos\left(\frac{\theta}{2}\right)\cos\left(\frac{3\theta}{2}\right)$$

$\sigma_z = 0$ (plane stress), $\sigma_z = v(\sigma_x + \sigma_y)$ (plane strain), *v* being the Poisson's ration, $\tau_{xz}, \tau_{yz} = 0$.

Equations (2-26) is valid for ductile materials in which the plastic deformation at crack tip is negligible. For $\theta = 0$, shear stress is zero and the equations can be written as follows:

$$\sigma_x = \sigma_y = \frac{K_I}{\sqrt{2\pi r}}$$

The linear elastic stress intensity factor K_I for Mode I loading is expressed as follows:

$$K_I = \sigma\sqrt{\pi a}.$$

Where a is the half length of the crack and σ is tensile stress acting far away from the crack tip. In general, the crack length is assumed to be very small compared to the size of the component. As the crack size increases, or the component boundary is decreased, the outer boundaries of the component begins to influence crack tip stress distribution. Under such condition, K_I takes the form:

$$K_I = \sigma\sqrt{\pi a}\, Y(a/w) \qquad (2-27)$$

Where *w* is the characterizing dimension of the component, like width, Y(a/w) is a case specific calibration function or correction factor.

2.6.1.3 Energy release rate

Crack propagation is accompanied with dissipation of energy because there is plastic deformation of the material ahead of the crack tip which causes growth and coalescences of micro voids in the material to form a new crack (figure 2.10). By considering fracture from an energy perspective, crack growth criteria can be expressed in terms of energy release rate, which is the energy needed

to propagate a unit surface of crack. Crack growth starts when the energy coming from the stress-strain field is adequate for the growth and coalescence of micro voids in the body.

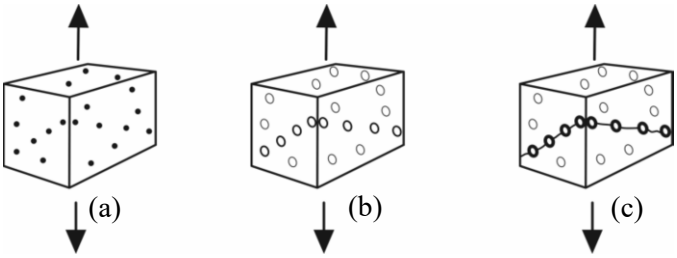

Figure 2.10 Fracture process in a ductile material: (a) Void nucleation (b) Void growth (c) Void coalescence

For ductile materials, a plastic zone develops ahead of the crack tip due to deformation of the material surrounding the crack tip and it acts as the fracture process zone. As the applied load is increased, the size of the process zone grows until the crack propagates and the material behind the crack tip unloads elastically. The plastic loading and unloading cycle near the crack tip causes dissipation of energy as heat. In physical terms, more energy is required for crack propagation in ductile materials compared to brittle materials. In brittle materials, the work of fracture w_f equals to the surface energy γ_s, expended in disruption of intermolecular bonds to create the fracture surface. In ductile materials, plastic dissipation of energy in process zone, γ_p also contributes to the work of fracture w_f, along with the surface energy. Figure 2.11 illustrates the mechanism for crack propagation through brittle and quasi-brittle elastic-plastic materials.

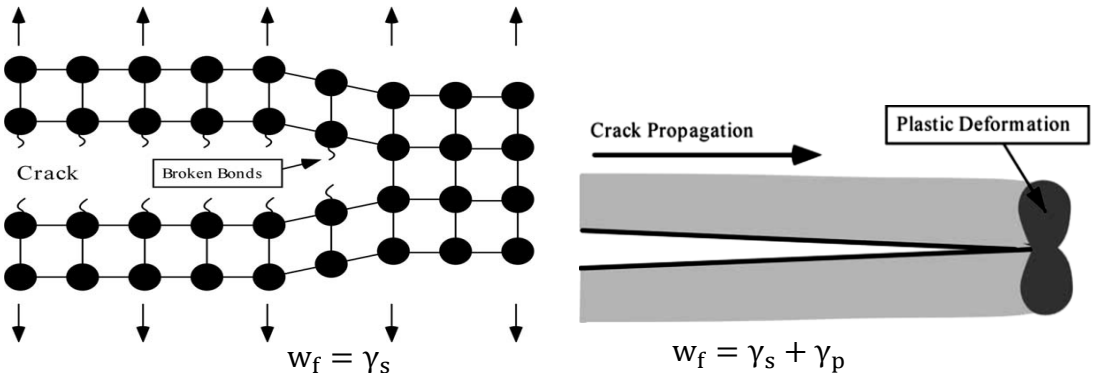

(a) Brittle materials (b) Quasi-brittle elastic-plastic materials

Figure 2.11 Crack propagation in brittle and quasi brittle materials [43]

Irwin (1957) observed that if the size of plastic zone is small compared to the size of the crack, then the energy required for crack growth is independent of stress distribution at crack tip. Therefore, the energy release rate for the fracture process is a constant referred to as fracture energy G_c, that depends only on the material and is independent of loading and geometry of the cracked body. The crack propagates when the energy release rate due to the applied load G exceeds the critical value for the material G_c.

The energy approach offers an alternative perspective to the stress intensity approach to fracture analysis but the two are related. The main difference is that fracture energy is a global parameter while stress intensity factor is a local parameter that defines the stress field at the crack tip only. Irwin (1957) showed that for a Mode I crack the strain energy release rate and the stress intensity factor are related as follows:

$$G = -\frac{\partial U}{\partial A} = \frac{K_I{}^2}{E'} \qquad (2-28)$$

Where E' is the effective Young's modulus, U is the strain energy stored in the body, A is the crack area and K_I is the stress intensity factor for Mode I loading.

For plane stress condition, $E' = E$ and for plane strain $E' = \frac{E}{1-\nu^2}$, where E is the Young's modulus, ν is Poisson's ratio.

2.6.1.4 Effect of specimen thickness on fracture

Figure 2.12 [47] shows variation of stress and strain at the front of a crack within a body of thickness, B. At the center of the crack front, contraction is restrained in all directions and the body is in a state of plane strain with high stress triaxiality near crack tip. The restraint relaxes progressively as one moves away from the centre of the crack front towards the external surface.

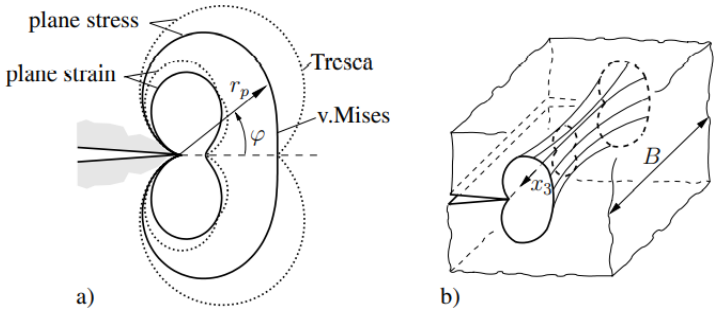

Figure 2.12 Effect of thickness on stress-strain field at crack front [47]

The body is free to deform at the external surface and is in a state of plane stress. The size of region with high stress triaxiality (under plane strain conditions) increases with thickness of the body as the size of plane stress regions simultaneously reduce. Studies show fracture strains are low where stress triaxialities are high [48,49] because deformation is restrained by the high hydrostatic stresses associated with high stress triaxialities.

The shape of the fractured surface varies with the state of stress and strain within the body, hence with thickness of the body as shown in figure 2.13. Fracture surface under plane strain conditions is flat, while slant (shear) fracture occurs under plane stress conditions as shown in Figure 2.13. The ratio of flat to slant fracture increases with specimen thickness (B) as the size of region under plain strain and high stress triaxiality increases. Apparent fracture toughness, K_c is high in thin specimens that exhibit full shear fracture (region I). This is because of the stress relaxation that occurs when the plastic zones developed under plain stress conditions coalesce to blunt the entire crack front, forming one bean shaped bulb through the thickness of the thin body (figure 2.12a). As the thickness increases, the plane stress regions reduce, and the plastic zones developed at the extremities of the body cannot coalesce hence reducing the overall size of plastic zone and its blunting action along the crack front as shown in region II. Regions of high triaxiality and plane strain increase and more flat fracture occurs. Stress relaxation is reduced, and apparent fracture toughness drops until a critical specimen thickness $B_{c.}$ where it then remains constant as shown in region III. Increasing thickness beyond B_c increases flat fracture and reduces slant fracture.

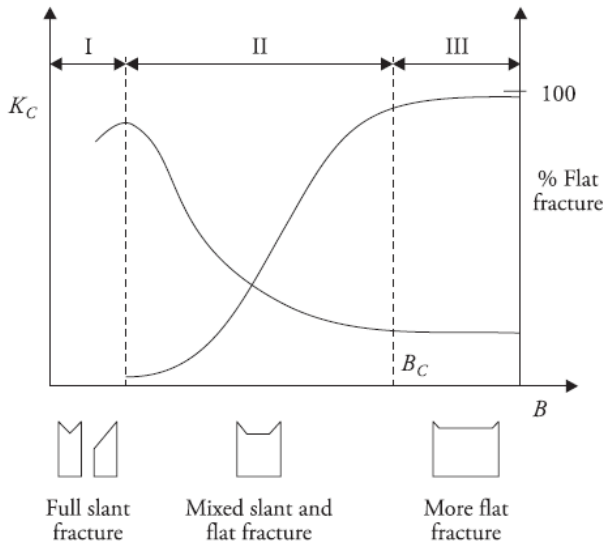

Figure 2.13 Effect of thickness on fracture toughness and type of fracture [43]

The size of test specimens in laboratory measurements of fracture toughness is limited (equation 2-29) to ensure it does not affect the measured toughness of the material. The restriction ensures that the test is conducted under plain strain conditions and the lowest possible fracture toughness of the material is measured. Slant fracture behavior is eliminated by using grooved samples in the fracture toughness tests.

$$a, B, (W - a) \geq 2.5 \left(\frac{K_{Ic}}{\sigma_{ys}}\right)^2 \qquad (2 - 29)$$

2.6.2 Elastic plastic fracture mechanics

The Linear elastic fracture mechanics (LEFM) theory only applies where plastic deformation occurs in an infinitesimal area of near the crack tip and plasticity does not control the fracture. The theory has limitations when plastic deformation ahead of the crack tip becomes significant. Elastic-plastic fracture mechanics (EPFM) extends the LEFM theory to nonlinear elastic materials having an initial crack, by considering that the body fails with plastic deformation and the size of fracture process zone is large compared to the original crack geometry. It is important to note that EPFM does not follow elastic-plastic material model but provides a solution for a nonlinear elastic material using the LEFM theory. Like the elastic-plastic materials with power law behavior, the nonlinear elastic material analyzed by EPFM exhibits a power law behavior between stress and strain but has a different unloading path (figure 2.14). The elastic-plastic material follows a linear unloading path with the slope equal to Young's modulus, while the nonlinear elastic material unloads along the same path it is loaded. The loading paths of the two materials are the same under monotonic loading. Thus, an analysis that assumes nonlinear elastic behavior is valid for elastic-plastic materials under monotonic loading without unloading.

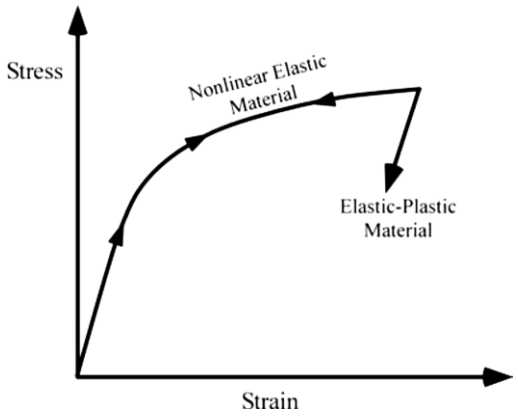

Figure 2.14 Stress-strain behaviors of elastic-plastic and nonlinear-elastic materials [43]

2.6.2.1 The J contour integral

Rice (1968) [24] showed that the energy release rate for a nonlinear material could be expressed in terms of a path independent contour integral known as J-Integral (figure 2.15), which has since become an efficient tool for solving energy problems in fracture mechanics.

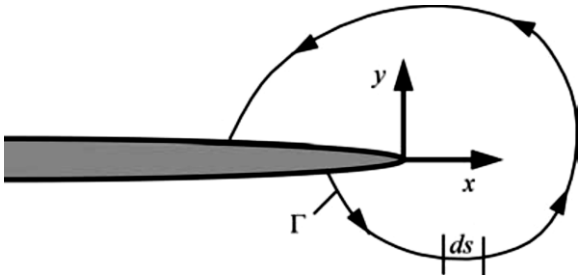

Figure 2.15 Arbitrary contour around the tip of a crack to characterize J [43]

The J-integral is determined as follows:

$$J = \int_{\Gamma} \left(w dy - T_i \frac{\partial u_i}{\partial x} ds \right) \qquad (2-30)$$

$$w = \int_0^{\varepsilon_{ij}} \sigma_{ij} d\varepsilon_{ij}$$

Where σ_{ij} and ε_{ij} are the stress and strain tensor components, T_i is the stress component vector at a given point on the contour. u_i is the displacement vector, w is the strain energy density, and ds is the incremental length along the contourΓ. If a free body diagram of the material inside the contour is constructed, T_i would define the stresses acting at the boundaries. The components of the traction vector are given by:

$$T_i = \sigma_{ij} n_j$$

Where n_j is a unit vector normal to the contour Γ.

Given that the path of the contour must be within the material, the J-integral analysis only applies to situations where plastic deformation at crack tip does not extend to the edge of the cracked body. The total J for an elastic-plastic material is the sum of elastic and plastic components.

$$J_{total} = J_{Elastic} + J_{Plastic}$$

Rice (1968) showed that the J-integral is equal to the strain energy release rate for a crack in a body subjected to monotonic loading and it is true for linear elastic and nonlinear elastic materials. For a linear elastic material, J integral is the same as G and for plane stress and plane strain conditions it follows that:

$$J = G = \frac{K^2}{E'}$$

Where E' is the effective Young's modulus, earlier defined for plane stress and strain conditions. For nonlinear elastic materials with a power law relationship between stress and strain, Hutchinson, Rice and Rosengren (HRR) [47] developed the J-integral relationships below to characterize the stress and strain conditions at the crack tip.

$$\varepsilon_{ij} = k_2 \left(\frac{J}{r}\right)^{\frac{n}{n+1}}, \quad \text{and} \quad \sigma_{ij} = k_1 \left(\frac{J}{r}\right)^{\frac{1}{n+1}} \qquad (2-31)$$

Where k_1 and k_2 are proportionality constants.

For a linear elastic material, n=1, and the two equations predict a stress and strain singularities of $1/\sqrt{r}$, like LEFM theory.

For elastic-plastic material with small scale yielding, there is an additional stress singularity of $r^{\frac{-1}{n+1}}$ due to plasticity at the crack-tip. Thus, the J-integral can be viewed as both an energy parameter and as a stress intensity parameter.

2.6.2.2 Effect of plasticity on stress fields at crack tip

Figure 2.16 illustrates the distribution of stresses at crack tip and the applicable methods for evaluating stresses at the crack tip. Figure 2.16(a) shows small scale yielding behavior where both stress intensity factor K and J-integral can be used to characterize crack tip stress and strain fields. At short distance away from the crack tip, the stress intensity factor completely defines the fields. A little closer to the crack tip is the plastic zone, where stresses and strain are completely defined by the J-integral. The small region very close the crack tip is the large plastic strain region where the HRR solution is no longer valid because of crack blunting by severe plastic deformation. In small scale yielding, both J and K can characterize the crack tip conditions because the region of large strain is very small.

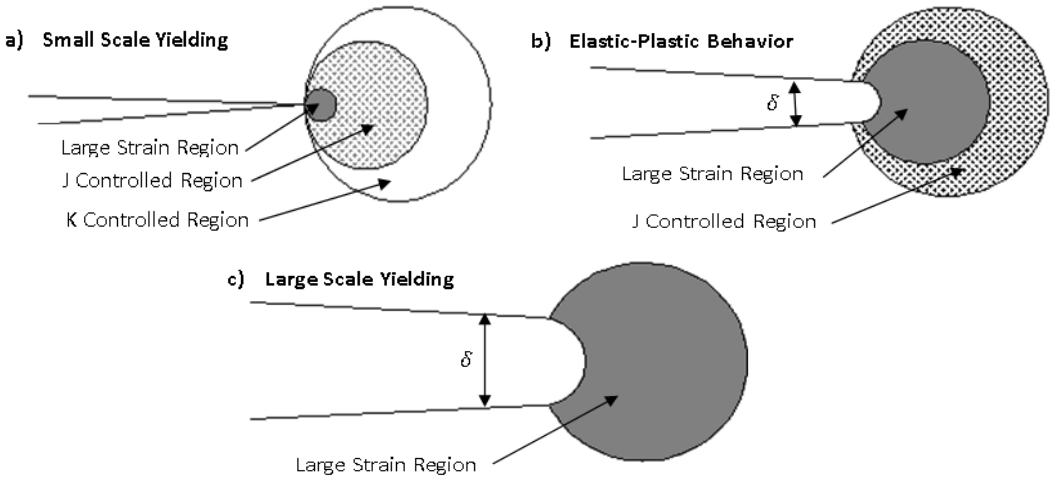

Figure 2.16 Effect of plasticity at crack tip on stress distribution [43]

Figure 2.16 (b) illustrates elastic-plastic conditions, where J-integral solution is still valid, but there is no longer a K-defined field. As the plastic zone size increases around the crack tip, the K-controlled region disappears and both the J-controlled, and large strain regions expand. Therefore, K is no longer a valid solution but, J-integral is still an appropriate fracture criterion. It is important to note that the size of large strain regions increase significantly as one moves from small scale yielding to elastic-plastic strain conditions and the crack tip/mouth opening displacements, δ increase in similar proportion. With large scale yielding (figure 2.16(c)), both K and J-integral solutions are no longer valid because the crack tip is blunted by severe plastic deformation. Crack tip constraint, which depends on specimen geometry controls the stress and strain fields at the and resistance to crack growth.

2.6.2.3 Crack growth resistance

Tough materials do not fail catastrophically when the critical values of crack growth criterion like J_{1c} and crack tip opening displacement (CTOD) are reached. The material's resistance to crack extension increases with crack growth such that successive crack extensions occur at higher values of J and CTOD, due to increase in apparent fracture toughness. Figure 2.17 shows a typical fracture resistance (R) curve for a ductile material. Initially, the curve is nearly vertical; crack growth is very small and crack tip is blunt. As applied J increases, material at crack tip fails locally and the crack extends. Because the curve is rising, the initial crack growth is usually stable, but may become unstable later as the curve flattens. Fracture toughness J_{Ic} is defined near the initiation of

stable crack growth but its exact location on the curve is uncertain like the location of yield point in stress-strain curves. The R-curve is not very sensitive to specimen geometry; therefore, it is a useful tool in calibration of numerical models.

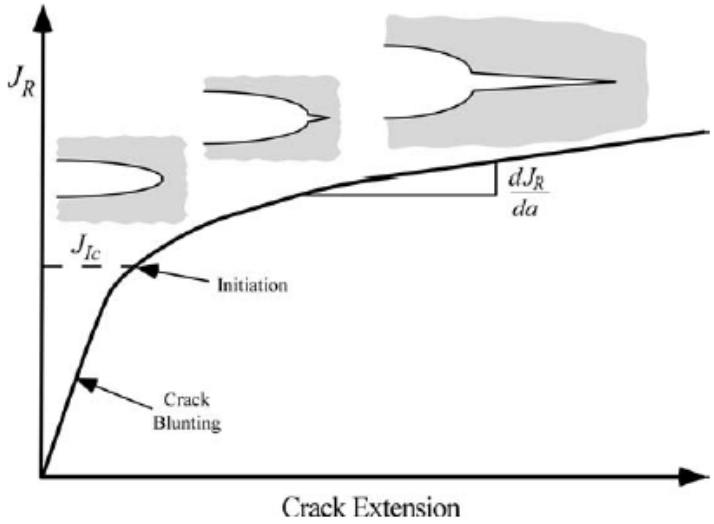

Figure 2.17 Typical crack growth resistance curve for ductile material [43]

2.6.2.4 Time dependent fracture

Fracture mechanics can also be used to analyze time dependent fracture mechanisms like fatigue and stress corrosion cracking. Generally, material property and loading determine whether time is a fracture variable and the applicable branch of fracture mechanics for the analysis. Time is not a fracture variable under static loads, like monotonically increasing internal pressure. Linear elastic and elastic plastic fracture mechanics deal with fracture under quasi static conditions. Dynamic fracture mechanics, viscoelastic fracture mechanics and viscoplastic fracture mechanics include time as a fracture variable. The grade of steel pipeline materials control fracture behavior. High strength steel pipelines fracture in a linear elastic manner while low to medium strength steels show elastic plastic fracture behavior [43,47].

The grade of the pipe analyzed in this study was API X70, which is considered a medium strength grade, suitable for analysis by elastic plastic fracture mechanics. In addition, the pipe was only subjected to monotonic pressure thus, fracture was independent of time. Fatigue and stress corrosion cracking were not part of this study.

2.6.3 Cohesive zone modelling

Both LEFM and EPFM apply when an initial crack exists in the structure and the region of large strain around the crack tip is small compared to structural dimensions hence, both methods are constraint and geometry dependent and cannot analyze crack initiation in uncracked bodies. Cohesive zone modelling (CZM) is a phenomenological local approach that represents an improvement on the LEFM and EPFM theories to allow for modelling of crack initiation and propagation problems.

Figure 2.18 shows an illustration of the CZM approach to modelling of fracture problems. Continuum elements are used to model the material's deformation based on its stress strain curve while damage and separation of fracture surfaces is modeled by a cohesive layer of zero thickness embedded within continuum elements (figure 2.18a), using a specific constitutive traction-separation law (TSL).

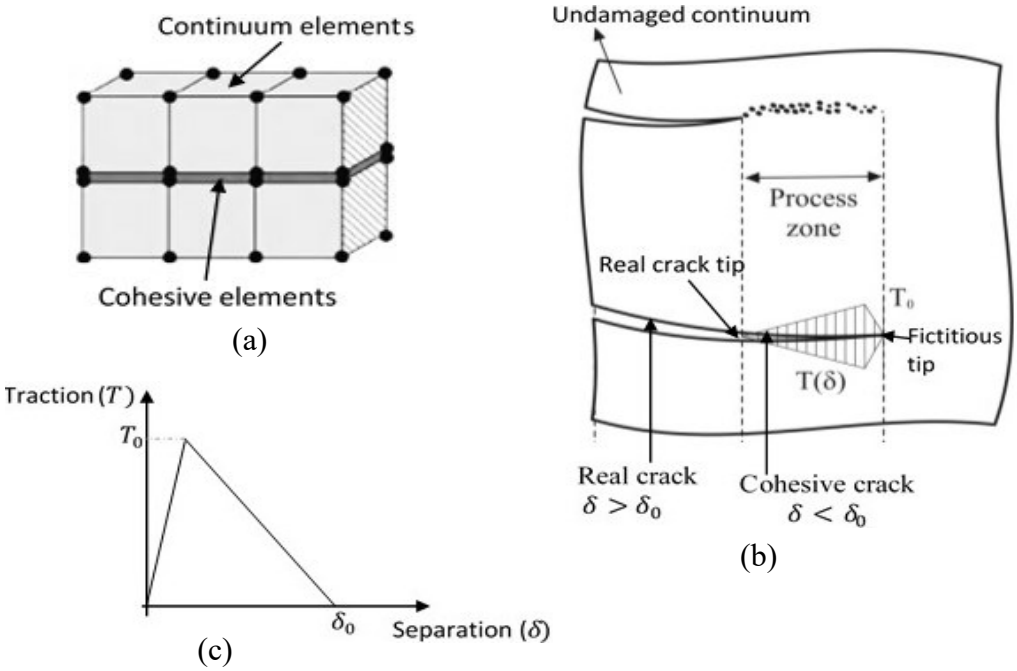

Figure 2.18 Showing (a) Ductile fracture concept for cohesive zone modelling (b) CZM and continuum elements (c) Traction separation law [46,53]

Fracture takes place inside a fracture process zone modeled as an extension of crack length up to a point referred to as the fictitious crack tip (figure 2.18b). The material in the process zone is still able to transfer stresses, although it is damaged. In this region, the TSL describes the relation

between the local stresses, $T(\delta)$ and separation δ of the crack surfaces. Stress increases up to a maximum value T_0, the cohesive strength of the material then decreases with increase in separation (figure 2.18c), following the specified TSL. The real crack tip is the point on the crack surface at which there is no stress and separation is at the maximum value,δ_0. The crack propagates when the stress at the tip exceeds cohesive strength. When the crack opens, the stress is not assumed to fall to zero instantaneously, but it decays progressively with increasing fracture surface separation until the critical displacement δ_0 is reached then it vanishes. Fracture is assumed to occur only in the cohesive layer while the continuum remains undamaged. The cohesive elements open progressively after damage and the elements lose stiffness at failure and disentangle the continuum elements into separate fracture surfaces. Crack propagation takes place along element boundaries and usually the crack path is known apriori but where it is not, mesh generation is done in a way that different paths are made possible.

2.6.3.1 Traction separation laws

Traction separation laws are uniquely characterized by a small number of parameters, which in the best case scenario like the exponential type laws, may be reduced to at least two parameters: the maximum traction at the surface of the continuum elements T_0 and the maximum separation between the fracture surfaces δ_0, where upon failure occurs and the crack propagates. A constitutive equation relates the traction, T, to the relative displacement, δ, at the interface. The form of the cohesive law is given by the function $T(\delta)$. The peak stress at the interface is the local strength of the material and is the condition for developing plastic deformation in the continuum. The area under the curve generated by the TSL represents the energy Γ_0 absorbed by the cohesive elements during the fracture process and is called the cohesive energy.

$$\Gamma_0 = \int_0^{\delta_0} T(\delta)\, d\delta \qquad (2-32)$$

If the shape of the TSL is known, any two of T, δ and Γ_0 are enough to characterize the cohesive law in numerical simulations. The local work of separation is equivalent to the material's fracture toughness, which is also defined by the energy release rate, G_c, when the material has a linear-elastic deformation behavior. For elastic plastic materials the cohesive energy, approximately corresponds to the J-integral at crack initiation, J_{1c} read from the crack growth resistance curve

and is the first guess for Γ_0 in simulations. The shape and input parameters of TSLs are always chosen to be as simple as practicable for numerical reasons, rather than being physically meaningful because the mechanisms that control them are yet to be quantified.

Basic forms of TSL comprise of bilinear curves but other forms including exponential curves for brittle metals, trapezoidal curves recommended for ductile metals, shown in figure 2.19 below are available. It is important to note that any of these cohesive laws can be used to model crack propagations in materials, but the values of cohesive parameters will vary and may not be physically meaningful for some materials with some TSLs.

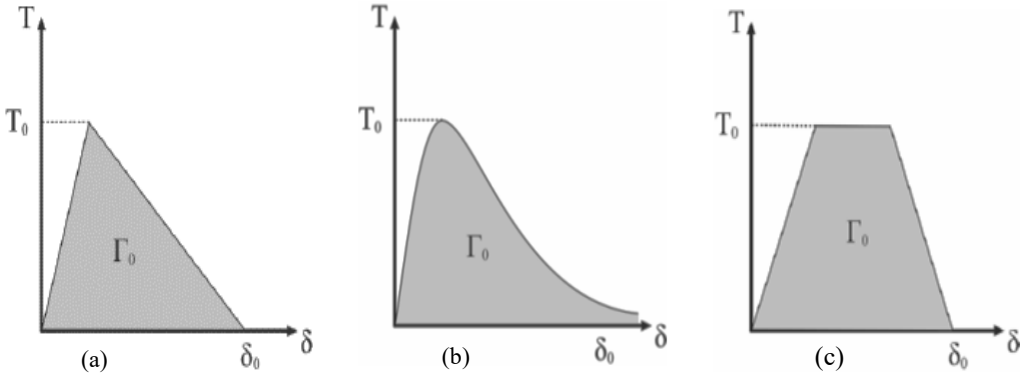

Figure 2.19 Forms of TSL (a) Bilinear (b) Exponential and (c) Trapezoidal [46,53]

The three fracture parameters T_0, G_c, and δ_0 can be relatively well determined experimentally: the cohesive fracture strength T_0 is approximately the ultimate strength of a smooth or notched tensile specimen, the fracture energy is estimated from fracture mechanics experiments like single edge notch tension test (SENT) via the critical stress intensity factors K_{Ic} or the J-integral. The cohesive energy for normal fracture, G_c, is estimated by the J-integral at crack initiation in Mode I fracture determined from crack growth resistance curves (figure 2.17). The crack tip opening displacement is measured from the fracture process zone.

2.6.3.2 Finite element methods

Finite element methods can be used to accurately solve boundary value problems in a continuum. But its application in crack problems is complicated by the inability to reproduce the singularity at crack tip using conventional finite elements. This is remedied in practice by using infinitesimally small mesh elements around the crack to approximate the infinite stresses at the tip, which of

course increases the time required for simulations and computing cost. Singularities of $r^{\frac{-1}{2}}$ and $r^{\frac{-1}{n+1}}$ were shown in previous sections to exist in linear and nonlinear elastic fracture mechanics respectively.

Figure 2.20 [50] shows a typical one-dimensional isoparametric element for traditional finite element modeling of a bar. Linear shape functions $N_a(\xi)$ are used to transform the body from undeformed to the deformed configuration. By shifting node 3 in the local coordinate system to the quarter point of the element, the conventional isoparametric element is modified into a quarter point element, which in theory accurately reproduces the singularity at the crack tip [51].

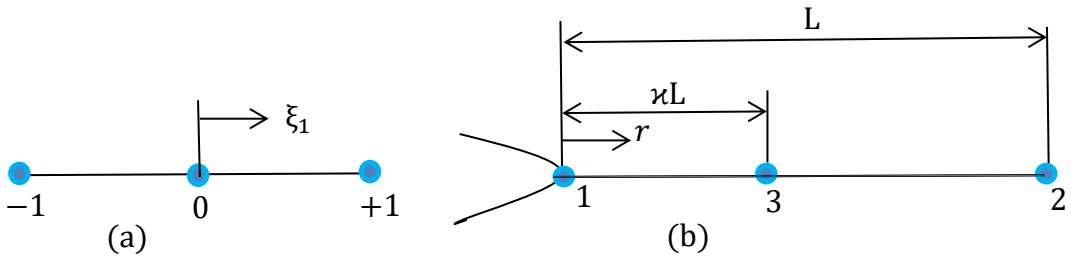

Figure 2.20 1-D finite elements in (a) natural, and (b) local cartesian coordinate system [50]

The quadratic one dimensional displacement field of this isoparametric finite element in its natural coordinate system is:

$$u(\xi) = \sum_{a=1}^{3} N_a(\xi)u^{(a)} = \frac{1}{2}\xi(\xi-1)u^{(1)} + (1-\xi^2)u^{(3)} + \frac{1}{2}\xi(\xi+1)u^{(2)} \qquad (2-33)$$

Where $N_a(\xi)$ is the linear shape function that maps the undeformed to deformed shape of the body. The same interpolation is valid for all coordinates in an isoparametric element formulation. In the local coordinates system (figure 2.20b), the nodes are: $r^{(1)} = 0, r^{(2)} = L, r^{(3)} = \varkappa L$. $\varkappa$ is a parameter that controls the location of node 3.

$$r(\xi) = \sum_{a=1}^{3} N_a(\xi)r^{(a)} = \frac{1}{2}\xi(\xi-1)r^{(1)} + (1-\xi^2)r^{(3)} + \frac{1}{2}\xi(\xi+1)r^{(2)} \qquad (2-34)$$

For a regular one dimensional finite element analysis, the value of $\varkappa = 1/2$

Therefore, $r(\xi) = \frac{L(1+\xi)}{2} \Rightarrow \xi = \left(\frac{2r}{L} - 1\right)$

And the displacement field in the local coordinates would be:

$$u(r) = u^{(3)} + \frac{1}{2}\left(u^{(2)} - u^{(1)}\right)\left(\frac{2r}{L} - 1\right) + \left[\frac{1}{2}\left(u^{(1)} + u^{(2)}\right) - u^{(3)}\right]\left(\frac{2r}{L} - 1\right)^2 \qquad (2-35)$$

Which is a second-degree polynomial in r, meaning the strain, a derivative of displacement is a linear function in *r* and the desired singularity of $r^{\frac{-1}{2}}$ or $r^{\frac{-1}{n+1}}$ at crack-tip is not achievable.

If $\varkappa = 1/4$, node 3 shifts closer to the crack:

$$r(\xi) = \frac{1}{4}L(1+\xi)^2 \Rightarrow \xi = 2\sqrt{\frac{r}{L}} - 1$$

And the new displacement field in the local coordinates would be:

$$u(r) = u^{(3)} + \frac{1}{2}\left(u^{(2)} - u^{(1)}\right)\left(2\sqrt{\frac{r}{L}} - 1\right) + \left[\frac{1}{2}\left(u^{(1)} + u^{(2)}\right) - u^{(3)}\right]\left(2\sqrt{\frac{r}{L}} - 1\right)^2 \qquad (2-36)$$

The resulting displacement function now reproduces exactly the displacement field at the crack tip, which comprises of a constant rigid body displacement, a linear displacement and a term in $r^{\frac{1}{2}}$ which addresses the singularity envisaged by linear elastic fracture mechanics.

2.6.3.3 Extended finite element method

Although the conventional finite element method can model stationary cracks accurately, it is not robust enough to model crack growth. It treats the crack a new discontinuity each time it grows, and the body is re-meshed to capture the new crack geometry. The basic concept of the extended finite element method (XFEM) is to enrich the approximation space so that it can reproduce certain features of a problem of interest, like cracks or interfaces wherever they exist in the body. The solution is executed in steps as follows: first, the usual conventional finite element discretization of the body is completed. Then, by considering the location of discontinuities, a few virtual degrees of freedom are added to the conventional finite element model at selected nodes near the discontinuity to improve accuracy of the approximation. The following expression is used to calculate the displacement of a point x located in the cracked domain.

$$u(x) = u^{FEM} + u^{enr} = \sum_{j=1}^{n} N_j(x)u_j + \sum_{k=1}^{N} N_k(x)\psi(x)a_k \qquad (2-37)$$

Where:

u^{FEM} is the conventional finite element solution for displacements field,

u^{enr} is the enrichment approximation to account for presence of discontinuity,

u_j is the vector of regular FEM nodal degrees of freedom,

a_k is the added set of virtual degrees of freedom to the regular FEM model,

$\psi(x)$ is the discontinuity enrichment function defined for the set of nodes influenced by the discontinuity (i.e. nodes in elements touched by the discontinuity).

The form of the enrichment function used depends on the type of discontinuity in the body. The Heaviside enrichment function $H(\xi)$ is commonly used to model strong discontinuities, like cracks. It takes the forms of step function, signed functions and smoothed functions.

i. Heaviside step function

$$H(\xi) = \begin{cases} 1 & \forall \xi > 0 \\ 0 & \forall \xi < 0 \end{cases}$$

ii. Heaviside signed function

$$H(\xi) = \begin{cases} +1 & \forall \xi > 0 \\ -1 & \forall \xi < 0 \end{cases}$$

iii. Smoothed functions help avoid numerical instabilities in the solution and can take the following forms:

$$H(\xi) = \begin{cases} 0 & \xi < -\beta \\ \frac{1}{2} + \frac{\xi}{2\beta} + \frac{1}{2\pi}\sin\frac{\pi\xi}{2\beta} & -\beta < \xi < \beta \\ 1 & \xi > \beta \end{cases}$$

β is very small compared to the size of the smallest element in the model. Figure 2.21 illustrates the effects of step and signed enrichment functions applied to a strong discontinuity in a one-dimensional (1-D) bar.

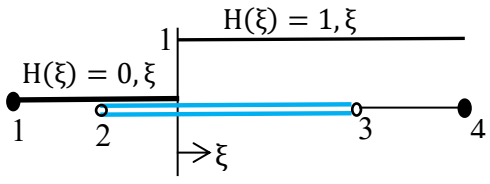

(a) Effect of step function

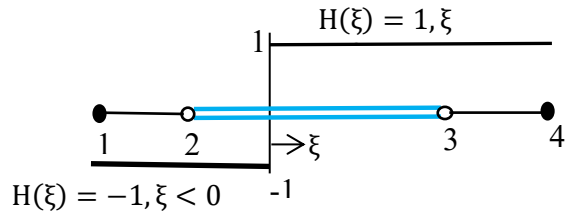

(b) Effect of sign function

Figure 2.21 Actions of Heaviside step and signed functions $H(\xi)$ on a discontinuity in a bar [52]

Figure 2.22 illustrates the steps followed in XFEM to model a one-dimensional bar problem having four nodes and three finite elements with a strong discontinuity (crack) at an arbitrary location $x_i\xi_i$ within the middle element. First, the conventional finite element solution is sought using linear shape functions $N_j(x)$(figure 2.22a). This step treats the body as a continuum and does not address the discontinuity. The approximate displacement field obtained from this step is:

$$u(x) = \sum_{i=1}^{n} N_j\,(x)u_j \qquad (2-38)$$

The shape functions N_j in the natural coordinate system were previously defined as:

$$N_1(\xi) = 1-\xi\,,\ N_2(\xi) = \xi, \text{ and } N_3(\xi) = 1+\xi.$$

In the second solution step, the Heaviside step function enrichment, $H(\xi)$ (figure 2.21a) is applied to nodes 2 and 3, of the element having the crack to obtain the result in figure 2.22b. The approximate displacement field then becomes:

$$u(x) = \sum_{j=1}^{n} N_j\,(x)u_j + \sum_{k=1}^{N} N_k\,(x)H(\xi)a_k \qquad (2-39)$$

Considering an enriched node i in the cracked element, the displacement of the node after enrichment is given by: $u(x_i) = u_i + H(\xi)a_i \neq u_i$

Clearly, the displacement obtained after enrichment is not equal to u_i, the actual nodal displacement of the enriched node i, hence this approximation is not an interpolation. The simple remedy to this shortcoming is to shift the step function around the node of interest so that the interpolation is automatically guaranteed as follows:

$$u(x) = \sum_{j=1}^{n} N_j\,(x)u_j + \big(H(\xi) - H(\xi_k)\big)a_k \qquad (2-40)$$

Such that: $\langle u(x)\rangle = u(x^+) - u(x^-) = \sum_{k=1}^{N} N_k\,(x)a_k$

The effect of shifting the step function around the node on the shape function is illustrated in figure 2.22c.

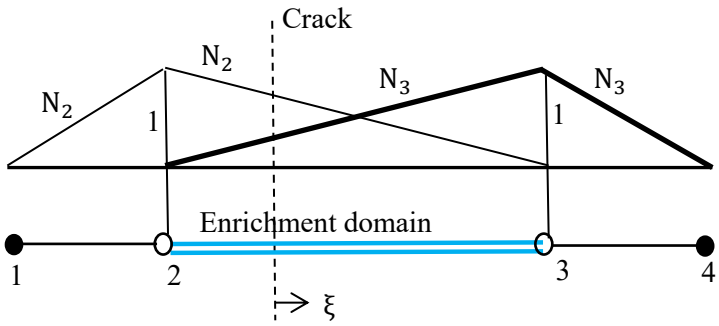

(a) Regular Finite element solution

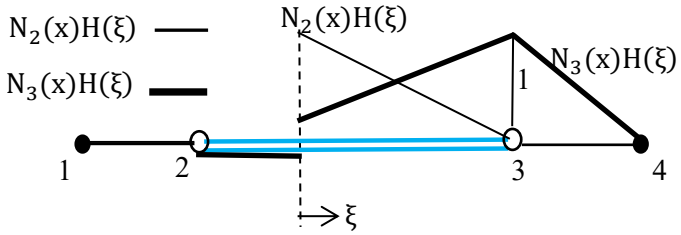

(b) Solution with Heaviside (step) enriched shape function solution

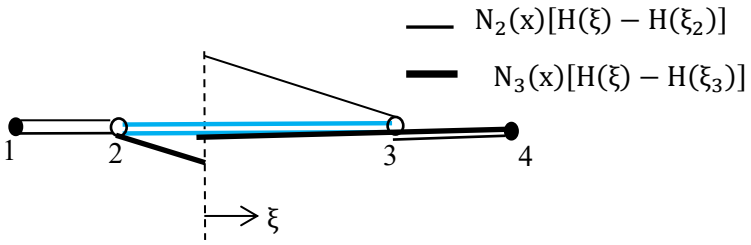

(c) Effect of shift in the enriched shape function

Figure 2.22 Heaviside step function enrichment of strong discontinuity in a one dimensional bar [52]

2.7 References

[1].Cosham, A., & Hopkins, P. (2004). The effect of dents in pipelines—guidance in the pipeline defect assessment manual. *International Journal of Pressure Vessels and Piping, 81*(2), 127-139.

[2].Mohr, W. 2003. "Strain-based design of pipelines-basic guidance on strain-based design, the Minerals Management Service (MMS) and the Office of Pipeline Safety (OPS)", Project No. 45892GTH.

[3]. Baker, M. 2004b. "Pipe Wrinkle Study". Delivery Order DTRS56-02-D-70036. Integrity Management Program. Office of Pipeline Safety.

[4]. Oshana, JJ., "Dent behavior of steel pipes under pressure load" (2014). Electronic Theses and Dissertations. 5025. https://scholar.uwindsor.ca/etd/5025.

[5]. D.B. Noronha Jr. et al. "Procedures for the strain-based assessment of pipeline dents", Int. Journal of Pressure Vessels and Piping 87 (2010) 254e265

[6]. Keith A, Escoe B. Piping and pipelines assessment guide. British library cataloguing-in publication data, vol. I. Elsevier; 2006.

[7]. Robert B Francini and Nader Yoosef-Ghodsi: "Development of a Model for Predicting the Severity of Pipeline Damage Identified by In-Line Inspection" Pipeline Research Council International (PRCI) Report, PR-218-063511-B, Final Report No. 08-124, December 2008.

[8]. Dawson, S.J., Russel, A., Patterson, A., "Emerging techniques for enhanced assessment and analysis of dents", IPC 2006-10264, Proceedings of 6th international conf. on pipelines, Calgary, Canada, 2006.

[9].Belanos S.P, Ryan R.S., "Dents in pipe.", Oil Gas J 1958; 56:155–61.

[10].Wang KC, Smith, E.D., "The effect of mechanical damage on fracture initiation in line pipe: part I—dents.", Report ERP/PMRL 82-11 (TR), Canada: Canadian Centre for Mineral and Energy Technology (CANMET) January 1982.

[11].Hopkins. P., Jones, D.G., Clyne, A.C., "Recent studies of the significance of mechanical damage in pipelines.", The American Gas Association and European Pipeline Research Group Research Seminar V, San Francisco, USA, September; 1983.

[12].Bjørnøy, O.H., Rengard, O., Fredheim, S., Bruce, P., "Residual strength of dented pipelines, DNV test results.", Tenth International Conf. on Offshore and Polar Engineering (ISOPE 2000) Seattle, USA, 28 May–2 June; 2000.

[13].Lancaster ER, Palmer S.C. Strain concentrations in pressurized dented pipes, Part E. J Process Mech Engng, Proc. Inst Mech Engng 1996; 210:29–38

[14].Beller M, Mattheck C, Zimmermann J. Stress concentrations in pipelines due to the presence of dents. Proceedings of the First International Offshore and Polar Engineering Conf. (ISOPE 1991), Edinburgh, United Kingdom, 11–19 August; 1991.p. 421–24

[15].Rosenfeld M.J., Pepper J.W, Lewis K., Basis of the new criteria in ASME B31.8 for prioritization and repair of mechanical damage, IPC02-27122. Proceedings of IPC 2002, International Pipeline Conf., Calgary, Alberta, Canada: American Society of Mechanical Engineers.

[16].Ong LS, Soh AK, Ong JH. Experimental and finite element investigation of a local dent on a pressurized pipe. J Strain Anal 1992;27(3):177–85.

[17].Pluvinage, G., Capelle, J., and Schmitt, C., "Handbook of Materials Failure Analysis with Case Studies from the Oil and Gas Industry", Chapter 3: Methods for assessing defects leading to gas pipe failure, Elsevier Ltd, 2016.

[18].Orynyak I.V., Bogdan A.V., Rozgonyuk C.V., Ductile fracture model for a pipe with a dent. Proc. 4th int. conf. on pipeline technology, Oostende, Belgium, 9–13 May, volume II; 2004. p. 949–60.

[19].Allouti, M., Schmitt, C., Pluvinage, G., Gilgert, J., & Hariri, S. (2012). Study of the influence of dent depth on the critical pressure of pipeline. *Engineering Failure Analysis, 21*, 40-51.

[20].ASME B31.8-2010, Gas Transmission Distribution Piping System, New York, USA 2010A

[21].Arumugam U, Gao M, Ravi K., Wang R, Kania R, "Study of plastic strain limit damage criterion for pipeline mechanical damage using FEA and full-scale denting tests", IPC2016, Paper 64548, 11th International Pipeline Conf., September 2016, Calgary, Canada.

[22].ASME Boiler & Pressure Vessel Code, Section VIII, Division 3, "Alternative Rules for Construction of High-Pressure Vessels" (2010).

[23].J. W. Hancock and A. C. McKenzie, "On the mechanisms of ductile failure in high-strength steels subjected to multi-axial stress-states". Journal of Mech. Phys. Solids, Vol. 24.

[24].J. R. Rice and D. M. Tracey, "On the ductile enlargement of voids in triaxial stress fields". Journal of Mech. Phys. Solids, Vol. 17, pp 201 to 217, 1969.

[25].CSA Z662-15, Oil and gas Pipeline Systems Ontario, Canada, June 2015

[26].ASME. (2012). “Pipeline transportation systems for liquids and slurries.” ASME B31.4. New York

[27].API1176-2016, Recommended practice for assessment and management of cracking in pipelines, Washington, USA.

[28].Kiefner, J. F., Maxey, W. A., Eiber, R. J., and Duffy, A. R., “Failure Stress Levels of Flaws in Pressurized Cylinders,” American Society of Testing and Materials Report No. ASTM STP 536, pp. 461–481, 1973

[29].Kiefner, J.F, “Defect Assessment – Conclusion: Modified Ln-Secant equation improves failure prediction” Oil and Gas Journal, 2008

[30].Jaske, C.E, “CorLAS User manual”, Version 2.25, 2010.

[31].ASME. “Fitness-for-service, API Recommended Practice 579-1/ASME FFS-1 2007, Second Edition”, The American Society of Mechanical Engineers, New York, USA, June 2007.

[32].BSI. BS7910: 2005, “Guide to methods for assessing the acceptability of flaws in metallic structure”, London, UK, British standards institution, July 2005.

[33].Folias, E.S., “An Axial Crack in a Pressurized Cylindrical Shell,” *International Journal of Fracture Mechanics* 1 (1965) pp. 104-113.

[34]. Shih, C.F., and Hutchinson, J.W., “Fully plastic solutions and large-scale yielding estimates for plane stress crack problems”, Report No. DEAP S-14, Harvard University, July 1975.

[35].Cravero, S. and Ruggeri, C., “Structural Integrity Analysis of Axially Cracked Pipelines Using Conventional and Constraint-Modified Failure Assessment Diagrams”, Int. J.of Pressure Vessels and Piping, 2006.

[36].Ghaednia, H., “Burst strength of NPS30 Steel pipes with dent-crack defect’(2015). Electronic theses and dissertation 5713. https://scholar.uwindsor.ca/etd/5713

[37].Ghaednia, H., Das, S., Wang, R., and Kania, R. (2015b). “Safe burst strength of pipeline with dent-crack defect: Effect of crack depth and operating pressure.” Eng. Fail. Anal.,55,288-299.

[38].Ghaednia, H., Das, S., Wang, R., and Kania, R. (2017). “Dependence of burst strength on crack length of a pipe with dent-crack defects”. Pipeline systems and Eng. Practice, 2017,8(2):04016019.

[39].Macdonald, K. A., & Cosham, A. (2005). Best practice for the assessment of defects in pipelines – gouges and dents. Engineering Failure Analysis

[40].Lancaster E.R., Palmer S.C.," Burst pressure of pipes containing dents and gouges", IMechE 1996, Proceedings of the Institution of Mechanical Engineers, UK, Vol 210

[41].Orynyak, I., Yakovleva, E., & Rozgonyuk, V. (2007). Application of the cheng-finnie method to the calculation of stress intensity factors in thin-walled pipes with long axial cracks with allowance for geometric nonlinearity. *Strength of Materials, 39*(5), 455-465.

[42].Bai, Y., & Song, R. (1997). Fracture assessment of dented pipes with cracks and reliability-based calibration of safety factor. *Int. J. of Pressure Vessels and Piping, 74*(3), 221-229.

[43].Anderson T.L, "Fracture mechanics fundamentals and applications", Taylor and Francis, 2005.

[44].Samarth, T., Ming G., Ravi K., Shahani K., Kania R., "Evaluation of existing fracture mechanics models for burst pressure predictions, theoretical and experimental aspects", IPC2014-33563 proceedings of the 10th international pipeline conf., Calgary Canada 2014

[45].Newman, J. C. and Raju, I. S. An empirical stress-intensity factor equation for the surface crack. Engineering Fracture Mechanics, 1981, 15(1-2), 85-191.

[46].Seif, T., "Ductile fracture analysis in a steel plate by cohesive zone modelling", MSc thesis, Memorial University of Newfoundland, Canada, 2014.

[47].Gross D, Seelig T., "Fracture mechanics with an introduction to micro mechanics", 3rd edition, Springer international, 2018.

[48].Y. Bao, T. Wierzbicki, "On fracture locus in the equivalent strain and stress triaxiality space", Int. J. Mech. Sci. 46 (1) (2004) 81–98.

[49].Y. Bai, T. Wierzbicki, "A new model plasticity and fracture with pressure and Lode dependence", Int. J. Plast. 24 (2008) 1071–1096.

[50].M. Kuna, (2013) Finite Elements in Fracture Mechanics, Solid Mechanics and Its Applications 201, DOI: 10.1007/978-94-007-6680-8_3, Springer Science+Business Media Dordrecht.

[51].Henshell, R.D., and Shaw, K.G., "Crack tip finite elements are unnecessary*", International Journal of Numerical methods in Engineering, Vol.9,495-507,1975.

[52].S. Moahammadi, (2008), Extended finite element method for fracture analysis of structures, Black well publishing, UK.

[53].Cornec, A., Scheider, I., Schwalbe, K.H., On the practical application of the cohesive model, Eng. Fract. Mech. 70 (14) (2003) 1963–1987

3. CRACK PROPAGATION AND BURST PRESSURE OF LONGITUDINALLY CRACKED PIPELINES USING EXTENDED FINITE ELEMENT METHOD

This chapter is derived from a research article published in the International Journal of Pressure Vessels and Piping, Elsevier Science Direct: Okodi, A., Lin, M., Yoosef-Ghodsi, N., Kainat, M., Hassanien ,S., Adeeb, S., Crack Propagation and Burst Pressure of Longitudinally Cracked Pipeline Using Extended Finite Element Method, International Journal of Pressure Vessels and Piping (2020), 10.1016/j.ijpvp.2020.104115.

3.1 Abstract

This paper presents an investigation of the potential of extended finite element method (XFEM) implemented in Abaqus standard software, with maximum principal strain and fracture energy as damage parameters for analysis of crack propagation and prediction of burst pressure in pipelines. Models of API 5L X60 pipe were calibrated first, using data from single edge notched tension test and then using burst pressures from 3 full scale tests. Both calibrations produced low fracture energy and marginally varied strains as XFEM damage parameters. The models were used to predict burst pressures of pipe specimens having varying sizes of longitudinal cracks that were rectangular in profile and located on the external surface of the pipes. Burst pressures were also predicted using analytical methods and the results compared with tests and XFEM predictions. All analytical methods accurately predicted burst pressures of specimens with shallow crack depth but were inaccurate for deeper cracks. XFEM predictions were satisfactory for all specimens. Although few cracks were analyzed, the results show XFEM can be effective for analysis of crack propagation and prediction of burst pressure in pipelines, but investigation using more crack sizes, pipe grades and pipe geometries is recommended for a firm conclusion.

Keywords: Extended finite element Crack propagation Burst pressure Principal strain Fracture energy

3.2 Introduction

Nearly 60% percent of energy consumed in Canada is delivered by pipelines [1,2] and their integrity is essential to energy supply in the country. 17% of Canadian pipeline safety incidents in 2017 were due to cracks [2]. Longitudinal cracks are particularly risky as they are likely to propagate at low internal pressure and careful analysis is paramount to keep affected pipes in service. Currently, there are many integrity models but studies [3-5] show most are conservative for deep cracks and non-conservative for shallow cracks. Caution is needed to avoid costly integrity decisions. Canadian companies did 2557 integrity digs in 2018 [1], some of which could arguably have been avoided with better integrity assessment. Finite element methods (FEM) can accurately simulate fracture in pipelines [6-8] but is widely regarded as tedious for modelling crack growth since it requires re-meshing to match crack geometry. Recently, the extended finite element method (XFEM), has been used successfully [9,10] without the requirement to match crack

geometry, which makes it more suitable for analysis of crack propagation, but its performance in pipelines has not yet been widely investigated.

3.2.1 Overview of the extended finite element method

XFEM uses the concept of partition of unity [11-13] to extend the conventional finite element method and by so doing, eliminates the need for conformity between the mesh and crack geometry. Local enrichment functions and additional degrees of freedom are introduced in FEM formulation, while retaining its core framework and properties such as sparsity [14]. Equation (3-1) shows partition of unity enrichment used to approximate nodal displacement vector function u in a body with a physical crack.

$$u = \sum_{I=1}^{N} N_I(x)\left[u_I + H(x)a_I + \sum_{\alpha=1}^{4} F_\alpha(x)b_I^\alpha\right] \qquad (3-1)$$

$N_I(x)$ is the nodal shape function, u_I the nodal displacement vector associated with the continuous part of the solution; $H(x)$ the discontinuous jump function that bridges over the crack; a_I, the enriched degree of freedom vector over the interior of crack. $F_\alpha(x)$ is the elastic asymptotic crack-tip function and b_I^α is the associated nodal enriched degree of freedom vector at the crack tip. The products $H(x)a_I$ and $F_\alpha(x)\, b_I^\alpha$ represent enrichments applied to nodes that are cut by the crack interior and nodes cut by the crack tip respectively. Implemented in a software, XFEM uses an intra element algorithm to freely lay the crack within the mesh and not tie it to element boundaries, thereby eliminating the need to match its geometry and re-mesh upon propagation [15]. The software searches for regions of crack initiation where stresses or strains exceed a user defined value, after which phantom nodes and their superposed original real nodes move apart as the crack propagates, following a user defined traction separation law (TSL) and evolution criterion.

XFEM in Abaqus standard [14] allows linear, exponential and tabular TSL to be specified. Applicable damage initiation criteria are maximum principal stress (*Maxps*) or strain (*Maxpe*) and maximum nominal stress or strain. Others are quadratic nominal stress, quadratic nominal strain and user defined damage initiation criterion. Supported damage evolution criteria are fracture energy and crack tip displacement. The damage parameters are unknown and are best estimated and optimized by calibration using test results. Cornec, et.al [16] proposed using maximum stress

over a notched tensile bar's instantaneous cross section at fracture as cohesive strength T_0, and criterion for damage initiation. This is equal to the true tensile strength of the bar σ_u, in brittle fracture but is higher in ductile fracture, due to localized necking. The energy release rate $G_{IC} = K_{IC}^2/E'$ is taken as the cohesive energy Γ_0, for brittle material while the J integral, $J_{IC} = K_{IC}^2/E'$ is used for ductile materials, where $E' = E$ for plane stress conditions and $E' = E/(1 - v^2)$ for plane strain conditions. Schwalbe et.al [17] suggested that applicable values of cohesive strength and cohesive energy for ductile materials can be estimated as $T_0 \approx 3\sigma_y$ and $\Gamma_0 \approx K_{IC}^2/E'$ respectively, where σ_y is the yield stress of the material.

Available calibrations of XFEM parameters [7,18] show fracture energy G_c with *Maxps* values ranging from $1.4\sigma_y$ to $4.5\sigma_y$ can satisfactorily simulate crack propagation in ductile materials. Li and Chandra [8] showed that *Maxps* greater than $1.5\sigma_y$ is required to develop significant plastic strains at crack tip in Aluminum Al2024-T3 alloy and that for *Maxps* $>1.5\sigma_y$, resistance to crack propagation is primarily by plastic dissipation of energy while for *Maxps* $<1.5\sigma_y$, resistance is primarily by the fracture energy, G_c. Based on this observation, Li and Chandra [8] claim that value of *Maxps* required to predict brittle fracture is comparable to yield strength; while for ductile fracture, the required Maxps are higher due to necking specimens.

Preliminary studies at the University of Alberta [9,18-19] show XFEM with *Maxps* and fracture energy, G_c as damage parameters can simulate crack propagation in pipelines. Results are obtained with relatively coarse mesh, but the *Maxps* required are sometimes too high compared to measured strength of materials, which seem unrealistic. Liu et.al [10] used XFEM with *Maxpe* to analyze crack propagation in beam specimens of thickness 7mm and 12.5mm extracted from X80 pipeline steel. Their result showed *Maxpe* required to simulate crack propagation increases with decrease in specimen thickness due to decreasing constraint at crack tip. According to Liu et.al, *Maxpe* is more suitable for simulating ductile fracture in pipelines.

This study used XFEM implemented in Abaqus standard [14], with *Maxpe* and fracture energy, G_c as damage parameters to predict burst pressure of three seam welded API 5L-X60 pipe specimens having rectangular shaped cracks on their external surfaces with crack lengths measured along the longitudinal axis of the pipe and crack depths in the thickness direction. Experimental

burst pressures and mechanical properties of the pipe material were known [20]. Analytical models were also used to predict burst pressures and compared with XFEM and test results.

3.2.2 Analytical models for assessing cracks in pipelines

Analytical models employ fracture mechanics principles to predict burst pressure of cracked pipes. The models do not require calibration with test results and are thus good for quick integrity assessment. Material properties, crack geometry and pipe dimensions are used as input parameters to predict remaining strengths of cracked pipes. Assessments are relatively fast, facilitating quicker integrity decision processes. Analytical models used in this study were: Modified NG-18 equation [21], CorLAS [22], and failure assessment diagrams (FAD) level 2B in API-579 [23] and BS7910[24] codes. The Modified NG-18 equation is a semi empirical model that uses Charpy impact energy and flow stress to predict failure pressure. The original version is deemed too conservative and the modified version [25] used in this study (equation 3-2) was released in 2008.

$$\sigma_{fs} = \frac{\left(\frac{\bar{\sigma}}{M_T}\right)\cos^{-1}(e^{-x})}{\cos^{-1}(e^{-y})} \qquad (3-2)$$

Where: $x = \left(\frac{12\frac{CVN}{A_0}E\pi}{8c\bar{\sigma}^2}\right)$ and $y = x\left(1-\left(\frac{d}{t}\right)^{0.8}\right)^{-1}$

$\sigma_{fs}, \bar{\sigma}, M_T, CVN, A_0, E, d, t, \text{and } 2c$ are failure stress, flow stress, Folia's factor, upper shelf impact energy, reference area, Young's modulus, crack depth, wall thickness, and crack length respectively. Flow stress is determined using the formula $\bar{\sigma} = \sigma_y + 68.95MPa$ [25] The predicted failure pressure is the one corresponding to the lowest failure stress. Folia's factor M_T and Fracture toughness K_c are calculated using the following relations.

$$M_T = \frac{1-\frac{a}{tM_t}}{1-\frac{a}{t}}, \text{ while } M_t = \sqrt{\left[1 + 1.255\left(\frac{C_{eq}^2}{Rt}\right) - 0.0135\left(\frac{C_{eq}^4}{R^2t^2}\right)\right]}$$

Equation (3-2) is used to determine failure stress used in equation (3-3) to predict failure pressure P_f of the component.

$$P_f = \sigma_{fs}\frac{2t}{D}\left(\frac{1-\frac{A}{A_0}}{1-\frac{A}{A_0 M_T}}\right) \qquad (3-3)$$

Where $P_f, D, A, t, \sigma_{fs}, A_0, M_T$ are failure pressure, external diameter, crack area, $t, \sigma_{fs}, A_0,$ and M_T are as defined above.

CorLAS [22] uses J integral based fracture toughness for prediction of crack growth and burst pressure with elastic-plastic pipeline materials. Values of applied J integral are iteratively computed using equation (3-4) and compared with fracture toughness, J_{crit} of the material, determined either from tests or by empirical correlations of Charpy impact energy.

$$J = Q_f F_{sf}\left[\frac{\sigma^2 \pi a}{E} + f_3(n) a \varepsilon_p \sigma\right] \qquad (3-4)$$

Where J, Q_f, F_{sf}, σ, a, E, $f_3(n)$, n, ε_p are respectively the J-integral value, elliptical shape factor, free surface factor, local stress, crack depth, Young's modulus, strain-hardening factor, strain hardening exponent, and plastic strain respectively. Failure is predicted when $J=J_{crit}$. CorLAS also predicts failure based on flow stress. Failure is evaluated using both criteria and the smaller value is the predicted failure pressure.

FAD is a graphical method composed of a failure line that relates fracture toughness to material strength. Its abscissa shows progress towards failure by plastic collapse, represented by load ratio L_r associated with the primary stress in the pipe. The ordinate shows progress towards failure by fracture represented by fracture ratio K_r. Where $K_r = \frac{K_I}{K_{mat}}$, $L_r = \frac{\sigma_{ref}}{\sigma_y}$, σ_{ref} is reference stress due to applied load, σ_y the yield strength , K_I is elastic stress intensity factor, K_{mat} is material's fracture toughness. The failure line defines limits of possible combinations of K_r and L_r for the component. Location of assessment point (K_r, L_r) with respect to the failure line determines whether the flawed component is safe or not. Increase in load and or defect size shifts assessment point along a loading path towards the failure line. Figure 3.1 shows a schematic illustration of FAD methodology.

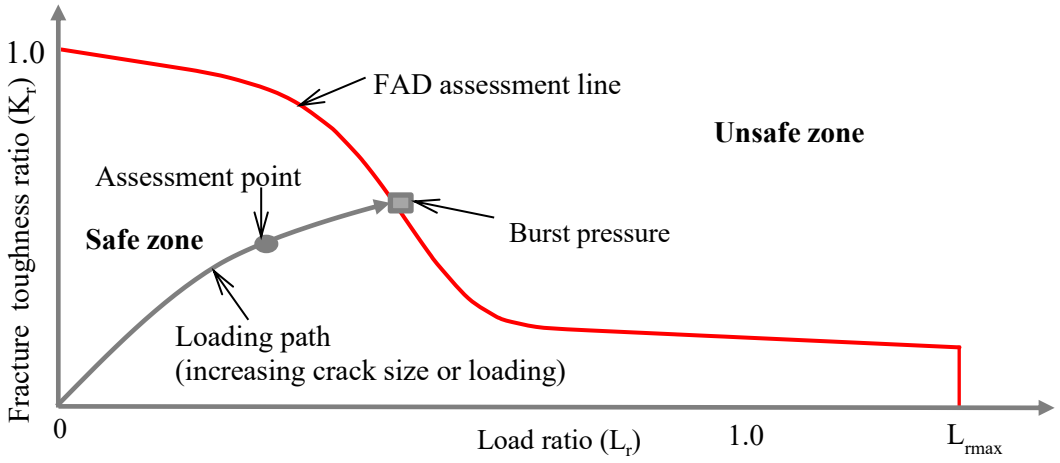

Figure 3.1 Schematic illustration of the FAD methodology

FAD has three levels and sub levels of assessment depending on the desired accuracy and availability of material data. This study used level 2B procedures in BS7910 and API 579 codes. Its failure line is given by equation (3-5).

$$K_r(L_r) = \left(\frac{E\varepsilon_{ref}}{L_r\sigma_y} + \frac{(L_r)^3\sigma_y}{2E\varepsilon_{ref}}\right)^{-0.5} \quad \text{for} \quad 0.0 < L_r \leq L_{rmax} \qquad (3-5)$$

$$K_r(L_r) = 1.0 \quad \text{for} \quad L_r = 0.0$$

K_r, L_r and E are as previously defined, ε_{ref} is load ratio obtained from true stress-strain curve at true stress = $L_r\sigma_y$. L_{rmax} =1.25 for carbon steels. The two codes differ in methods for determining reference stress, σ_{ref}. API 579 reference stress is based on net section collapse criterion while BS7910 reference stress is based on local ligament criterion and has a built-in factor of safety of 1.2 which makes it more conservative.

3.2.3 Overview of experimental data

3.2.3.1 Burst tests

This study used experimental results from literature [20,26], which comprised of three full-scale burst tests conducted at room temperature on longitudinally cracked end capped seam welded API 5L X60 pipes of external diameter D_e = 508mm, wall thickness t =15.8mm, and lengths, L=3m with a 20mm thick steel plate as endcap.

The cracks were created as rectangular notches in three sizes described by their depths and length $(a \times 2c)$: $3mm \times 60mm, (19\%t), 7mm \times 140mm, (44\%t), and\ 10mm \times 200mm, (63\%t)$, at 180 degree location away from the seam weld to minimize effect of weld on properties of base metal near crack. Ultrasonic pulse technique was used to measure crack propagation. Small amounts of ductile tearing prior to failure was reported, indicating intense plastic strains occurred at crack tip. Figures 3.2a and 3-2b are schematic illustrations of a typical specimen. Detailed experiment is reported in [20,26].

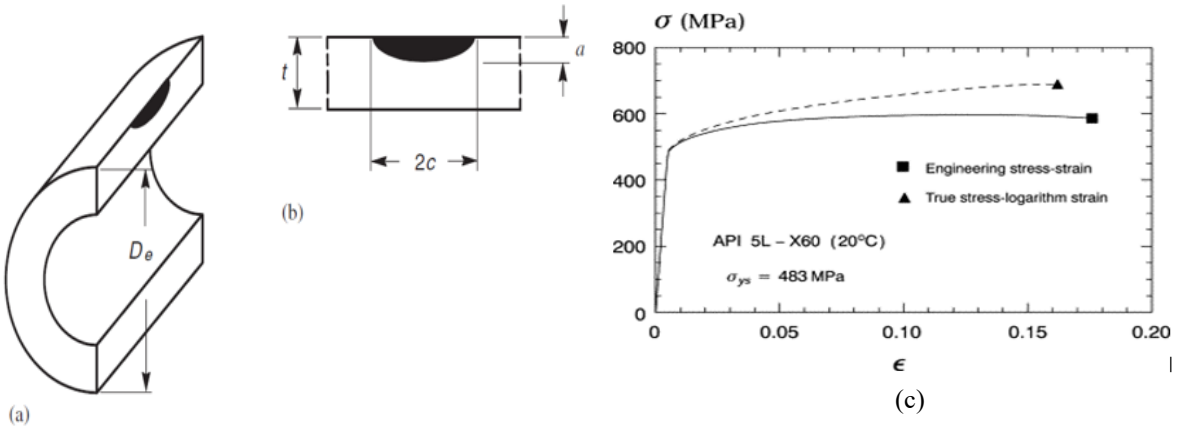

Figure 3.2 (a) and (b); schematic illustration of specimen with crack;(c) Stress-strain curve [20,26]

3.2.3.2 Material properties

Tensile and Charpy V-notch impact tests were used [20] to determine mechanical properties of pipe material given in table 3.1 and the stress-strain curve in figure 3.2c. 13mm thick rectangular specimens extracted in the circumferential direction of the pipe in accordance with ASTM A370 were used in the tensile coupon tests. The material had Young's modulus E=210GPa, and Poisson's ratio $\nu = 0.3$. Fifteen Charpy-V notch impact specimens were tested following requirements of ASTM E23 standard. The material was reported to present a fully ductile fracture behavior with approximate Charpy impact energy of 135J at room temperature. The fracture toughness of the material K_{mat}, was estimated based on provisions in Appendix F of API-579 to be $177MPa\sqrt{m}$ and this value was used in analytical predictions.

Table 3.1 Mechanical properties of API 5L-X60 pipe steel at room temperature [20]

σ_{ys} (MPa)	σ_u(MPa)	ε_t(%)	σ_u/σ_y
483	597	29	1.24

σ_{ys}: 0.2% proof stress; σ_u:ultimate tensile strength; ε_t: uniform elongation (gauge length =50mm)

In using the above test results, the authors were mindful of the following assumptions: that the cracks in the burst test specimens were rectangular and in the longitudinal axis of the pipe; the material properties obtained from the small scale tests were representative of the properties of the full pipe; the pipe was perfectly circular and of uniform wall thickness throughout its entire length. The authors considered internal pressure to be the only external load acting on the pipe.
The severity of cracks on integrity of the pipeline depends on crack geometry and orientation on the pipeline. Longitudinal cracks, being in the plane of the maximum principal (hoop)stress are more severe and would propagate at lower pressure than circumferential cracks. Rectangular cracks are more severe than elliptical cracks because they are associated with greater loss of material from the pipe wall.

The burst pressures used to calibrate and validate the XFEM model were from tests on pipes having longitudinal, rectangular shaped cracks. Changing the defect parameters would lead to a different set of burst test results for use in the calibration and validation of the model, but it would not significantly change the calibrated XFEM damage parameters of the pipe. This was the outcome in this study when calibration was accomplished using burst test results and repeated using crack growth resistance curve from SENT test of the same pipe. In both cases, the fracture strains (*Maxpe*) obtained were of the same order of magnitude and the fracture energies (G_c) were low. However, changing the material property of the pipe would give a different set of XFEM damage parameters because fracture strains vary with material toughness.

3.3 Numerical analysis, results and discussion

3.3.1 Set up of the xfem model

Specimens of longitudinally cracked API 5L- X60 pipes were modelled in Abaqus [14]. The pipe was modelled as elastic-plastic material with isotropic hardening while the endcap was modelled as elastic material of same Young's modulus and Poisson's ratio as pipe.

The model (figure 3.3a), comprised of a deformable solid strip of length 125mm, width 20mm, and thickness 15.8mm coupled to a deformable shell using shell-solid coupling constraint to form pipe. Shell section was offset at top surface and was attached to top edge of the solid strip. A 20mm thick deformable solid plate was tied to the end of pipe as endcap and rigid body constraint was assigned to it to prevent deformation. The longitudinal cracks were formed in the solid strip by embedding a rectangular planar shell with length placed in the longitudinal direction (z-axis) of pipe and depth in thickness direction (y-axis) of the pipe. By combining shell and solid parts in the pipe, it was possible to vary element type and mesh size and reduce computation cost.

Pipelines, being long structures deform radially with negligible change in length when subjected to internal pressure in experiments and in the field. The condition is considered plane strain and there is symmetry in the longitudinal direction (z-axis) of the pipe for both deformed and undeformed configurations.

The symmetry was used to model half of the pipe and further reduce computational cost by applying z-symmetry boundary condition at mid length of the pipe along the circumferential cross section, to restrain deformation in the longitudinal (z) direction and rotation in the radial directions. Pin boundary condition was applied at the end of the pipe to prevent rigid body motion in the x and y directions. Internal pressure was applied cumulatively in small increments to provide static loading.

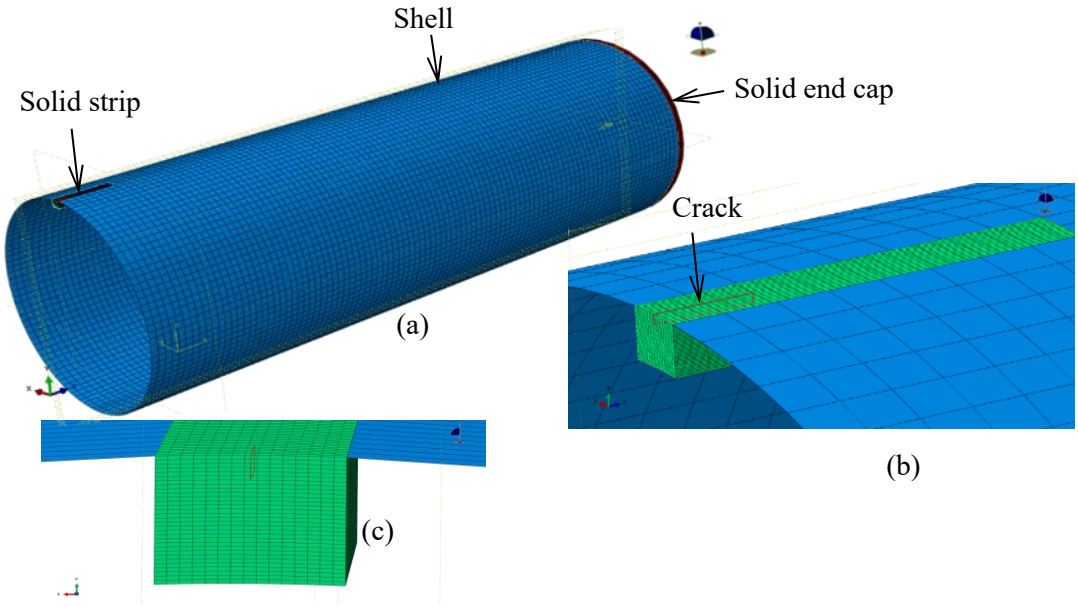

Figure 3.3 Showing (a) model set up and mesh distribution; (b) crack orientation in solid strip; (c) fine mesh in solid strip

3.3.2 Mesh details

Figures 3b and 3c show mesh distribution in the model. Linear brick elements (C3D8R) with reduced integration and hexagonal structured mesh was used in the solid while S4R elements with quad dominated free mesh was used in the shell. Mesh in the solid strip was refined to smaller sizes represented by $l_l \times l_h \times l_t$ to improve accuracy of prediction, where l_l, l_h and l_t are element dimensions in longitudinal, circumferential and thickness directions of pipe respectively. Mesh sensitivity analysis was done to optimize computation cost with respect to accuracy of prediction. Predicted burst pressures stabilized when element size of 2.5mm×1.8mm×0.75mm or smaller was used in the solid strip, resulting into 21 or more elements in thickness direction of the pipe. Instance element sizes of 15mm and 20mm in shell part of the pipe and endcap respectively were satisfactory.

3.3.3 Model calibration and burst pressure prediction

Plasticity was used to model material behavior with fracture strain and fracture energy as damage parameters. A linear traction separation law was used to specify evolution of the damage material to an open crack. Studies [10] show fracture behavior is influenced by material properties and

specimen geometry, thus, XFEM damage parameters are best estimated and optimized by calibration with test results. This is usually accomplished by numerically fitting experimental results, like load versus crack tip opening displacement (CTOD) or crack mouth opening displacement (CMOD) curves. Schwalbe et.al [17] recommend use of crack growth resistance curve (R-curve) since they do not vary a lot with specimen configuration. Agbo et.al [19] used similar procedure to calibrate *Maxpe* and G_c parameters of API X42 pipe and successfully used it to predict the experimentally obtained tensile strain capacity of the pipe. Liu et.al [10] calibrated damage parameters (*Maxpe* and G_c) of X80 pipe using load versus CMOD curve obtained from small-scale three-point bending test of beams extracted from the pipe material. Ameli et.al [18] used CTOD curves from SENT tests to calibrate damage parameters (*Maxps,* G_c) of API X42 pipe.

This study used results of SENT [15,18] and burst tests separately to calibrate XFEM damage parameters (*Maxpe* and G_c) of API X60 pipe. First, the load versus CMOD curve from SENT test [27] was numerically fitted by trial and error. *Maxpe*=0.034 with G_c=150N/mm satisfactorily fitted the experiment and were used as damage parameters of the pipe to predict burst pressures. It's interesting to note that the calibrated G_c =150N/mm is close to the critical J integral (149N/mm) estimated from fracture toughness and CVN value of the material. Figure 3.4 shows Von Misses stress distribution in the XFEM model and the fitted Load versus CMOD curve of the SENT test. The second calibration process used burst test results to estimate damage parameters without recourse to small scale tests. Each of the three burst tests specimens was modelled in XFEM. Damage parameters were adjusted until values that satisfactorily predicted the specimen's burst pressure were obtained. It was quickly established that small changes in *Maxpe* affected burst pressure more than large changes in G_c. High values of G_c with the same *Maxpe*, did not significantly change predictions. Li and Chandra [8] assert that crack growth resistance in ductile materials is primarily by its cohesive strength. Therefore, the calibration process sought to maximize *Maxpe* and keeping G_c as low as possible.

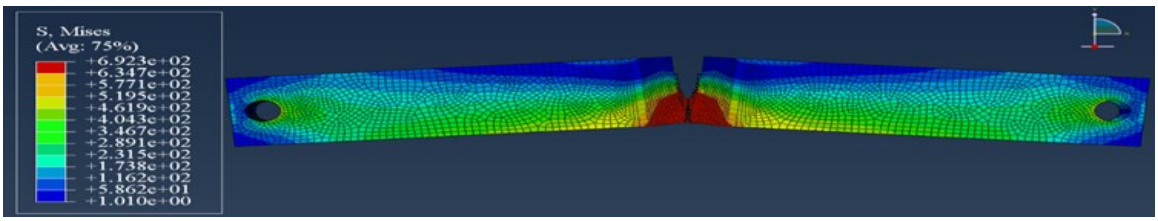

(a)

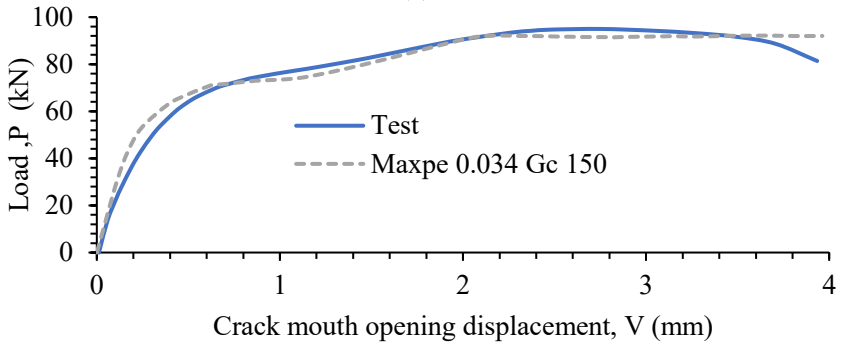

(b)

Figure 3.4 Showing (a) Stress distribution in SENT model, (b) Load-CMOD curves

Table 3.2 shows burst pressures and stress triaxialities, obtained using specimen specific damage parameters. Triaxiality $(\eta) = \sigma_p/\sigma_{eq}$ where $\sigma_p = (\sigma_{11} + \sigma_{22} + \sigma_{33})/3$, where σ_p is the pressure on an element, σ_{eq} is the corresponding Von Mises stress, σ_{11}, σ_{22}, and σ_{33} are principal stresses. *Maxpe* values were higher in the deeply flawed specimens, a sign of a more ductile fracture behavior [10]. The average of the three specimens' damage parameters was: *Maxpe* = 0.0383 and G_c = 23.33N/mm and were used as API X60 pipe's parameters.

Table 3.2 Burst pressure and triaxiality predicted with specimen-specific damage parameters

Crack (mm×mm)	Damage parameters		Pressure (MPa)			Triaxiality at start of propagation
	Maxpe (mm/mm)	G_c (N/mm)	At fracture of crack tip element	At burst	Burst test	
3×60	0.02	50	33.1	33.8	31.5	1.132
7×140	0.03	10	23.8	25.6	25	1.235
10×200	0.065	10	19.2	20.1	21	1.024
Average	0.0383	23.33				

Damage parameters obtained in the two calibrations varied. This is in part a result of using burst pressures obtained from single tests in the second method. Load and strength are random variables [28], thus burst tests repeated with the same size of crack are likely to give varied results. In addition, crack orientation in thin walled pipes may vary during propagation [17] such that an initially planar flat crack may get inclined to the load direction as it propagates. Its therefore erroneous to assign a burst pressure to a crack based on a single test; the mean of a series of tests would be more appropriate. Estimation of the inherent error in calibrated damage parameters caused by using few test results is beyond the scope of this work.

Tables 3.3a and 3.3b show burst pressure predicted using the two sets of damage parameters. The two sets of damage parameters are equally accurate when used to predict burst pressure, with absolute average error in prediction of 11.5% and 11%. Accuracy of the second calibration is of course a result of using burst pressures to estimate the damage parameters.

Table 3.3a Burst pressures predicted with damage parameters derived from SENT test

Crack (mm×mm)	Predicted pressure (MPa)	Test pressure (MPa)	Error in prediction (%)
3×60	35.6	31.5	+13.0
7×140	28	25	+12.0
10×200	19	21	-9.5
Average error (absolute)			11.5

Table 3.3b Burst pressures and triaxiality predicted with average of specimen-specific parameters

Crack (mm×mm)	Pressure (MPa)			Stress triaxiality at crack	
	At damage of crack tip element	At burst	Error in prediction (%)	At start of pressurization	At start of propagation
3×60	32.6	35.2	+11.7	0.97	1.11
7×140	24.6	26.9	+7.6	1.33	1.19
10×200	14.5	18.1	-13.8	1.43	1.22
Average error (absolute)			11		

It is clear from table 3.2 that the specimen-specific XFEM damage parameters vary with crack geometry. The damage parameters required to accurately predict propagation of the shallow

cracks are lower than those for the deep cracks, which shows that failure mechanisms for cracked specimens vary with crack geometry. Cravero and Ruggieri [20], observed that significant ductile tearing accompanies failure of specimens with deep cracks while no tearing occurs as specimens with shallow cracks fail.

The results in table 3.3 were obtained using a single set of damage parameters for all specimens. As observed above, the damage parameters that best predict test results vary with crack geometry. Therefore, using a single set of damage parameters across different sizes of cracks could be inaccurate for some of the cracks. The error could be mitigated by varying the damage parameters automatically during the analysis to avoid using the same parameters for all cracks. One example would be to use stress triaxiality at the crack tip as a criterion for material damage and crack propagation. The software would analyze the stress distribution at crack tip and the crack would propagate if the triaxiality exceeds a threshold value. This would eliminate the need to calibrate damage parameters altogether but is currently not a capability of the XFEM methodology in Abaqus [14]. In absence of such capability, it is recommended to ensure that data used to calibrate and validate the models are accurate by repeating tests and taking the average.

The pipe was also analyzed using a fully solid model and using a shell solid coupled model in which the shell section was offset at the mid surface. Additionally, the solid endcap was replaced with a planar shell to assess its effect on burst pressure. Figure 3.5 shows variation of burst pressures with crack depth for the different cases. There was no significant difference between burst pressures predicted using SENT derived fracture parameters and average of specimen specific parameters as seen from figure 3.5a. Similarly, changing solid end cap to shell endcap did not significantly alter the burst pressure (figure 3.5b) because rigid body constraint was used in both. There was 4 to 8 % increase in burst pressure of the three specimens when fully solid model was used compared to model predictions with shell section offset at top surface. The highest increment was observed in the specimen with 10mm×200mm crack (figure 3.5c).

Similar increments were observed upon analysis with shell solid coupled model in which shell section was offset at mid surface, proving that shell elements work best when the section is offset at mid surface, and that shell solid coupling constraint has no significant effect on burst pressure. The drawback is in the increased analysis time, yet the results are similar. For the pipe with

3mm× 60mm crack, with the fully solid model, the analysis was 9 times longer than when the shell section was offset at top surface. With shell section offset at mid surface, the analysis time was 4 times longer. The analysis time for all models reduced with increasing crack depth and decreasing size of remaining ligament.

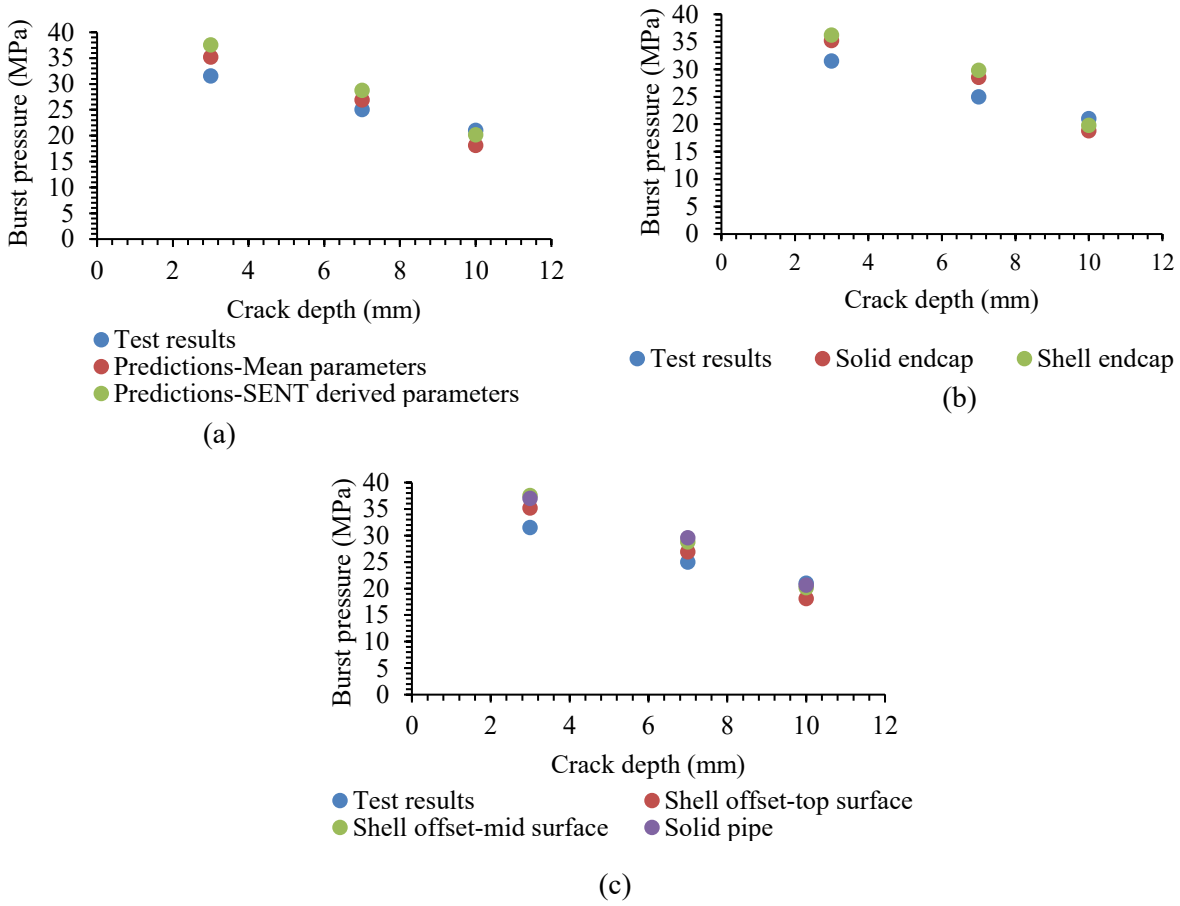

Figure 3.5 Showing variation of burst pressure with crack depth (a) for SENT and pressure derived damage parameters (b) with solid and shell endcaps (c) with fully solid model, and models with shell sections offset from mid-surface and top surface

Fracture strain(ε_f) varies with stress triaxiality (η) [29-33], with the simplest general relationship usually taking the form $\varepsilon_f = \beta e^{-\alpha\eta}$, where α and β are constants, determined by calibration. The relationships show fracture strains are low at high triaxialities, which is synonymous with tensile loading. Figure 3.6 shows 2-dimensional fracture loci of selected materials, reproduced here to demonstrate variation of fracture strains with triaxiality in the tensile loading regime.

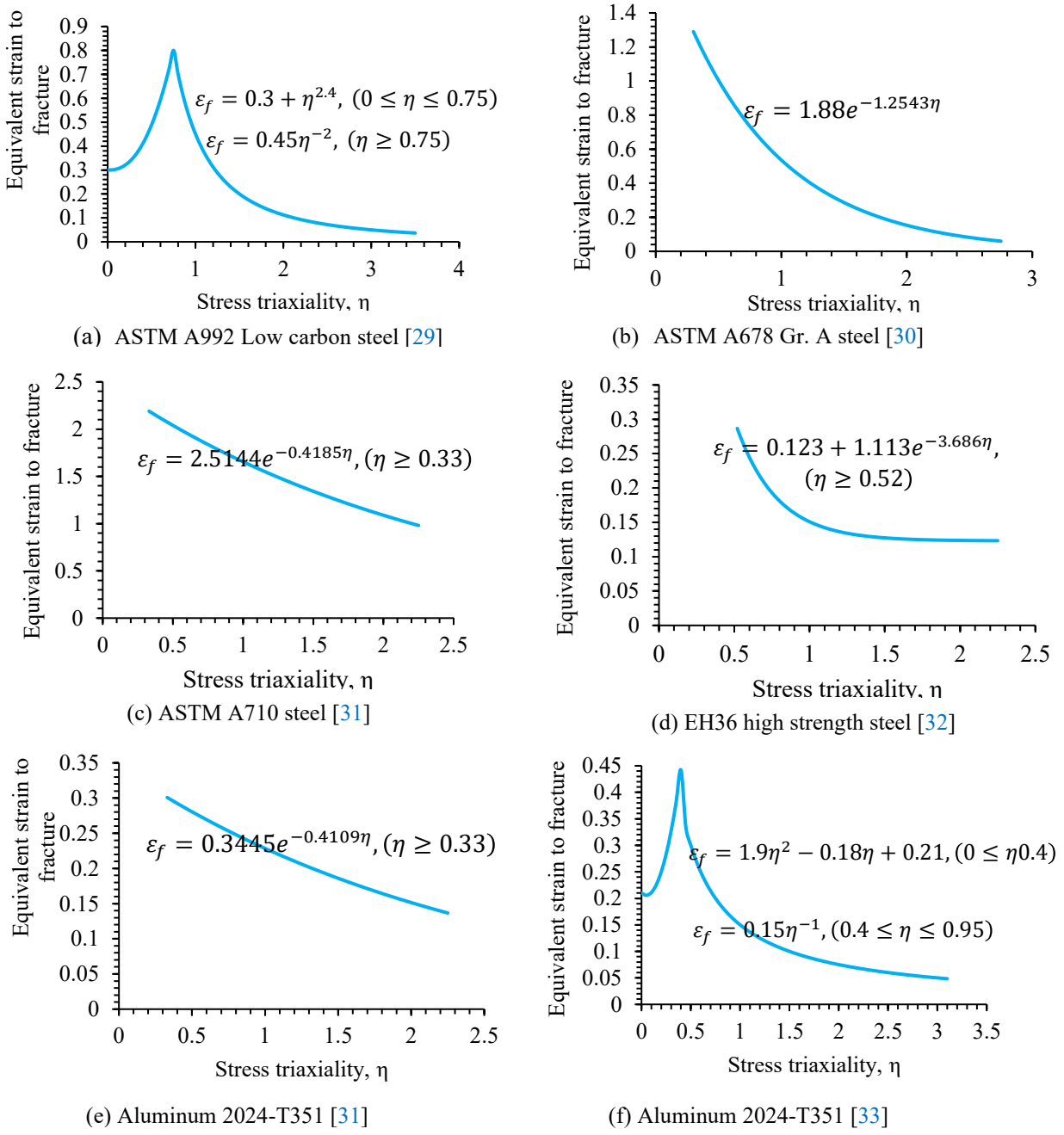

Figure 3.6 Showing 2-dimensionl fracture loci in the higher stress triaxiality regime

High triaxialities($\eta \ge 1$) were observed in all specimens, showing tensile stresses were dominant and the cracks were constrained, resulting in low fracture strains. For the specimens with 3mm×60mm and 7mm×140mm cracks, table 3b shows there was little difference between pressure at onset of crack propagation, when the crack tip element is damaged, and pressure at full crack propagation, when the last ligament element is damaged. This is because fracture energy was low,

and propagation was controlled by fracture strain. The corresponding difference in pressure was higher in the specimen with 10mm×200mm crack showing it exhibited a more ductile fracture behavior. Stress triaxiality in the specimen dropped with crack growth, allowing larger plastic straining in the specimen (more ductility) and improved fracture resistance.

Figure 3.7 shows variation of Von Mises stress and equivalent plastic strain in the remaining ligament of different specimens. 0% ligament loss is the point of imminent propagation: the crack-tip is open, but no propagation has taken place. 75% ligament loss is the point at which 25% of the original ligament length remains. The remaining ligament lengths at that stage were 2.6mm, 1.6mm and 0.5mm in specimens with 3mm×60mm, 7mm×140mm and 10mm×200mm cracks respectively.

Investigation of the curves shows that Von Mises stress hovered between 200MPa and 700MPa as the crack propagated through the specimens. However, equivalent plastic strains in the different specimens, differed greatly. Plastic deformation before crack propagation (0% ligament loss) was negligible in all specimens. At 75% ligament loss, plastic deformation was highest in the specimen with 3mm×60mm crack (PEEQ = 40%), and lowest in the one with 10mm×200mm crack with equivalent plastic strain of 10%. Thus, crack propagation in all specimen occurred with some plastification at crack tip. Ultrasonic measurements during burst tests [20], showed small ductile tearing (0.5mm-1mm) occurred in all specimens, providing evidence that significant plasticity preceded crack propagation and failure was controlled by plastic collapse rather than unstable fracture. However, the varied levels of equivalent plastic strains observed in this study showed plastic collapse was more likely in the shallow cracked specimens.

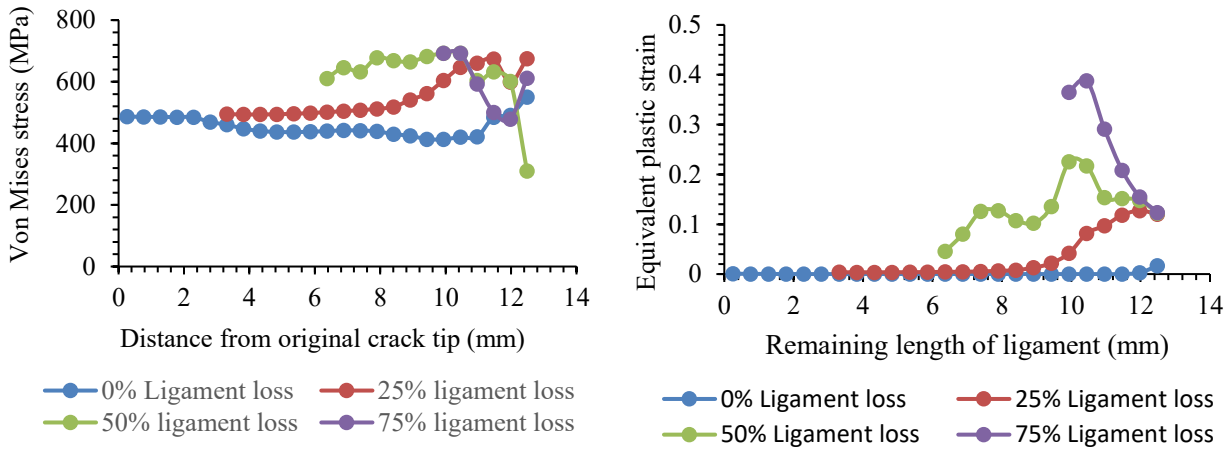

(a) Specimen with 3mm×60mm crack

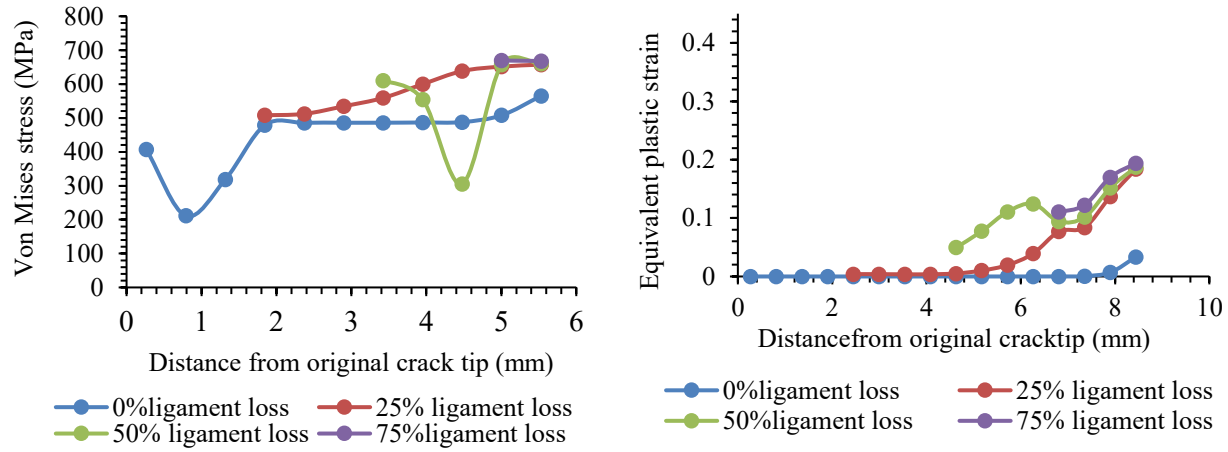

(b) Specimen with 7mm×140mm crack

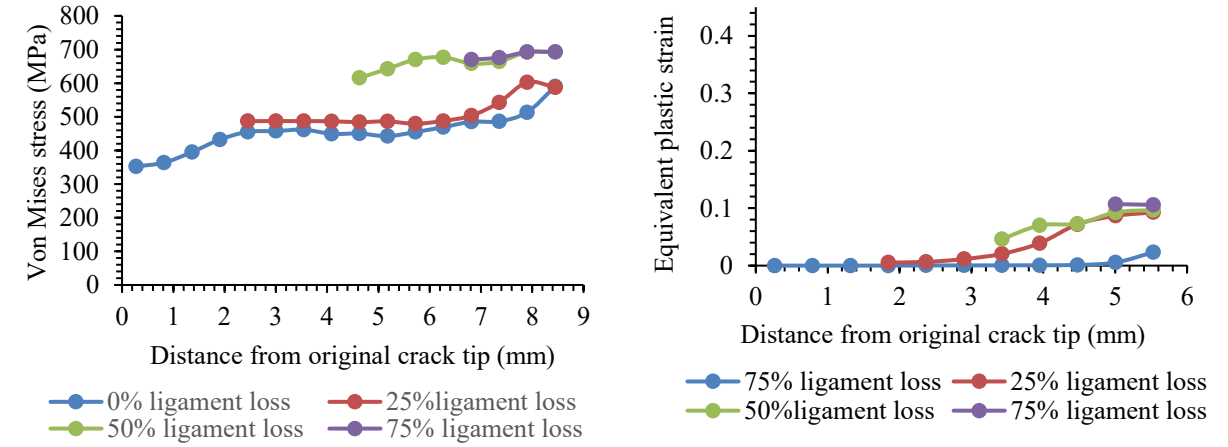

(c) Specimen with 10mm×200mm crack

Figure 3.7 Variation of von Mises stress and equivalent plastic strain with distance from crack tip

Figure 3.8 shows contours of Von Mises stress in the three specimens at failure. Large stresses in the deeply cracked specimens were limited to the neighborhood of the crack but covered a wider area of pipe wall in the specimen with 3mm×60mm crack. The difference in the response of the specimens is attributed to the varied magnitudes of internal pressure they sustained before failure. Visible radial upward displacement of the pipe wall occurred in all specimens due to plasticization and was more pronounced in specimen with 3mm×60mm crack compared to the deeply cracked specimens. This provides evidence that the mode of failure in the pipes varied with size of crack. Yielding of ligaments in the deeply cracked specimens was limited to the neighborhood of the crack with the rest of the pipe remaining elastic until the last elements in the ligaments were fractured. In the specimen with shallow crack, yielding of the entire pipe wall occurred before the last 25% of the remaining ligament was damaged. Therefore, fracture in the deeply cracked specimens were likely to be accompanied with ductile tearing of the ligaments, while in the specimen shallow crack, fracture was accompanied by plastic collapse of part of the remaining ligament due to the high pressure it sustained before failure. Available studies [34] show pipes with deep cracks are susceptible to failure by fracture and those with shallow cracks are susceptible to plastic collapse.

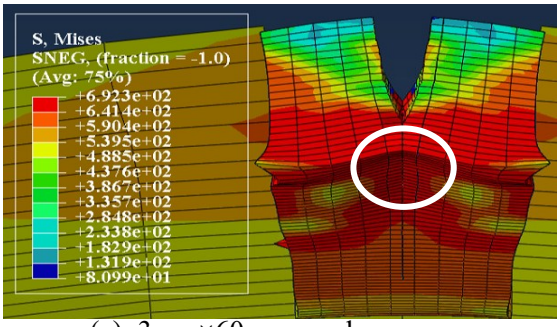

(a) 3mm×60mm crack

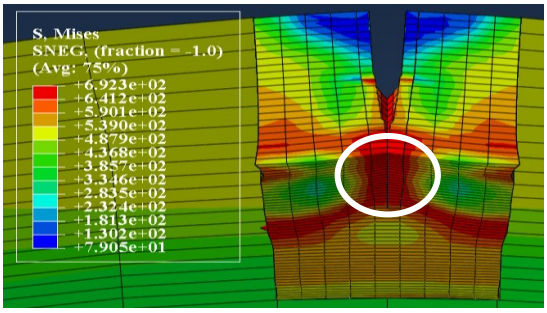

(b) 7mm×140mm crack

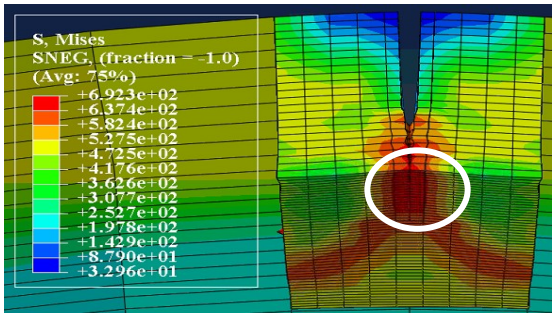

(c)10mm×200mm crack

Figure 3.8 Showing distribution of Von Mises stresses and upward displacement of internal surfaces (encircled)

The specimens were also analyzed using Modified NG-18 equation, CorLAS and FAD Level 2B methodologies in BS7910 and API 579 codes. Table 3.4a shows burst pressures of the three specimens obtained using different methods. Table 3.4b shows the corresponding burst pressure ratios (BPR) determined by dividing the test result by the predicted burst pressure. BPR >1 show prediction less than test result and such prediction is considered conservative. BPR<1 show non-conservative predictions. The means of the burst pressure ratios were used to characterize bias in predictions.

Table 3.4a Measured and predicted burst pressure (XFEM parameters: Maxpe/Gc =0.034/150)

Crack (mm×mm)	Burst pressure (MPa)					
	Test	XFEM	API 579 FAD	BS7910 FAD	CorLAS	Modified NG-18 equation
3×60	31.5	35.6	34.4	30.4	34.2	30.5
7×140	25	28	27	22	25.6	19.4
10×200	21	19	21	7.9	17.2	10.8

Table 3.4b Burst pressure ratios

Crack (mm×mm)	XFEM	API 579 FAD	BS7910 FAD	CorLAS	Modified NG-18 equation
3×60	0.885	0.916	1.036	0.921	1.033
7×140	0.893	0.926	1.136	0.977	1.289
10×200	1.105	1	2.658	1.221	1.944
Mean	0.961	0.947	1.61	1.04	1.422

Figure 3.9 compares burst pressure ratios of different methods with test results. All models satisfactorily predicted burst pressure of specimen with 3x60mm crack. Error in prediction increased with crack depth. XFEM and API-579 FAD Level 2B and CorLAS were non conservative for specimens with 3mm×60mm and 7mm×140mm cracks but conservative for the specimen with 10mm×200mm crack. BS7910 FAD Level 2B and Modified NG-18 equation were conservative for all specimens, with BS7910 being the most conservative. Previous studies [20] show analytical models are accurate for predicting burst pressure of pipelines with shallow cracks but are generally inaccurate and conservative for deep cracks, which is consistent with the findings

of this study. Analytical models can therefore be relied upon for assessment of shallow cracks as they are relatively easy to use and do not require calibration with tests.

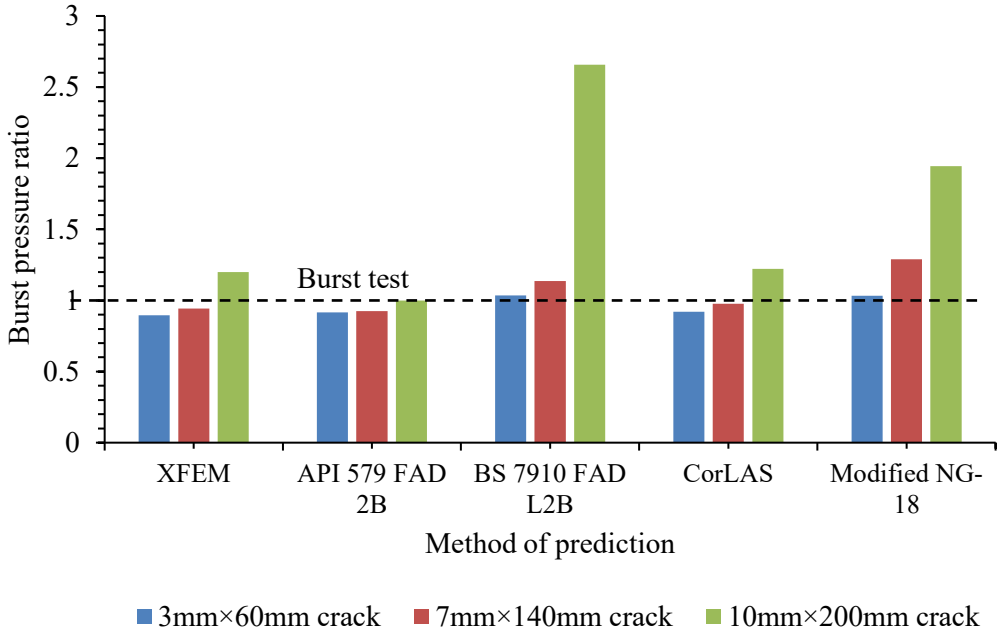

Figure 3.9 Comparison of predicted and test burst pressures

Failure of analytical models to predict burst pressure of specimens with deep cracks is mainly attributed to their inability to include ductile tearing in the analysis [20,34]. Additionally, FAD being a fitness for service model is by design conservative when used for failure analysis. The BS7910 FAD methodology applies a factor of safety of 1.2 for reference stress which makes it especially conservative when used for failure analysis. Accuracy of CorLAS prediction depends on how close the geometry of the crack in the model matches the geometry in the pipe. Rectangular cracks were used in this study and the geometry was accurately defined in the model.

Overall, satisfactory prediction of burst pressures of the three specimens were obtained using XFEM, CorLAS, and API 579 FAD Level 2B. All had mean BPR within ±5% of the test results (BPR =1), which is a bit conservatively biased but acceptable. Modified NG-18 equation and BS7910 FAD Level 2B were especially conservative for deep cracks, with mean BPR of 1.42 and 1.61 respectively.

Zijian et. al [5] assessed error in burst pressure predicted by various models and found CorLAS to most accurate while NG-18 and BS7910 FAD were inaccurate and conservative. Yan et.al [35] found CorLAS accurate, precise and less conservative for rectangular cracks than API579 FAD and Modified NG-18 equation. Bedairi et.al [34] used FEM, to predict onset of crack propagation in a 5.7mm thick, 508mm diameter APIX52 pipe, with four 200mm long cracks of depths 38%wall thickness (t), 47%t, 48%t and 51%t. The result showed all specimens failed by plastic collapse, and all predictions were conservative, with conservativeness increasing with crack depth. Fracture occurred in all specimens in this study. The specimens were thick (t =15.8mm), highly constrained resulting in low fracture strains [10], depicted by high stress triaxiality. But failure modes varied with crack depth. Specimens with crack depths of 7mm×140mm (44%t) and 10mm×200mm (63%t) failed by ductile fracture, while failure in the specimen with 3mm×60mm (19%t) crack occurred by ductile fracture with plastic collapse of the last 25% of ligaments, demonstrated by significant upward push of the internal surface of the pressurized pipe (figure 3.8).

3.4 Conclusion

Burst pressures of 3 API 5L X60 pipe specimens having longitudinal rectangular cracks were predicted using XFEM and analytical methods. The predictions were compared with burst test results to assess potential of XFEM (with *Maxpe* and G_c as damage parameters) implemented in Abaqus for analyzing crack propagation and prediction of burst pressure in pipelines. Calibration of XFEM models were accomplished using load versus crack mouth opening displacement curves from SENT test of samples extracted from the pipe and then using measured pressures from full scale burst tests.

The pipe fractured at low strain and low energy. Fracture strains obtained using the two calibration approaches were similar, but fracture energies varied widely. Calibration using SENT data gave a fracture energy of 150N/mm. Fracture energy obtained using the burst test data was very low compared to fracture toughness of the material. The difference is attributed to the limited data used in the calibration. It is expected that using more burst tests in the calibration would bring the energy closer to the fracture toughness of the material. In absence of extensive full scale burst test data, it is recommended that small scale tests of the material are used to calibrate the XFEM damage parameters.

All analytical models used in the study satisfactorily predicted burst pressures of the specimen with shallow crack and regardless of the method, accuracy of prediction reduced as the crack depth increased. Only API 579 Level 2B FAD, CorLAS, and XFEM were accurate for the deeply cracked specimens. Modified NG-18 equation and BS7910 Level 2B FAD were too conservative for specimens with deep cracks.

Although few cracks were analyzed, the results show XFEM can be effective for analysis of crack propagation and prediction of burst pressure in pipelines, but an investigation using more crack sizes, pipe grades and pipe geometries is recommended for a firm conclusion. Our future work will focus on assessment of combined cracks and dents and implementing a new XFEM damage criterion based on stress triaxiality in Abaqus to eliminate the need for calibration.

3.5 References

[1].Canadian Energy Pipeline Association, Transmission Pipeline Industry Performance Report, 2018.

[2].National Energy Board, Canada, Annual Report to Parliament, 2017, p. 18.

[3].A.B. Rothwell, R.I. Coote, A critical review of the assessment methods for axial planar surface flaws in pipe, in: Paper#21009, 52, Pipeline Technology Conference, Ostend, Belgium, 2009.

[4].T. Samarth, G. Ming, K. Ravi, K. Shahani, R. Kania, Evaluation of existing fracture mechanics models for burst pressure predictions, theoretical and experimental aspects, in: IPC2014-33563 Proceedings of the 10th International Pipeline Conference, Calgary Canada, 2014.

[5].Y. Zijian, S. Zhang, W. Zhou, Model Error Assessment of Burst Capacity Models for Energy Pipelines Containing Surface Cracks, International Journal of Pressure Vessels and Piping, 2014.

[6].R.D. Henshell, K.G. Shaw, Crack tip finite elements are unnecessary*, Int. J. Numer. Methods Eng. 9 (1975) 495–507.

[7].T.R. Hojjati, S. Cooreman, D. Van Hoecke, Finite element simulation of dynamic brittle fracture in pipeline steel: a XFEM-based cohesive zone approach, J. Mater.: Design and Applications 232 (5) (2018) 357–370.

[8].H. Li, N. Chandra, Analysis of crack growth and crack-tip plasticity in ductile materials using cohesive zone models, Int. J. Plast. 19 (2003) 849–882.

[9].M. Lin, S. Agbo, J.J.R. Cheng, N. Yoosef-Ghodsi, S. Adeeb, Application of the extended finite element method (XFEM) to simulate crack propagation in pressurized steel pipes, in: Proceedings of ASME 2017 Pressure Vessels and Piping Conference, volume 3B, 2017.

[10].X.B. Liu, H. Zhang, Y. Han, M. Xia, Y. Ji, Numerical and Experimental study on critical crack tip opening displacement of X80 pipeline steel, Mechanika 23 (2) (2017) 204–208, 2017.

[11].T.P. Fries, T. Belytschko, The extended/generalized finite element method: an overview of the method and its applications, Int. J. Numer. Methods Eng. (2000) 1–6.

[12]. J.M. Melenk, I. Babuska, The Partition of Unity Finite Element Method: Basic Theory and Applications, Computer methods in Applied mechanics and Engineering, 1996.

[13].N. Moes, J. Dolbow, T. Belytschko, A finite element method for crack growth without remeshing, Int. J. Numer. Methods Eng. 46 (1999) 131–150.

[14].Abaqus 6.14, Documentation,2014. Dassault Systèmes

[15].Z. Zhang, J. Xu, B. Nyhus, E. Østby, SENT (single edge notch tension) methodology for pipeline applications, in: Proceedings of the 18th European Conference on Fracture, Dresden, Germany, 2010.

[16].A. Cornec, I. Scheider, K.H. Schwalbe, On the practical application of the cohesive model, Eng. Fract. Mech. 70 (14) (2003) 1963–1987.

[17].K.-H. Schwalbe, I. Scheider, A. Cornec, The SIAM Method for Applying Cohesive Models to the Damage Behavior of Engineering Materials and Structures, GKSS 2009/1, 2009. ISSN 0344-9629.

[18].I. Ameli, A. Behrouz, M. Lin, S. Sylvester Agbo, R. Cheng, D. Da-Ming, S. Adeeb, Estimation of the CTOD- crack growth curves in SENT specimens using the extended finite element method, Int. J. Pres. Ves. Pip. 169 (2019) 16–25.

[19].S. Agbo, M. Lin, I. Ameli, A. Imanpour, D.-M. Duan, J.J.R. Cheng, S. Adeeb, Evaluation of the Effect of Internal Pressure and Flaw Size on the Tensile Strain Capacity of X42 Vintage Pipeline using Damage Plasticity Model in Extended Finite Element Method (XFEM). PVP2019-94005, Proceedings of the ASME 2019 Pressure Vessels & Piping Conference, July 2019, San Antonio, Texas, USA.

[20].S. Cravero, C. Ruggeri, Structural integrity analysis of axially cracked pipelines using conventional and constraint-modified failure assessment diagrams, Int. J. Pres. Ves. Pip. 83 (2006) 607–617.

[21].J.F. Kiefner, W.A. Maxey, R.J. Eiber, A.R. Duffy, “Failure Stress Levels of Flaws in Pressurized Cylinders,” American Society of Testing and Materials Report No, ASTM STP 536, 1973, pp. 461–481.

[22].C.E. Jaske, CorLAS User Manual, 2010, Version 2.25.

[23].ASME. “Fitness-For-Service, API Recommended Practice 579-1/ASME FFS-1 2007, second ed.”, The American Society of Mechanical Engineers, New York, USA, June 2007.

[24].B.S.I. BS7910, Guide to Methods for Assessing the Acceptability of Flaws in Metallic Structure, British standards institution, London, UK, 2005. July 2005.

[25].J.F. Kiefner, “Defect Assessment – Conclusion: Modified Ln-Secant Equation Improves Failure Prediction” Oil and Gas Journal, 2008.

[26].F. Dotta, C. Ruggeri, Structural Integrity assessment of high-pressure Pipelines with axial flaws Using a micromechanics model, Int. J. Pres. Ves. Pip. 81 (2004) 761–770.

[27].S. Cravero, C. Ruggeri, Evaluation of crack growth resistance cures of pipeline steels using constraint designed fracture specimens, in: IPC2006-10075, Proceedings of the 6th International Pipeline Conference, September 2006 (Calgary, Alberta, Canada).

[28].S. Abdelatif Hassanien Sherif, S. Adeeb, Probabilistic-based assessment of Corroded Pipelines: a comparison between closed form and surrogate limit states, in: IPC2006-10247, Proceedings of the 6th International Pipeline Conference, September 2006 (Calgary, Alberta, Canada).

[29].K. Ravi, K. Kapil, Computational models for ductile fracture prediction in structural engineering applications, Procedia Material Science 3 (2014) 1947–1955.

[30].Andrzej, G. Jaroslaw, L. Sebastian, D. Ihor, Estimation of the onset of crack growth in ductile materials, MDPI J. Materials 11 (2018) 2026.

[31].Y. Bai, T. Wierzbicki, A new model plasticity and fracture with pressure and Lode dependence, Int. J. Plast. 24 (2008) 1071–1096.

[32].J. Choung, W. Nam, D. Lee, C.Y. Song, Failure strain formulation via average stress triaxiality of an EH36 high strength steel, J. Ocean Eng. 91 (2014) (2014) 218–226.

[33].Y. Bao, T. Wierzbicki, On fracture locus in the equivalent strain and stress triaxiality space, Int. J. Mech. Sci. 46 (1) (2004) 81–98.

[34]. B. Bedairi, D. Cronin, A. Hosseini, A. Plumtree, Failure prediction for crack-in corrosion defects in natural gas transmission pipelines, Int. J. Pres. Ves. Pip. 96–97 (2012) 90–99.

[35].J. Yan, S. Zhang, S. Kariyawasam, M. Pino, T. Liu, Validate crack assessment models with in-service and hydrotest failures, in: IPC2018-78251, Proceedings of the 12th International Pipeline Conference, September 2018 (Calgary, Alberta, Canada).

4. EXTENDED FINITE ELEMENT INVESTIGATION OF BURST PRESSURE OF PIPELINE WITH COMBINED DENT AND CRACK DEFECTS

This chapter is derived from the published conference proceeding: Okodi, A., Cheng, J.J.R., Li, Y., Kainat, M., Adeeb, S., Yoosef-Ghodsi, N., Extended Finite Element Investigation of Burst Pressure of Pipeline with Combined Dent and Crack Defects, Proceedings of the ASME 2020 Pressure Vessels & Piping Conference, July 19-24, 2020, Minneapolis, Minnesota, USA, PVP2020-21318.

4.1 Abstract

Cracks within dents (dent-crack) are more degrading of pipeline integrity than the individual dents or cracks that form them since the constituting dents and cracks augment the degrading effect of each other. Dent-crack defects composed of a longitudinal crack in dent are critical for pipelines because the affected pipelines have a higher probability of mode 1 fracture under internal pressure. Currently, no analytical models for assessing integrity of pipelines with dent-crack defects exists, yet models for cracks or dents occurring separately are not applicable. The ASME B31.4 code recommends removal of the flawed pipeline sections without fitness for service assessment. However, recent experimental and finite element studies show there are sizes of cracks and dents for which the flawed sections remain serviceable, suggesting the ASME B31.4 code is conservative. In the classical finite element method, the crack domain is re-meshed each time the crack propagates, which makes the analysis tedious. The more recently developed extended finite element method offers a robust algorithm which eliminates the requirement to re-mesh crack domain upon propagation. This study explored the capability of the existing extended finite element method implemented in Abaqus standard software for burst pressure prediction for pipelines with dent-crack defects, considering different crack sizes and locations in a dent.

Key words: Dents, cracks, strength, integrity, extended finite element, internal pressure

Nomenclature

XFEM	Extended Finite Element Method
EDM	Electro-Discharging Machine
LVDT	Linear Variable Differential Transducer
ASME	American Society of Mechanical Engineers
ASTM	American Society for Testing and Materials
API	American Petroleum Institute
BSI	British Standards Institution
FEA	Finite element Analysis
Maxpe	Maximum principal strain
Maxps	Maximum principal stress

G_c	Fracture energy
D	Outside/external diameter
t	Pipe thickness
P_y	Yield pressure
E	Young's Modulus

4.2 Introduction

Mechanical damage by external interference such as impact of excavator bucket on pipe surfaces during repair digs and laying of pipes on rocks is a major source of dents and other defects in pipelines. Dents may occur alone, as plain dents, or in combination with other defects (Figure 4.1). An example combined defects is the dent-crack which is a combination of dent and crack within the same region of the pipe wall. A lot of research has been conducted on the effects of dents and cracks on the integrity of pipelines and several widely accepted models have been developed. Some of the models, like failure assessment diagram have been developed into engineering codes of practice such as the API 579[1] and BS7910 [2].

Dents are synonymous with stress concentration and large plastic strains in pipelines, which are conditions for crack initiation and growth [3]. Studies show that shape of dent affects location of peak stress, strain inside the dent and path of possible crack initiation and growth under internal pressure [4-6]. This is the rationale for strain-based evaluation of in line inspection (ILI) data to determine possibility of presence of combined defects such as dent-crack, dent-gouge, or dent-corrosion from inline inspection data [3]. Sharp and strong signals indicate the dent is accompanied with a crack, while in the cases where the signal strength is strong but distributed, a gouge is likely to be inside the dent. Combined defects are more severe on the integrity of pipelines that plain defects. Vilkys et.al [7] showed that gouge depths greater that 50% of wall thickness lead to stresses above the yield strength of the pipe material and are likely to initiate crack growth under normal operating pressure.

The maximum principal stresses developed in the gouge are amplified in the presence of dents. Therefore, a dent-gouge defect increases the risk of crack initiation and propagation under normal operating pressure even where the gouge depths are less than 50% of wall thickness. Hoff et.al [8] also showed that the driving force, represented by the hoop stress increases with internal

pressure and is higher in pipelines with dents and gouges than in pipelines with plain gouges alone. Thus, very small gouges in dented pipelines will significantly reduce the fatigue and burst strength of the pipelines.

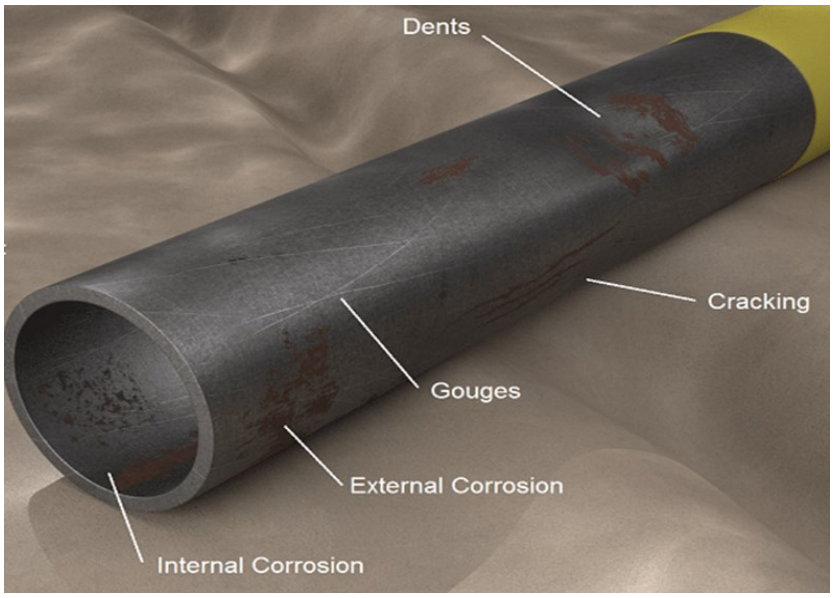

Figure 4.1 Showing common defects in pipelines
https://atteris.com.au/wpcontent/uploads/2017/04/pipe-render.png, accessed August 23, 2019

Very little work has been done on dent-crack defect so far [9-11], partly due to the practical difficulty of creating artificial cracks for experiments. Usually the cracks are created as notches and gouges with a small fatigue crack at the tip. There are currently no analytical models for assessing the integrity of pipelines with dent-crack defect that is accepted by the pipeline industry. The pipeline defect assessment manual [12,13] recommends the use of dent-gouge fracture model for assessing a dent combined with any other defect than a gouge. But the model is considered conservative and is unsuitable for dent-crack defect. The ASME B31.4 code recommends that pipelines with dent crack defects be discarded without fitness for service assessment, but recent research findings suggest its very conservative [9-11]

Oryniak et.al [14] proposed an analytical solution for stress distribution in a dent having an axial crack starting from the deepest point of a dent. The effect of dent is accounted for by allowing for geometric nonlinearity in the model. Bending stresses through the crack caused by the geometric nonlinearity are added to the stresses caused by the internal pressure and the sum of stresses is

used to calculate the stress intensity factor. Knowing the stress intensity factor, and the bending stresses due to denting, the formula can theoretically be used to determine the pressure required to propagate a part wall crack to a through wall crack. The pressure required to develop a through-wall crack being the remaining strength of the pipe. However, the formula is conservative as it does not capture re-rounding behavior of the dent and its effect on the bending stresses through the crack. Another expression was proposed by Bai and Song [15] to calculate the burst strength of pipes having dent-crack defects by considering a notch inside an infinitely long dent. Burst stress is computed as a fraction of the collapse stress of the pipe material. The collapse stress is modified to account for deterioration in material properties due to mechanical damage and the notch shape. The burst pressure is easily computed once the burst stress is known. The limitation is that the expression is derived using a notch not a crack. A factor of safety is applied to ensure safety of cracked pipes assessed using equations derived.

In the absence of industry accepted analytical models, assessments of pipelines with dent-crack defect in literature are done experimentally and by numerical modelling, which are expensive and not timely for integrity decision making purposes. The finite element method (FEA) allows for predicting and evaluation of the failure pressures of pipelines with more complex defects. However, Rosenfield et.al [16] assert that the analysis must account for both material and geometric non linearities to be accurate which increases the complication of the process. Material properties are altered by the indenting and rebounding effects of dent, which introduce uncertainties in the analysis.

More uncertainties result from the fact that there is no universally agreed criteria for interpreting FEA results and users of FEA software must decide on a criterion for a decision on failure. Das et.al [17] in their analysis of fatigue fracture of pipelines used the equivalent plastic strain as the criterion for failure; Pipeline failure was deemed to have occurred when a threshold value of equivalent plastic strain was reached. Adeeb and Horsey [18] suggested 20% as the critical strain for safe excavation of defective pipes in a rock ditch, believing that the material fails when the maximum principal strain reaches 20%. Tian and Zhang [19] utilized the equivalent stress as failure criterion to analyze burst strength of pipes with dent-scratch. Failure occurred when the equivalent stress equaled the true tensile strength of the material. Muntaseer et.al [5] used maximum strain as a measure of failure in dents and to identify areas within the dent to locate

cracks. They then used the fracture mechanics principals of J-integral in FEA to assess the safe operating pressure of the pipeline having a dent and potential crack. Similarly, Ghaednia et.al used the J-integral [9-11] at the integration point as the failure criterion to analyses the burst pressure of pipeline with dent crack defect using Abaqus software [20]. Failure occurred when the J-integral at any integration point in the model equaled the critical value J_{IC} of the material.

Thus, there are many possible criteria to determine failure in FEA and the user has the responsibility to choose the appropriate criterion. In addition, the traditional finite element methods are known to be tedious and costly for modeling propagating cracks due to the need to re-mesh the crack domain as it propagates. Using the extended finite element method (XFEM), the burst pressure is simply the pressure required to propagate a crack to make it a through-wall crack and can be easily observed from the post processing graphics, which makes it easy to use. XFEM has in-built algorithms that eliminate the requirement to re-mesh crack domain, making it less tedious and convenient for modelling propagating cracks.

The aim of this paper is to provide some insights into the capability of the existing extended finite element methods implemented in Abaqus standard software for analysis of crack propagation and burst pressure prediction in pipelines. Specimens of pipeline with longitudinal cracks in dents are modeled in XFEM and subjected to internal pressure to initiate and sustain crack propagation. Burst pressure is predicted when the initially part-wall cracks become through-wall cracks, with the predicted pressure representing the remaining strength of the flawed pipe.

4.3 Methodology

4.3.1 Creation of notch and fatigue cracks in the specimens

This study utilized experimental results from Ghaednia et.al [10], which comprises of four full-scale burst tests conducted at room temperature on API X70 pipes with longitudinal cracks in dents. The external diameter of the pipe, D =762mm, wall thickness t = 8.5mm, and lengths L = 2.5m. The cracks were created at the tip of fine crack-like, longitudinal electro-discharging machine, (EDM) cut V-shaped notches located at the 12 O'clock position of the pipe by applying a fatigue load using a fatigue load actuator. It was reported that the EDM cut notch had a depth of 4mm and the real crack was 0.3mm deep. The crack depths were determined by examining cut samples of the defect area after burst tests using Scanning Electron Microscopes. The

examinations showed three clear regions of crack: the crack-like v-notch, the fatigue crack and finally the ductile crack caused by propagation. Thus, the total crack-like defect was 4.3mm, approximately 50% of wall thickness (t).

The four cracks created in the different specimens, described by their depths and length (a×2c) were: 4.3mm×20mm, 4.3mm×60mm, 4.3mm×100mm, and 4.3mm×200mm. Only the crack length was varied in order to assess its effect on burst strength. Figure 4.2a is an illustration of the fatigue loading procedure and figure 4.2b shows the resulting notch and fatigue crack [10]. Figure 4.1c shows the set-up of the denting process.

It is important to note that creating identical fatigue cracks in different specimens is very difficult. Usually the geometry and orientation of the cracks vary upon repeating the experiments and the variations would affect results of burst tests. Cracks in the longitudinal plane of the pipe would cause lower burst pressures than circumferential cracks and the burst pressures would decrease with increase in crack geometry. In using the experimental results [20] to calibrate and validate numerical models, the authors assume that the fatigue cracks were longitudinal in orientation and rectangular in geometry, with the cracks in different specimens used in the burst test has same depths. A discrepancy in crack orientation and geometry would produce a different set of burst test results but it would not necessarily change the XFEM damage parameters if the same material properties are used for numerical modelling.

4.3.2 Overview of denting and pressurization of the specimens

A 50mm×100mm rigid rectangular steel block was used to create a dent at the location of the notched and fatigue crack resulting in a combined dent-crack defect [10]. The denting load was applied using a universal loading actuator and the operating pressure during the denting process was 3.8MPa, corresponding to 30% the yield pressure, P_y of the pipe material. The pressure was administered using a hydrostatic pump and monitored both manually and electronically through transducers attached to the specimen. Two linear variable differential transducers (LVDTs) were used to monitor the dent depth and plastic deformation realized during the denting process. Strain gauges were also arranged along the crack length to measure the denting strains. The measured strains and displacements of the indenter during the loading and unloading regimes were used to validate the finite element models. Approximately 28mm of the displacement remained as

permanent dent depth on the pipe upon release of the indenter. This is approximately 4% of the external diameter (D) of the pipe which is 30.48mm.

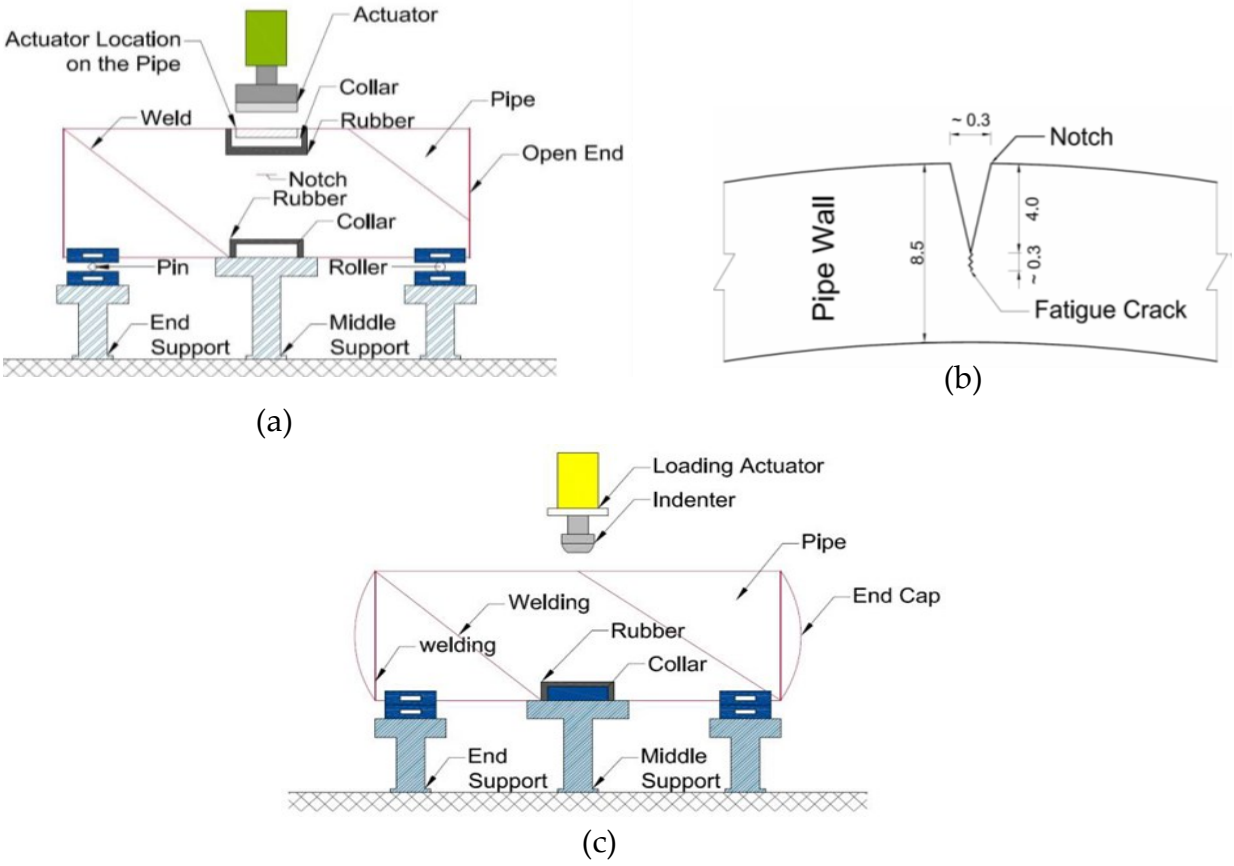

Figure 4.2 Schematic diagram showing (a) fatigue loading, (b) fatigue crack, and (c) denting process [10] (used with publisher's consent granted under license number 1528-896X)

The damaged pipes were subjected to monotonically increasing water pressure supplied by a water pump and monitored mechanically using a pressure gauge and electronically using a pressure transducer. The pipes were loaded until a leakage or burst occurs where upon the test were discontinued. The pressure that caused leakage or ruptured was the burst pressure the sample under test.

4.3.3 Tests of material properties

Tensile and Charpy V-notch impact tests were performed as part of the experimental program to determine the mechanical properties of the pipe material [10]. The tensile tests were conducted on

samples extracted for the pipes in accordance with the recommendations of ASTM E8. The pipe material had a yield stress of 540MPa for a proof strain of 5%, and tensile strength of 620MPa. Young's modulus E = 204GPa, Poisson's ratio $\nu = 0.3$. The material's stress-strain curve is shown in Figure 4.3. Five sub-size samples (full wall thickness specimen sizes) were used to conduct Charpy-V notch impact tests to ensure the pipe material was sufficiently ductile. The material presented fully ductile fracture with approximate Charpy impact energy of 152J at room temperature.

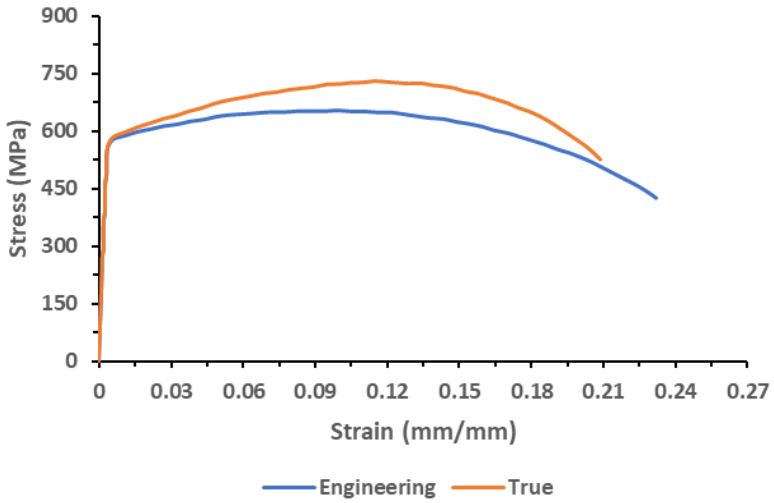

Figure 4.3 Stress-strain curves of the pipe material

4.4 XFEM modelling, burst pressure predictions, results and discussion

The general-purpose finite element software Abaqus [20], version 2017 was used in this paper for finite element analysis, making use of its in-built XFEM criterion. Fracture strain and energy were used as damage parameter. Specimens were modelled as elastic-plastic with isotropic hardening by inputting plastic stress- plastic strain data. The maximum displacement of the indenter was -63.53mm and the maximum denting load was 508kN for a target dent depth of 4%D (30.48mm).

4.4.1 Set up of the model

Models of specimens of APIX70 pipe with varying sizes of longitudinal rectangular dent-crack defects were created using XFEM in Abaqus [20], (Figure 4.4a). The models comprised of a deformable solid strip of length 250mm, width 50mm, and thickness 8.5mm coupled to a deformable shell using shell-solid coupling constraint to form the pipe body. The shell geometry

was defined by top surface of the pipe and assembly was done by fitting the top surface of the shell to the top surface of the solid for 3-dimensional alignment. Tie constraint was used to attach a 12mm thick flat deformable solid end-closer to the pipe-shell. The crack was formed as a rectangular planar shell embedded in the solid strip and the depth of crack used in the model was 4mm, which approximates the 4.3mm created in burst test specimens. The pipe was supported on two discrete rigid shell blocks placed at the bottom. A discrete rigid solid block placed at the center of the pipe, and over the crack was used as the indenter. Surface to surface standard contact was prescribed between the pipe surface and the surfaces of the discrete rigid supports. Similarly, contact was used between the indenter and pipe surfaces. Symmetry of the pipe along the along Z-axis (along pipe length) was used to model half of the pipe and reduce the computation cost. Thus, Z-symmetry boundary condition was applied at the center of pipe along the circumference to restrain longitudinal deformation. The pipe was restrained from vertical motion by setting the degree of freedom U2 at the bottom of the pipe to zero. This condition is fulfilled in real life by the self-weight of pipe and content.

4.4.2 Mesh details

Figure 4.4 shows mesh distribution in the model. Coupling of deformable shell and solid parts to form the pipe model allowed us to use different element types, mesh sizes and techniques in the pipe to further reduce computational time and cost. The solid part in the model was partitioned into three regions using datum planes to allow for mesh transition in the circumferential direction of the pipe, from fine mesh near the crack to coarse mesh away from the crack to reduce the number of elements in the model and lower cost of computation. Hexagonal sweep elements with advancing front, allowing for mapped meshing, were used in the finely meshed region close to the crack, while hexagonal structured elements were used in the solid region away from the crack. All solid regions used the 8-node linear brick elements (C3D8R) with reduced integration and 4-node S4R elements with quad-dominated free mesh were used in the shell parts.

Mesh sensitivity analysis was done to optimize computation cost with respect to accuracy of prediction. Predicted burst pressures stabilized when at least 17 elements were used in the thickness direction of the pipe in the region closest to the crack, corresponding to 0.5mm element thickness. With 17 elements, the tip of the 4mm deep crack rested at the bottom edge of the 8th

element, which is important for XFEM analysis. Predictions were not very sensitive to element sizes away from the crack in both longitudinal and circumferential directions of the pipe. Hence the element size of 1.7mm was used in the circumferential direction close to the crack. The element size in the length direction varied with length of crack. The 4mm×20mm and 4mm×60mm cracks had a longitudinal element length of 5mm while for the 4mm×100mm and 4mm×200mm cracks, satisfactory results were obtained with an element size of 25mm in the longitudinal direction of the pipe.

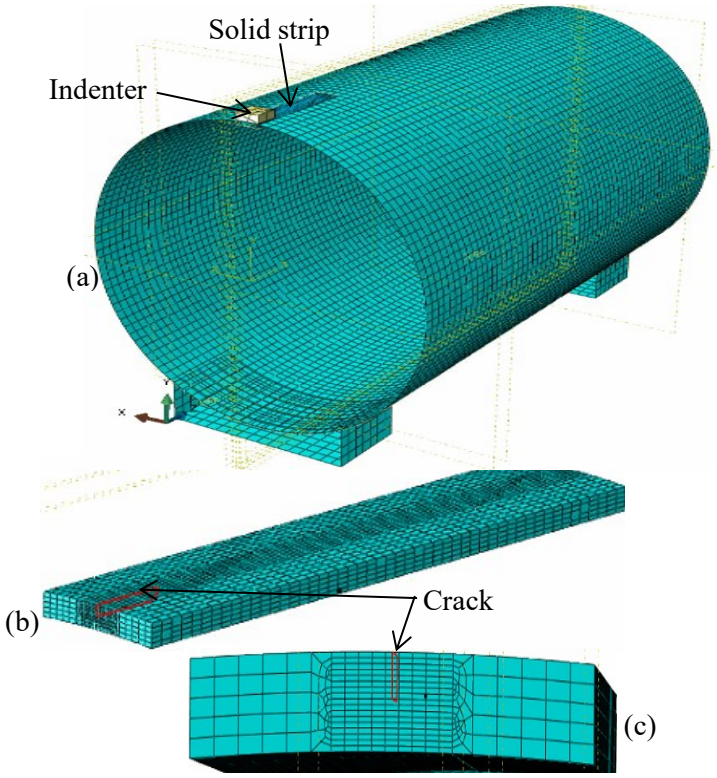

Figure 4.4 Showing (a) Model set up and mesh distribution, (b) Mesh in the solid part, (c) Mesh near crack

4.4.3 Loading procedure

Figure 4.5 shows the model loading process used in this study. Loading of the pipe was executed in four steps namely: Operating pressure of 3.8MPa, indentation, release of indenter, and finally internal pressure to burst the pipe. The indentation and release of the indenter were applied as displacement boundary conditions through the reference point of the discrete rigid solid rectangular indenter. A downward vertical displacement of 63.53mm was applied to the indenter

in step 2 of the analysis to dent the pipe surface. This was followed in step 3 by an upward displacement of 30mm to release the indenter and free the pipe surface, leaving a permanent plastic deformation on the pipe surfaces as dent depths. Internal pressure was applied cumulatively in small increments to provide static loading. First, a 3.8MPa, corresponding to approximately $0.3P_y$ was applied in step 1 as operating pressure during dent formation. This pressure remained active during indentation and release of indenter (steps 2 and 3) but was deactivated in step 4 when a pressure of 15MPa, was applied to propagate the crack and burst the pipe. The pressure in step 4 was deliberately chosen to be greater than the highest burst pressure obtained during test.

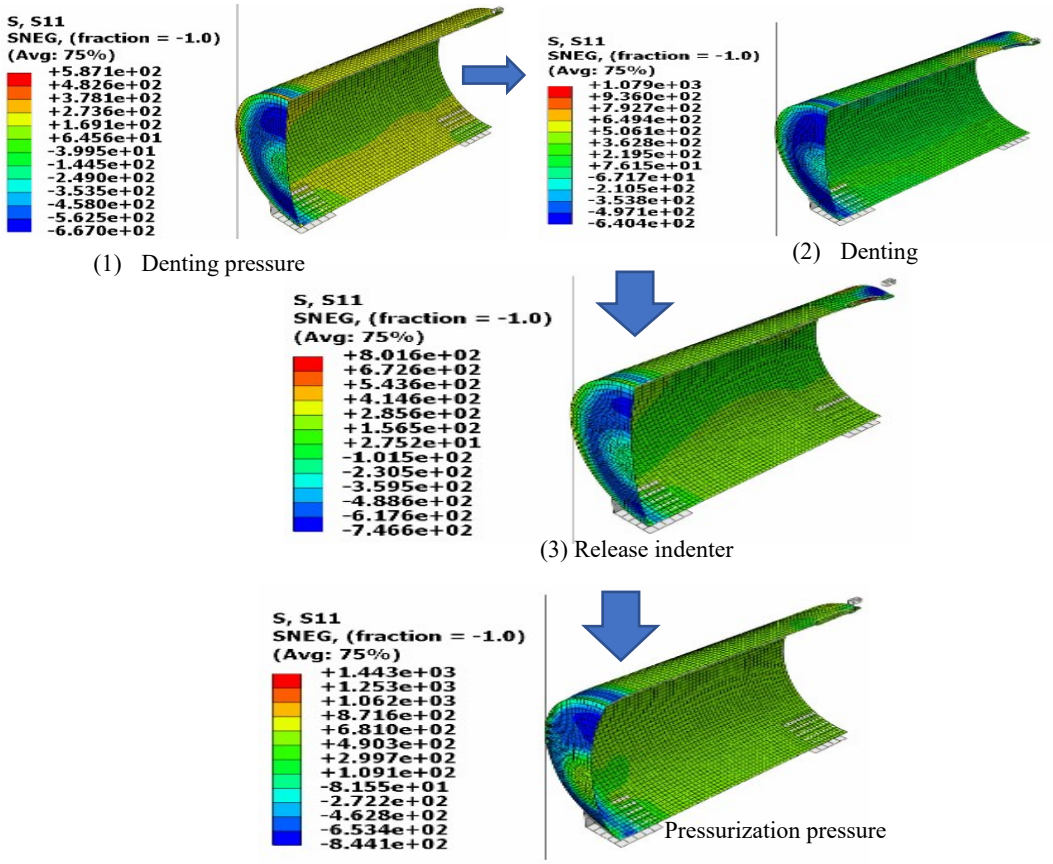

Figure 4.5 Showing the loading steps for numerical modelling

4.4.4 Model calibration, and burst pressure prediction

XFEM criterion requires damage parameters, specified in material properties to define the conditions for crack propagation. This allows for a direct prediction of failure pressure since propagation occurs when the specified parameters are realized at the crack tip. However, the

parameters are not part of the measured material properties and are determined by the user through a calibration process. Abaqus [20] provides amongst others, the options of maximum principal stress (*Maxps*) or maximum principal strain (*Maxpe*) as criteria for initiation of damage leading to development and propagation of cracks in the material. Previous studies [21-24] show that the values of *Maxps* required to propagate the cracks are usually very high, in multiples of the yield strength of the Material. The high *Maxps* values cannot be justified for ductile materials, where significant plasticization occurs at the crack tip and moderates the intensity of the stresses. Liu et.al [25] used *Maxpe* to analyze crack propagation in beam specimens of APIX80 pipeline steel and found that the *Maxpe* required increases with decrease in specimen thickness due to decreasing crack tip constraint and increasing ductility. And according to Liu et.al [25], the *Maxpe* is more suitable for simulating ductile fracture in pipelines than the *Maxps* criterion. This study therefore used *Maxpe* and fracture energy G_c as model damage parameters.

The parameters that best predicted the test results for each of the four specimens were determined individually and the average was used as the approximated damage parameters of pipe. Table 4.1 shows the damage parameters for each specimen, calibrated using burst pressure from tests and their averages. Adjustments were made to the average values by rounding of the figures to convenient numbers, with little change in the results. Thus, the damage parameters used for prediction in this paper were: fracture strain and fracture energy of 0.036 and 120 J/m^2 respectively.

Table 4.1 Calibrated damage parameters

Crack (mm×mm)	Damage parameters	
	Fracture strain (*Maxpe)*	Fracture energy, G_c (J/m^2)
4.3×20	0.033	100
4.3×60	0.035	100
4.3×100	0.032	100
4.3×200	0.043	150
Average	0.036	112.5

Validation of the calibrated models was done by comparing experimental and predicted load-displacement curves for the four pipe specimens as shown in Figure 4.6a. There is good agreement between the experiment and finite element derived curves for all the specimens. The dent depths obtained in the modelling process were: 29.5mm for the two shortest cracks (lengths 20mm and

60mm) and 30.5mm for the two longer cracks (lengths of 100mm and 200mm). The difference is attributed to the variation in the sizes of mesh used along the length of the cracks. Thus, the average permanent plastic deformation of the pipe surface for the four specimens was 30mm, which is closer to the 4%D (30.48mm) dent depth addressed in this study compared to the 28mm obtained experimentally.

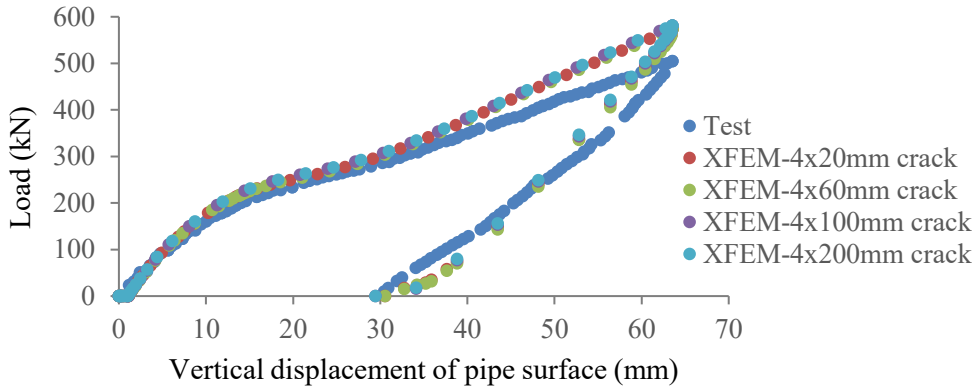

(a) Loading-displacement curves for dent

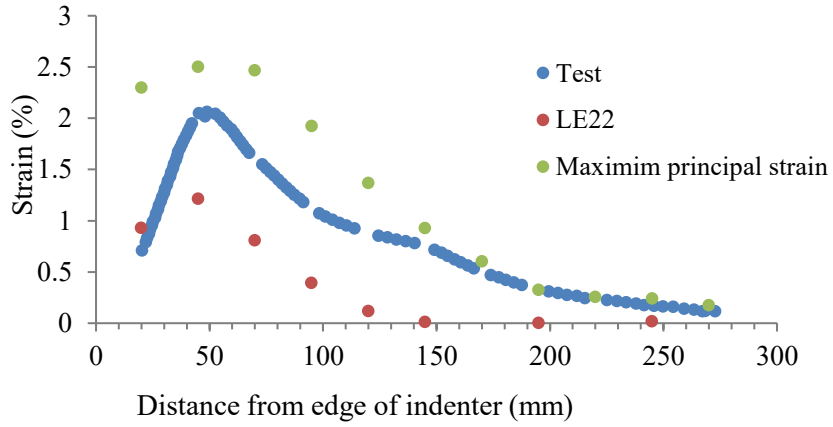

(b) Strain distribution along length of pipe

Figure 4.6 Showing (a) application and release of indenter (b) variation of strain with distance along pipe length

Similarly, the denting loads varied with crack lengths, which is also partly attributable to the size of elements used in the longitudinal direction of the crack to obtain acceptable predictions. The denting loads for the smaller cracks, having 5mm long elements in the crack length direction were 573kN and for the longer cracks, having 25mm long elements in the crack length directions were

581.kN, giving an average of 577kN which is 14% higher than the test load. The higher denting loads for the models also show that the model was stiffer than the test specimen. It should be remembered here that the cohesive crack used in the XFEM model was 4mm deep. But the crack in the experiment was 4.3mm deep and comprised of a 4mm EDM cut v-notch and a 0.3mm deep fatigue crack. Thus, the model was expected to be stiffer than the tested specimens.

The experimental and predicted strain distributions in the longitudinal direction of the pipe were compared as shown in Figure 4.6b to further validate the model. The strain variations have similar trends, although the predicted maximum principal strains are higher in the region closer to the indenter, which was modeled as a solid and sustained higher bending stresses and strains.

The measured and predicted strains match in locations far away from the edge of indenter where bending strains and effect of crack on stress distribution are minimal and membrane strains due to the applied internal pressure are dominant. It's important to note that the hoop strains in the damaged pipe were predominantly tensile. This agrees with the findings of Rafi et.al [26] who experimentally investigated the strength of pipeline with dent-crack defects. Their analysis of strain distribution along the length of the crack showed that strains are predominantly tensile in the circumferential direction (hoop strains). On the other hand, both compressive and tensile strains exist in the longitudinal direction due to the end cap indenter effects. The results indicate that cracks in longitudinal orientation are predominantly under tensile tress and likely to propagate under internal pressure by mode-I fracture and is the reason why this study focused on longitudinal cracks in dents.

The calibrated damage parameters were included in the material property definition and the resulting model used to predict burst pressure of the four pipe specimens. Table 4.2 shows the burst pressures predicted using the calibrated model damage parameters, alongside the test results. The model predictions agree with the test results. Figure 4.7 shows a plot of predicted burst pressure against the burst pressures obtained from tests. The dashed line shows equality of prediction and test burst pressures. With exception of the specimen with 4.3mm×100mm crack, the predictions of burst pressures of the rest of the specimens plot closer to the equality line, indicating general agreement between the predicted and test results.

Table 4.2 Predicted burst pressure for different specimens

Crack (mm×mm)	Burst pressure (MPa)		
	Model prediction	Experiment results	Error (%)
4×20	13.95	13.55	3
4×60	11.13	11.28	-1.33
4×100	10.80	9.48	14
4×200	7.09	7.82	-9.3

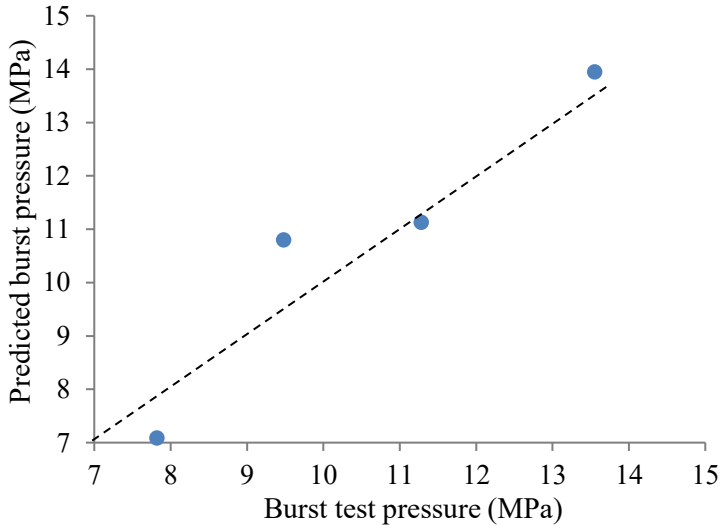

Figure 4.7 Comparison of predicted and test burst pressures

The behavior of the specimen with 4mm×100mm crack is influenced by the fact that its length matched the length of the indenter. Thus, the entire surface of the pipe carrying the indenter, being weakened by the crack experienced less bending stress than the region beyond the edge of indenter. The critical strain required to match the experimental burst pressure with the XFEM prediction was lower than the average strain (0.0316 vs. 0.03565) and when the average damage parameters were used in the model, the predicted burst pressure was higher than test result. The opposite occurred in the specimen with 4mm×200mm crack. Since the crack length was longer than the indenter length, part of it was in the rim of the dent under high bending stresses and strains. The critical strain required to match the experimental and XFEM prediction was higher than the calibrated average strain (0.043 vs. 0.03565) implying the fracture behavior was more ductile.

Ghaednia et.al [9] reported that the specimens having 4mm×20mm,4mm×60mm cracks showed less ductile failure than the specimen with 4mm×100mm crack. The specimen the 4mm×200mm crack failed by sudden rupture. The longer cracks have less constraint thus develop larger plastic stresses and strains over a large region of the pipe, and a more ductile failure and sudden rupture for the very long cracks.

The average absolute error in prediction is approximately 7% which closely matches the 5% average error of obtained by Ghaednia et.al [9] based on fracture mechanics principal of J-integral determined by finite element analysis. The J-integral predictions of Ghaednia et.al [9] were generally conservative, whereas the XFEM predictions here shows the models non conservative predictions are also possible for dent-crack defected pipes.

4.5 Conclusion

The effectiveness of XFEM (with *Maxpe* and G_c as damage parameters) implemented in Abaqus for analysis of crack propagation and prediction of burst pressure in pipelines with dent-crack was investigated in this paper.

Models of APIX70 pipe specimens having 4mm×20mm, 4mm×60mm, 4mm×100mm and 4.3mm×200mm longitudinal external surface cracks centered inside a dent of depth 4% external diameter of the pipe were calibrated with data from full-scale burst tests to determine fracture strain and fracture energy that accurately re-produced their burst pressures. The fracture strains required for satisfactory predictions were similar and did not vary significantly with crack length. The average fracture strain and average fracture energy of the three specimens was used as the damage parameters of the pipe to burst pressure.

XFEM predicted burst pressure generally matched the burst test results, within an average error of 7%. This compares well with the 5% error obtained using finite element analysis of the same pipes based on J-integral fracture mechanics principals implemented in Abaqus.
The location of the region where the through wall crack first appeared varied with the crack length. It first developed at the center of the specimens with the 4mm×20mm and 4mm×60mm cracks, while for the specimens with 4mm×100mm and 4mm×200mm cracks, the through wall crack and burst started away from the center because the cracks are long enough to influence stress

distribution in the rim of the dent where bending strains are highest under internal pressure. The 4mm×20mm crack exhibited brittle fracture compared to its longer counterparts.

The results show XFEM (with maximum strain and fracture energy as damage parameters) can be used as an effective tool to analyze crack propagation and predict burst pressure. A well calibrated XFEM model can also be used to predict possible failure modes for specimens with varying sizes of dent-crack defects. A study involving wider range of cracks and dent sizes will be conducted in the future to confirm this potential.

4.6 References

[1]. ASME. "Fitness-for-service, API Recommended Practice 579-1/ASME FFS-1 2007, Second Edition", The American Society of Mechanical Engineers, New York, USA, June 2007.

[2]. BSI. BS7910: 2005, "Guide to methods for assessing the acceptability of flaws in metallic structure", London, UK, British standards institution, July 2005

[3]. Ming Gao, Ravi Krishnamurthy, Samarth Tandon, & Udayasankar Arumugam.*Critical strain based ductile damage criterion and its application to mechanical damage in pipelines.* Proceedings of the 13th International Conf. on Fracture June 16-21, 2013, Beijing, China

[4]. Lancaster, E. R., & Palmer, S. C. (1996). Burst pressures of pipes containing dents and gouges. *Proceedings of the Institution of Mechanical Engineers, Part E: Journal of Process Mechanical Engineering, 210*(1), 19-27.

[5]. Muntaseer Kainat, Doug Langer, Sherif Hassanien, (2018). Do we need a safe excavation pressure for dented pipelines: How should it be defined? *Proceedings of the 12th international pipelines conference. Ipc2018-78376, Calgary, Alberta, Canada*

[6]. Zimmermann, J., Beller, M., & Mattheck, C. (1991). Stress concentrations in pipelines due to the presence of dents. Paper presented at ISOPE-I-91-121

[7]. Vilkys, T., Rudzinskas, V., Prentkovskis, O., Tretjakovas, J., Višniakov, N., & Maruschak, P. (2018). Evaluation of failure pressure for gas pipelines with combined defects. *Metals, 8*(5), 346. doi:10.3390/met8050346

[8]. Ronny, H., Espen, B., & Lijana, D.O., *Damage Assessment of Pipelines with Dents, Cracks – Proposal for Methodology for Calculation of Acceptable Dimensions of a Combination of Crack, & Dent in Subsea Pipelines*. Proceedings of the ASME 29th International Conference on Ocean, Offshore and Arctic Engineering, Shanghai, China (2010). *Omae2010-2*

[9]. Ghaednia, H., Das, S., Wang, R., & Kania, R. (2017). Dependence of burst strength on crack length of a pipe with a dent-crack defect. *Journal of Pipeline Systems Eng. and Practice, 8*(2).

[10]. Ghaednia, H., Das, S., Wang, R., & Kania, R. (2015a). Effect of operating pressure and dent depth on burst strength of NPS30 line pipe with Dent–Crack defect. *Journal of Offshore Mechanics and Arctic Engineering, 137*(3), 031402-8.

[11]. Ghaednia, H., Das, S., Wang, R., & Kania, R. (2015b). Safe burst strength of a pipeline with dent–crack defect: Effect of crack depth and operating pressure. *Engineering Failure Analysis, 55*, 288-299.

[12].Cosham, A., & Hopkins, P. (2004). The effect of dents in pipelines—guidance in the pipeline defect assessment manual. *International Journal of Pressure Vessels and Piping, 81*(2), 127-139.

[13].Macdonald, K. A., & Cosham, A. (2005). *Best practice for the assessment of defects in pipelines – gouges and dents. Engineering Failure Analysis*.

[14].Orynyak, I., Yakovleva, E., & Rozgonyuk, V. (2007). Application of the cheng-finnie method to the calculation of stress intensity factors in thin-walled pipes with long axial cracks with allowance for geometric nonlinearity. *Strength of Materials, 39*(5), 455-465.

[15].Bai, Y., & Song, R. (1997). Fracture assessment of dented pipes with cracks and reliability-based calibration of safety factor. *Int. J. of Pressure Vessels and Piping, 74*(3), 221-229.

[16]. Rosenfield, M.J., Pepper, J.W., & Lewis, K., Basis of the new criteria in ASME B31.8 for prioritization, & repair of mechanical damage. (2002). *Ipc2002-27122 ipc02-27122 dented pipes with cracks*

[17]. Das S., Cheng, J.J.R., Murray D.W., Prediction of fracture in wrinkled energy pipelines subjected to cyclic deformations, Int. J. Offshore Polar Eng. 17 (3) (2007) 205–212

[18].Adeeb S.M., Horsley D.J., A numerical procedure to establish a safe working pressure during excavation of a pipeline in a rock ditch, Int. J. Press. Vessel. Pip. 83 (7) (2006) 488–497.

[19]. Tian, X., & Zhang, H. (2017). *Failure criterion of buried pipelines with dent and scratch defects.* Journal of *Engineering Failure Analysis.*

[20]. Abaqus 6.14, Documentation,2014. Dassault Systèmes

[21].Lin M., Agbo S., Cheng J.J.R., Yoosef-Ghodsi N., Adeeb S., Application of the extended finite element method (XFEM) to simulate crack propagation in pressurized steel pipes, in: Proceedings of ASME 2017 Pressure Vessels and Piping Conference, volume 3B, 2017.

[22].Ameli I., Behrouz A., Lin M., Agbo S., Cheng J.J.R., Da-Ming D., Adeeb S., Estimation of the CTOD- crack growth curves in SENT specimens using the extended finite element method, Int. J. Pres. Ves. Pip. 169 (2019) 16–25.

[23].Agbo S., Lin M., Ameli I., Imanpour A., Duan D.-M., Cheng J.J.R., Adeeb S., Evaluation of the Effect of Internal Pressure and Flaw Size on the Tensile Strain Capacity of X42 Vintage Pipeline using Damage Plasticity Model in Extended Finite Element Method (XFEM). PVP2019-94005, Proceedings of the ASME 2019 Pressure Vessels & Piping Conference, July 2019, San Antonio, Texas, USA.

[24].Li H., Chandra N., Analysis of crack growth and crack-tip plasticity in ductile materials using cohesive zone models, Int. J. Plast. 19 (2003) 849–882.

[25].Liu X.B., Zhang H., Han Y., Xia M., Ji Y., Numerical and Experimental study on critical crack tip opening displacement of X80 pipeline steel, Mechanika 23 (2) (2017) 204–208, 2017.

[26].Rafi, A., Silva, J., Kenno, S., Das, S., Kania, R., & Wang, R.Y., (2010). Strength of line pipe with dent and crack d effect. *Proceedings of the 8th international pipelines conference. IPC 2010-31095, Calgary, Alberta, Canada.*

5. CRACK PROPAGATION AND BURST PRESSURE OF PIPELINE WITH RESTRAINED AND UNRESTRAINED CONCENTRIC DENT-CRACK DEFECTS USING EXTENDED FINITE ELEMENT METHOD

This chapters is derived from a research article published in the MDPI Journal of Applied Sciences, Special issue on Advanced Numerical Approaches for Crack Growth Simulation: Okodi, A., Li, Y., Cheng, J.J.R., Kainat, M.,Yoosef-Ghodsi, N., Adeeb, S., Crack Propagation and Burst Pressure of Pipeline with Restrained and Unrestrained Concentric Dent-Crack Defects Using Extended Finite Element Method, Journal of Applied Sciences (2020), 10.3390/app10217554

5.1 Abstract

Mechanical damage in form of dents, cracks, gouges, and scratches are common in pipelines. Sometimes, these damages form in proximity of each other and act as one defect in the pipe wall. The combined defects have been found to be more injurious than individual defects. One of the combined defects in pipeline comprises of a crack in a dent, also known as dent-crack defect. This paper discusses the development of finite element models using extended finite element criterion (XFEM) in Abaqus to predict burst pressure of specimens of API X70 pipeline with restrained and unrestrained concentric dent-crack defects. The models are calibrated and validated using results of full-scale burst tests. The effects of crack length, crack depth, dent depth, and denting pressure on burst pressure are investigated. The results show that restrained dent-crack defects with shallow cracks (depth less than 50% of wall thickness) inside dents do not affect pipeline operations at maximum allowable operating pressure if crack lengths are less than 200 mm. Releasing restrained dent-cracks when the pressure is at maximum allowable operating pressure can cause propagation of deep cracks (depth of 50% of wall thickness or more) longer than 60 mm. However, only very long cracks (200 mm and higher) propagate to burst the pipe. Cracks of depth less than 20% of wall thickness inside dents formed at zero pressure are not propagated by the maximum allowable operating pressure. Dent-crack defects having dents of depth less than 2% outside diameter of pipe behave as plain cracks if the dents are formed at zero denting pressure but are more injurious than plain cracks if the dents are formed in pressurized pipes.

Keywords: Dents; Cracks; Strength; Integrity; Extended finite element; Burst pressure; Stress; Strain

5.2 Introduction

Mechanical damage like cracks, scratches, and gouges often occur inside dents in pipelines. The combined defects are considered more injurious to pipeline integrity than plain defects [1-6]. An example of combined defects found in pipelines is a crack inside a dent, also known as a dent-crack defect [2-4]. Vilkys et al. [7] showed that gouge depths greater than 50% of wall thickness cause stresses higher than yield strength of pipe material and cracks are likely to initiate at the tip of such gouges under normal operating pressure. The dent magnifies the maximum principal stresses developed in the gouge, increasing susceptibly to cracking. Ronny et al. [8] also showed

that hoop stresses are higher in a pipeline with combined dent and gouge defects than in a pipeline with plain gouges and concluded that dent-gouge defects significantly lower the burst strength of pipelines. Very few full-scale experimental studies on dent-crack defects in pipelines have been accomplished [2-5], mainly because of the difficulty in creating artificial cracks for experiments. Usually, the cracks are represented by notches and gouges [9] with a small fatigue crack at the tip. Currently, there are no analytical models for assessing the integrity of a pipeline with dent-crack defects. The pipeline defect assessment manual [10,11] recommends use of the dent-gouge fracture model to assess dent-crack defects, for cases where single longitudinal part-wall cracks occur inside longitudinally oriented continuous dents of constant width in pipes loaded by static internal pressure. But there is very limited experimental validation of the model for dent-crack defect assessment, and since the difference between the stress environment at the base of a gouge and the stress environment at the tip of a crack is not accounted for in the model, its suitability for assessing integrity of pipeline with dent-crack defects is questionable.

Oryniak et.al [12] proposed a model for assessing dent-crack defects based on the stress distribution in a dent with an axial crack lodged at its deepest point by treating the dent as a source of geometric nonlinearity. Bending stresses through the crack caused by the geometric nonlinearity were added to the stresses caused by the internal pressure and the sum used to calculate the stress intensity factor used to analyze crack propagation. The model is considered conservative because it does not account for the effect of re-rounding of dents under internal pressure on the bending stresses through the crack. Bai and Song [13] used a notch in an infinitely long dent to represent a dent-crack defect and then modified the plastic collapse stress of the pipe material to account for deterioration in the material properties due to the mechanical damage during defect formation and the effect of notch shape. They considered the modified collapse stress as the burst stress of the pipe, and a fraction of it was used to compute burst pressure. The main limitation of their approach is that they used a notch instead of a crack.

In the absence of analytical models, the finite element method (FEA) has been successfully used to evaluate burst pressures of pipelines with dent-crack defects [2-4]. But it lacks an in-built criterion for determining burst pressure. The software user must choose one out of several that have been suggested in literature. Das et. al [14] used a threshold for equivalent plastic strain in the defect area to analyze fatigue fracture. Adeeb and Horsey [15] used 20% maximum principal

strain as the critical strain for safe excavation of defective pipes in a rock ditch, considering material fails at 20% strain. Tian and Zhang [16] used an equivalent stress criterion to assess burst strength of pipes with dent-scratch defect, considering failure to occur when the equivalent stress equals the true tensile strength of the pipe material. Other studies [2-4,17] used the J-integral concept, assuming failure occurred when the J-integral at any integration point in the model equaled a critical value J_{1c} of the material. All the above FEA failure criteria use material properties and geometry of pipe, which are altered by denting and rebound action of dents [18], further introducing uncertainty in the results.

The extended finite element method (XFEM) uses damage parameters determined through calibration and input in the model as material properties [19]. Any moderating effects of denting and re-rounding of dents on material properties and fracture behavior is considered in the calibration process. The cracks propagate when the value of strains, stresses, and fracture energy or displacements at any integration point within the pipe exceed the calibrated damage parameters. Crack growth in the XFEM models can be observed from the post processing graphics, which makes it easy to accurately determine the burst pressure.

The XFEM criterion uses the partition of unity concept to waive the need for mesh geometry to match crack geometry by introducing local enrichment functions and additional degrees of freedom in the standard FEM formulation [20-22]. An intra-element algorithm freely lays the crack within the mesh without tying it to element boundaries, thus overcoming the requirement to match the geometry of mesh to crack geometry. The software searches for regions of crack initiation where stresses and strains exceed a critical value, after which phantom nodes and their superposed original real nodes move apart as the crack propagates, following a specified traction separation law (TSL) and damage evolution criterion. Abaqus standard [23] provides linear, exponential, and tabular TSL options and maximum principal stress (*Maxps*) or strain (*Maxpe*), and maximum nominal stress or strain for damage initiation criterion. Other damage initiation criteria options include quadratic nominal stress, quadratic nominal strain, and user-defined criterion. Damage evolution criteria include fracture energy and crack tip displacement.

This paper used the XFEM procedure in Abaqus [23] to analyze propagation of longitudinal cracks inside restrained and un-restrained dents and predict burst pressure of pipeline with dent-crack defects. Pipe specimens with longitudinal part-wall cracks inside longitudinal rectangular dents

were modeled and subjected to internal pressure to initiate and sustain crack propagation and burst the pipe. The pipe was considered to have failed when the part-wall crack propagated through the last element in the pipe wall to become a through-wall crack. The pressure required to propagate the part-wall crack to form a through-wall crack is the burst pressure of the pipe and it represents the remaining strength of the flawed pipe.

5.3 Materials and methods

5.3.1 Overview of burst tests and material properties

Burst test results and material properties of API X70 pipe samples with dent-crack defects were obtained from literature [2] and used to calibrate and validate numerical models developed in this study. Details of the set-up of the burst test and material properties have been provided in chapter 4. Table 5.1 shows a summary of the burst test results for the pipe specimens used in the calibration and validation. The pipes had 28mm deep rectangular dents, equivalent to 4% of the external diameter (D). The dents were formed when the pipe was under a pressure of 3.8MPa, equivalent to 30% of the yield pressure, P_y of the pipe (P_y =12.67MPa).

Table 5.1 Burst pressures of different specimens

Crack size (mm × mm)	Burst pressure (MPa)
	Burst test results
4×20	13.56
4×60	11.28
4×100	9.48
4×200	7.82

The material had a yield stress of 540 MPa (5% proof strain), tensile strength of 620 MPa, Young's modulus, E of 204 GPa, and Poisson's ratio v of 0.3. The material was reported to present a fully ductile fracture behavior, with approximate Charpy impact energy of 152 J at room temperature.

5.3.2 Numerical modelling

5.3.2.1 Overview

The XFEM in Abaqus [23] was used to model the crack propagation. Maximum principal strain (*Maxpe*) and fracture energy (G_c) were used as damage parameters. The pipe material was

modelled as elastic-plastic with isotropic hardening behavior. Denting of the pipe was accomplished by prescribing a maximum downward displacement load to the indenter as a boundary condition. A displacement load of 63.53 mm left an unrestrained dent of 4%D depth upon releasing the rigid indenter from the pipe surface. details of the procedures followed to develop the model was discussed in chapter 4.

5.3.2.2 Setup of the model

Figure 5.1a shows the setup of the model and the boundary conditions. Symmetry of the burst test set up along the *Z*-axis (along pipe length) was used to model half of the pipe and reduce computational cost. The model comprised of a deformable solid strip of length 250 mm, width 20 mm, and thickness t =8.5 mm, a deformable shell of external diameter, D =762mm, length, L=1250 mm, with part of it cut out and replaced with the solid strip in which the crack was embedded. Shell geometry was defined by the top surface such that the pipe was assembled by joining the top edge of the shell to the top edge of the solid strip. Previous studies [19] show that shell elements work best when the section is offset at mid surface. The predictions are closer to predictions made using a fully solid model. But the analysis time is significantly longer than the time taken when shell geometry was offset at the top surface. Predictions with shell section offset at the top surface were within 10% of the solid model predictions and yet the analysis time was at least 4 times faster. Shell-solid coupling constraint was used for the transition between solid and shell elements in the pipe body. The crack was modelled as a rectangular planar shell embedded in the solid strip, while the indenter was modelled as a discrete rigid solid block placed at the 12 O'clock position of the pipe and over the crack. Surface-to-surface standard contact was prescribed between the pipe and the indenter. Z-symmetry boundary condition was applied along the circumferential edge of the pipe for symmetry along the *Z*-axis. Vertical support was provided at the bottom of the pipe by restraining degree of freedom U2 against vertical displacement at locations on the pipe surface that were placed on steel blocks during the burst test. Kinematic constraint was used at the ends of the pipe with the geometric centers as reference points, fixed against displacement and rotation but allowing the pipe to freely expand.

5.3.2.3 Mesh distribution

Eight-node linear brick elements (C3D8R) with reduced integration were used in the solid part of the pipe, while four-node (S4R) elements with quad-dominated free mesh were used in shell parts

of the pipe. Mesh sensitivity analysis was done to optimize accuracy of prediction and reduce the time required to complete analysis. Predictions were very sensitive to size of elements in the solid part of the pipe having the crack. Therefore, fine mesh distribution was used in it, and coarse mesh in the rest of the pipe. Final element dimensions in the solid were 5mm×2.86mm×0.85 mm in the longitudinal, circumferential, and thickness directions of the pipe respectively, and element size of 18 mm was used for the shell elements. Figure 5.1b shows mesh distribution in the model, with fine mesh near the crack and coarse mesh away from the crack to reduce computation cost. A total of 10 elements were used in the thickness direction of the pipe.

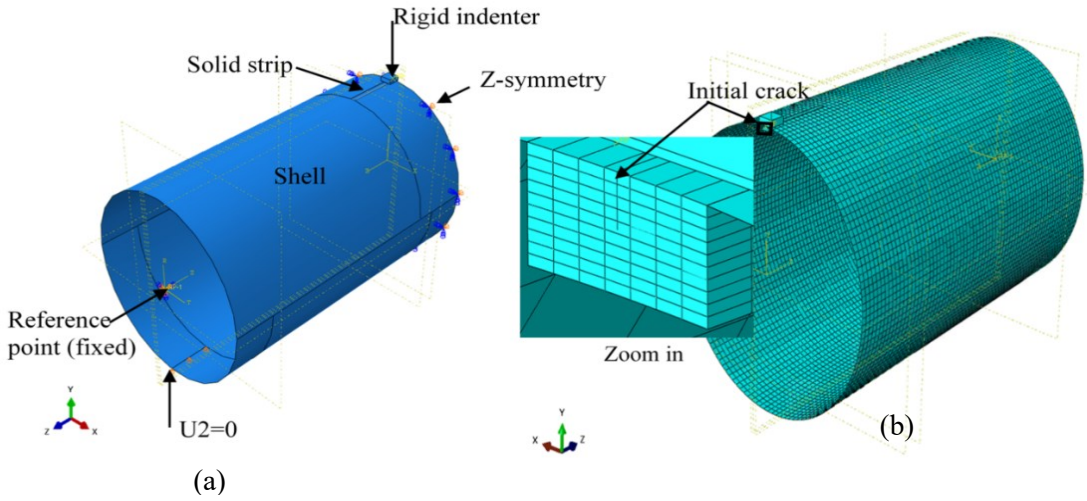

Figure 5.1 Showing (a) Model geometry; (b) Mesh distribution in the model.

5.3.2.4 Defect configuration and loading sequence

Three common pipeline dent-crack defect configurations were investigated. The first defect configuration investigated was a pipe with an unrestrained dent-crack defect subjected to internal pressure. The denting load was applied through the indenter as a displacement. The indenter was released from the surface of the cracked pipe after loading, to create the unrestrained dent-crack and the flawed pipe was then subjected to internal pressure to propagate the crack. The second defect configuration was a pipe with a restrained dent-crack subjected to internal pressure. The indenter was left on the pipe surface after applying denting load and internal pressure was then applied to propagate the crack. This configuration simulates a pipe dented and cracked by a hard object on which it is placed during construction. The last configuration was a pipe with a restrained dent-crack defect, subjected to pressure equivalent to 80% of the yield pressure, P_y of the pipe,

considered to be the maximum allowable operating pressure (MAOP) of the pipe. The indenter was gradually released from the pipe surface with the pipe still at MAOP. The objective was to assess whether releasing the indenter at MAOP would propagate the dent-crack. Often in the field, an initially restrained dent is unrestrained circumstantially. In such a scenario, getting the maximum safe operating pressure that does not propagate an existing crack as the restraint is released becomes paramount. Figure 5.2 shows the steps used to vary the defect configurations investigated in this study. Different permutations of the steps produce different defect and loading scenarios in the pipe.

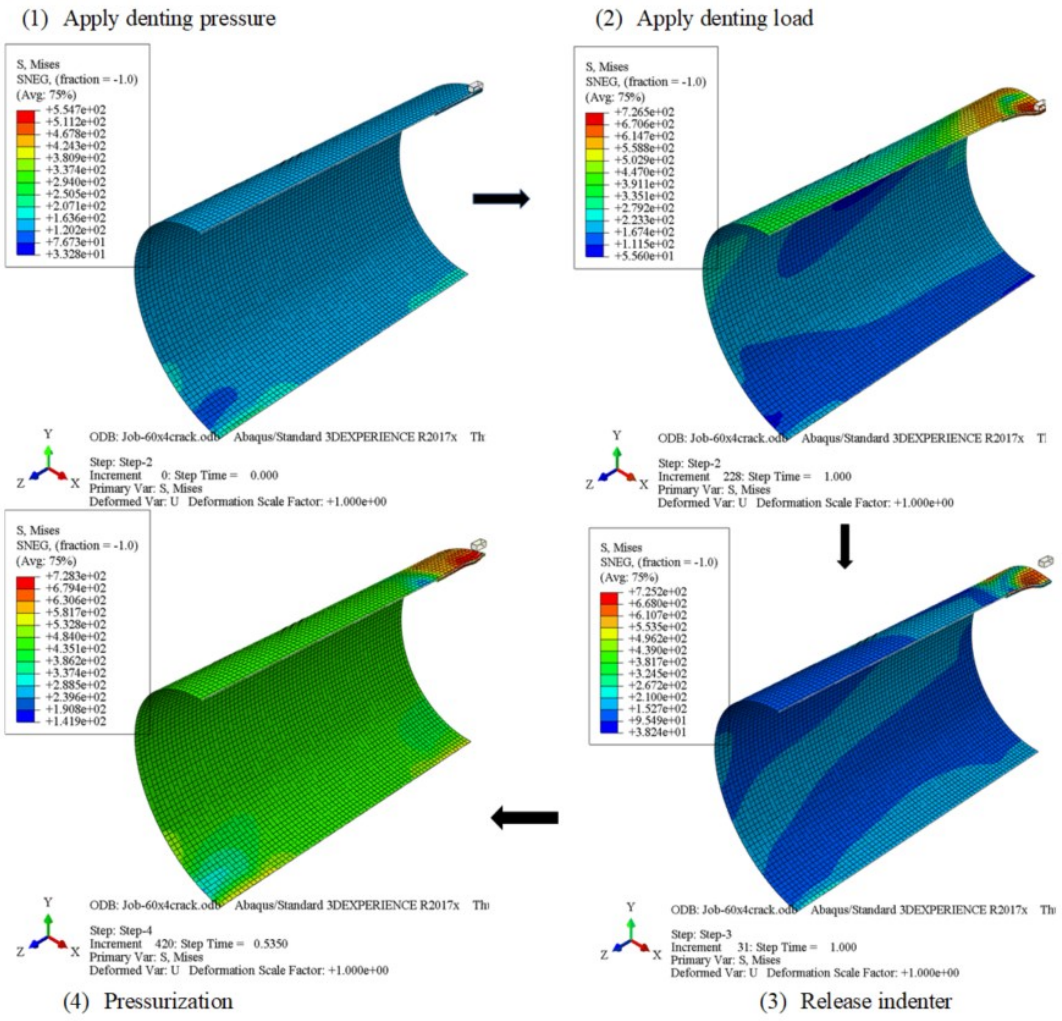

Figure 5.2 Loading steps for numerical model

Unrestrained dent-crack defects under internal pressure were realized using steps 1-4. Restrained dent-crack under internal pressure was created using steps 1, 2, and 4, eliminating step 3 altogether.

Finally, the third scenario (release of indenter at MAOP) was simulated using steps 1, 2, 4, and 3, in that order, with the amount of pressure used in step 4 being the MAOP of the pipe. Parametric studies were conducted for the three defect scenarios by varying denting pressure, dent depth, and crack dimensions.

5.3.2.5 Calibration and validation of the model

Maximum principal strain (*Maxpe*) with exponential traction separation law, were used as damage parameters for XFEM crack propagation. Available studies [19] show that model calibration can be successfully accomplished using either small-scale or full-scale test results. Burst test results were used to calibrate and validate the model in this study. Burst pressure of the specimen with 4mm×100mm crack was used for calibration. The crack length in the specimen matched the dent length perfectly. Results of the three remaining specimens (4mm×20mm, 4mm×60mm, and 4mm×200mm cracks) tested were used in validation. Damage parameters obtained from the calibration and validation process were fracture strain, *Maxpe* = 0.045, and fracture energy, G_c = 2 kJ/m^2. High fracture strain and low fracture energy cause large plastic deformation followed by brittle crack propagation [24]. Resistance to propagation of a cohesive crack in elastic-plastic materials depends on material properties and damage parameters (cohesive strength and energy). According to Li and Chandra [25], the resistance is effected through plastic dissipation of energy in the material surrounding the fracture process zone and dissipation of cohesive energy inside the fracture process zone itself. Increasing cohesive strength (fracture strain) and strain hardening exponent increases the contribution of plasticity towards resistance of crack propagation but lowers contribution of cohesive energy (fracture energy). Large fracture strains show that the material has a high flow stress and require large loads to plasticize. The large loads produce large traction within the fracture process zone resulting in greater resistance to fracture. Low fracture energy shows that resistance to crack propagation is fundamentally by the plastic dissipation of energy in the material around the fracture process zone. A very low amount of energy is required to separate the surfaces within the cohesive zone to form the crack. Table 5.1 above shows burst pressures of four specimens obtained from test and predictions made using the calibrated model. The result shows that the model is generally non-conservative, and predictions were within 10% of the test results.

Load-displacement curves [2] for the dent formation process in the experiments were used to validate the denting of the numerical model. Figure 5.3 shows load-displacement curves for application and release of the rigid indenter from the pipe surface. There is good agreement between test and model-derived curves for all specimens, but the maximum denting load of the model was on average 13% higher than maximum load from tests, showing the models was stiffer than the experiments. This is attributed to the firm supports achieved in modelling compared to supports used in experiments.

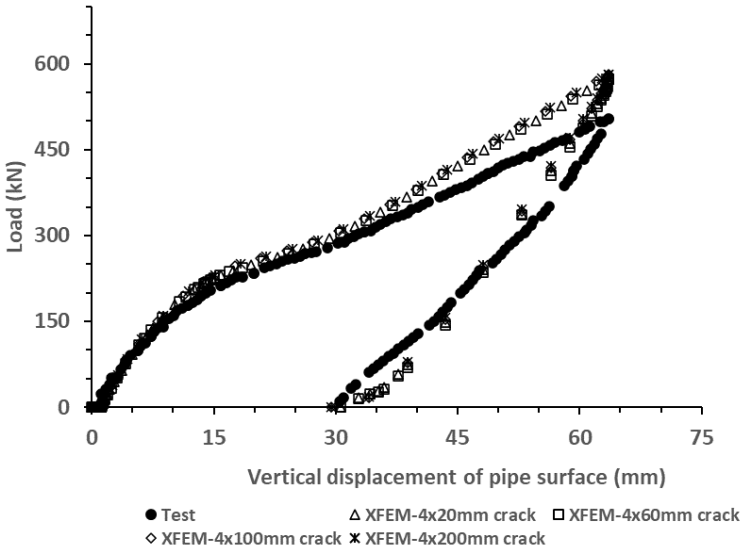

Figure 5.3 Load-displacement curves for application and release of indenter

5.4 Results and discussion

5.4.1 Unrestrained concentric dent-crack defects

Figure 5.4 shows the Von Mises stress distribution at different stages of crack propagation through the wall of the specimen having a 4mm×60mm crack at the center of a 4%D deep unrestrained dent formed at $0.3P_y$ denting pressure. The crack did not propagate during dent formation but stresses at the tip were higher than the yield stress of the material (Figure 5.4b). When internal pressure is applied, the dent rebounds and the pipe recovers some of its circular geometry before the crack begins to propagate at high pressure as shown in Figure 5.4c. The pressure was applied monotonically, hence fracture was independent of time [26]. Crack growth was initiated when the strain at the tip of the existing crack exceeded the critical value of 0.045, determined through calibration of the XFEM model. The growth occurred with visible upward displacement of the

internal surface of the pipe (Figure 5.4d, and 5.4e) due to plasticization under sustained pressure, typical of specimens with deep cracks [24,27].

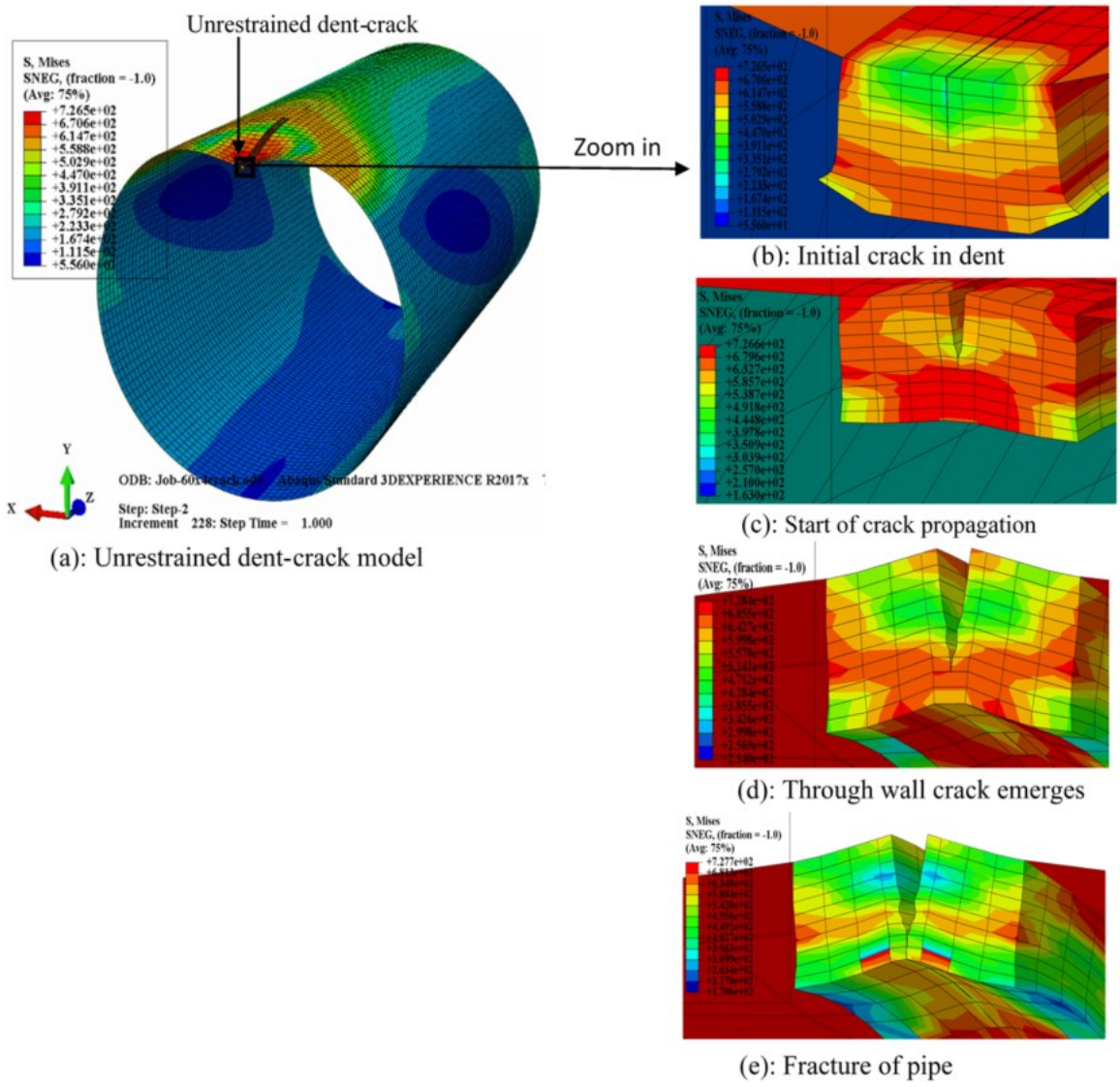

Figure 5.4 Distribution of von Mises stress in pipe wall at various stages of propagation of a crack inside unrestrained dent: (a) Model of pipe with unrestrained concentric dent-crack; (b) Before applying pressure; (c) At start of crack propagation; (d) After through wall crack emerges inside pipe; (e) When crack has fully opened and fracture is complete

Table 5.2 shows the effect of varying the defect parameters on the burst pressure of a pipe with unrestrained concentric dent-crack defect, considering crack depths of 1.7mm (0.2t) and 4mm (0.5t). Internal pressure (denting pressure) ranging from 0% to 80% of yield pressure, P_y (P_y = 12.67 MPa), was maintained in the pipe during dent formation as crack length and dent depths

were varied. Denting the pipe at a pressure of $0.8P_y$ (=10.13MPa) caused cracks to propagate in the circumferential direction during formation of the unrestrained dent-crack because the total bending and membrane strains normal to the circumferential plane surpassed the threshold fracture strain in the process. The risk of circumferential propagation increased with dent depth and denting pressure. It was impossible to dent the pipe to 6%D depth at $0.3P_y$ denting pressure with 200mm long crack. Similarly, creating 6%D deep dents at 0.5Py denting pressure was generally problematic for all crack lengths because large strains are involved.

Table 5.2 Burst pressure of pipes with unrestrained concentric dent-crack defects

Crack size mm)		Denting pressure (MPa)											
Depth	Length	$0.0P_y$			$0.3P_y$			$0.5P_y$			$0.8P_y$		
		Dent depth (%OD)											
		2%	4%	6%	2%	4%	6%	2%	4%	6%	2%	4%	6%
		Burst pressure (MPa)											
0.2t	20	15.08[i]	15.12[i]	15.25[i]	15.49[i]	15.69	14.29[i]	15.51[i]	15.16[i]	**	**	**	**
	60	15.11[i]	15.13[i]	15.21[i]	15.71[i]	15.83[i]	14.5	15.58[i]	14.8[i]	**	**	**	**
	100	15.03[i]	15.26i	15.18[i]	15.59[i]	15.64	14.37	15.17[i]	14.66[i]	6.3*	**	**	**
	200	15.96	16.42i	15.19[i]	15.65[i]	15.64[i]	**	15.3[i]	10.8	**	**	**	**
0.5t	20	15.01	15.13	15.19	15.59	14.9	14.15	15.33	13.7	10.45	**	**	**
	60	13.63	10.51	10.12	11.78	11.14	11.66	10.7	11.76	**	**	**	**
	100	12.68	10.28	9.89	11.07	10.12	3.8*	10.14	6.3*	6.3*	**	**	**
	200	11.18	9.57	9.62	10	8.34	**	8.18	**	**	**	**	**

[i]: Pipe plasticizes without crack propagation; *: Crack propagated by denting pressure; **: Crack propagates during denting, dent formation unsuccessful; t: wall thickness; OD: Outside diameter; P_y: yield pressure

5.4.1.1 Effect of crack depth on burst pressure

Unrestrained dent-cracks having 0.2t deep cracks of any length inside dents less than 6%D deep had no tangible effect on the burst pressure if the defects were formed at $<0.5P_y$ denting pressure. A denting pressure of $0.5P_y$ for dents of depths <6%D and crack of lengths ≤ 200mm, was not consequential to operations of pipeline if crack depths were ≤ 0.2t. The pipes sustained pressures higher than 10.13 MPa ($80\%P_y$), the MAOP of the pipe without bursting. Most specimens with 0.2t deep cracks inside dents sustained very high internal pressure and plasticized significantly without crack propagation. On the other hand, all specimens with 0.5t deep crack in the dent failed by fracture and their burst pressures decreased with crack length, for all dent depths and denting pressures. Specimens with shallow cracks tend to fail by plastic collapse, while deeply cracked specimens tend to fail by fracture [19,24].

5.4.1.2 Effect of crack length on burst pressure

Crack length was varied from 20mm to 200mm while maintaining crack depth at 0.5t, varying dent depths from 0% to 6%D, and denting pressures from 0 to $0.8P_y$. Increasing crack length from 20mm to 200mm in a 2%D deep dent formed at zero pressure caused a 25% drop in the burst pressure and a 36% drop for dent depths ≥ 4%D. Dent-crack defects with ≤2%D dent depths formed at zero pressure had the same burst pressure as plain cracks (Figure 5.5a). With cracks of lengths > 20 mm and dent depth > 2%D, dent cracks were more severe than plain cracks, as shown in figure 5.5b, and figure 5.5c, with the disparity increasing with crack length and denting pressure.

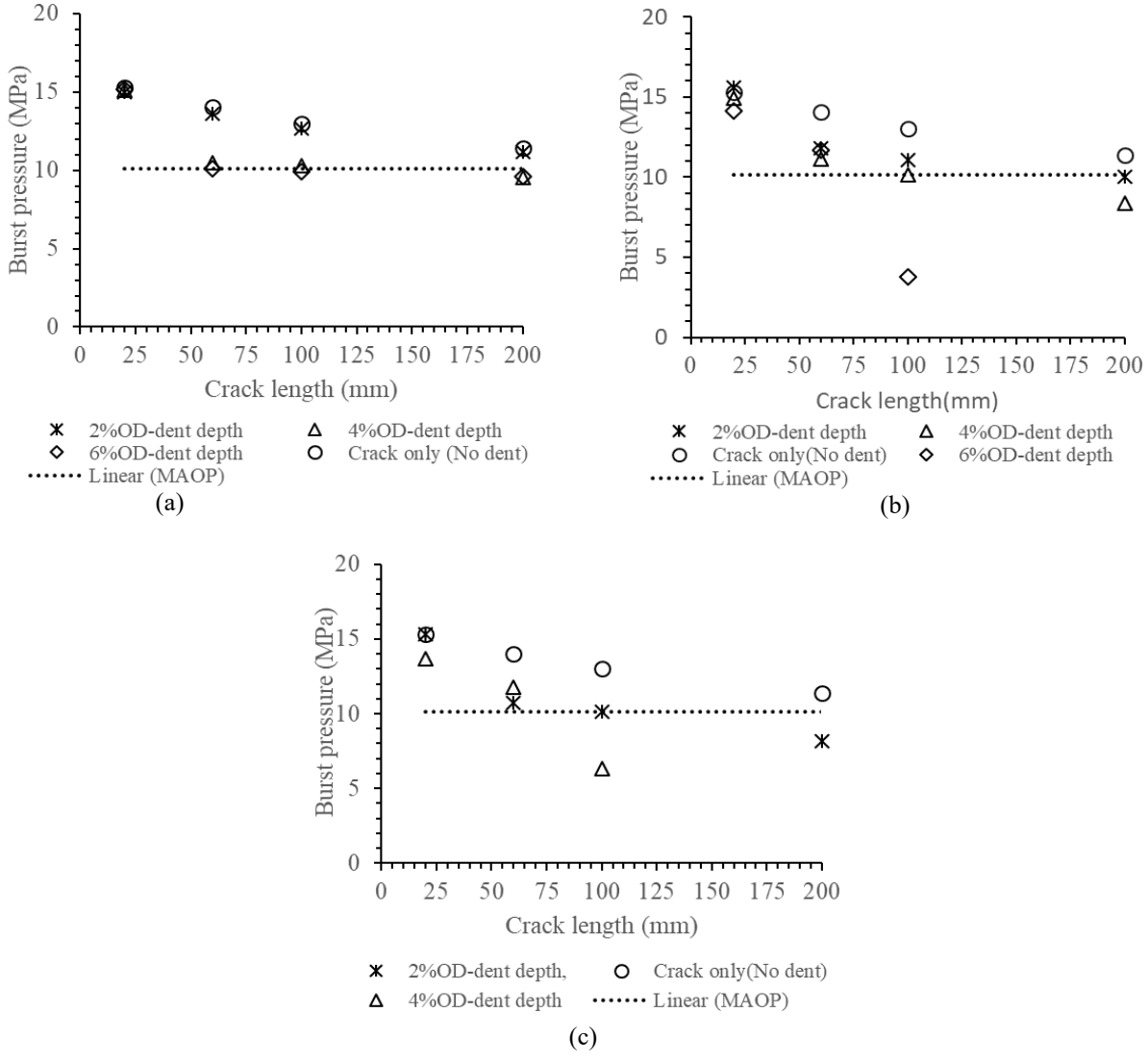

Figure 5.5 Variation of burst pressure of specimens with 0.5t deep crack in dents of different depths formed at (a) Denting pressure =0, (b) Denting pressure $=0.3P_y$; (c) Denting pressure $=0.5P_y$

According to Ghaednia et al. [2-4], dent-crack defects with cracks of 0.5t depth inside dents of 4%D depths were unable to sustain pressure equivalent to the MAOP of the pipe if crack lengths were greater than 75mm, regardless of the pressure at which the dents were formed. This study shows that the margin of safety is higher and varies with pressure. All dents formed at zero pressure with a 0.5t crack would sustain the MAOP for crack lengths < 200mm as shown in figure 5.5a, while figure 5.5b shows that 0.5t deep cracks inside 4%D deep dents formed at $0.3P_y$ denting pressure have limiting length of 100mm. The same defect if formed at $0.5P_y$ would have a limit length less than 100mm.

Ghaednia et al. [2] applied the J-integral concept to decide whether the pipe had failed. Failure occurred when the J-integral value at any point in the crack reached $1.15J_{1c}$, the critical value of J-integral at which the material fractured. We believe, based on our analysis, that using the J-integral value at the tip of an existing crack to determine burst pressure of pipeline is conservative. Whereas crack growth in the model initiated at lower pressure, its progression beyond the immediate vicinity of the original crack tip was slowed by plasticity, enabling the pipes to sustain more pressure before bursting.

5.4.1.3 Effect of dent depth on burst pressure

Increasing the dent depth from 0% to 6%D while keeping the crack length and the crack depth constant did not change the burst pressure if the dent was formed at zero pressure (Figure 5.6a). But, where denting of the pipe was accomplished with the pipe already under pressure, increasing the dent depths at constant crack length and crack depth reduced the burst pressure, as shown in Figure 5.6b, and figure 5.6c. The rate of drop in the burst pressure with dent depth increased with crack length and denting pressure.

Dent-crack defects having dents > 4%D deep, formed at denting pressure > $0.3P_y$ with a crack of length > 100mm and depth ≥ 0.5t were likely to burst at pressures lower than MAOP of the pipe. All dents formed at $0.5P_y$ denting pressure and having crack of lengths >100mm inside them did not sustain the MAOP ($80\%P_y$) of the pipe.

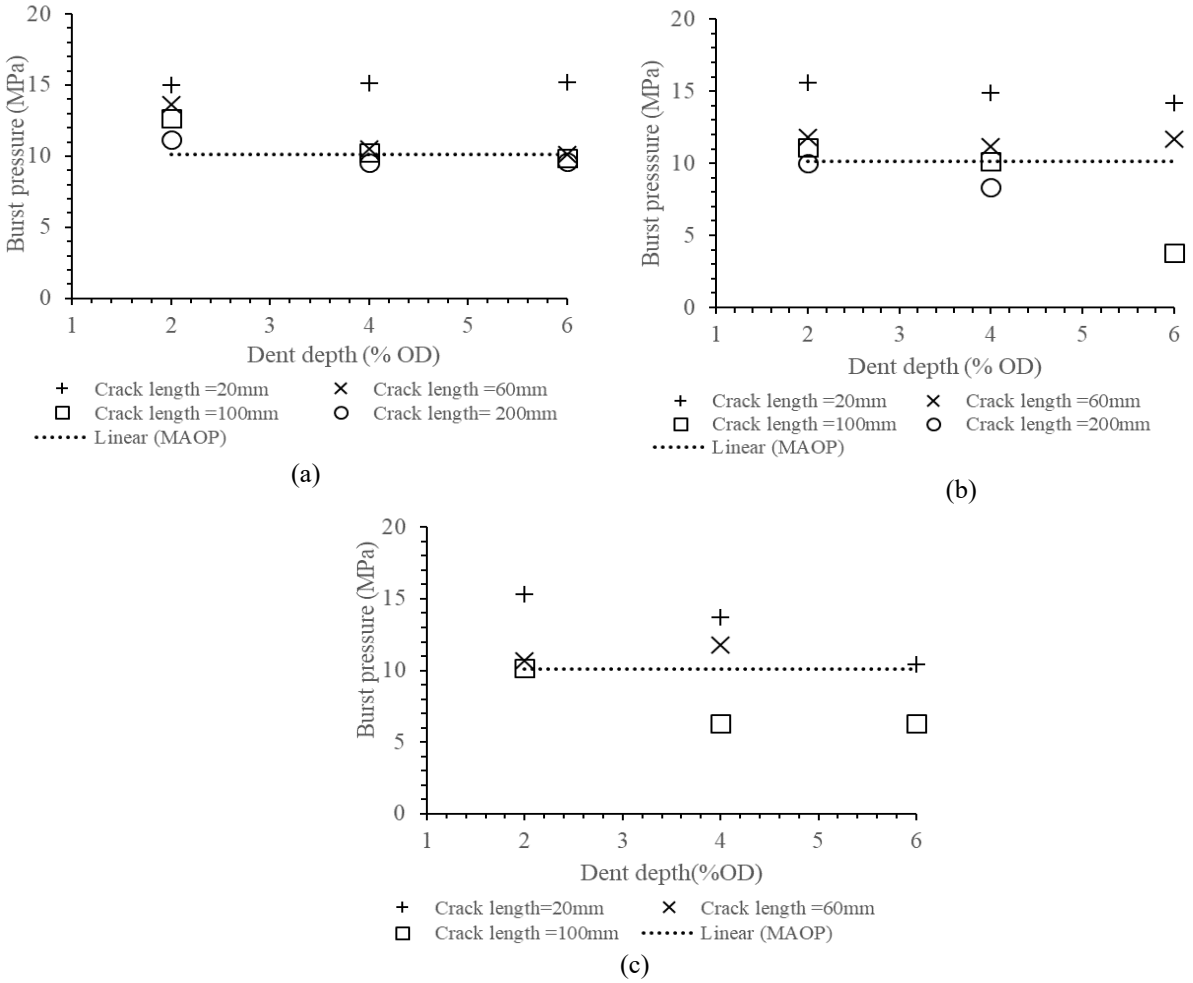

Figure 5.6 Variation of burst pressure with dent depth, for pipes having 0.5t deep cracks of various lengths inside dents formed at: (a) Denting pressure =0, (b) Denting pressure =0.3P_y; (c) Denting pressure =0.5P_y

5.4.1.4 Effect of denting pressure

Figure 5.7 shows the variation of the burst pressure with denting pressure for pipes having different dent depths and crack dimensions. The results show that dent-crack defects formed when the pipe was under pressure were more severe on burst strength. For a given crack length and dent depth, burst pressure dropped with increase in denting pressure. Specimens having crack length ≥100 mm in dents of depth ≥ 4%D formed at 0.3P_y were likely to burst at pressures lower than MAOP of the pipe. All specimens with dents formed at 0.5P_y and having crack length ≥100mm burst at pressures lower than MAOP. It is thus valid to say that dents augmented the effect of cracks on burst pressure, and denting pressure magnified the effect of the dent depth. Dent-crack defects formed

at $0.3P_y$ or lower denting pressures sustained the MAOP if the dent depths are less than 4%D and cracks inside the dents were less than 100mm long and 0.5t deep. Defects formed at $0.5P_y$ only sustained the MAOP if the crack lengths were less than 100 mm. As concluded by Ghaednia et al. [2], dent-crack defects having 4%D deep dents formed at $0.3P_y$ are likely to sustain the MAOP if the crack length is <75mm and crack depth is 0.5t.

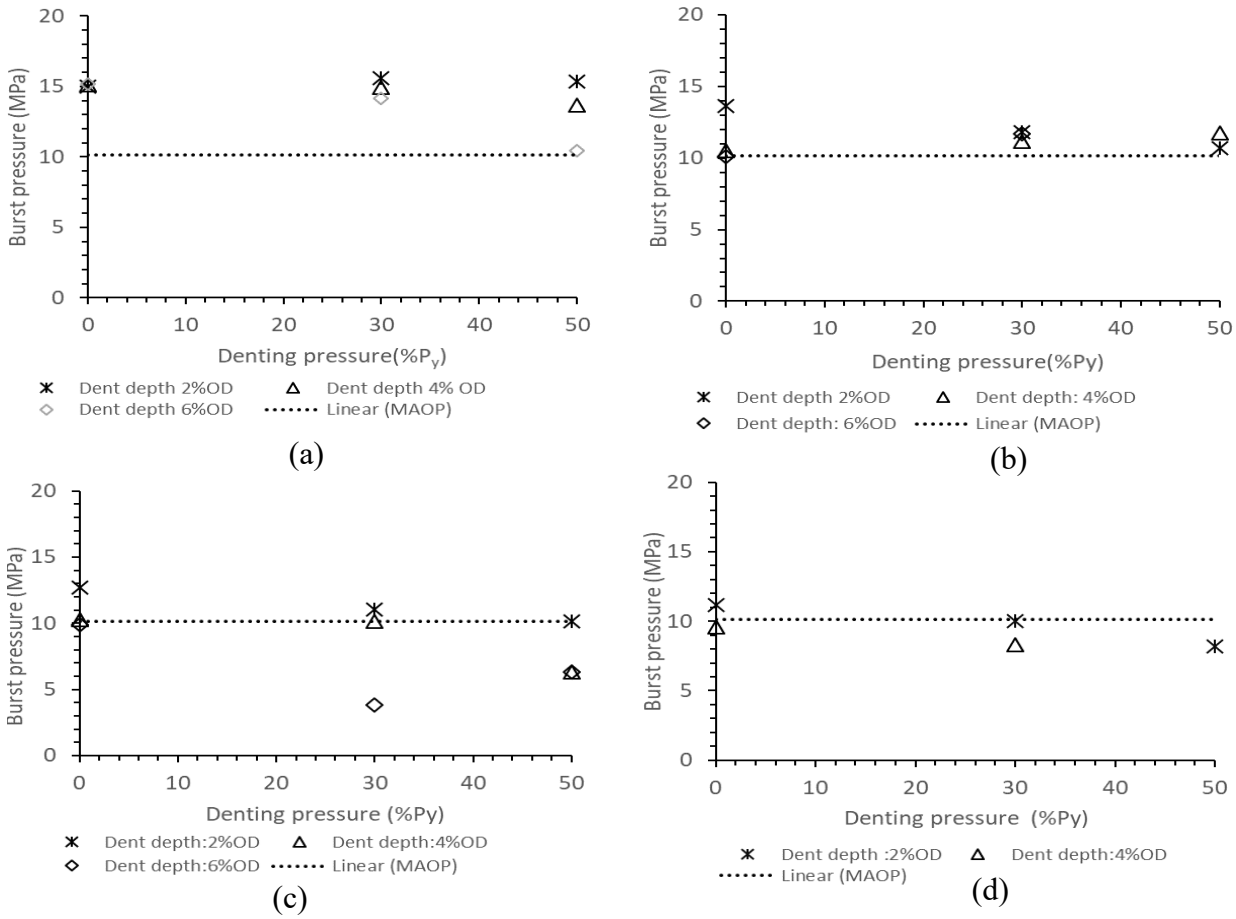

Figure 5.7 Variation of burst pressure with denting pressure, for pipes with 0.5t deep cracks of varied lengths inside dents of varied depths: (a) Crack length = 20mm, (b) Crack length = 60mm, (c) Crack length =100mm and (d) Crack length = 200mm

5.4.2 Restrained concentric dent-crack defects

Figure 5.8 shows the von Mises stress distribution at different stages of crack propagation through the wall of the specimen having a 4mm×60mm crack in a 4%D deep restrained dent formed at $0.3P_y$ denting pressure. The remaining ligaments in the pipe sustained high stresses in excess of

the yield strength (σ_y=540MPa) of the material prior to the start of crack propagation (figure 5.8a), like in the unrestrained dent (figure 5.4a).

Before internal pressure was applied, the von Mises stresses in the restrained dent (figure 5.8b) were lower than the von Mises stresses in the pipe with unrestrained dent (figure 5.4b). This is because a smaller displacement (load) is required to form restrained. Large displacement loads are required to form unrestrained dents of the same depth as part of the displacement is recovered during elastic spring back of the dent. Thus, for dents of the same depth in unpressurised pipes, large stresses detected in the pipe wall are a sign that an unrestrained dent could be present in the pipe, while lower stresses suggest the dent is restrained.

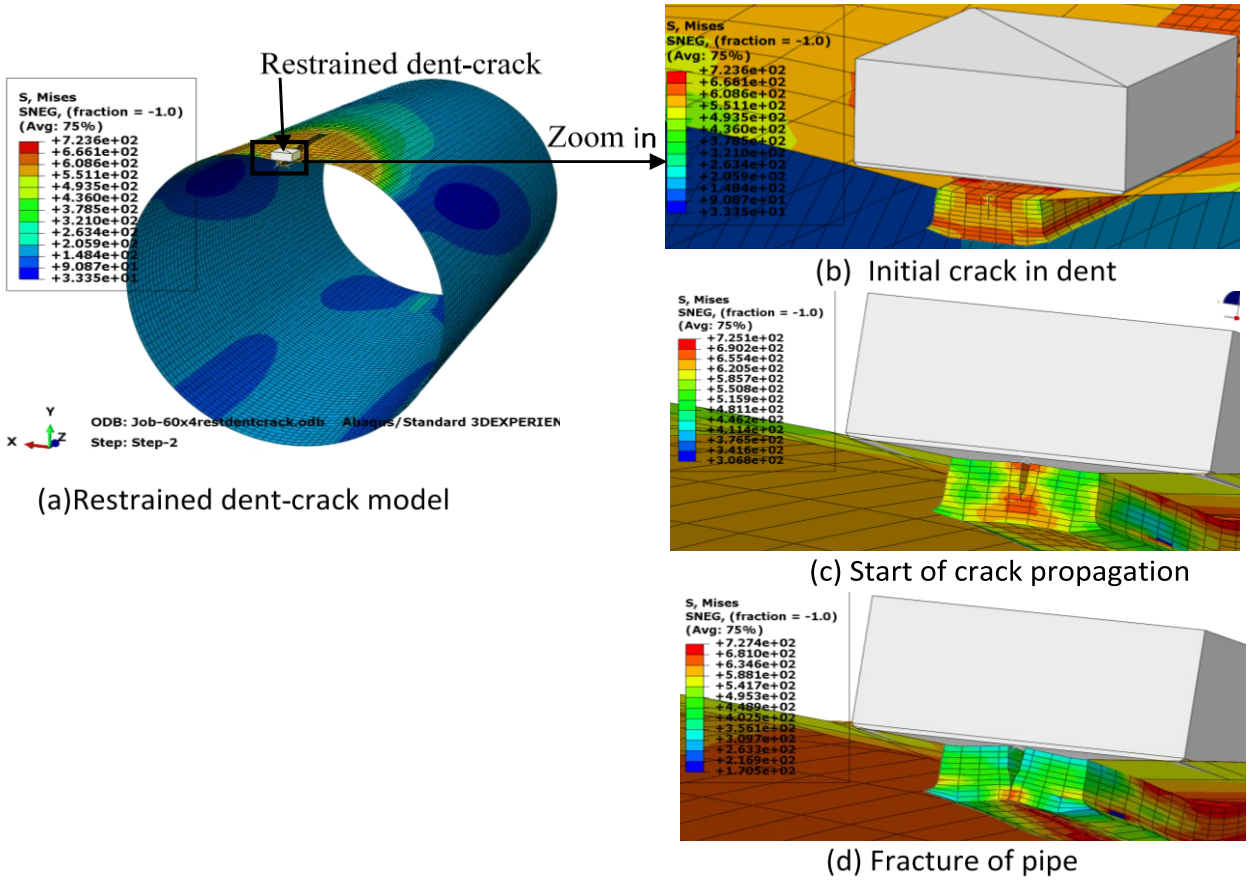

Figure 5.8 Distribution of von Mises stress in pipe wall at various stages of propagation of a crack inside a restrained dent: (a) Model of pipe with restrained dent-crack; (b) Before applying pressure; (c) At start of crack propagation; (d) After fracture is complete

After application of internal pressure to initiate crack propagation, the von Mises stress distribution in the restrained dents (figure 5.8c) become more severe than the von Mises distribution in the unrestrained dent(figure 5.4c), because of a relaxation of stresses within the unrestrained as it rebounds under internal pressure [28], a process that is restricted by the restraining feature in the restrained dents. Thus, detection of large stresses in a dent that has been subjected to large pressure would show the likely hood that the dent is constrained. Low stresses within the dented region suggests presence of unrestrained dents. This agrees with the findings by Alexander and Kiefner [29], who showed that even very deep dents will rebound under pressure if it is unrestrained. Therefore, if a deep dent is detected in a pipe after it has been subjected to significant internal pressure, it is likely that the dent is restrained. But if the dent is very shallow dents after the pipe is pressurized, it is more likely to be an unrestrained dent.

At the point of fracture of the pipe, the von Mises stress distribution in the restrained and unrestrained dents are similar (figures 5.4e and 5.8d). This is would also be expected in a physical pipe when the internal pressures drop due to loss of content from the fractured pipe. But unlike the unrestrained dent, failure of the restrained dent was not accompanied with significant upward displacement of the internal surface of the pipe, showing that the restraint dent prevented rebound by internal pressure.

Currently, there are no studies on the effect of dent restraint on propagation of pre-existing cracks inside dented pipes. However, studies of restrained plain dents show that their primary mode of failure is by puncture of the pipe if the restraining feature is sufficiently pointed [30]. The high stress at the tip of the pointed restraining feature initiates a small crack on the surface of the pipe which then propagates under internal pressure and punctures the pipe. This suggests that a pre-existing stress riser like a crack inside a restrained dent of any shape would similarly propagate at high internal pressure.

It was observed in this study that the pressure required to initiate propagation of cracks found inside restrained dent was very close to the burst pressure of the pipe. While for the unrestrained dent-crack, the burst pressure was significantly higher than the pressure at which the crack begins to propagate. The 4mm×60mm crack inside the 4%D deep unrestrained dent formed at $0.3P_y$ denting pressure (figure 5.4) begun to propagate at a pressure of 9MPa and burst at 11.14MPa.

The difference can be attributed to the ability of the unrestrained dents to rebound under internal pressures. The stresses in the dent are redistributed in the pipe wall according to the extent of dent rebound and the stress concentration within the dent relaxes, allowing it to sustain additional pressure. The rebound is prevented in restrained dent-crack defects and it was also observed that the burst pressure of the pipe with restrained dent-cracks were always higher than those of corresponding unrestrained dent-cracks.

Table 5.3 shows the predicted burst pressure of specimens with various sizes of restrained dent-crack defects. All specimens with cracks of depth 0.2t inside dents sustained pressures greater than the yield pressure, P_y of the pipe without fracturing. Crack length, dent depth, and denting pressures had no measurable effect on the burst pressure of the specimens, as they failed by plastic collapse. Releasing the indenter from the pipe surface with the pipe operating at 80% of the yield pressure (MAOP) did not cause crack propagation in the specimens (Table 5.4).

With a crack of depth 0.5t, burst pressures dropped with increasing crack length, dent depth, and denting pressure like the pipes with unrestrained dent-crack defects. However, burst pressure of specimens with restrained dents-cracks were generally higher than burst pressures of the corresponding specimens with unrestrained dent-cracks (Table 5.2) and plain cracked specimens (Table 5.5). Restraining dents contribute in two ways to improve pipe resistance to fracture. First, compressive stresses from the restraint reduce stress triaxiality at the crack tip and secondly, they counteract hoop stresses from internal pressure. Therefore, high pressure is required to develop the fracture strain and propagate cracks in restrained dents.

Restrained dent-crack defects with crack lengths ≥100mm inside dents of depth ≥ 6%D formed at any pressure were problematic as they displayed susceptibility to unstable crack propagation in circumferential and longitudinal directions. Denting pipes at $0.8P_y$ propagated cracks of length ≥ 100mm inside dents of depths ≥4%D. Releasing the dent restraint at MAOP did not propagate cracks of length <60mm. Cracks of length >60mm propagated but only those with lengths >100 mm and inside dents of depth ≥4%D deep formed at $0.8P_y$ denting pressure propagated until the pipes burst when the dent restraint was released.

Table 5.3 Burst pressure of pipes with restrained concentric dent-crack defect

Crack size (mm)		Denting pressure (MPa)											
Depth	Length	$0.0P_y$			$0.3P_y$			$0.5P_y$			$0.8P_y$		
		Dent depth (%OD)											
		2%	4%	6%	2%	4%	6%	2%	4%	6%	2%	4%	6%
		Burst pressure (MPa)											
0.2t	20	16.76[i]	15.97[i]	15.83[i]	15.73[i]	15.72[i]	15.94[i]	15.75[i]	16.26[i]	15.81[i]	16.05[i]	15.80[i]	15.98[i]
	60	17.25	16.87[i]	15.80[i]	15.69[i]	15.63[i]	15.78[i]	15.62[i]	15.68[i]	15.91[i]	16.06	15.95[i]	15.88[i]
	100	16.62	15.82[i]	15.93[i]	15.66[i]	15.79[i]	15.91[i]	15.59[i]	15.63[i]	15.60[i]	15.95[i]	15.80[i]	15.81[i]
	200	16.45	15.84[i]	15.79[i]	15.60[i]	15.93[i]	15.65[i]	16.01[i]	15.75[i]	16.10[i]	15.74	16.03	16.47[i]
0.5t	20	16.26[i]	16.22[i]	16.03[i]	15.95[i]	15.83[i]	15.98[i]	15.76[i]	15.71[i]	16.06[i]	16.03[i]	16.04[i]	16.03[i]
	60	15.67	16.03	16.18[i]	15.53	15.61[i]	16.10[i]	15.76	15.98	16.14[i]	15.58	15.91	16.06
	100	15.35	15.86	15.97[h]	15.5	15.65[i]	14.06[h]	15.45	15.71	6.47[h]	15.28	15.22	**
	200	14.93	15.23	13.76[h]	14.83	15.16	11.82[h]	14.77	15.09	10.06[h]	14.36	**	**

[i]: Pipe plasticizes without crack propagation; [h]: Longitudinal crack propagates in circumferential direction; *: Crack propagated by denting pressure; **: Crack propagates during denting, dent formation unsuccessful; t: wall thickness; OD: Outside/external diameter; P_y: yield pressure

Table 5.4 Effect of releasing indenter at maximum allowable operating pressure ($80\%P_y$)

Crack size (mm)		Denting pressure (MPa)											
Depth	Length	$0.0P_y$			$0.3P_y$			$0.5P_y$			$0.8P_y$		
		Dent depth (%OD)											
		2%	4%	6%	2%	4%	6%	2%	4%	6%	2%	4%	6%
0.2t	20	✓	✓	✓	✓	✓	✓	✓	✓	✓	✓	✓	✓
	60	✓	✓	✓	✓	✓	✓	✓	✓	✓	✓	✓	✓
	100	✓	✓	✓	✓	✓	✓	✓	✓	✓	✓	✓	✓
	200	✓	✓	✓	✓	✓	✓	✓	✓	✓	✓	✓	✓
0.5t	20	✓	✓	✓	✓	✓	✓	✓	✓	✓	✓	✓	✓
	60	✓	✓	✓	✓	✓	✓	✓	✓	✓	✓	✓	✓
	100	✓	✓	✓	✓	✓	✓[h]	✓	✓	✓[h]	✓	✓	✗[3]
	200	✗	✗	✗	✗	✗	✗	✗	✗	✓[h]	✗	✗	✗[2]

✓: No crack propagation, ✓: Crack propagates but does not burst the pipe; ✓[h]: Crack propagated in circumferential direction but no burst; ✗: Pipe burst as indenter is released; ✗[2]: Pipe bursts during denting, ✗[3]: Pipe bursts during pressurization, with dent restrained; ***t***: wall thickness.

Table 5.5 Burst pressure of specimens having plain cracks

Crack size (mm)		Burst Pressure (MPa)
Depth	Length	
0.2t	20	15.75
	60	15.62
	100	15.43
	200	15.00
0.5t	20	15.32
	60	14.04
	100	13.00
	200	11.39

5.5 Conclusion

Burst pressure of pipeline with restrained and unrestrained concentric dent-crack defects was investigated in this study, considering the effect of varying crack geometry, dent depth, and denting pressure. Predicted burst pressures are compared with burst pressure of longitudinally cracked pipes without dents. Lastly, the effect of releasing the indenter from pipe surface when the pipe is operating at its maximum allowable operating pressure on crack propagation was assessed.
Specimens with unrestrained concentric dent-crack defects with dent depth of 2%D formed at zero denting pressure had the same burst pressure as plain cracked specimens, but dent-crack defects were more injurious than plain cracks with increasing dent depth and denting pressures. A 0.2t deep crack in dents formed at zero pressure was not problematic because the affected specimen sustained the MAOP of the pipe without the crack propagating, for crack lengths ≤ 200mm and dent depths ≤ 6%D.

Unrestrained dents of depth 6%D formed at pressures $>0.3P_y$, with cracks of depth ≥ 0.2t, did not sustain the MAOP of the pipe. The cracks propagated at pressures lower than MAOP of the pipe, and risk of bursting at pressure lower than MAOP increased with crack length and denting pressure.

Specimens with restrained dent-crack defects had higher burst pressure than the corresponding specimens with unrestrained dent-crack defects and releasing the restraint at MAOP did not propagate 0.2t deep cracks but propagated 0.5t deep cracks. Risk of propagation and bursting increased with crack length, denting pressure, and dent depth. All cracks with length >60mm propagated but only those of length > 100mm propagated until the pipes burst when dent restraint was released at MAOP of the pipe.

Increasing crack depth, crack length, and dent depth were more detrimental to pipe integrity than increasing denting pressure. But, deep dents (>4%D) disproportionately increased the effect of the other defect parameters on pipeline integrity and burst pressure.

Pipelines with restrained concentric dent-crack defects are safe for service at maximum allowable operating pressure of the pipe if the restraints remain in position on the pipe surface. Integrity of

pipelines with unrestrained concentric dent-cracks vary with defect geometry. Affected pipelines retain significant strength and may be maintained in service with careful assessment.

Although only two crack depths were considered in this study, the results suggest that dent-crack defects are not too severe on integrity of pipelines subjected to monotonically increasing pressure. A study involving more crack depths and locations within dents other than the dent center (apex) is required for a broader understanding of the effect of dent-crack defects on the integrity of pipelines. Our future work will investigate more crack depths and the effect of cracks located in the flank of dents on burst pressure. Additionally, the fatigue life of pipelines with dent-crack defects, which has not been the focus of the present study, will be investigated.

5.6 References

[1].The American Society of Mechanical Engineers. *Gas Transmission and Distribution Piping System: ASME Code for Pressure Piping, B31*; ASME-B31.8; Revision to B31.8-1999; The American Society of Mechanical Engineers, New York, USA ,2003.

[2].Ghaednia, H.; Das, S.; Wang, R.; Kania, R. Dependence of burst strength on crack length of a pipe with a dent-crack defect. *J. Pipeline Syst. Eng. Pract.* 2017, *8*, 4016019.

[3].Ghaednia, H.; Das, S.; Wang, R.; Kania, R. Effect of operating pressure and dent depth on burst strength of NPS30 line pipe with Dent-Crack defect. *J. Offshore Mech. Arct. Eng.* 2015, *137*, 031402-8.

[4].Ghaednia, H.; Das, S.; Wang, R.; Kania, R. Safe burst strength of a pipeline with dent-crack defect: Effect of crack depth and operating pressure. *Eng. Fail. Anal.* 2015, *55*, 288–299.

[5].Rafi, A.; Silva, J.; Kenno, S.; Das, S.; Kania, R.; Wang, R.Y. Strength of line pipe with dent and crack defect. In Proceedings of the 8th International Pipelines Conference, IPC 2010-31095, Calgary, AB, Canada, 27 September–1 October 2010.

[6].Bedairi, B.; Cronin, D.; Hosseini, A.; Plumtree, A. Failure prediction for crack-in corrosion defects in natural gas transmission pipelines. *Int. J. Press. Vessel. Pip.* 2012, *96*, 90–99.

[7].Vilkys, T.; Rudzinskas, V.; Prentkovskis, O.; Tretjakovas, J.; Višniakov, N.; Maruschak, P. Evaluation of failure pressure for gas pipelines with combined defects. *Metals* 2018, *8*, 346.

[8].Ronny, H.; Espen, B.; Lijana, D.O. Damage assessment of pipelines with dents and cracks, proposal for methodology for calculation of acceptable dimensions of a combination of crack, & dent in subsea pipelines. In Proceedings of the ASME 29th International Conference on Ocean, Offshore and Arctic Engineering, Shanghai, China, 6–11 June 2010.

[9].Lancaster, E.R.; Palmer, S.C. Burst pressures of pipes containing dents and gouges. *Proc. Inst. Mech. Eng. Part E J. Process Mech. Eng.* 1996, *210*, 19–27.

[10].Cosham, A.; Hopkins, P. The effect of dents in pipelines—Guidance in the pipeline defect assessment manual. *Int. J. Press. Vessel. Pip.* 2004, *81*, 127–139.

[11].Macdonald, K.A.; Cosham, A. Best practice for the assessment of defects in pipelines—Gouges and dents. *J. Eng. Fail. Anal.* 2005, *12*, 720–745.

[12].Orynyak, I.; Yakovleva, E.; Rozgonyuk, V. Application of the cheng-finnie method to the calculation of stress intensity factors in thin-walled pipes with long axial cracks with allowance for geometric nonlinearity. *Strength Mater.* 2007, *39*, 455–465.

[13].Bai, Y.; Song, R. Fracture assessment of dented pipes with cracks and reliability-based calibration of safety factor. *Int. J. Press. Vessel. Pip*. 1997, *74*, 221–229.

[14].Das, S.; Cheng, J.J.R.; Murray, D.W. Prediction of fracture in wrinkled energy pipelines subjected to cyclic deformations. *Int. J. Offshore Polar Eng*. 2007, *17*, 205–212.

[15].Adeeb, S.M.; Horsley, D.J. A numerical procedure to establish a safe working pressure during excavation of a pipeline in a rock ditch. *Int. J. Press. Vessel. Pip.* 2006, *83*, 488–497.

[16].Tian, X.; Zhang, H. Failure criterion of buried pipelines with dent and scratch defects. *J. Eng. Fail. Anal.* 2017, *80*, 278–289.

[17].Kainat, M.; Langer, D.; Hassanien, S. Do we need a safe excavation pressure for dented pipelines: How should it be defined? In Proceedings of the 12th International Pipelines Conference, Ipc2018-78376, Calgary, AB, Canada, 24–28 September 2018.

[18].Rosenfield, M.J.; Pepper, J.W.; Lewis, K. Basis of the New Criteria in ASME B31.8 for Prioritization, & Repair of Mechanical Damage. *Int. Pipeline Conf.* 2002, *36207*, 647–658.

[19].Okodi, A.; Lin, M.; Yoosef-Ghodsi, N.; Kainat, M.; Hassanien, S.; Adeeb, S. Crack propagation and burst pressure of longitudinally cracked pipeline using extended finite element method. *Int. J. Press. Vessel. Pip.* 2020, *184*, 104115.

[20].Melenk, J.M.; Babuska, I. The partition of unity finite element method: Basic theory and applications. *Comput. Methods Appl. Mech. Eng.* 1996, *139*, 289–314.

[21].Moes, N.; Dolbow, J.; Belytschko, T. A finite element method for crack growth without remeshing. *Int. J. Numer. Methods Eng.* 1999, *46*, 131–150.

[22].Fries, T.P.; Belytschko, T. The extended/generalized finite element method: An overview of the method and its applications. *Int. J. Numer. Methods Eng.* 2000, *84*, 253–304.

[23].Dassault Systèmes. *Abaqus Documentation* ; Dassault Systèmes : Velizy-Villacoublay, France, 2016.

[24].Liu, X.B.; Zhang, H.; Han, Y.; Xia, M.; Ji, Y. Numerical and Experimental study on critical crack tip opening displacement of X80 pipeline steel. *Mechanics* 2017, *23*, 204–208.

[25].Li, H.; Chandra, N. Analysis of crack growth and crack-tip plasticity in ductile materials using cohesive zone models. *Int. J. Plast.* 2003, *19*, 849–882.

[26].Anderson T.L, “Fracture mechanics fundamentals and applications”, Taylor and Francis, 2005.

[27].Cravero, S.; Ruggeri, C. Structural Integrity Analysis of Axially Cracked Pipelines Using Conventional and Constraint-Modified Failure Assessment Diagrams. *Int. J. Press. Vessel. Pip.* 2006, *83*, 607–617.

[28].Race J.M, "Integrity assessment of plain dent subject to fatigue loading", University of Newcastle, School of Marine Science and Technology, Report prepared for UKOPA, 2008.

[29]. Alexander C.R., Kiefner J.F., "Effect of smooth and rock dents on liquid petroleum pipelines", American Petroleum Institute, API 1156, 1997.

[30].Kiefner J.F., and Alexander C.R., "Effect of smooth and rock dents on liquid petroleum pipelines (Phase II)", American Petroleum Institute, Addendum to API 1156, 1999.

6. EFFECT OF LOCATION OF CRACK IN DENT ON BURST PRESSURE OF PIPELINE WITH COMBINED DENT AND CRACK DEFECTS

This chapter is derived from a research article submitted for publication in the Journal of Pipeline Sciences and Engineering: Allan Okodi, Yong Li, Cheng, J.J.R., Muntaseer Kainat, Nader Yoosef-Ghodsi, Samer Adeeb, Effect of location of crack in dent on burst pressure of pipeline with combined dent and crack defects

6.1 Abstract

Burst pressure of pipelines with longitudinal cracks located at the centre of rectangular dents varies with defect size and recent reports indicate that it could be very high for shallow cracks inside shallow dents and for cracks inside restrained dents. However, it is not clear whether cracks located in the flank of dents would have the same impact on burst pressure of pipelines with dent-crack defects. In addition, studies show that the location of maximum strain in circular dents shifts away from the centre towards the flank when dented pipes are pressurized, but the implication on the propagation of longitudinal cracks located in various parts of a dent has not yet been widely investigated. In this paper, models of pipelines with longitudinal cracks inside rectangular dents were created using the Finite Element Methods software Abaqus to analyze crack propagation and predict the associated burst pressure. The in-built Extended Finite Element procedure in Abaqus was used to model crack propagation through the pipe. The models were calibrated and validated using previously published results of burst tests and tests of material properties. The effect of longitudinal cracks in both the flank and centre of the dents on the burst pressure was analyzed by varying the crack length, the crack depth, the dent depth, the internal pressure during dent formation and the dent constraint condition. The results show that longitudinal cracks in the flank of rectangular dents are more severe for pipeline integrity than cracks located in the centre of dents. Crack depth and crack location inside the dents are the most influential parameters when assessing dent-crack defects in pipelines. Their effects on burst pressure are magnified by crack length, dent depth and denting pressure.

Keywords: Combined defect; pipeline; surface crack; through wall crack; burst pressure; flank of dent; finite element method; extended finite element method.

6.2 Introduction

Over eighty percent of excavated pipelines have some form of dents [1], often in combination with other defects such as cracks and metal losses in the forms of scratches, gouges, and corrosion. It is therefore practically impossible to repair all dents found in pipeline and an engineering assessment is usually conducted to prioritize them for digs and repair. Dents adjacent to welds may cause cracks to develop in the welds, resulting in a combined defect commonly referred to as crack in dent or dent-crack defect, which has been found to cause premature failure of pipelines [2] and

are prioritized for attention by pipeline operators. Dents in onshore pipelines are mainly caused by third party activities along the pipeline, such as the impact of an excavator bucket during excavations for new developments. But they may also be the result of placing pipes on hard rocks during construction, producing a constrained or rock dent in the pipeline [3].

Research shows that dents are regions of stress and strain concentration in pipelines and represent areas for potential crack initiation and growth. The distribution of stress and strain in a dent varies with the dent shape [4-6]. The profiles of stress and strain along the axis of a pipe having a long dent are constant but they vary sharply with length in pipes with short (local) dents. The maximum stress and strain occur at the root of long dents, and in the flank of short dents. Ong et al. [6] experimentally investigated strain distribution in small mild steel pipes with short, plain dents subjected to modest internal pressure. The results confirmed the existence of high external strains in the flanks of a short dent along its longitudinal axis when the pipe is pressurized. Lancaster and Palmer [7] investigated strain concentrations in pressurized dented small aluminum pipes. Their analysis of elastic strain distribution within the dents similarly showed that high external strains and stresses existed in the axial extremities of the dents. Furthermore, fatigue tests [8,9] show cracks are more likely to initiate in the flanks of short dents and at the root of long dents, which is more evidence that the location of peak hoop stress and strain vary with the shape of dent. Tian and Zhang [10] and Vilkys et.al [11] also found that the location of maximum strain in circular dents shift from the centre towards the flanks when the dented pipe is pressurized.

Studies on dent-crack defects are very scarce, particularly studies on the effect of location of cracks in dents on burst pressure [12-15]. A useful study for understanding the potential effect of location of cracks inside dents on burst pressure of pipeline was conducted by Lancaster and Palmer [16], who showed that the burst pressure of small aluminum pipes having gouges inside dents is influenced by the relative location of the gouge inside the dent. Pipes having long axial gouges in dents and those with gouges located at the axial extremities of the dents had lower burst pressure than those with axial gouges at the center of the dents. However not all gouges located within axial extremities had low burst pressure, although all low burst pressures were due to gouges in the axial extremities of dent. This shows there is a specific zone within the axial extremities of dent where hoop stresses and strains are the highest. Understanding the profile of hoop strain and stress distributions inside a dent of a particular shape is necessary to understand the development and

propagation of planar surface defects like cracks and gouges inside the dent and how the crack and dent interact to degrade the integrity of the pipe. The stress environment at the tip of cracks is more severe than the environment at the tip of other planar defects like scratches and gouges therefore dent-cracks are expected to be more severe on the integrity of pipeline than dents combined with scratches and gouges.

The implications of these results for propagation of cracks in dented pipelines have not been analyzed but it strongly suggests that the location of a crack inside a dent could influence the burst pressure. Ghaednia [15] tested two pipes with rectangular dent-crack defects, considering a dent placed parallel to the longitudinal axis of the pipe and another placed at an angle of 26 degrees to the longitudinal axis of the pipe. In both cases, the crack was parallel to the longitudinal axis of the pipe and inside the dent. Hence the defect in the first test was a concentric dent-crack defect, and the one in the second test had the crack along the diagonal of the rectangular dent and passing through one corner of the dent. The pipes were reported to have the same burst pressure regardless of the orientations of the cracks in the dents, leading to the conclusion that the location of crack does not affect burst pressure if the crack is inside the dent. The conclusion is not supported by relevant literature on strain and stress distribution in dents and more investigation is needed. Okodi et. al [17] previously investigated the burst pressure of pipelines with longitudinal cracks of depth to wall thickness ratio (a/t) of 0.2 and 0.5 located at the centre of dents, considering both restrained and unrestrained dent conditions. The results show that the burst pressure varies with defect geometry and are relatively high for shallow cracks in dents, suggesting that concentric dent cracks are not always severe on the pipeline integrity and affected pipes may be retained in service with a fitness for service assessment. However, it is not clear if similar behavior could be obtained with cracks located away from the center of dents considering that the distribution of strain and stress in dents varies with location.

Currently, there are no analytical models accepted by the pipeline industry for assessment of burst pressure of pipelines with dent-crack defects [18]. The assessment could be performed using costly full-scale burst tests and traditional finite element method (FEM), which do not give timely results for quick integrity decision requirements. Although the traditional FEM could provide accurate predictions and can evaluate complex defect geometries, it lacks an in-built criterion for determining failure and is also not suitable for analyzing propagating cracks because the crack

domain must be re-meshed with each crack extension. The Extended Finite Element Method (XFEM) [19-21] is a relatively new extension of the traditional FEM that is suitable for analysis of propagating cracks. It uses an intra element algorithm incorporated in the standard FEM algorithm to freely lay a crack inside the domain without tying it to boundaries of mesh elements, thus overcoming the requirement to match mesh geometry to crack geometry. The software searches for regions of crack initiation where stresses and strains due to the applied load exceed specified damage parameters of the model, after which the software generated phantom nodes and their superposed original real nodes separate and the crack propagates, following a specified traction separation law (TSL) and damage evolution criterion. The burst pressure of the pipe with a surface crack inside a dent is the pressure required to propagate the crack until it penetrates the full thickness of the pipe. The XFEM procedure in Abaqus finite element analysis software [22] was used in this study to predict the burst pressure of pipelines with longitudinal cracks of depth to wall thickness ratio (a/t) of 0.2, 0.35 and 0.5 located at the centre and in the flank of dent (figure 6.1). Denting was done at different internal pressures and both restrained and unrestrained dent conditions were considered. Defects formed when the pipe is under internal pressure represent defects formed in in-service pipelines, while defects formed in unpressurised pipe represent those formed before the pipeline is commissioned for operation, like during construction or transportation of the pipes to construction site. The flawed pipes were subjected to monotonically increasing internal pressure until burst occurred and the results for different crack locations are compared to assess the effect of crack location inside dents on the burst pressure.

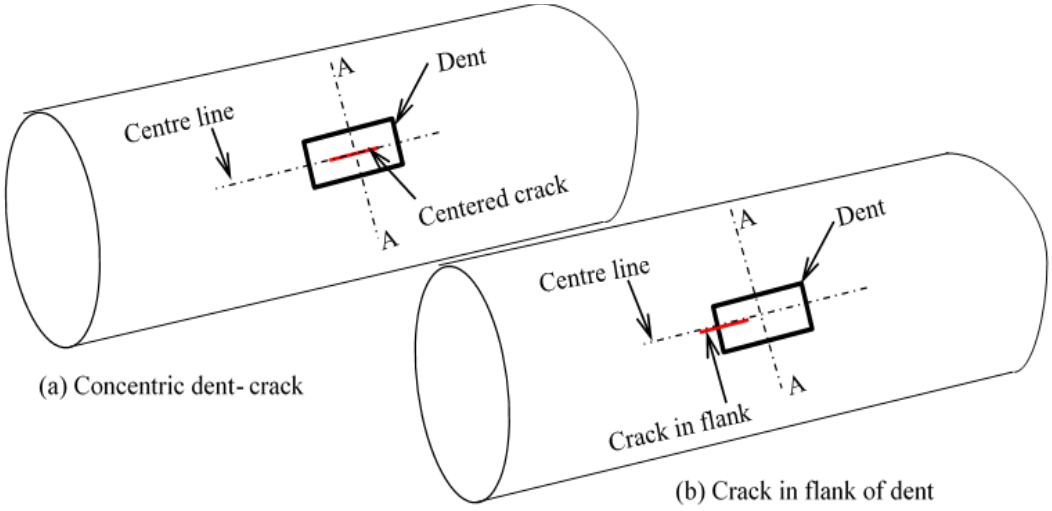

Figure 6.1 Location of cracks inside dents in pipeline having dent-crack defects

6.3 Methodology

Parametric analysis of the burst pressure of pipeline with dent-crack defects was conducted for cracks located in the flank of dents and for cracks located at the center of the dents. Table 6.1 shows a summary of defect parameters used in the analysis. Cracks in the flanks were positioned by moving the crack along the longitudinal axis of the dent to begin at an offset distance of 40mm from the centre of the dent. This ensured that all cracks extended into the axial extremities of the dent, including the shortest crack. Axially centred cracks were obtained by placing the cracks concentric with the dent.

Table 6.1 Parameters of the dent-crack defects

Defect parameter						
Crack location	Dent condition		Crack length (mm)	Crack depth (a) (%t)	Dent depth (%D)	Denting pressure (% P_y)
Flank	Restrained	Unrestrained	20, 60, 100, 150	20, 35, 50	2,4,6	0,30,50
Centre	-	Unrestrained	20, 60, 100, 150	20*, 35, 50*	2,4,6	0,30,50

(*) These results were reported in our previous study [17], t-Wall thickness, D-Outside pipe diameter, P_y-Yield pressure.

The calculated yield pressure P_y, of the pristine pipe was 12.67MPa, determined based on the nominal dimensions and yield stress of the pipe using the formula: $P_y = {}^{2t\sigma_y}/_{D}$ where σ_y is the yield stress of the pipe material, t and D are as defined in table 6.1 and had values of 8.5mm and 762mm respectively.

6.3.1 Numerical modelling

Maximum principal strain (Maxpe) and fracture energy (G_c) were used as the XFEM damage parameters for crack initiation and evolution respectively, with exponential traction separation law, which is recommended for cohesive zone modelling of fracture in ductile metals [23]. The pipe material was modelled as elastic-plastic with isotropic hardening behavior, based on the average stress-strain curve obtained from tensile tests. Dents were formed in the pipe wall by applying vertical downward displacements to the surface of the pipe through a rigid rectangular indenter. The indenter was left on the surface of the pipe after applying the displacement to form restrained or constrained dents, while the unrestrained dents were formed by releasing the rigid indenter from the pipe surface to allow for elastic spring back of the dent to the desired permanent depth. The

displacements required to form the dents increased with dent depth and denting pressure. Larger displacements were required to form unrestrained dents than restrained dents because of the elastic spring back in unrestrained dents. The applied denting displacements for the restrained dents are equivalent to the desired dent depths (2%, 4% and 6%D) because the indenter remains on the pipe after denting. The depths of the unrestrained dents are determined after elastic spring back. Table 6.2 shows the denting displacements used in forming restrained and unrestrained dents of various depths for different denting pressures.

Table 6.2 Displacements required to form restrained and unrestrained dents in the pipes

Denting pressure (%P_y)	Dent depth %D (mm)	Denting displacements (mm)	
		Restrained dent	Unrestrained dent
0	2 (15.7)	15.7	32
	4 (30.48)	30.48	53
	6 (45.7)	45.7	67
30	2 (15.7)	15.7	38
	4 (30.48)	30.48	60
	6 (45.7)	45.7	78
50	2 (15.7)	15.7	43
	4 (30.48)	30.48	66
	6 (45.7)	45.7	86

6.3.1.1 Set up of the model

Figure 6.2 shows the model setup, boundary conditions and mesh distribution. Detailed description can be found in a previous study [17] involving longitudinal cracks of depth to wall thickness ratios (a/t) of 0.2 and 0.5 located at the centre of rectangular dents (table 6.1). A third crack, with a/t = 0.35 located at the centre of the dent was modelled in the current study. In addition, the three cracks (a/t = 0.2,0.35 and 0.5) were modelled when located in the flank of the dent. The flank cracks were placed in such a way that the whole length would be within the flank of the dent if they were short, while a small portion of long cracks would extend into the rim of dent. Defects located at the centre of the dent allow symmetry boundary conditions to be used at the centre of the pipeline so that only half of the pipe is modelled. But this is not possible when the cracks are in the flanks of dents even if the dents are centred on the pipeline. Therefore, the flank cracks models in this study comprised of full lengths of the pipe, cracks, and indenters. The models consisted of a deformable solid strip 500mm in length, 20mm in width, and 8.5mm thick coupled to a deformable shell with outside diameter of 762mm, 2500mm long and 8.5mm thick using shell solid coupling constraint in Abaqus [22]. Shell geometry was defined by the top surface such that

the pipe was assembled by joining the top edges of the shell and the solid strip. The crack was modelled as a planar shell of elliptic geometry embedded in the solid strip. The indenter was modelled as a discrete rigid solid rectangular block. Surface to surface standard contact was used between the pipe and the indenter. Vertical support was provided at the bottom of the model by restraining the degree of freedom U2 at locations that were placed on steel blocks during the reported experimental burst test [12-13]. Kinematic coupling constraint was used at the ends of the pipe, such that it was fixed against displacement and rotation but allowed to freely expand under internal pressure.

6.3.1.2 Mesh distribution

Eight-node linear brick elements (C3D8R) with reduced integration were used in the solid part of the pipe, while four-node (S4R) elements with quad-dominated free mesh were used in the shell. Mesh sensitivity analysis was done to optimize the accuracy of prediction against the time taken to complete the analysis. Predictions were more sensitive to the size of elements in the solid part because it had the crack. Therefore, mesh refinement was done in the solid, while a coarser mesh was used in the shell. Element dimensions in the solid were 5mm×2.86mm×0.85mm in the longitudinal, circumferential and, thickness directions of the pipe respectively, resulting in a total of 10 elements in the thickness direction. The size of the shell elements was 18mm.

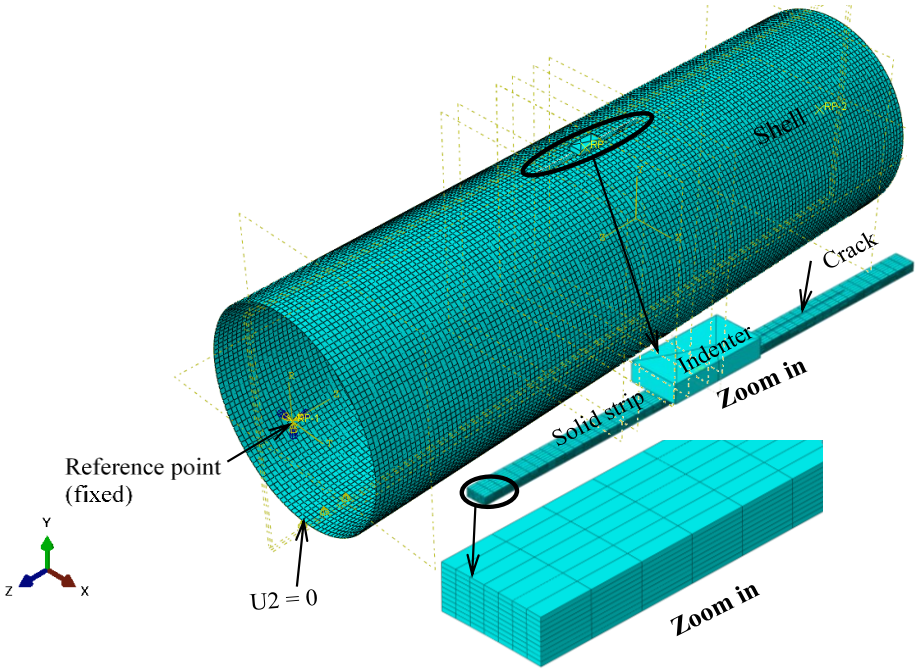

Figure 6.2 Model set up and mesh distribution

6.3.1.3 Calibration and validation of the model

Results of four full-scale burst pressure tests and material properties of specimens of API X70 pipeline were obtained from published literature [18] and used to calibrate and validate the numerical XFEM models for parametric analysis. The material property data obtained were the stress-strain curve, the yield stress, the ultimate tensile stress, the Poison's ratio and the elastic Young's modulus of the pipeline steel. Details of the calibration and validation procedure have been published previously [17]. It was determined through the calibration and validation process that the model predictions using maximum principal strain (Maxpe) of 0.045 and fracture energy (G_c) of 2kJ/m^2 as XFEM damage parameters agreed with the results of the full-scale burst tests.

6.4 Results and discussion

6.4.1 Strain and stress distribution in plain rectangular rents

6.4.1.1 Dents formed when the pipe is not pressurized

Figure 6.3 shows the variation of circumferential (hoop) strain, equivalent plastic strain and circumferential stress along the longitudinal axial centerline of a 2%D deep plain dent formed at zero denting pressure. The strains and stresses were extracted from the external surface of the dent at different stages of loading. The curves are computer generated, to show trends of distribution. The grey colored lines show strain and stresses in the restrained dent (indenter kept on dented pipe), the red lines show distributions in the unrestrained dent (after elastic spring back), and the blue lines show distributions after moderate pressurization of the unrestrained dent. The peak strain and plastic deformation occur within the central region of the dent (figures 6.3a and 6.3b). The gap in figure 3a between the strain distribution curves for restrained and unrestrained dents are a result of the elastic spring back, while the gap between the distributions in unrestrained dent and the moderately pressurized dent precipitated by the rebound under pressure. The gaps are small and uniform within the central region of the dent but widen towards the extremities of the dent, suggesting that more plastic strains develop in the extremities of dent than at the centre after pressurization. This is confirmed by plotting the distribution of the equivalent plastic strain (PEEQ) along the pipe length (figure 6.3b). The PEEQ curves for restrained and unrestrained dents overlap, confirming elastic spring back is not associated with any plastic strain. The gap created by moderate pressurization is wide in the extremities of the dent where growth in the plastic strain

is the highest. This is in keeping with studies that show that maximum strains in circular dents shift from the center to the flanks after pressurization [24].

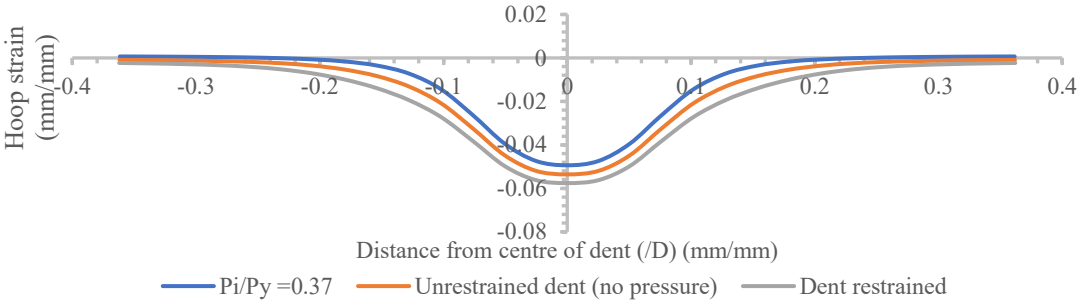

(a) Hoop strain distribution along the longitudinal axis of

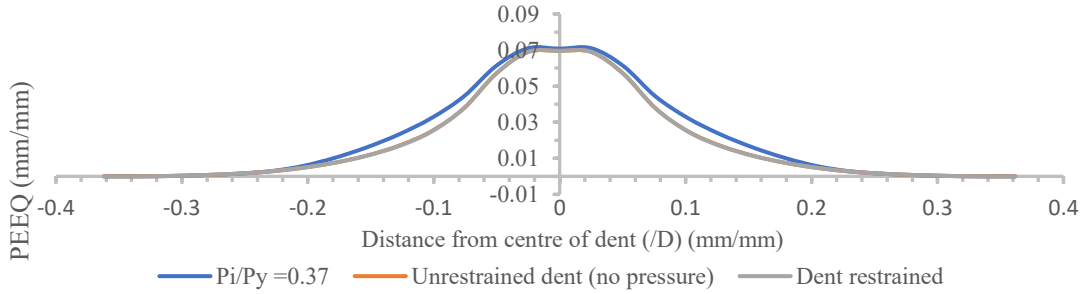

(b) Equivalent plastic strain distribution along the longitudinal

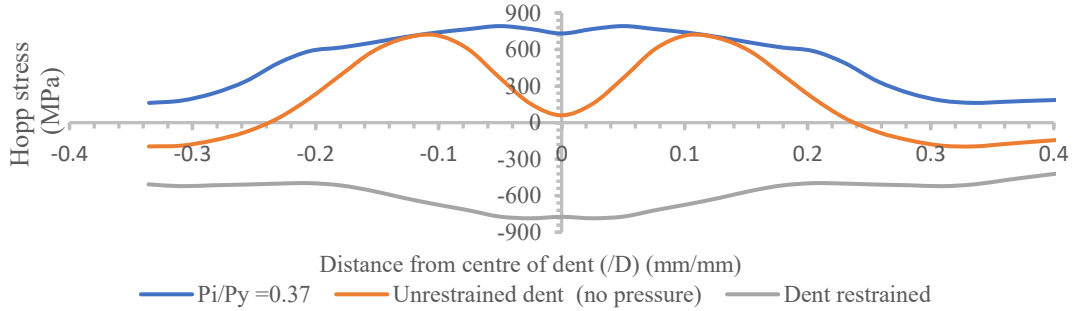

(c) Hoop stress distribution along the longitudinal axis of the

Figure 6.3 Variation of hoop stresses and strains along the longitudinal axis of dent at different stages of loading: Dent depth=2%D and dents formed at denting pressure, P_d /P_y=0

The maximum hoop stress in the restrained 2%D deep dent occurs in the central region of the dent and is negative in value (figure 6.3c). However, the location of the maximum hoop stress shifts to the flanks in the unrestrained dent and the sign is reversed by the elastic spring back. The distribution of hoop stress within the unrestrained dent becomes uniform when the pipe is moderately pressurized. The internal pressure causes the bending strains and stresses within the unrestrained dent to reduce in absolute value as the pipe regains original geometry during dent

rebound. The membrane stresses and strains due to the internal pressure increasingly dominate the distribution with increasing internal pressure, resulting in uniform stress distribution when the rebound is complete. Lancaster and Palmer [7] assert that dent rebound is greatest within the region close to the center of the dent and it delays the onset of membrane stresses from internal pressure within that region, which is the more reason why the growth of plastic strain under internal pressure begins from the axial extremities of the dents. Similar variations of stresses and strains were obtained with deeper dents (4%D and 6%D) formed at zero denting pressure. However, elastic spring back of the unrestrained dent did not flip the sign of the circumferential (hoop) stresses and the rebound was slow, requiring high internal pressure to complete, suggesting that cracks in deep dents could propagate before the rebound of the dent is completed if the applied pressure is enough to develop the critical strain for crack propagation. The rebound of the 2%D (shallow dent) occurred at low internal pressure, insufficient to develop the critical strain for crack propagation. Therefore, the cracks in shallow the dents were likely to propagate after the rebound/re-rounding of the pipe.

Figures 6.4 and 6.5 respectively show the contours of the equivalent plastic strain (PEEQ) and the circumferential stress on the external surface of the pipe with 2%D unrestrained plain rectangular dent formed under zero denting pressure. The spectra show that the peak PEEQ before pressurization is within the central region of the dent, while the peak stress is in the flanks (figures 6.4a and 6.5a respectively). Figure 6.4b shows the PEEQ spectrum in the pressurized pipe. Moderate pressurization of the dent does not change the distribution of PEEQ within the central region of the dent. Rather, it causes a sharp growth in the PEEQ within the axial extremities (flank and rim) of the dent compared to the growth in the central region of the dent as was also shown in figure 6.3b. The difference in the plastic strain growth rates between the centre region of the dent and the extremities of the dent can be attributed to the rebound of the central region of the dent under internal pressure, which delays the onset of plastic straining of the region by the membrane stresses from internal pressure [7]. In addition, Allouti et.al [25] have shown that micro hardening of the material during the denting process is greater in the central region of the dent than at the extremities of the dent, contributing to the variation in strain growth within the two regions when the pipe is pressurized. It is this difference in plastic straining rates and the variation of stress distribution within the pressurized pipes with dents that potentially governs the initiation and

propagation of cracks inside the dents, but it has not been verified. Lancaster and Palmer [16] observed that leakage of pipes with axial gouges inside dents begin at the axial extremities of the gouge. Figure 6.5b shows the contours of hoop stress in the pipe with 2%D deep dent after pressurization. The distribution of the stresses within the dented region of the pipe is generally uniform as was shown in figure 6.3c because the dent rebounds under moderate internal pressure and the membrane stress due to the internal pressure dominate the stress distribution.

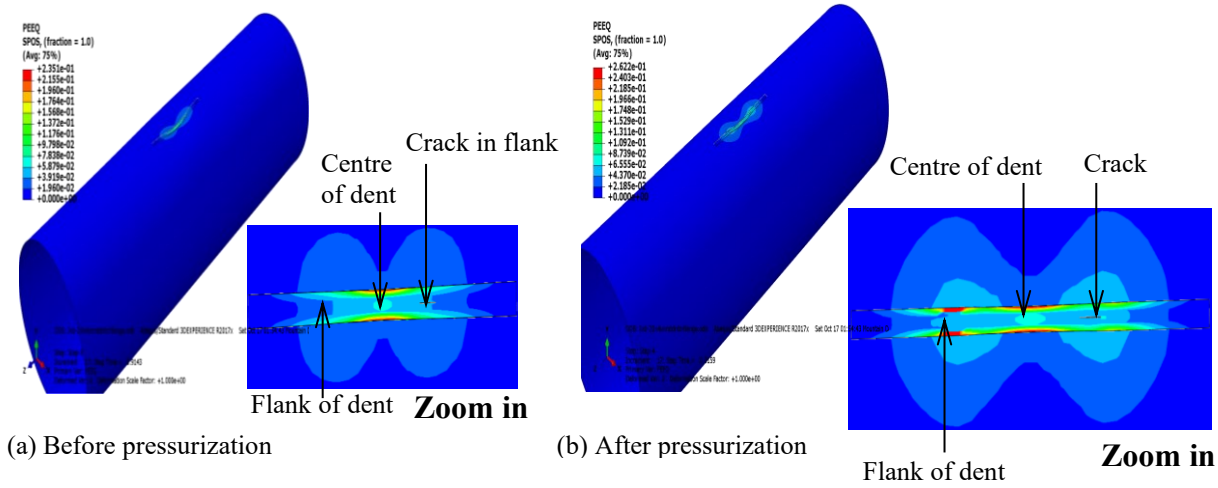

Figure 6.4 Equivalent plastic strain on the external surface of the pipe with a 2%D deep unrestrained dent-crack defect formed at zero denting pressure

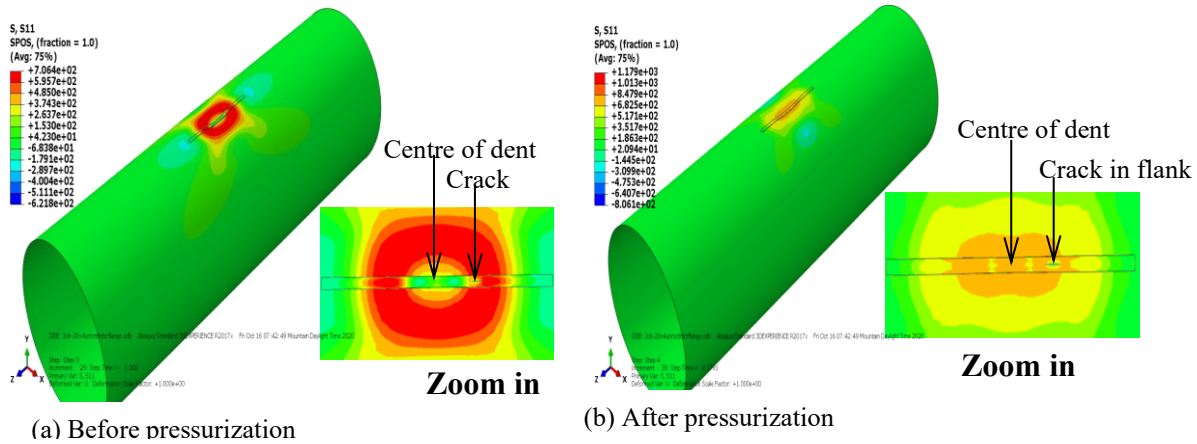

Figure 6.5 Circumferential stresses on the external surface of the pipe with a 2%D deep unrestrained dent-crack defect formed at zero denting pressure

6.4.1.2 Dents formed when the pipe is under internal pressurized

Figure 6.6 shows the variation of the circumferential strain, the equivalent plastic strain (PEEQ) and the circumferential stress on the external surface of the 2%D deep plain dent along the longitudinal axis of the dent. The dent was formed at an internal pressure of 3.8MPa (P_d/P_y=0.3) in the pipe.

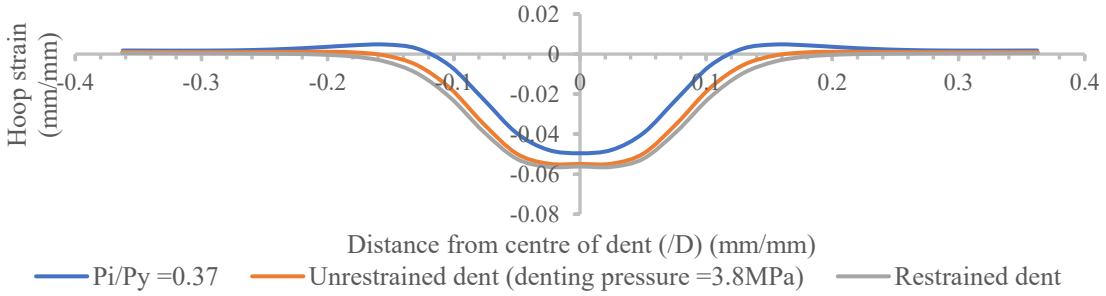

(a) Hoop strain variation along the longitudinal axis of the dent

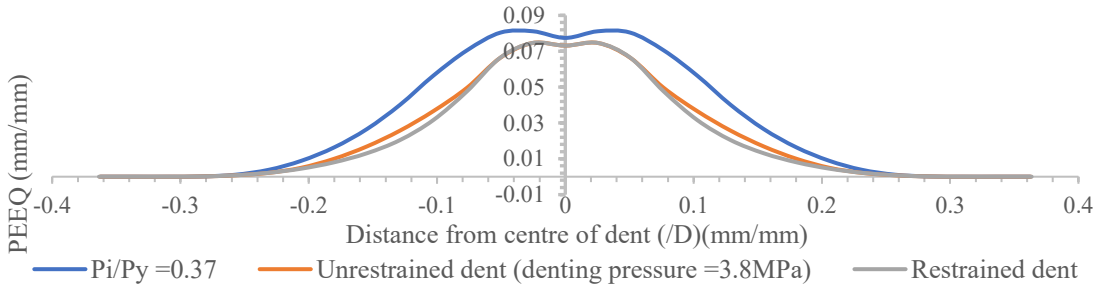

(b) Equivalent plastic strain variation along the longitudinal axis of the dent

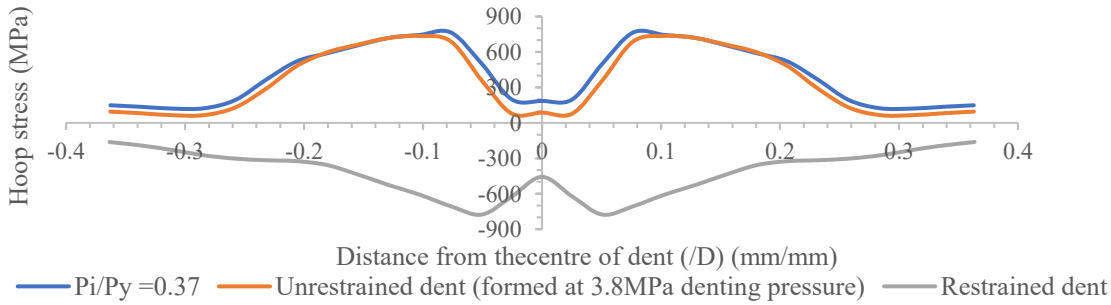

(c) Hoop stress variation along the longitudinal axis of the dent

Figure 6.6 Variation of stresses and strains along the longitudinal axis of the dent. Dent depth = 2% D, denting pressure, P_d/P_y = 0.3, (=3.8MPa)

Although the dents formed in pressurized pipe are more representative of defects formed in pipeline under operation than dents formed when the pipe is empty, it can be observed from figure

6.6 and figure 6.3 that there is strong similarity in the distribution of stresses and strains in the resulting dents. The maximum circumferential strain, and the maximum PEEQ occur in the central region of the dents and are the same if the dents have the same depth. The location of the maximum circumferential stress also shifts to the extremities of the dent when the dent is unrestrained, similar to the situation of dents formed when the pipe is not under pressure. However, there is a large gap between the distribution of the circumferential strain in the unrestrained dent and the distribution after moderate pressurization of the dent formed in the pressurized pipe (figure 6.6a) compared to the gap for dents formed when the pipe is not pressurized (figure 6.3a). The gap is narrower in the central region of the dent and widens towards the extremities of the dent. This indicates that elastic spring back of the 2%D deep dent is greater when the dent is formed at zero denting pressure and the pressurization leads to an increase in the circumferential strain in the flanks of the dents at a higher rate compared to the increase within the centre of the dent. A comparison of the gaps between the curves for PEEQ distribution for the two dents (figures 6.3b and 6.6b) affirms this observation.

Lancaster and Palmer [16] have shown that denting pressure acts as the transition pressure for transition from elastic to plastic deformation within the dent. Therefore, applying internal pressure in excess of the denting pressure causes more plastic deformation in pipes dented under pressure than in those dented at zero pressure. A comparison of the strain distribution for the restrained and the unrestrained dents shows that elastic spring back of dents formed in pressurized pipes are less than the spring back in dents formed in empty pipes as indicated by the negligible gap between the curves for dents formed under pressure (figure 6.6a and 6.6b). The stiffening effect of denting pressure [26] reduces the ability for elastic spring back. However, the dent rebounds significantly when pressurized beyond the denting pressure. Similar response is observed in deep dents (4%D and 6%D) formed in pressurized pipes. Increasing the dent depth increases the bending strains and stresses, while increasing denting pressure increases the membrane strains and stresses and the stiffness of the pipe such that creating deep dents under high pressure may propagate existing cracks in the pipe.

6.4.2 Implications of the strain and stress distribution in the dents on crack propagation

6.4.2.1 Cracks in unrestrained dents formed in unpressurized pipe

Effect of crack length and location inside the dent

Figure 6.7 shows the variation of the burst pressure of specimens of API X70 pipe with crack length and location of the cracks inside the rectangular dent. The cracks had depths (a/t) of 0.2, 0.35 and 0.5 and the depth of the unrestrained dent was 32mm, equivalent to 4%D of the pipe. 4%D being the depth of the intermediate of three dents (2, 4, and 6%D) analyzed in this study. Its response offers useful insight into the potential response of the other two dents.

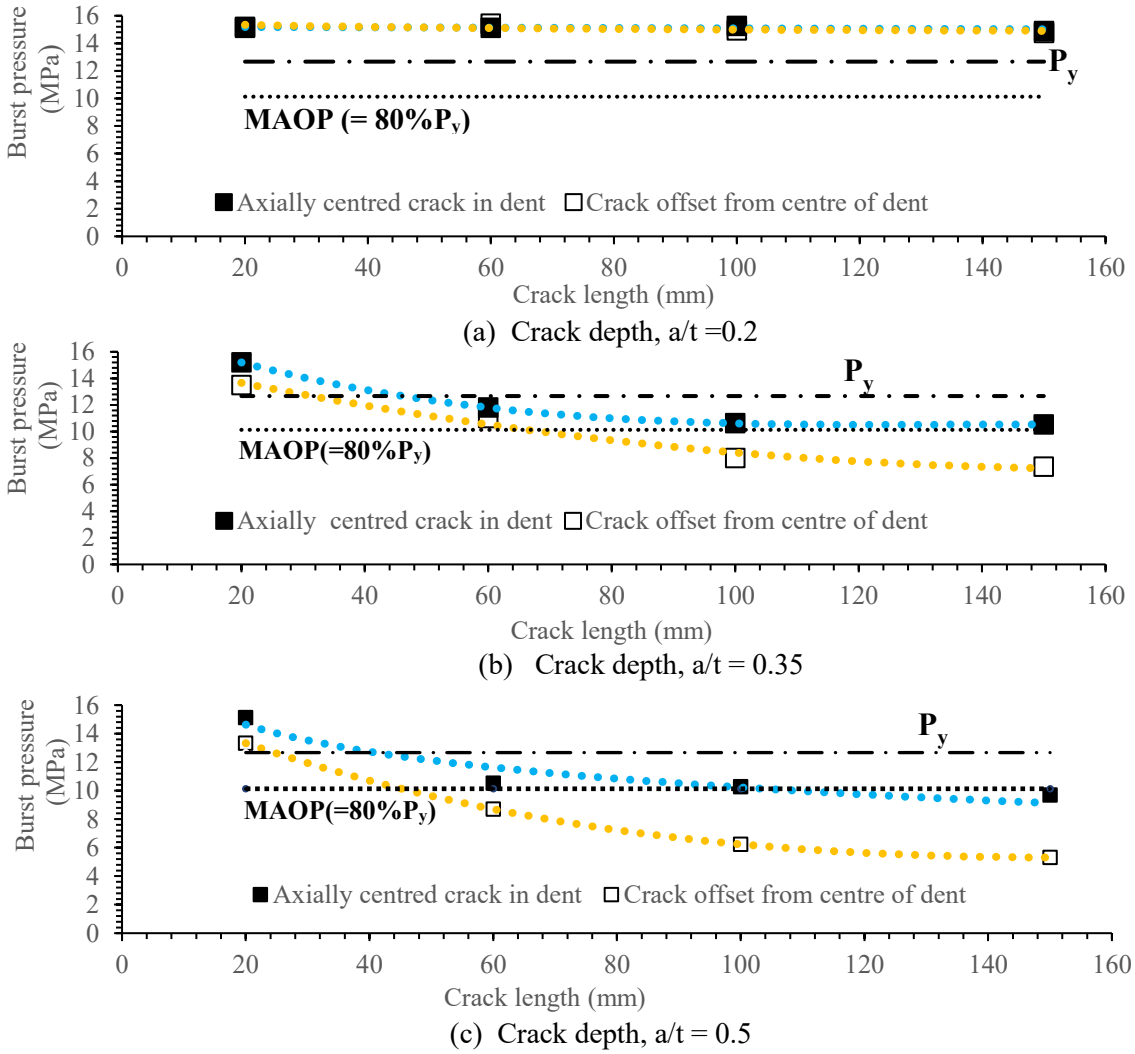

Figure 6.7 Variation of the burst pressure with crack length and crack location inside the dent formed at zero pressure. Dent depth = 4%D

Denting was done when the pipes had no internal pressure (P_d /P_y= 0). The burst pressure was determined when the cracks were at the center of the dent and repeated with the cracks in the flank of the dent, giving the two sets of results shown in the figure for each crack. The solid markers in the figure show axial cracks located at the center of the dent while the clear markers are for axial cracks located in the flank of the dent. The dashed line indicates the yield pressure of the pipe (12.67MPa), while the dotted black line shows the maximum allowable operating pressure (MAOP) of the pipe, which was determined to be 10.13MPa, and is equivalent to 80% of the yield pressure [27,28]. The colored lines are logarithmic fitted trendlines of the predicted burst pressures for specimens having cracks at the center of the dent and those with cracks in the flank of the dent.

Crack length and location inside the dent did not affect burst pressure of specimens with the crack of depth a/t = 0.2 (figure 6.7a). Failure in the specimens occurred at pressures greater than the yield pressure of the pipe, with extensive plasticization of the pipe wall. Burst pressure of specimens with cracks of depths a/t = 0.35 and a/t = 0.5 varied with crack length and location inside the dent (figures 6.7b and 6.7c). The burst pressures dropped steadily with increase in crack length but stabilized at crack lengths >100mm. The contrast in the variation of burst pressure between specimens with shallow cracks in the dent and specimens with deep cracks in the dent points to the well-established view [29] that shallow cracks generally cause failure by plastic collapse while deep cracks tend to cause fracture at low pressure.

Cracks were more severe on burst strength when located in the flank of the dent than when at the center of the dent. It is observed that all specimens with a/t =0.35 and a/t = 0.5 cracks at the center of the dent sustained the MAOP of the pipe, but only the specimens with the shortest cracks (20mm and 60mm) of depth a/t = 0.35 located in the flanks sustained MAOP and with a/t =0.5, only the 20mm long crack in the flank of the dent sustained the MAOP. Crack propagation and burst pressure of pressurized pipes is ordinarily controlled by the crack depth and least by the crack length [29]. But in the presence of dents, the burst pressure of cracked pipes is sensitive to crack length because bending moments develop around the crack, and it is well known that cracks have very low resistance against bending [4-6]. The resistance reduces with increase in crack length and crack depth. In addition, the distribution of stresses and strains in unrestrained rectangular dents have been shown to be non-uniform (figure 6.3 and 6.6). Before pressurization, rotational

deformation is highest within the central region of the dent and less in the flanks and rims of dent [4]. But when the dent is pressurized, plastic strains develop rapidly in the extremities (flanks and rims) of the dent (figure 6.3b). The circumferential strains also increase towards the critical positive values causing crack propagation in the flanks of the dents much faster than at the centre (figure 6.3a). Therefore, the crack located in the flank of the dent encounters large plastic strains and positive circumferential stresses at low internal pressure leading to crack propagating and pipe burst at pressures lower than the MAOP. Long crack in the flank of the dent is particularly vulnerable because they extend into the region of high plastic strain and high positive circumferential strains. Lancaster and Palmer [7] showed that the rebound of dents by internal pressure is limited within the central region. The crack at the center of the dent does not encounter the large plastic strains and the circumferential strains stay negative while the pipe is being pressurized.

Effect of dent depth and location of crack inside the dent

Figure 6.8 shows the variation of the burst pressure with dent depth and location of the crack inside the dent. The solid markers in the graphs show the burst pressure of specimens having cracks at the centre of the dent, while the clear markers show burst pressure for pipes having cracks in the flank of the dent. The crack length was fixed at 100mm, while varying the dent depth, the crack depth and location inside the dent which was formed under zero internal pressure ($P_d/P_y=0$). The dotted coloured lines are the logarithmic fitted trendlines of predicted burst pressures.

It is observed from figure 6.7 and figure 6.8 that the variation of burst pressure with dent depth and crack location inside the dent is similar to the variation with crack length and location in the dent for dents formed under zero internal pressure. Burst pressure of the shallow cracked specimen (a/t = 0.2) is independent of dent depth (figure 6.8a) and the crack length (figure 6.7a). Burst pressure of specimens with the deeper cracks (a/t =0.35 and 0.5) inside the dents reduced with the increase in dent depth and crack length. Similarly, the drop in the burst pressure between specimens with 2%D and 4%D deep dents was steeper than the drop in burst pressure between specimens with 4%D and 6%D deep dents. Denting of the pipe creates bending moments across the crack, which increases with dent depth [4] while on the other hand, the resistance of the crack to the bending moments reduce with crack length.

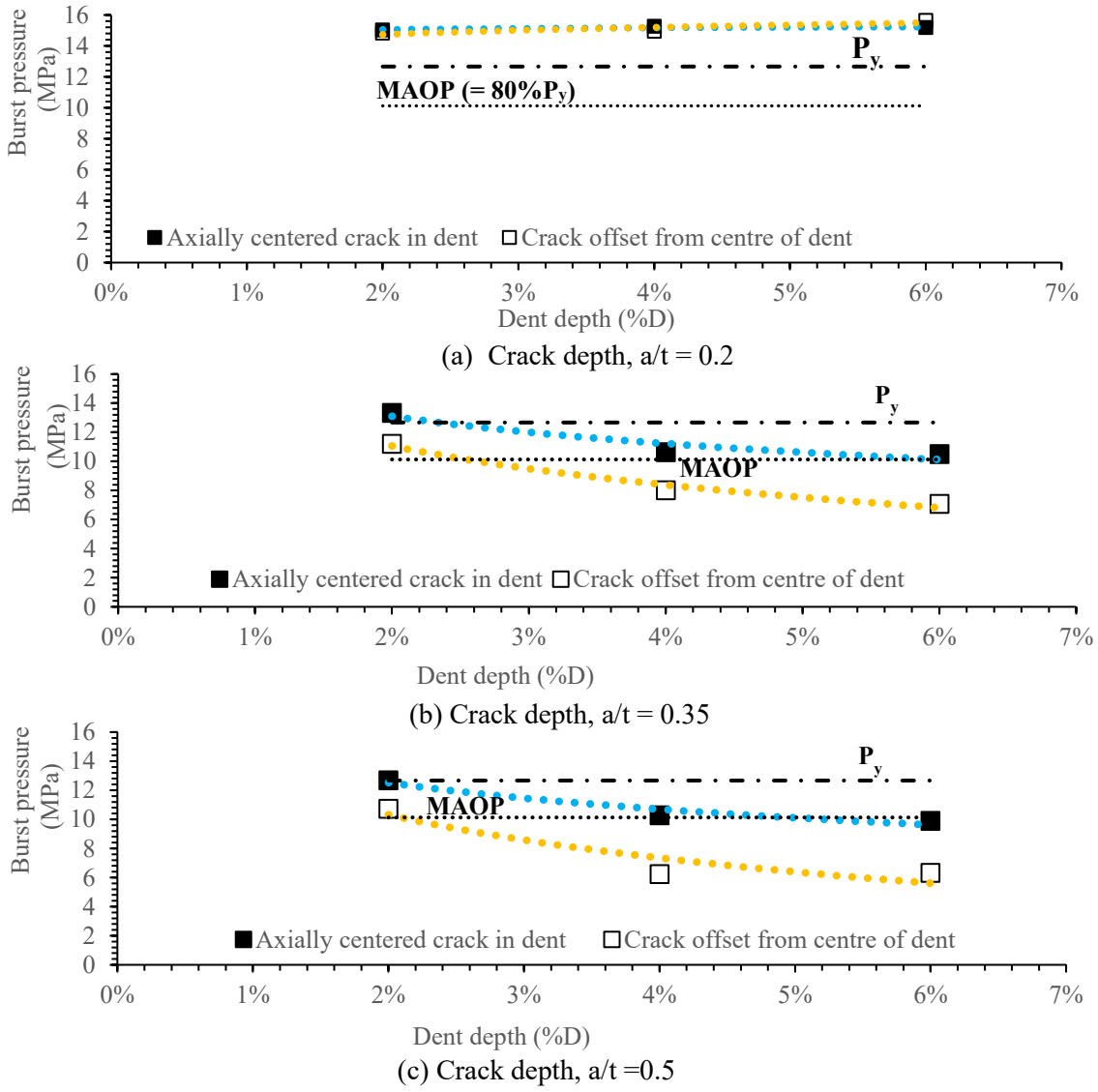

Figure 6.8 Variation of burst pressure with dent depth and location of crack inside dents formed at zero denting pressure, Crack length =100mm.

The striking resemblance in trends of variation of burst pressure with dent depth and crack length strongly suggests that the loss of bending resistance with increasing crack length is proportional to the increase in bending moment with dent depth and it is sufficient proof that long axial cracks inside deep dents are more severe on the strength of pipeline than short axial cracks in shallow dents, regardless of location of the crack within the dent. It is also observed that the cracks inside the 2%D deep dent sustained very high pressure regardless of crack depth and location inside the dent. Failure of the specimens with cracks in the deep dents (4% D and 6%D) was heavily

influenced by the location of the crack inside the dent, with centered cracks failing at higher pressure than cracks in the flank of the dents. The discrepancy in burst pressure of deeply dented specimens due to crack location is of course attributed to the relative rebounds and the relative plastic straining that occur at the centre and in the flanks of the dent after pressurization. Shallow dents formed at zero pressure typically rebound at low to moderate internal pressure without causing significant additional plastic strains in the axial extremities of the dent. The effect of the dent is neutralized by the rebound and the defect behaves as a plain crack resulting in very high burst pressure. Okodi et.al [17] showed that the burst pressure of pipes with cracks inside 2%D deep dents formed at zero denting pressure is the same as burst pressure of the pipe with a plain crack.

6.4.2.2 Cracks in unrestrained dents formed when the pipe is under internal pressure

Effect of crack length, location inside the dent and denting pressure

Figure 6.9 shows the variation of burst pressure with crack length and location of the crack inside 4%D deep dents. Denting of the pipe was done under zero internal pressure ($P_d/P_y = 0$) and under 3.8MPa ($P_d/P_y = 0.3$) internal pressure. The analysis was performed for cracks located at the centre of the dent and then repeated with cracks in the flank of dent. The solid markers in the graphs show cracks located at the center of the dent while the clear markers are for cracks in the flanks. The square markers show denting at zero pressure while the triangles show dents formed at 3.8MPa denting pressure. The dotted coloured lines are the logarithmic fitted trendlines of predicted burst pressures. It is observed from the figure that the burst pressure reduces with crack length and that cracks in the flanks were more severe on burst strength than cracks at the centre of the dent. Increasing the denting pressure from 0 to 3.8MPa did not affect the burst pressure of specimens with cracks at the centre of the dent. But it significantly reduced the burst pressure of specimens with cracks in the flank of the dent. The observation is in keeping with the finding of Lancaster and Palmer [16] that burst pressure of gouges located at the centre of circular dents in aluminum pipes did not change significantly with the increase in denting pressure. According to Lancaster and Palmer [16] the maximum plastic strains in the dent develops in the axial extremities of the dent when the pipe is pressurized, and it increases with internal pressure. The results of this study (figure 6.6b) shows that the plastic strains within the axial extremities of the rectangular dent increases rapidly with denting pressure, while the growth in plastic strains within the central region

of the dent is slow. Hence, the sign of the circumferential strain in the flank becomes positive (tensile) with increasing internal pressure much earlier than in the centre of the dent. This is why the burst pressure of specimens with cracks in the flank of the dent reduces with the increase in denting pressure while the corresponding specimens with cracks at the center of the dent were not significantly affected by the increase in denting pressure.

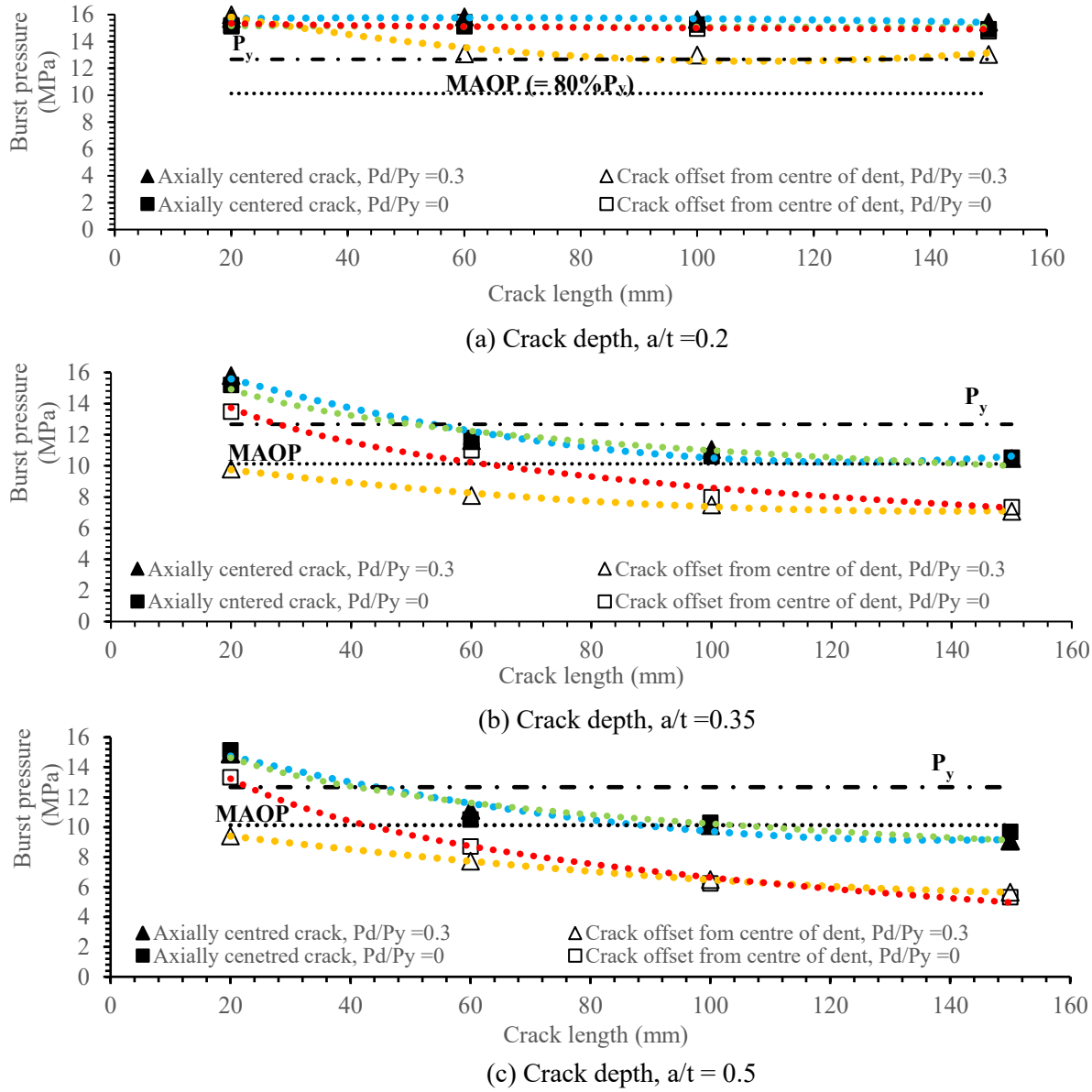

Figure 6.9 Variation of burst pressure with crack length and crack location inside the dent. Dent depth = 4%D. Denting pressures, P_d / P_y = 0 and 0.3

Effect of dent depth, location of crack inside the dent and denting pressure

Figure 6.10 shows the variation of the burst pressure with dent depth and location of the crack in the dents for specimens having 100mm long cracks located at the centre and in the flanks of the dents. Denting was done at zero internal pressure(P_d/P_y=0) and under internal pressure of 3.8MPa (P_d/P_y=0.3). The solid markers in the graphs indicate cracks at the center of dents, while the clear markers are for cracks in the flanks (offset from the center along the longitudinal axis of dent). The square shaped markers show the specimens dented zero internal pressure while the triangular shaped markers show the specimens whose dents were formed when the pipe was under pressure. Burst pressure generally reduced with the increase in dent depth. Specimens with cracks at the centre of the dent had higher burst pressures than specimens with the same cracks located in the flank of the dent. Denting pressure did not significantly affect the burst pressure of specimens with cracks at the centre of dents. But burst pressure of all specimens with cracks in the flank of dents reduced with the increase in denting pressure regardless of the depth of the crack. Forming deep dents (>4%D) under pressure was problematic and, in most cases, was unsuccessful especially with deep cracks in the flank of dent, as cracks would propagate during denting. Even where denting was successful, the pipes did not sustain additional pressure before bursting as shown in figures 6.10b and 6.10c for dents formed under 3.8MPa internal pressure.

The difference in strength between specimens with cracks at the centre of dents and specimens with cracks in the flanks has been attributed to the plastic strain growth rates and dent rebound in the two regions[16]. Plastic strain development with increasing pressure is rapid in the flanks but slow at the centre of dents, while rebound is limited to the central region of dents. Thus, the crack at the centre encounters less plastic straining and is shielded from membrane stresses until high internal pressure acts in the pipe. It is interesting that burst pressure of the specimen with the a/t=0.5 deep crack in the 6%D dent (figure 6.10c) formed at 3.8MPa denting pressure was lower with the crack at the centre of dent than when the crack was in the flank of the dent. This shows burst pressure can vary randomly in pipes with very long and deep cracks inside deep dents. But failure pressure is always very low regardless of the location of the crack in the dent.

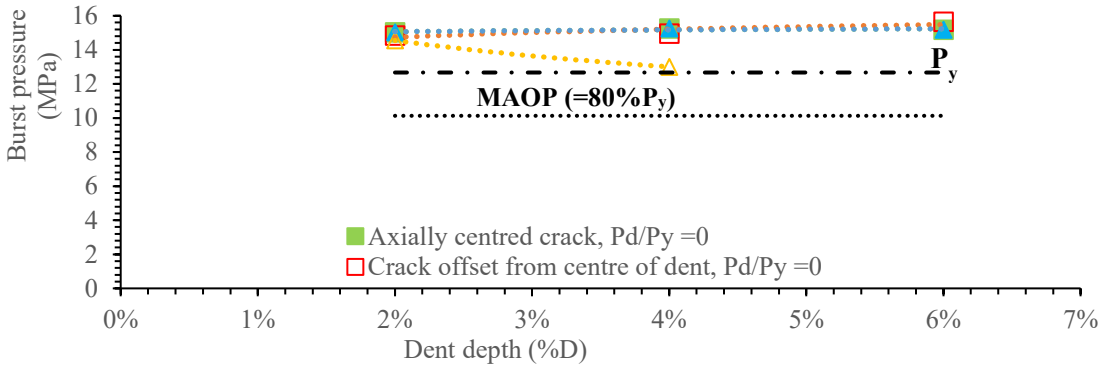

(a) Crack depth, a/t =0.2

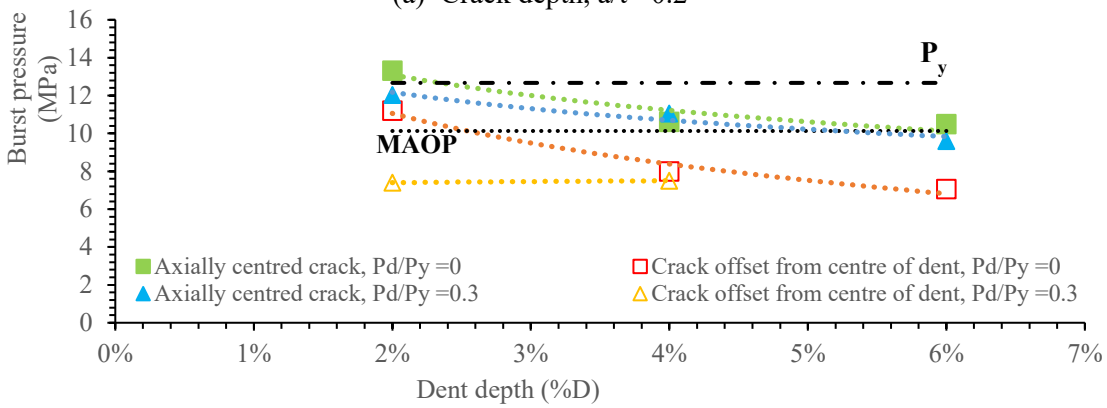

(b) Crack depth, a/t = 0.35

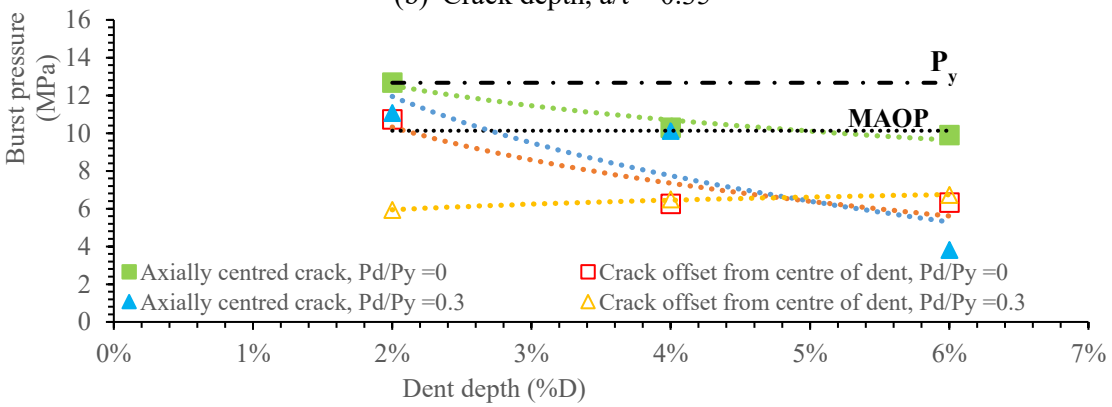

(c) Crack depth, a/t = 0.5

Figure 6.10 Variation of burst pressure with dent depth and location of crack inside dents. Crack length =100mm, Denting pressures, P_d /P_y=0 and 0.3., MAOP =0.8P_y

6.4.2.3 Cracks in restrained dents

Effect of dent restraint and denting pressure on burst pressure

Figure 6.11 compares the variation of the burst pressure with crack length for pipes having cracks of depth a/t of 0.5 in the flanks of restrained and unrestrained dents. The dents are 4%D (32mm) deep and were formed at denting pressures P_d/P_y of 0, 0.3 and 0.5. The solid markers show burst pressure of pipes with cracks in the restrained dents formed at various denting pressures, while the clear markers indicate burst pressure of specimens with cracks in the unrestrained dents formed at the different denting pressures. The trendlines are logarithmic fittings of the data points. The blue curves show trends for restrained dent-cracks. The red lines are for the unrestrained dent-cracks. The curves generally plot close to each other, showing that denting pressure generally did not significantly vary burst pressure except for the short (20mm and 60mm) cracks inside the unrestrained dent. The pipes with restrained dent-cracks had higher burst pressure than those with unrestrained dent-cracks, showing the restraining forces counteract the effect of internal pressure and prevent propagation of cracks at low pressure.

Increasing crack length reduced burst pressure of both the restrained and the unrestrained dent-cracked specimens because of the reduction in bending resistance with increase in crack length and the large plastic strains and positive circumferential strains that long cracks and cracks in flanks encounter within the extremities of the pressurized dent. It is observed that increasing the denting pressure from P_d/P_y of 0.3 to 0.5 did not significantly change the burst pressure of the pipes with unrestrained dent-cracks. Defects with same dent depths formed under the two denting pressures had similar burst pressures. Lancaster and Palmer [7] showed that failure in unrestrained dents depends on the loading history (denting pressure) and the original dent depth. The denting pressure acts as the transition pressure for transitioning from elastic to plastic behavior and eventual full plastification and loss of load carrying capacity within the dented region of the pipe. The burst pressures reduce with dent depth as observed in the previous sections.

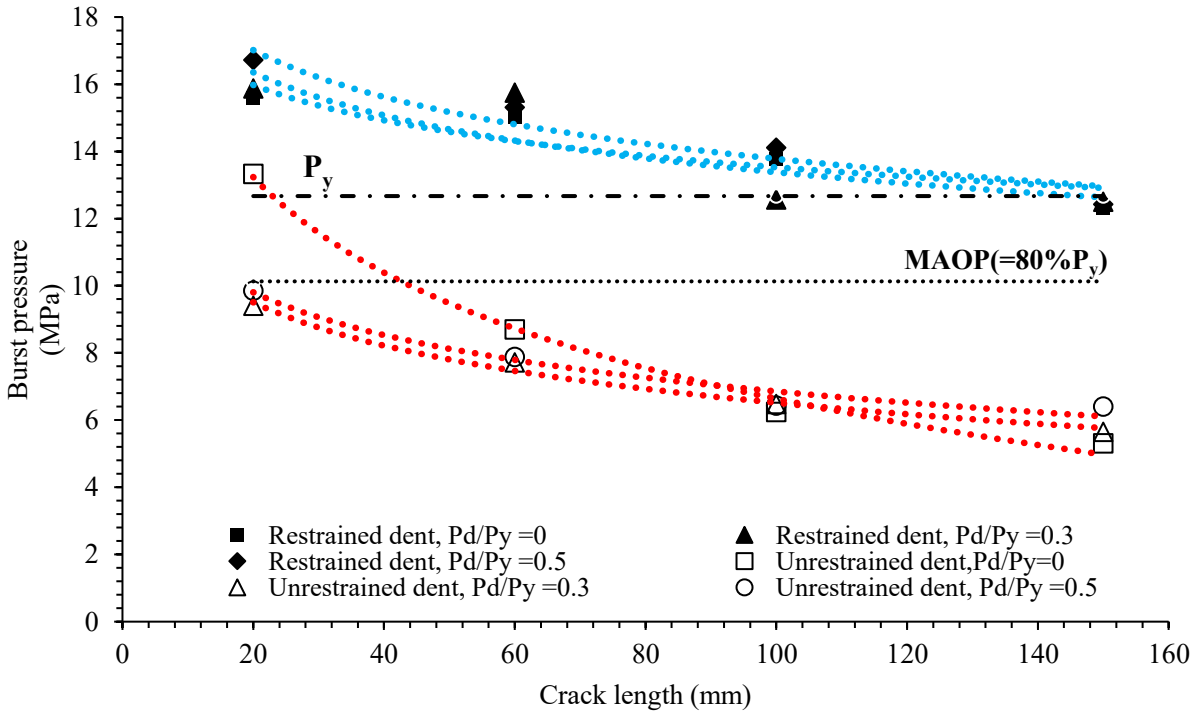

Figure 6.11 Showing variation of burst pressure with crack length, for cracks of depth a/t =0.5 located in the flanks of constrained and unconstrained dents of depth 4%D, formed at denting pressure P_d/P_y=0, 0.3 and 0.5

6.5 Conclusion

The effect of location of cracks inside dents on burst pressure of pipeline with dent-crack defects was investigated using cracks placed at the centre of rectangular dents and cracks placed in the flanks of the dents. Crack length, crack depth, dent depth and denting pressure were varied and their effect on the burst pressure determined for each crack location in the dent. In addition, the effect of dent restraint on burst pressure of pipes with cracks in the flank of the dent was assessed and the following conclusions were drawn.

The peak (negative) hoop strain and plastic strain on the external surface of the pipe with unrestrained rectangular dent occurs in the central region of the dent before the pipe is pressurized. The development of tensile hoop strains occurs much earlier in the flanks of the dent than at the centre of the dent when the pipe is pressurized. Plastic strains also develop rapidly in the extremities of the dent, than at the centre of the dent when the internal pressure is applied.

The peak hoop stress on the external surface of the unrestrained rectangular dent occurs in the extremities of the dent. The location of the hoop stress does not vary with internal pressure.
Elastic spring back of dents is greater in dents formed in empty pipes. But dents formed in pressurized pipes rebound faster than dents formed in empty pipes. The rebound begins when the applied pressure exceeds the denting pressure.

Cracks located in flank of dents are more injurious to the integrity of pipes than cracks located at the centre of dents.

Long and deep cracks in the flank of unrestrained dents were found to be the most severe combination of defect parameters for burst pressure. Their effects are aggravated by denting pressure and dent depth.

Burst pressure of pipeline with shallow cracks in dents formed at zero denting pressure are not influenced by crack length and dent depths.

Restraining dents improves burst pressure of pipes with dent crack defects regardless of location of the crack in the dent.

6.6 Limitations of the study

The results and conclusions of this study are based on the numerical analysis conducted on API X70 pipe grade with pre-existing longitudinal crack inside rectangular dent. The pipe is assumed to be regular in shape, with constant thickness and diameter and subjected to monotonically increasing internal pressure only. The material properties used in the analysis is for the base metal. The weld metal and the heat affected zone were not modelled. The fatigue life of the pipe with dent was not part of the analysis. The burst pressure represents the remaining strength of the pipe and is the pressure required to propagate the pre-existing crack in dent to puncture the pipe.

6.7 References

[1] Dawson, S.J., Russel, A., Patterson, A., "Emerging techniques for enhanced assessment and analysis of dents", IPC 2006-10264, Proceedings of 6th international conference on pipelines, Calgary, Canada, 2006.

[2] Rosenfeld, M. 2001. "Proposed New Guidelines for ASME B31.8 on Assessment of Dents and Mechanical Damage". Topical Report GRI-01/0084. Des Plaines, IL: GRI.

[3] Alexander, C, and Kiefner, J. 1997. Final Report on Effects of Smooth and Rock Dents on Liquid Petroleum Pipelines: To the American Petroleum Institute, October 10, 1997. American Petroleum Institute

[4] Ong LS, Chan YW, Seet G. The elastic analysis of a dent on pressurized pipe. Int J Pressure Vessels Piping 1989; 38:369–83.

[5] Ong LS. Derivation of stresses associated with a long axial dent in a pressurized cylinder. Int J Mech Sci 1991;33(2):115–23.

[6] Ong LS, Soh AK, Ong JH. Experimental and finite element investigation of a local dent on a pressurized pipe. J Strain Anal 1992;27(3):177–85.

[7] Lancaster ER, Palmer SC. Strain concentrations in pressurized dented pipes, Part E. J Process Mech Engng, Proc Inst Mech Engng 1996; 210:29–38.

[8] Fowler JR, Alexander CR, Kovach PJ, Connelly LM. Cyclic pressure fatigue life of pipelines with plain dents, dents with gouges, and dents with welds. AGA Pipeline Research Committee, Report PR-201-927 and PR-201-9324, June; 1994.

[9] Alexander CR, Kiefner JF. Effects of smooth and rock dents on liquid petroleum pipelines. Final report to the American Petroleum Institute, Stress Engineering Services, Inc., and Kiefner and Associates, Inc., 10 October 1997, API Publication 1156, November; 1997.

[10] Tian, X., & Zhang, H. (2017). "Failure criterion of buried pipelines with dent and scratch defects." J. Eng. Failure Anal. 80(2017)278-289

[11] Vilkys, T., Rudzinskas, V., Prentkovskis, O., Tretjakovas, J., Višniakov, N., & Maruschak, P., (2018)." Evaluation of failure pressure for gas pipelines with combined defects." *Metals, 8*(5), 346.

[12] Ghaednia, H., Das, S., Wang, R., & Kania, R. (2015a). "Effect of operating pressure and dent depth on burst strength of NPS30 line pipe with Dent–Crack defect." *J. Offshore Mech. and Arctic Eng., 137*(3), 031402-8.

[13] Ghaednia, H., Das, S., Wang, R., & Kania, R. (2015b). “Safe burst strength of a pipeline with dent–crack defect: Effect of crack depth and operating pressure.” *Eng. Failure Analysis, 55*, 288-299

[14] Rafi, A., Silva, J., Kenno, S., Das, S., Kania, R., & Wang, R.Y., (2010).” Strength of line pipe with dent and crack defect.” *Proceedings of the 8th international pipelines conference. IPC 2010-31095, Calgary, Alberta, Canada.*

[15] Ghaednia, H. (2015). Burst pressure of NPS30 steel pipes with dent-crack defect (Ph.D. Dissertation). University of Windsor, Windsor, Ontario, Canada.

[16] Lancaster ER, Palmer SC. Burst pressures of pipes containing dents and gouges, Part E. J Process Mech Engng, Proc Inst Mech Engng 1996;210:19–27.

[17] Okodi A, Li Y, Cheng R, Yoosef-Ghodsi N, Kainat M, & Adeeb S., (2020), “Crack Propagation and Burst pressure of Pipeline with Restrained and Unrestrained Concentric Dent-crack defects using Extended finite element method” ***J.*** *Applied sciences*,(2020), 10.3390/app10217554

[18] Ghaednia, H., Das, S., Wang, R., & Kania, R. (2017). “Dependence of burst strength on crack length of a pipe with a dent-crack defect.” *J. Pipeline Syst. Eng.& Practice, 8*(2), 4016019.

[19] Melenk J.M, Babuska, I. “The partition of unity finite element method: Basic theory and applications.” *Computer methods in Applied mechanics and Engineering*, 1996.

[20] Moes, N., Dolbow, J., and Belytschko, T. “A finite element method for crack growth without remeshing.” *Int.J. Numer. methods in Eng*, 46 (1999) 131–150.

[21] Fries, T.P., and Belytschko, T. “The extended/generalized finite element method: An overview of the method and its applications.” *Int.J. Numer. methods in Eng*, (2000) 1-6.

[22] Abaqus Documentation,2016. Dassault Systèmes.

[23] Needleman, A., "An Analysis of Decohesion along an Imperfect Interface”, International Journal of Fracture, 1990; 42:21-40

[24] Tian, X., & Zhang, H. (2017). “Failure criterion of buried pipelines with dent and scratch defects.” J. Eng. Failure Anal. 80(2017)278-289

[25] Allouti M, Schmitt C, Pulvinage G, Gilgert J & Hariri S. (2012). “Study of the influence of dent depth on the critical pressure of pipeline” *J. Eng. Failure Anal.* 21 (2012) 40–51

[26] Cosham, A.; Hopkins, P. The effect of dents in pipelines—Guidance in the pipeline defect assessment manual. *Int. J. Press. Vessel. Pip.* 2004, *81*, 127–139.

[27] ASME-B31.8, 2003, Revision to B31.8-1999. Gas transmission and distribution piping system: ASME Code for Pressure Piping, B31, The American Society of Mechanical Engineers.

[28] CSA Z662-2007, Oil and gas Pipeline Systems Ontario, Canada, 2007

[29] Cravero, S. and Ruggeri, C. "Structural Integrity Analysis of Axially Cracked Pipelines Using Conventional and Constraint-Modified Failure Assessment Diagrams." *Int. J. Press. Vessel. Pip,* 83(2006) 607-617.

7. SUMMARY, SCIENTIFIC CONTRIBUTION, CONCLUSION AND ROMMENDATIONS

This chapter presents a summary of the work conducted in this research project and the contributions made. Suitable conclusions drawn and recommendations of additional work that is needed in order to develop acceptable predictive models that can be used for assessment of pipelines with dent-crack defects.

7.1 Summary

This research was designed to study the effect of dent-crack defects on integrity of pipeline. The effects of varying defect geometry, location of crack inside dent, and prevailing pressure during denting, on burst strength of pipeline with longitudinal cracks inside dents was evaluated. The overall objective was to propose a method for assessing pipeline with dent-crack defects, subjected to monotonically increasing internal pressure.

Review of literature revealed a profound deficiency of research on dent-crack defects in pipeline as well as a lack of predictive analytical models for burst strength of affected pipeline. On the other hand, over 80% of excavated pipeline present with some form of dents, often accompanied by metal loss and cracking due to electro chemical action and mechanical interference. Dents on their own are locations of strain and stress concentration and are active sites for stress corrosion cracking. Field reports indicate that pipes with dent-crack defects fail at very low pressure even where the sizes of constituting cracks and dents were initially small at the time of detection. Failure is usually by leakage or rupture with substantial loss of content, leading to shutdowns of pipeline operations. It is against this background that this research project was developed to gain insight on the remaining strength of pipeline with various sizes of dent-crack defects, in the interest of understating how the individual defect parameters contribute to degrade the integrity of pipelines. The extended finite element method implemented in Abaqus software was used in this research to numerically investigate crack propagation and predict burst pressure of pipelines having longitudinal cracks inside rectangular dents. Maximum principal strain and fracture energy were used in the numerical models as damage parameters to specify conditions for propagation of cohesive cracks through pipe wall. Data from single edge notch tension tests, full-scale burst tests, and material property tests were obtained from literature and used to calibrate and validate the models.

The first stage of the research focused on assessing the effectiveness of the extended finite element criterion implemented in Abaqus software to analyze crack propagation in pipelines. Numerical models of API X60 pipelines having longitudinal cracks were developed and used to investigate crack propagation and predict burst pressure of pipelines with plain cracks. The models were calibrated and validated using a crack mouth opening displacement curve generated from single edge notch tension test. The calibration and validation of the model was repeated using burst

pressure of pipes with longitudinal cracks from full scale tests. The two calibration and validation efforts produced comparable damage parameters. Analytical methods for crack assessment, available in the pipeline industry, namely: Modified NG-18 equation, Failure Assessment Diagram (FAD) and CorLAS were then used to predict failure pressure of the API X60 pipeline. Numerical model predictions and predictions made using the three analytical methods were compared with burst pressure tests of the pipe specimens in order to assess the suitability of the extended finite element method in Abaqus as a tool for analysis of crack propagation and prediction of bust pressure in pipelines. The results showed that model calibration can be successfully accomplished using results of small scale tests. But where such is not forthcoming, the calibration can also be done using part of the results of full scale burst tests, with the rest of the results used for validation. The extended finite element method with principal strain and fracture energy as damage parameters is effective for analysis of crack propagation and prediction of the burst pressure of longitudinally cracked pipelines.

The second part of the research extended the investigation to dent-crack defects. Models of API X70 grade of pipeline with dent-crack defects were calibrated and validated using results of full-scale burst tests obtained from the literature. The maximum principal strain and fracture energy were used as damage parameters as earlier stated, with exponential traction separation law, to model crack propagation through the dented pipe. The models were used in a parametric study to analyze crack propagation and predict burst pressure of pipelines having dent-crack defects considering the following locations of cracks inside dents.

i. Longitudinal cracks located at the center of rectangular dents, and
ii. Longitudinal cracks located in the flanks of rectangular dents.

For each scenario, crack depth, crack length, dent depth, denting pressure, dent restraint/constraint condition were varied. The dents were either in a restrained or unrestrained condition and the dent depths, expressed as a percentage of the outside diameter (D) of pipe were 2%, 4% and 6%. Denting pressure measured as a percentage of the yield pressure of pipe was varied from 0 to 80% of the yield pressure. Crack depth measured as a fraction of the wall thickness (t) of the pipe was varied from 0.2t to 0.5t; and crack length was varied from 20mm to 200mm.

7.2 Scientific contribution

This research has rendered the following scientific contributions:

i. evaluated the effectiveness of extended finite element methods for analysis of crack propagation in pipeline,
ii. showed that XFEM can be successfully calibrated and validated using data from full scale burst tests as well as small scale tests,
iii. evaluated and facilitated broader understanding of the nature of interaction between dents and cracks and their individual and combined effect on pipeline integrity,
iv. assessed the remaining strength of pipeline with dent-crack defects and determined required derating pressure for different combinations of dent-crack defect parameters,
v. generated data from parametric analyses that can facilitate future research on the effect of dent-crack defects on pipelines.

7.3 Conclusion

The current research was initiated to investigate burst pressure of pipeline with dent-crack defects. The effect of defects comprised of longitudinal cracks inside rectangular dents on burst pressure of specimens of API X70 grade of pipeline subjected to monotonically increasing internal pressure was evaluated, considering different sizes of cracks and dents and various operating conditions for dent formation. Lower grades of pipeline steel were not assessed. Therefore, the conclusions of this study do not apply to lower grades of pipeline steel but may be extended to higher grades of pipeline with similar strength to the current pipe, like the APIX80 grade. In addition, the pipes were assumed to be geometrically perfect and of uniform strength. Based on the results, significant insight has been gained on the contribution of various defect parameters towards reducing burst pressure of pipeline, leading to the following conclusions.

- The effect of dent-crack defects on the integrity of pipeline varies with location of cracks inside dents. Specimens with longitudinal cracks at the center and concentric with rectangular dents had higher burst pressure than those with longitudinal cracks located in the flank of rectangular dents.
- In either case, defects having cracks inside restrained dents had higher burst pressure than corresponding defects with cracks inside unrestrained dents.

- Restrained dent-crack defects fail with significant plasticity, while in unrestrained dent-crack defects, plasticity becomes significant if the cracks are shallow in depth.
- Stress distribution within a dent before the pipe is pressurized varies with the location within the dent and contributes towards variation of the burst pressure. Bending stress in the flanks and rims of rectangular dents are generally tensile, while the stress at the center of rectangular dents vary with dent depth, being tensile in shallow dents less than or equal to 2%D deep and compressive inside dents that are 4%D deep and 6%D deep.
- Similarly, before a pipe is pressurized, the strain distribution show that the circumferential strain is maximum and primarily compressive at the center of the dent. After the dent is pressurized, the strains and stresses within the flanks increase at a higher rate than the increments within the center of dent until the dent rebounds under internal pressure.
- Burst pressure decreased with increases in dent depth. Deep dents have greater concentrations of strains and stresses within the dented area. Cracks inside deep dents propagated at lower pressure and the affected specimens had lower burst pressure than specimens with cracks inside shallow dents.
- Dent-crack defects comprising of cracks inside shallow rectangular dents, less than or equal to 2%D deep formed in empty pipes behave like plain cracks, regardless of crack location and crack geometry inside the dent. Affected pipes have the same burst pressure as specimens with plain cracks.
- Denting a pipe when it is under pressure is more severe for pipeline integrity than denting an empty pipe. But denting pressure has a marked effect on the integrity when the dents are deep. On the other hand, the burst pressure of pipeline with shallow crack (0.2t deep) inside shallow dents (2% D deep) is not affected by the denting pressure.
- Denting pressure stiffens the pipe and improves bending resistance therefore denting under pressure uses more load than denting empty pipe, the stiffness increases with denting pressure. Forming deep dents in pipes pressurized to more than 50% of the yield pressure of the pipe is problematic as cracks in the pipe can propagate during dent formation. It can also puncture the pipe if a pointed indenter is used.
- Burst pressure of pipelines with dent-crack defects drop with the increase in crack length and crack depth. Total bending stresses across cracks increase with crack length and for

cracks in the flanks of dent, the stresses are tensile and augment hoop stresses from internal pressure, resulting in failure at low pressure.

- Crack length does not significantly affect burst pressure of pipeline if the cracks are shallow (0.2t deep) and inside dents formed at zero denting pressure, regardless of where in the dent the cracks are located. But where the dents are formed under pressure then the variation of burst strength with crack length becomes significant.
- Burst pressure was more sensitive to increment in crack depth than increase in crack length. Defects having deep cracks inside dents tend to fail by fracture while those with shallow cracks inside dents tend to fail by plastic collapse due to severe plasticization of the pipe wall by the internal pressure.
- Regardless of the location of the crack inside dent, releasing the indenter did not propagate shallow cracks, 0.2t deep inside dents.
- Deep cracks of depth of 0.35t and 0.5t depth inside restrained rectangular dents propagate when the restraint is released from the pipe surface at a pressure equivalent to 80% of the yield pressure of the pipeline. Risk of propagation increased with crack length and crack location inside the dent. Cracks located in the flanks of the dent are more likely to propagate than cracks at the center of the dents. Similarly, cracks longer than 60mm propagate but only those longer than 100mm will propagate to burst the pipeline.
- This study has therefore established that crack depth and crack location inside dents are the most severe parameters of dent-crack defects on pipeline integrity. Particularly, deep cracks located in the flanks of dents are the most severe and are detrimental to pipeline integrity. Crack length, dent depth and denting pressure aggravate the effect of crack depth and crack location.
- There is a critical size of a dent-crack defect that allows the pipeline to operate at its maximum allowable operating pressure(80%of yield pressure) without bursting, but it varies with denting pressure. A 200mm long longitudinal crack that is 0.5t deep, inside a 4%D deep dent formed in an empty pipe can sustain the maximum allowable operation pressure of the pipe. But the length would have to be reduced to 100mm if the dent is formed at a denting pressure equivalent to 30% of the yield pressure of the pipe and 75mm if the pipe is formed at a denting pressure equivalent to 50% of the yield pressure of the pipe.

- The extended finite element methods implemented in Abaqus software, with maximum principal strain and fracture energy as damage parameters is effective for analysis of crack propagation and prediction of burst pressure of pipeline. The models can be calibrated using crack growth resistance curves generated from small scale tests or results of full scale burst tests.

7.4 Recommendations

This research has contributed significantly towards understanding of the effects of dent-crack defects on burst pressure of pipelines. However, there are gaps that remain to be addressed in order to further the progress made, hence the following recommendations.

i. More burst tests are required to generate data for a wider range of grades of pipeline steels.
ii. More parametric numerical studies on the burst pressure of a wider range of pipe grades, with different dent shapes other than rectangular shape, to generate enough data and enable development of a predictive analytical model for assessment of burst strength of pipeline with dent-crack defects.
iii. The effect of fatigue loads arising from pressure fluctuations on crack propagation and burst pressure of pipeline with dent-crack defects need to be assessed.
iv. Other damage initiation criteria for crack propagation need to be explored, including automatically varying the damage criterion based on triaxiality.

BIBLIOGRAPHY

[1].Abaqus Documentation,2016. Dassault Systèmes.

[2].Abdelatif Hassanien Sherif, S., Adeeb, S, Probabilistic-based assessment of Corroded Pipelines: a comparison between closed form and surrogate limit states, in: IPC2006-10247, Proceedings of the 6th International Pipeline Conference, September 2006 (Calgary, Alberta, Canada).

[3].Adeeb, S.M.; Horsley, D.J. A numerical procedure to establish a safe working pressure during excavation of a pipeline in a rock ditch. *Int. J. Press. Vessel. Pip.* 2006, *83*, 488–497.

[4].Agbo S., Lin, M., Ameli, I., Imanpour, A., Duan, D.-M., Cheng, J.J.R., Adeeb S., Evaluation of the Effect of Internal Pressure and Flaw Size on the Tensile Strain Capacity of X42 Vintage Pipeline using Damage Plasticity Model in Extended Finite Element Method (XFEM). PVP2019-94005, Proceedings of the ASME 2019 Pressure Vessels & Piping Conference, July 2019, San Antonio, Texas, USA.

[5].Alexander, C, and Kiefner, J. 1997. Final Report on Effects of Smooth and Rock Dents on Liquid Petroleum Pipelines: To the American Petroleum Institute, October 10, 1997. American Petroleum Institute

[6].Allouti M, Schmitt C, Pulvinage G, Gilgert J & Hariri S. (2012). "Study of the influence of dent depth on the critical pressure of pipeline" *J. Eng. Failure Anal.* 21 (2012) 40–51

[7].Ameli, I., Behrouz, A., Lin, M., Agbo, S., Cheng, R., Da-Ming, D., Adeeb, S., Estimation of the CTOD- crack growth curves in SENT specimens using the extended finite element method, Int. J. Pres. Ves. Pip. 169 (2019) 16–25.

[8].Anderson T.L, "Fracture mechanics fundamentals and applications", Taylor and Francis, 2005.

[9].API 1176-2016, Recommended practice for assessment and management of cracking in pipelines, Washington, USA.

[10].API 1160-2001, Managing System Integrity for Hazardous Liquid, Washington DC, USA 2001

[11].Arumugam U, Gao M, Ravi K., Wang R, Kania R, "Study of plastic strain limit damage criterion for pipeline mechanical damage using FEA and full-scale denting tests", IPC2016, Paper 64548, 11th International Pipeline Conference, September 26-30, 2016, Calgary, Canada.

[12].ASME. (2012). “Pipeline transportation systems for liquids and slurries.” ASME B31.4. New York.

[13].ASME B31.8-2010, Gas Transmission Distribution Piping System, New York, USA 2010A

[14].ASME Boiler & Pressure Vessel Code, Section VIII, Division 3, “Alternative Rules for Construction of High-Pressure Vessels” (2010).

[15].ASME. “Fitness-for-service, API Recommended Practice 579-1/ASME FFS-1 2007, Second Edition”, The American Society of Mechanical Engineers, New York, USA, June 2007.

[16].Bai, Y.; Song, R. Fracture assessment of dented pipes with cracks and reliability-based calibration of safety factor. *Int. J. Press. Vessel. Pip*. 1997, *74*, 221–229.

[17].Bai, Y., Wierzbicki, T., A new model plasticity and fracture with pressure and Lode dependence, Int. J. Plast. 24 (2008) 1071–1096Bedairi, B.; Cronin, D.; Hosseini, A.; Plumtree, A. Failure prediction for crack-in corrosion defects in natural gas transmission pipelines. *Int. J. Press. Vessel. Pip.* 2012, *96*, 90–99.

[18].Baker, M. 2004a. “Dent Study”. Delivery Order DTRS56-02-D-70036. Integrity Management Program. Office of Pipeline Safety.

[19].Baker, M. 2004b. “Pipe Wrinkle Study”. Delivery Order DTRS56-02-D-70036. Integrity Management Program. Office of Pipeline Safety.

[20].Bao, Y., Wierzbicki, T., On fracture locus in the equivalent strain and stress triaxiality space, Int. J. Mech. Sci. 46 (1) (2004) 81–98.

[21].Belanos S.P, Ryan R.S., “Dents in pipe.”, Oil Gas J 1958; 56:155–61.

[22].Beller M, Mattheck C, Zimmermann J. Stress concentrations in pipelines due to the presence of dents. Proceedings of the First International Offshore and Polar Engineering Conference (ISOPE 1991), Edinburgh, United Kingdom, 11–19 August; 1991.p. 421–24

[23].Bjørnøy, O.H., Rengard, O., Fredheim, S., Bruce, P., “Residual strength of dented pipelines, DNV test results.”, Tenth International Conference on Offshore and Polar Engineering (ISOPE 2000) Seattle, USA, 28 May–2 June; 2000.

[24].BSI. BS7910: 2005, “Guide to methods for assessing the acceptability of flaws in metallic structure”, London, UK, British standards institution, July 2005

[25].Canadian Energy Pipeline Association, Transmission Pipeline Industry Performance Report, 2018 snapshot, https://pr18.cepa.com/, Accessed April 2018

[26].Choung, J., Nam, W., Lee, D., Song, C.Y., Failure strain formulation via average stress triaxiality of an EH36 high strength steel, J. Ocean Eng. 91 (2014) (2014) 218–226.

[27].Cosham, A.; Hopkins, P. The effect of dents in pipelines—Guidance in the pipeline defect assessment manual. *Int. J. Press. Vessel. Pip.* 2004, *81*, 127–139.

[28].Cosham, A., and Hopkins, P. 2001. "A New Industry Document Detailing Best Practices in Pipeline Defect Assessment." In Fifth International Onshore Pipeline Conference, Amsterdam, The Netherlands. http://www.penspenintegrity.com/downloads/virtual-library/industry-bestpractice.pdf.

[29].Cornec, A., Scheider, I., Schwalbe, K.H., On the practical application of the cohesive model, Eng. Fract. Mech. 70 (14) (2003) 1963–1987.

[30].Cravero, S. and Ruggeri, C. "Structural Integrity Analysis of Axially Cracked Pipelines Using Conventional and Constraint-Modified Failure Assessment Diagrams." *Int. J. Press. Vessel. Pip,*83(2006) 607-617

[31].Cravero, S. Ruggeri, C., Evaluation of crack growth resistance curves of pipeline steels using constraint designed fracture specimens, in: IPC2006-10075, Proceedings of the 6th International Pipeline Conference, September 2006 (Calgary, Alberta, Canada).

[32].CSA Z662-2007, Oil and gas Pipeline Systems Ontario, Canada, 2007

[33].CSA Z662-15, Oil and gas Pipeline Systems Ontario, Canada, June 2015

[34].Das, S.; Cheng, J.J.R.; Murray, D.W. Prediction of fracture in wrinkled energy pipelines subjected to cyclic deformations. *Int. J. Offshore Polar Eng*. 2007, *17*, 205–212.

[35].Dassault Systèmes. *Abaqus Documentation* ; Dassault Systèmes : Velizy-Villacoublay, France, 2016.

[36].Dawson, S.J., Russel, A., Patterson, A., "Emerging techniques for enhanced assessment and analysis of dents", IPC 2006-10264, Proceedings of 6th international conference on pipelines, Calgary, Canada, 2006.

[37].Dotta, F., Ruggeri, C., Structural Integrity assessment of high-pressure Pipelines with axial flaws Using a micromechanics model, Int. J. Pres. Ves. Pip. 81 (2004) 761–770.

[38].Folias, E.S., "An Axial Crack in a Pressurized Cylindrical Shell," *International Journal of Fracture Mechanics* 1 (1965) pp. 104-113.

[39].Fowler, J. 1993. “Criteria for Dent Acceptability in Offshore Pipeline.” In the Offshore Technology Conference, Houston, Texas, May 1993. doi:10.4043/7311-MS. http://www.onepetro.org/mslib/servlet/onepetropreview?id=OTC-7311-MS.

[40].Fries, T.P., and Belytschko, T. “The extended/generalized finite element method: An overview of the method and its applications.” *Int.J. Numer. methods in Eng*, (2000) 1-6.

[41].Ghaednia, H., Das, S., Wang, R., & Kania, R. (2017). “Dependence of burst strength on crack length of a pipe with a dent-crack defect.” *J. Pipeline Syst. Eng.& Practice, 8*(2), 4016019.

[42].Ghaednia, H., Das, S., Wang, R., & Kania, R. (2015a). “Effect of operating pressure and dent depth on burst strength of NPS30 line pipe with Dent–Crack defect.” *J. Offshore Mech. and Arctic Eng., 137*(3), 031402-8.

[43].Ghaednia, H., Das, S., Wang, R., & Kania, R. (2015b). “Safe burst strength of a pipeline with dent–crack defect: Effect of crack depth and operating pressure.” *Eng. Failure Analysis, 55*, 288-299

[44].Ghaednia, H. (2015). Burst pressure of NPS30 steel pipes with dent-crack defect (Ph.D. Dissertation). University of Windsor, Windsor, Ontario, Canada.

[45].Gross D, Seelig T., “Fracture mechanics with an introduction to micro mechanics”, 3rd edition, Springer international, 2018.

[46].Hancock, J. W., and McKenzie, A. C., “On the mechanisms of ductile failure in high-strength steels subjected to multi-axial stress-states”. Journal of Mech. Phys. Solids, Vol. 24, pp 147 to 169, 1976.

[47].Henshell, R.D., Shaw, K.G., Crack tip finite elements are unnecessary*, Int. J. Numer. Methods Eng. 9 (1975) 495–507.

[48].Hojjati, T.R., Cooreman, S., Van Hoecke, D., Finite element simulation of dynamic brittle fracture in pipeline steel: a XFEM-based cohesive zone approach, J. Mater.: Design and Applications 232 (5) (2018) 357–370.

[49].Hopkins. P., Jones, D.G., Clyne, A.C., “Recent studies of the significance of mechanical damage in pipelines.”, The American Gas Association and European Pipeline Research Group Research Seminar V, San Francisco, USA, September; 1983.

[50].Jaske, C. E, CorLAS User Manual, 2010, Version 2.25.

[51].Kainat, M.; Langer, D.; Hassanien, S. Do we need a safe excavation pressure for dented pipelines: How should it be defined? In Proceedings of the 12th International Pipelines Conference, Ipc2018-78376, Calgary, AB, Canada, 24–28 September 2018.

[52].Keith A, Escoe B. Piping and pipelines assessment guide. British library cataloguing-in publication data, vol. I. Elsevier; 2006.

[53].Kiefner, J. F., Maxey, W. A., Eiber, R. J., and Duffy, A. R., "Failure Stress Levels of Flaws in Pressurized Cylinders," American Society of Testing and Materials Report No. ASTM STP 536, pp. 461–481, 1973.

[54].Kiefner, J.F, "Defect Assessment – Conclusion: Modified Ln-Secant Equation Improves Failure Prediction" Oil and Gas Journal, 2008.

[55].Kuna, M., (2013) Finite Elements in Fracture Mechanics, Solid Mechanics and Its Applications 201, DOI: 10.1007/978-94-007-6680-8_3, Springer Science+Business Media Dordrecht.

[56].Lancaster E.R., Palmer S.C.," Burst pressure of pipes containing dents and gouges", IMechE 1996, Proceedings of the Institution of Mechanical Engineers, UK, Vol 210

[57].Lancaster, E. R., & Palmer, S. C. (1996). Burst pressures of pipes containing dents and gouges. *Proceedings of the Institution of Mechanical Engineers, Part E: Journal of Process Mechanical Engineering, 210*(1), 19-27.

[58].Li, H.; Chandra, N. Analysis of crack growth and crack-tip plasticity in ductile materials using cohesive zone models. *Int. J. Plast.* **2003**, *19*, 849–882.

[59].Lin, M., Agbo, S., Cheng, J.J.R., Yoosef-Ghodsi, N., Adeeb, Application of the extended finite element method (XFEM) to simulate crack propagation in pressurized steel pipes, in: Proceedings of ASME 2017 Pressure Vessels and Piping Conference, volume 3B, 2017.

[60].Liu, X.B.; Zhang, H.; Han, Y.; Xia, M.; Ji, Y. Numerical and Experimental study on critical crack tip opening displacement of X80 pipeline steel. *Mechanics* **2017**, *23*, 204–208.

[61].Macdonald, K.A.; Cosham, A. Best practice for the assessment of defects in pipelines—Gouges and dents. *J. Eng. Fail. Anal.* 2005, *12*, 720–745.

[62].Melenk J.M, Babuska, I. "The partition of unity finite element method: Basic theory and applications." *Computer methods in Applied mechanics and Engineering*, 1996.

[63].Ming Gao, Ravi Krishnamurthy, Samarth Tandon, & Udayasankar Arumugam.*Critical strain based ductile damage criterion and its application to mechanical damage in pipelines.* Proceedings of the 13th International Conference on Fracture June 16-21, 2013, Beijing, China

[64].Moahammadi, S., (2008), Extended finite element method for fracture analysis of structures, Black well publishing, UK.

[65].Moes, N., Dolbow, J., and Belytschko, T. "A finite element method for crack growth without remeshing." *Int.J. Numer. methods in Eng*, 46 (1999) 131–150.

[66].Mohr, W. 2003. "Strain-based design of pipelines- basic guidance on strain-based design, the Minerals Management Service (MMS) and the Office of Pipeline Safety (OPS)", Project No. 45892GTH.

[67].National Energy Board, Canada, annual report to parliament, 2017-18, https://www.neb-one.gc.ca/, Accessed April 2019

[68].National Energy board, Safety advisory NEB SA 2010-01, 18th June 2010; http://www.neb-one.gc.ca, Accessed 11 July 2019

[69].Natural Resources Canada (NRCan) Energy fact book 2019-2020

[70].Neimitz. A, Galkiewicz, J., Lipiec, S., Dzioba I., Estimation of the onset of crack growth in ductile materials, MDPI J. Materials 11 (2018) 2026.

Newman, J. C. and Raju, I. S. An empirical stress-intensity factor equation for the surface crack. Engineering Fracture Mechanics, 1981, 15(1-2), 85-191.

[71].Noronha D.B. Jr. et al. "Procedures for the strain-based assessment of pipeline dents", Int. Journal of Pressure Vessels and Piping 87 (2010) 254e265

[72].Okodi A, Li Y, Cheng R, Yoosef-Ghodsi N, Kainat M, & Adeeb S., (2020), "Crack Propagation and Burst pressure of Pipeline with Restrained and Unrestrained Concentric Dent-crack defects using Extended finite element method" ***J.*** *Applied sciences*, (2020), 10.3390/app10217554

[73].Okodi, A.; Lin, M.; Yoosef-Ghodsi, N.; Kainat, M.; Hassanien, S.; Adeeb, S. Crack propagation and burst pressure of longitudinally cracked pipeline using extended finite element method. *Int. J. Press. Vessel. Pip.* 2020, *184*, 104115.

[74].Ong LS, Soh AK, Ong JH. Experimental and finite element investigation of a local dent on a pressurized pipe. J Strain Anal 1992;27(3):177–85.

[75].Orynyak I.V., Bogdan A.V., Rozgonyuk C.V., Ductile fracture model for a pipe with a dent. In: Denys R, editor. Proc. 4th int. conf. on pipeline technology, Ostend, Belgium, 9–13 May, volume II; 2004. p. 949–60.

[76].Orynyak, I.; Yakovleva, E.; Rozgonyuk, V. Application of the cheng-finnie method to the calculation of stress intensity factors in thin-walled pipes with long axial cracks with allowance for geometric nonlinearity. *Strength Mater.* 2007, *39*, 455–465.

[77].Oshana, JJ., "Dent behavior of steel pipes under pressure load" (2014). Electronic Theses and Dissertations. 5025. https://scholar.uwindsor.ca/etd/5025.

[78].Pluvinage, G., Capelle, J., and Schmitt, C., "Handbook of Materials Failure Analysis with Case Studies from the Oil and Gas Industry", Chapter 3: Methods for assessing defects leading to gas pipe failure, Elsevier Ltd, 2016.

[79].Rafi, A., Silva, J., Kenno, S., Das, S., Kania, R., & Wang, R.Y., (2010)." Strength of line pipe with dent and crack defect." *Proceedings of the 8th international pipelines conference. IPC 2010-31095, Calgary, Alberta, Canada.*

[80].Ravi, K., Kapil, K., Computational models for ductile fracture prediction in structural engineering applications, Procedia Material Science 3 (2014) 1947–1955.

[81].Rothwell, A.B., Coote, R.I., A critical review of the assessment methods for axial planar surface flaws in pipe, in: Paper#21009, 52, Pipeline Technology Conference, Ostend, Belgium, 2009.

[82].Rice, J. R., and Tracey, D. M., "On the ductile enlargement of voids in triaxial stress fields". Journal of Mech. Phys. Solids, Vol. 17, pp 201 to 217, 1969.

[83].Rinehart, A., and Keating, B. 2007. "Stress Concentration Solution for a 2D Dent in an Internally Pressurized Cylinder." Journal of Engineering Mechanics 133 (7) (July): 792–800. doi:10.1061/(ASCE)0733-9399(2007)133:7(792).

[84].Robert B Francini and Nader Yoosef-Ghodsi: "Development of a Model for Predicting the Severity of Pipeline Damage Identified by In-Line Inspection" Pipeline Research Council International (PRCI) Report, PR-218-063511-B, Final Report No. 08-124, December 2008.

[85].Ronny, H.; Espen, B.; Lijana, D.O. Damage assessment of pipelines with dents and cracks, proposal for methodology for calculation of acceptable dimensions of a combination of crack, & dent in subsea pipelines. In Proceedings of the ASME 29th International Conference on Ocean, Offshore and Arctic Engineering, Shanghai, China, 6–11 June 2010.

[86].Rosenfeld, M. 2001. “Proposed New Guidelines for ASME B31.8 on Assessment of Dents and Mechanical Damage”. Topical Report GRI-01/0084. Des Plaines, IL: GRI.

[87].Rosenfield, M.J.; Pepper, J.W.; Lewis, K. Basis of the New Criteria in ASME B31.8 for Prioritization, & Repair of Mechanical Damage. *Int. Pipeline Conf.* 2002, *36207*, 647–658.

[88].Rosenfield, M.J., Pepper, J.W., & Lewis, K., Basis of the new criteria in ASME B31.8 for prioritization, & repair of mechanical damage. (2002). *Ipc2002-27122 ipc02-27122 dented pipes with cracks*

[89].Samarth, T., Ming, G., Ravi, K., Shahani, K., Kania, R., Evaluation of existing fracture mechanics models for burst pressure predictions, theoretical and experimental aspects, in: IPC2014-33563 Proceedings of the 10th International Pipeline Conference, Calgary Canada, 2014.

[90].Schwalbe, K.H., Scheider, I., Cornec, A., The SIAM Method for Applying Cohesive Models to the Damage Behavior of Engineering Materials and Structures, GKSS 2009/1, 2009. ISSN 0344-9629.

[91].Seif, T., “Ductile fracture analysis in a steel plate by cohesive zone modelling”, MSc thesis, Memorial University of Newfoundland, Canada, 2014.

[92].Shih, C.F., and Hutchinson, J.W., “Fully plastic solutions and large-scale yielding estimates for plane stress crack problems”, Report No. DEAP S-14, Harvard University, July 1975.

[93].The American Society of Mechanical Engineers. *Gas Transmission and Distribution Piping System: ASME Code for Pressure Piping, B31*; ASME-B31.8; Revision to B31.8-1999; The American Society of Mechanical Engineers, New York, USA ,2003.

[94].Tian, X., & Zhang, H. (2017). “Failure criterion of buried pipelines with dent and scratch defects.” J. Eng. Failure Anal. 80(2017)278-289

[95].Vilkys, T., Rudzinskas, V., Prentkovskis, O., Tretjakovas, J., Višniakov, N., & Maruschak, P. (2018).” Evaluation of failure pressure for gas pipelines with combined defects.” *Metals, 8*(5), 346.

[96].Wang K.C, Smith, E.D., “The effect of mechanical damage on fracture initiation in line pipe: part I—dents.”, Report ERP/PMRL 82-11 (TR), Canada: Canadian Centre for Mineral and Energy Technology (CANMET) January 1982.

[97].WRC Bulletin 465, “Technologies for the Evaluation of Non-Crack-Like Flaws in Pressurized Components,” September 2001, Welding Research Council

[98].Yan, J., Zhang, S., Kariyawasam, S., Pino, M., Liu, T., Validate crack assessment models with in-service and hydrotest failures, in: IPC2018-78251, Proceedings of the 12th International Pipeline Conference, September 2018 (Calgary, Alberta, Canada).

[99].Zijian, Y., Zhang, S., Zhou, W., Model Error Assessment of Burst Capacity Models for Energy Pipelines Containing Surface Cracks, International Journal of Pressure Vessels and Piping, 2014.

[100].Zhang, Z., Xu, J., Nyhus, B., Østby, E., SENT (single edge notch tension) methodology for pipeline applications, in: Proceedings of the 18th European Conference on Fracture, Dresden, Germany, 2010.